Title
Mitochondrial Segregation in Budding Yeast Gametogenesis

Author
Sawyer, Eric M

Publication Date
2019

Peer reviewed|Thesis/dissertation

Mitochondrial Segregation in Budding Yeast Gametogenesis

By

Eric M. Sawyer

A dissertation submitted in partial satisfaction of the

requirements for the degree of

Doctor of Philosophy

in

Molecular and Cell Biology

in the

Graduate Division

of the

University of California, Berkeley

Committee in charge:

Professor Elçin Ünal, Chair
Professor David Drubin
Professor Karen Davies
Professor James Olzmann

Spring 2019

Abstract

Mitochondrial Segregation in Budding Yeast Gametogenesis

by

Eric M. Sawyer

Doctor of Philosophy in Molecular and Cell Biology

University of California, Berkeley

Professor Elçin Ünal, Chair

Cellular differentiation involves remodeling cellular architecture to transform one cell type into another. An important and conserved cellular differentiation program is gametogenesis, the process by which sexually reproducing organisms produce gametes. Gametogenesis involves specialized cell division as well as extensive cellular remodeling. Here, we investigated mitochondrial dynamics during gametogenesis in budding yeast to determine how regulators of meiotic differentiation act to control organelle morphogenesis. We found that mitochondria detach from the plasma membrane during meiosis II in a temporally controlled manner. Mitochondrial detachment is regulated by the induction of a transcription factor, Ndt80, which promotes the activation of a protein kinase, Ime2. Ime2 induces mitochondrial detachment by promoting the destruction of the mitochondria-endoplasmic reticulum-cortex anchor (MECA), which normally attaches mitochondria to the plasma membrane. Destruction of MECA involves Ime2-dependent phosphorylation and proteolysis that target both known subunits of the complex. We next investigated the fate of the mitochondrial network after its detachment. Consistent with previous studies, we found that the detached mitochondria gained associations with meiotic nuclei. By light and electron microscopy, we determined that the association between mitochondria and the nucleus is a developmentally regulated membrane contact site. Formation of the nucleus-mitochondria contact site required Ndt80 but not Ime2, indicating that the contact site is potentiated prior to destruction of MECA. We analyzed the potential involvement of two known ER-mitochondria tethers, ERMES and Ltc1/Lam6, but our data disfavor their potential roles in this process. Instead, novel factors are likely responsible for generating the nucleus-mitochondria contact site. Our study defines key mechanisms that coordinate mitochondrial morphogenesis with the landmark events of meiosis. Further, our work demonstrates that cells can developmentally regulate tethering to induce organelle remodeling.

for Andy

Table of Contents

Acknowledgments

I thank all past and present members of the Brar and Ünal laboratories for their advice, technical assistance, and friendship. I give additional thanks to the following people who contributed to the execution of this work, its motivation, or its presentation: Juliet Barker, Gloria Brar, Christiane Brune, Jingxun Chen, Yuzhang Chen, Leon Chan, Katie Conlon, Karen Davies, David Drubin, Jay Goodman, Devon Harris, Victoria Jorgensen, Pallavi Joshi, Grant King, Barbara Meyer, James Olzmann, Michael Rape, Jasper Rine, Tina Sing, Amy Tresenrider, and Jing Zhang. In addition, Julius Yunus and Luke Berchowitz provided critical insights and experimental support for the analysis of Ime2 in Chapter 2. Lori Kohlstaedt and the Vincent J. Coates Proteomics/Mass Spectrometry Laboratory provided critical technical assistance for mass spectrometry analysis. Kent McDonald and the UC Berkeley Electron Microscope Lab provided extensive knowledge, experimental assistance, and training for the electron microscopy experiments. The Spring 2017 MCB 140L course performed the genetic screen described in Section A.1. I also thank Laura Lackner, Gavin Schlissel, and Kevan Shokat for generously providing reagents and protocols. Finally, I thank Jeremy Thorner for stimulating discussions that influenced the course of this work.

Most of all, I would like to thank Elçin Ünal for creating a fantastic laboratory environment in which to conduct this work. This work would not have been possible without Elçin's generous mentorship and enthusiasm for biology throughout the course of my graduate studies.

I also thank the following funding sources for their support of this and other work in the Ünal lab: the Pew Charitable Trusts (00027344), Damon Runyon Cancer Research Foundation (35-15), National Institutes of Health (DP2 AG055946-01), and Glenn Foundation for Medical Research. My graduate training was further supported by a National Science Foundation Graduate Research Fellowship (DGE 1752814 and DGE 1106400) and National Institutes of Health Traineeship (T32 GM007127). Mass spectrometry was performed by the University of California, Berkeley, Coates Proteomics Lab, which is supported by the National Institutes of Health S10 Instrumentation Grant S10RR025622.

Chapter 1

Introduction

1.1 Mitochondrial structure and inheritance

Mitochondria are dynamic organelles responsible for energy harvesting and other metabolic activities. Mitochondria are present in essentially all eukaryotic cells and are descended from bacteria. The genome within mitochondria is both remnant and reminder of their origins. The sequences of mitochondrial genomes resemble modern obligate intracellular pathogens within the alphaproteobacter class, suggesting an endopathogen-to-endosymbiont origin (Ferla et al., 2013; Lane, 2006; Wang and Wu, 2015).

1.1.1 Mitochondria: conserved organelles with diverse forms and functions

Mitochondria are extraordinary organelles. Mitochondria contain a genome that is transcribed and translated within the organelle by dedicated factors. Mitochondria are also metabolic hubs, facilitating ATP production by oxidative phosphorylation, lipid synthesis, and iron-sulfur cluster synthesis (Friedman and Nunnari, 2014; Mishra and Chan, 2014). Remarkably, yeast mitochondria contain a complex proteome estimated to contain approximately 1000 different proteins (Fox, 2012). In all but perhaps a few obscure eukaryotes, mitochondria are essential for life. Clearly, mitochondria are a multifaceted and important organelle.

In most cell types, mitochondria exist as a highly dynamic and interconnected network (Friedman and Nunnari, 2014; Mishra and Chan, 2014). In yeast cells, mitochondria form a branched tubular structure that is dynamically remodeled but stably anchored to the plasma membrane (Hoffmann and Avers, 1973; Nunnari et al., 1997). In both yeast (Nunnari et al., 1997) and cultured mammalian cells (Chen et al., 2003), remodeling of the mitochondrial network is mediated by fusion and fission. Although at the microscopic scale, mitochondrial structure is highly unstable, the net balance of mitochondrial fusion and fission provides a stable structure to the overall organelle network (Bleazard et al., 1999; Tieu and Nunnari, 2000).

In individual cells, the microscale morphology of mitochondria is dynamic. However, coordinated changes in the shapes of mitochondria also occur during development. The first discovered molecular mediator of mitochondrial dynamics, the mitochondrial fusion GTPase Fuzzy onions, was identified due to its specialized role

in *Drosophila* spermatogenesis (Hales and Fuller, 1997). Fuzzy onions is specifically produced in germ cells to induce a programmed and cell-wide wave of mitochondrial fusion that occurs during postmeiotic differentiation. Many structural specializations of mitochondria are also visible in comparisons between somatic cell types. Cristae, where the respiratory complexes in the inner mitochondrial membrane reside, differ widely in their morphology across cell types (Zick et al., 2009). These specializations are likely tailored to meet the metabolic demands unique to particular tissues, with metabolically active cell types requiring more densely packed cristae. Neurons contain small, individual mitochondria, amenable to axonal transport, rather than the extensive fused networks found in most other cell types (Schwarz, 2013). In general, the mechanisms that give rise to cell type-specific mitochondrial architectures are poorly understood but likely play critical roles in organismal homeostasis.

1.1.2 Shaping and positioning mitochondria

The steady-state morphology of the mitochondrial network arises from the balance between several remodeling processes, which may vary in their activities between cell types or developmental contexts. Mitochondrial fusion promotes the joining of two mitochondria into one. Because mitochondria contain both inner and outer membranes, correct joining of the organelles requires two rounds of specific homotypic fusion. Fusion of the outer mitochondrial membrane is accomplished by the mitofusins, a family of dynamin-related GTPases (Hales and Fuller, 1997; Mishra and Chan, 2014). Yeast contain a single mitofusin, Fzo1 (Hermann et al., 1998). Subsequent inner membrane fusion requires a different dynamin-related GTPase, OPA1, and known as Mgm1 in yeast (Cipolat et al., 2004). Importantly, inner mitochondrial membrane fusion also requires the electrochemical gradient, thereby coupling the physiology of the organelle to its dynamic behavior (Meeusen et al., 2004).

Mitochondrial fusion is balanced by fission, which serves to divide the organelle. Like fusion, membrane scission is catalyzed by dynamin-related GTPases. The GTPase DRP1, or Dnm1 in yeast, constricts mitochondria to promote fission (Bleazard et al., 1999; Smirnova et al., 1998) by coupling GTP hydrolysis to constriction of oligomeric assemblies (Kalia et al., 2018). The initial recruitment of DRP1 to dividing mitochondria occurs at mitochondrial constrictions where ER tubules wrap around mitochondria (Friedman et al., 2011), and the final step of mitochondrial division requires membrane scission by a classical dynamin, dynamin-2 (Lee et al., 2016). Together, over two decades of study has underscored the importance of dynamin-related GTPases—and now classical dynamics—in controlling the structure of mitochondria.

The morphology of the mitochondrial network is also controlled by extrinsic factors that influence the localization of the organelle. Mitochondria-cytoskeleton

interactions play key roles in both the intracellular distribution and inheritance of mitochondria. It has been known for many years that animal cells harness the ATP-hydrolyzing activities of microtubule motors (such as kinesins) to facilitate the motility of organelles, including mitochondria (Vale, 1987). Mitochondrial association with spindle microtubules has also been observed in fission yeast (Yaffe et al., 2003) and in some animal cells, such as *Drosophila* spermatids (Fuller, 1993). In budding yeast, where an actin cytoskeleton predominates, mitochondrial motility instead relies on actin and myosin motors (Boldogh et al., 2001).

Proper mitochondrial motility and distribution is critical to cellular health. In the absence of the kinesin adapter protein Milton, mitochondria cannot be transported to synapses, leading to defective synaptic transmission (Stowers et al., 2002). Concerted mitochondrial movements occur during *Drosophila* female gametogenesis (Cox and Spradling, 2003) and male gametogenesis (Aldridge et al., 2007; Fuller, 1993) to ensure proper morphogenesis and transmission of the organelle. Finally, retention of mitochondria at particular sites is critical for organelle communication and homeostasis (see Section 1.2).

1.1.3 Mitochondrial segregation during cell division

The molecular mechanisms that influence the shapes and positions of mitochondria, described above, must ultimately allow proper segregation of the organelle during cell division. Whether segregation of mitochondria is active or passive, and whether active segregation mechanisms discriminate between subpopulations of mitochondria, have attracted much interest but appear to vary across different biological contexts.

Mitochondria-cytoskeleton interactions are ubiquitious in most cells (including in interphase), providing an opportunity for co-option of the cell division machinery by mitochondria. In fission yeast, mitochondria associate with microtubules and are transported to the spindle poles during mitosis alongside the chromosomes (Yaffe et al., 2003). Perturbation of fission yeast mitochondria-microtubule interaction leads to reduced fidelity of mitochondrial inheritance due to their improper subcellular distribution (Jajoo et al., 2016). In budding yeast, the actin cytoskeleton and a type V myosin motor, Myo2, play essential roles in mitochondrial segregation. Myo2 mediates mitochondrial transmission from the mother cell into the bud in a transport process regulated by the adapter protein Mmr1 and the Rab GTPase Ypt11 (Altmann et al., 2008; Boldogh et al., 2004; Chernyakov et al., 2013; Itoh et al., 2004). Despite their structural dissimilarity, Mmr1 and Ypt11 are functionally redundant (Chernyakov et al., 2013). Mitotic roles for mitochondria-cytoskeleton interaction factors are less understood in mammalian cells. However, in mammalian cells, mitochondrial distribution during mitosis is controlled at least in part by association of mitochondria with dynamic microtubule tips (Kanfer et al., 2015).

Is mitochondrial segregation biased? Yeast cells undergo replicative aging, with a distinct mother-daughter asymmetry in lifespan (Mortimer and Johnston, 1959). Mitochondrial function declines dramatically as mother cells age (Hughes and Gottschling, 2012; Veatch et al., 2009). Actin-based motility favors the distribution of high quality mitochondria to daughter cells (Higuchi et al., 2013), though the effect is modest in unchallenged cells, perhaps due to redundancy with constitutive quality control mechanisms such as fusion and fission (Osman et al., 2015). Additionally, a mother-daughter asymmetry in lysosomal function may promote daughter mitochondria rejuvenation independent of or in parallel to the initial distribution of mitochondria (Henderson et al., 2014). A similar asymmetric distribution of old and young mitochondria was found to play a critical role in human stem cell maintenance (Katajisto et al., 2015), indicating asymmetric mitochondrial segregation may be a conserved feature of asymmetric cell division.

1.2 Tethers and membrane contact sites

The concept of membrane tethering was developed by studies of the secretory pathway. Studies of membrane trafficking identified the presence of heterotypic membrane-membrane tethering (or "docking") as a distinct precursor to membrane fusion (Waters and Pfeffer, 1999). Later, this concept was applied to actively tethered membranes not destined for fusion. In this work, we use the term "tethering" in this more recent sense, referring to the anchoring of different organelles. We refer to tethered membranes as "membrane contact sites." Tethering to establish membrane contact sites has proved ubiquitous, with a growing number of pairwise organelle-organelle interactions being identified in yeast and in cultured animal cells. While the roles of most organelle interactions are largely unknown, several particularly well-studied cases point to importance in organelle distribution, lipid homeostasis, and communication between organelles.

1.2.1 Bridging organelles with protein tethers

The interaction between organelles does not occur spontaneously but instead is mediated by protein assemblies called tethers (Eisenberg-Bord et al., 2016; Gatta and Levine, 2017; Lackner, 2019; Prinz, 2014; Scorrano et al., 2019). At a basic level, the function of all tethers is the same: pulling membranes together. However, the structural and biochemical details of the many tethers discovered so far have turned out to be extraordinarily diverse. Despite this complexity, tethers can be understood on the basis of their general, defining features as well as specializations that enable their individual biological functions (Eisenberg-Bord et al., 2016; Scorrano et al., 2019).

Perhaps the prototypical tether is a protein complex that bridges the ER and mitochondria in yeast, called the ER-mitochondria encounter structure, or ERMES

(Kornmann et al., 2009). ERMES contains four core subunits, all of which are required for its function (Kornmann et al., 2009). Mmm1 is an integral ER membrane protein, while Mdm34 and Mdm10 are integral mitochondrial outer membrane proteins, and Mdm12 binds the complex from the cytosol (Kornmann et al., 2009). Tethering specificity is provided by protein-protein interactions between the ER- and mitochondria-targeted subunits (Kornmann et al., 2009). In addition, the small GTPase Gem1 transiently associates with ERMES (Murley et al., 2013). The function of ERMES can be partially complemented by a synthetic tether, indicating that a major function of ERMES is to simply tether the ER and mitochondria, independent of other catalytic functions it might have (Kornmann et al., 2009). Three of the four ERMES subunits (Mmm1, Mdm12, and Mdm34 but not Mdm10) contain predicted synaptotagmin-like, mitochondrial and lipid-binding protein (SMP) domains (Kopec et al., 2010). Proteins containing SMP domains commonly localize to membrane contact sites, providing many opportunities for detailed structure-function analysis of this conserved protein module (Reinisch and De Camilli, 2016).

Additional mitochondria-organelle contact sites, and tethers localized to the contact sites, have been identified. The vacuole and mitochondria patch (vCLAMP) is a contact site between mitochondria and the lysosome/vacuole and contains the tether Vps39/Vam6 and the Rab GTPase Ypt7 (Elbaz-Alon et al., 2014; Honscher et al., 2014). Interestingly, Vps39/Vam6 and Ypt7 also participate in the endosome-vacuole tethering HOPS complex, but this role is genetically separable from mitochondria-vacuole tethering (Elbaz-Alon et al., 2014; Honscher et al., 2014). Removal of vCLAMP or ERMES is tolerated, but simultaneous removal of both is lethal (Elbaz-Alon et al., 2014; Honscher et al., 2014). This type of genetic interaction is common among tethers.

In yeast, the ER and mitochondria mostly localize to the cell cortex. In both cases, this distribution is due to the actions of protein tethers. ER-plasma membrane tethering is controlled by at least six different proteins: the tricalbins Tcb1/2/3, the VAP homologs Scs2/22, and Ist2 (Manford et al., 2012). In contrast, a single protein complex is required for mitochondria-plasma membrane tethering: the mitochondria-ER-cortex anchor, or MECA (Cerveny et al., 2007; Klecker et al., 2013; Lackner et al., 2013; Ping et al., 2016). MECA contains two known subunits, Num1 and Mdm36 (Lackner et al., 2013; Ping et al., 2016). Num1 is a massive (~300 kDa) protein that contains a C-terminal Pleckstrin homology (PH) domain and a N-terminal coiled coil domain (Lackner et al., 2013; Ping et al., 2016; Tang et al., 2012; Yu et al., 2004). The PH domain promotes plasma membrane binding through its association with the plasma membrane-specific lipid phosphatidylinositol (4,5)-bisphosphate (Tang et al., 2012; Yu et al., 2004). The N-terminal coiled coil domain can bind directly to the mitochondria-specific lipid cardiolipin *in vitro* (Ping et al., 2016). Therefore, the tethering specificity of MECA is conferred by the distinct lipid binding specificities of its N- and C-terminal

domains (Ping et al., 2016). The second MECA subunit, Mdm36, supports but is not absolutely required for the function of Num1 (Lackner et al., 2013; Ping et al., 2016).

MECA plays two distinct roles: it is the cortical anchor for mitochondria as well as cytoplasmic dynein (Heil-Chapdelaine et al., 2000; Kormanec et al., 1991; Kraft and Lackner, 2017; Omer et al., 2018; Tang et al., 2012). Deletion of the major MECA subunit, Num1, leads to detachment of mitochondria from the cell cortex (Cerveny et al., 2007; Klecker et al., 2013; Lackner et al., 2013) and defective nuclear migration from the mother cell into the bud during mitosis (Kormanec et al., 1991). To direct nuclear movements through dynein-astral microtubule binding, Num1 acts by directly binding dynein (Tang et al., 2012). In addition to serving as the cortical receptor for dynein, Num1 also activates the motor activity of bound dynein. Binding of dynein to Num1 leads to the removal of the dynein inhibitor Pac1/LIS1 (Lammers and Markus, 2015). The two roles of Num1 are genetically separable, as Num1 bearing two amino acid substitutions in the dynein-binding region (L167E L170E) cannot anchor dynein but efficiently anchors mitochondria (Tang et al., 2012). Recent work suggests that the dual roles of MECA in tethering mitochondria and dynein may be intertwined. Mitochondria have been proposed to nucleate cortical MECA assemblies (Kraft and Lackner, 2017). In the absence of Num1, Mdm36, or bud-segregated mitochondria, spindle positioning is defective (Kraft and Lackner, 2017). Another study found that the ER tethering proteins Scs2 and Scs22 govern Num1 distribution across competing microtubule sliding and end-on capture, suggesting that multiple, functionally distinct populations of MECA exist within cells (Omer et al., 2018). More work is required to determine how MECA is assembled and how its distinct functions are regulated.

Determining the functions of tethers at contact sites is an area of active investigation. Tether functions are likely quite diverse. A family of sterol transporters that contain Steroidogenic Acute Regulatory Transfer (StART) domains have been implicated in lipid transport at membrane contact sites as well as tethering (Elbaz-Alon et al., 2015; Gatta et al., 2015; Murley et al., 2015; Tong et al., 2018). The protein Ltc1/Lam6 is a StART domain-containing sterol transporter that localizes to ER-mitochondria and ER/nucleus-vacuole contact sites, and perhaps others (Elbaz-Alon et al., 2015; Murley et al., 2015). Importantly, the protein physically associates with ERMES, and simultaneous deletion of an ERMES subunit and *LTC1/LAM6* leads to a synthetic growth defect (Elbaz-Alon et al., 2015; Murley et al., 2015).

The excellent genetic tools in budding yeast, as well as the fact that many tethers exhibit genetic interactions with one another, has been a boon for the yeast tether field. Identifying tethers in mammalian cells has lagged behind, but nonetheless many interesting cases have come to light. In yeast, the enigmatic protein Vps13 is synthetically lethal with deletion of ERMES, and some alleles of *VPS13* are

dominant bypass suppressors of ERMES deletions (Lang et al., 2015). Humans have four Vps13 orthologs, which localize to different ER-organelle contact sites where they transport lipids (Kumar et al., 2018). In addition, human ER-plasma membrane contact sites appear to use very similar tethering machinery as that described in yeast, though with an additional level of regulation by Ca^{2+} signaling (Saheki and De Camilli, 2017). In other cases, structurally dissimilar proteins may serve functionally similar roles.

1.2.2 Functions of tethering and membrane contact sites

Tether-mediated membrane contact sites have now been observed for nearly all major organelles, indicating the phenomenon is widespread (Eisenberg-Bord et al., 2016; Gatta and Levine, 2017; Lackner, 2019; Prinz, 2014; Scorrano et al., 2019). As the 'census' of tethers and membrane contact sites has grown, so too has the opportunity to systematically assess the functional relevance of membrane contact sites.

It is highly likely that the majority of tethers promote lipid transport between organelles. This activity can occur through lipid transporting activity present in the tethering proteins themselves or indirectly by inducing membrane-membrane contact that can be exploited by a transporter protein (Eisenberg-Bord et al., 2016). Sterol lipid transporting activity is clear in the case of the StART domain proteins (Elbaz-Alon et al., 2015; Gatta et al., 2015; Murley et al., 2015; Tong et al., 2018). In addition, the SMP domain (present in ERMES) has clear lipid binding and likely transport activity (AhYoung et al., 2015; Saheki and De Camilli, 2017; Schauder et al., 2014). In the case of ERMES in particular, any putative lipid transporting function appears to be functionally dispensable due to complementation of the tether by a biochemically inert artificial tether (Kornmann et al., 2009). It was previously hypothesized that ERMES may play a key role in phospholipid synthesis due to the division of the phosphatidylcholine biosynthetic pathway between the ER and mitochondria (Kornmann et al., 2009). Only recently was it appreciated that the enzyme responsible for the sole step thought to occur in mitochondria (phosphatidylserine decarboxylase) is actually also present in the ER due to dual co-translational targeting of the polypeptide (Friedman et al., 2018; Jan et al., 2014; Williams et al., 2014). ERMES-mediated lipid transit therefore likely occurs in parallel to other mechanisms, both organelle intrinsic and involving organelle crosstalk. A similar principle may apply to other contact sites where removal of the contact leads to only a mild or no lipid homeostasis defect.

Perhaps the most surprising development in the organelle contact site field has been the discovery that interactions between organelles can influence their behaviors. In both yeast and animal cells, transient ER-mitochondria contacts are precursors to mitochondrial fission (Friedman et al., 2011). In animal cells, the basis of this phenomenon appears to originate with the ER-localized formin, INF2,

which induces actin polymerization to promote mitochondrial constriction (Korobova et al., 2013). Mitochondrial constriction alone (even by exogenous means) is sufficient to induce division of the organelle (Helle et al., 2017). Importantly, ER-mitochondria contact sites are also spatiotemporally coupled to the replication of the mitochondrial genome in both yeast and human cells (Lewis et al., 2016; Meeusen and Nunnari, 2003; Murley et al., 2013). ER-endosome contact sites are also precursors to endosome fission (Hoyer et al., 2018; Rowland et al., 2014). This finding indicates that contact with the ER may be integrated into the division and other behaviors of many organelles.

Tethers can also play roles in organelle inheritance. In yeast, the myosin adapter protein Mmr1 (Altmann et al., 2008; Boldogh et al., 2004; Chernyakov et al., 2013; Itoh et al., 2004) is also tethered at the bud tip to retain mitochondria there (Chen et al., 2018a; Swayne et al., 2011). An analogous repurposing of a motor protein adapter for tethering occurs in *Drosophila* spermatogenesis, where the kinesin adapter Milton promotes mitochondria-nucleus tethering during postmeiotic differentiation (Aldridge et al., 2007). Finally, an alternative isoform of the germ plasm protein Oskar promotes mitochondrial tethering at the posterior pole of *Drosophila* oocytes (Hurd et al., 2016). This Oskar isoform locally alters the actin cytoskeleton to promote mitochondrial entrapment and inheritance by the primordial germ cells (Hurd et al., 2016). Further work will be required to clarify the extent to which tethering contributes to organelle inheritance across the diverse biological contexts in which tethering is observed.

1.2.3 Regulation of membrane contact sites

Membrane contact sites are widespread and have generally been studied under uniform growth conditions in yeast or cultured animal cells. Although studies cannot uncover environmental or developmental regulation of tethers by performing experiments in a single growth condition, genetic perturbations hint at tether regulation mechanisms.

The deletion of a single tether often has no consequence on growth rate in laboratory conditions but can lead to compensatory remodeling of other contact sites (Eisenberg-Bord et al., 2016; Scorrano et al., 2019). Examination of one contact site in mutants lacking a different contact site can demonstrate this effect. For example, when the vCLAMP subunit Vps39 is absent, ERMES punta approximately triple in number (Elbaz-Alon et al., 2014). The reciprocal experiment gave the same result: deletion of an ERMES subunit led to marked expansion of the vCLAMP site (Elbaz-Alon et al., 2014). In other cases, a single tether can change its localization to dynamically respond to local needs. Vps13 uses distinct adapters to target it to different membrane contact sites (Bean et al., 2018), and consistent with a compensatory function, simultaneous deletion of *VPS13* and any ERMES subunit is lethal (Lang et al., 2015). The ability of tethers to dynamically remodel one contact

site to compensate for deficiency in another indicates that tethers are subject to regulation that stabilizes organelle homeostasis. However, the pathways responsible for sensing contact site dysfunction and inducing contact site remodeling are not known.

Contact site remodeling can also occur in response to changing environmental conditions. The nucleus-vacuole junction in yeast, which tethers the nucleus and vacuole, expands in stationary phase when nutrients are depleted (Pan et al., 2000). In medium with glycerol as the sole carbon source, ERMES sites increase in number, and vCLAMPs are reduced (Honscher et al., 2014). The reduction in mitochondria-vacuole tethering was shown to be caused by phosphorylation of the vCLAMP subunit Vps39 (Honscher et al., 2014). Similar examples of phosphoregulation have been reported for other tethering factors, including Osh2, Osh3, OSBP, and CERT (Kumagai et al., 2014; Nhek et al., 2010). These findings indicate that posttranslational modification of tethers can influence membrane contact sites. These observations also bolster the possibility that tethers may be integrated into signaling pathways that regulate their activity.

Tethers and the membrane contact sites they establish play widespread roles in the organization and homeostasis of cells. The fact that cellular organization and physiology both differ remarkably between cell types indicates that tethers must be regulated by cell type. How tethering is integrated into cellular differentiation is the major focus of this work. First, we introduce meiotic differentiation (gametogenesis), the developmental program addressed in this work.

1.3 Meiotic differentiation in budding yeast

Meiosis is a specialized cell division, where a single round of DNA replication is followed by two rounds of chromosome segregation. As a result, ploidy is halved. While mitosis is ubiquitous, meiosis is employed in a single biological context—to generate reproductive cells, or gametes. Because of its specialized role, meiosis occurs in conjunction with cellular differentiation programs that give rise to gametes. This differentiation program is gametogenesis. Meiosis and gametogenesis involve elaborate transformations to gene regulation, cell cycle regulation, and cellular organization. The proper coordination of each is critical to reproductive success.

1.3.1 The importance of meiosis and gametogenesis

In sexually reproducing species, meiosis is responsible for the two-fold reduction in chromosome number that occurs during gamete formation. As a result, meiosis allows offspring to have two parents without runaway ploidy increases every generation. Due to the manner in which ploidy reduction is achieved, meiosis also results in the formation of recombinant chromosomes. By generating new

combinations of alleles, meiosis provides genetic variety for interrogation by natural selection.

Using genetics to study meiosis is a form of introspection, as meiosis is the cellular basis of many genetic phenomena. The unbiased segregation of unlinked loci during the meiotic divisions explains the Mendelian phenomenon of "independent assortment." The allelic nature of the two copies of a single gene explains Mendel's "segregation." And the biased segregation of linked loci is due to the limited numbers of crossovers that occur between homologous chromosomes in a single round of meiosis. Without meiosis, genetics would not be the same.

Although ploidy reduction and other chromosome-centric aspects of meiosis are undeniably important, much more is involved. The genetic products of meiosis are housed in highly specialized cells called gametes. Gametes exist on the cellular extremes. Eggs are some of the largest cells and sperm some of the smallest. Eggs can exist in precise, reversible cell cycle arrests for decades. Eggs also contain large maternal contributions to the embryo in the form of RNAs, proteins, and nutrients. Gametes of both sexes have the remarkable ability to fuse to one another in a precise manner that guarantees each offspring has precisely two parents. Most importantly, gametes are the only cells that give rise to offspring, and so gametes ensure the continuity of the species by allowing development to begin anew each generation.

Due to its critical importance to sexually reproducing organisms, meiosis is deeply conserved across species. However, meiosis varies in detail not just between species but between the two sexes of a single species. In female animals, only one of the four possible haploid genomes produced from meiosis becomes the egg. In males, all meiotic products become sperm. In fungi, all meiotic products become gametes, making fungal meiosis akin to animal spermatogenesis. The fungus whose meiotic development has been most intensely studied is the ascomycete *Saccharomyces cerevisiae*, commonly called budding yeast or baker's yeast. In fact, studies in budding yeast have been instrumental in advancing our understanding of meiosis.

In budding yeast, meiosis and gametogenesis are called sporulation (Neiman, 2005; Neiman, 2011). This is because the gametes are environmentally resilient, specialized cells called spores. As each spore is haploid and has one of two sexes (mating types), the similarity to animal gametes is clear. However, unlike animal gametes, the four spores produced from a single meiosis are essentially identical and physically associated with one another in a structure called a tetrad. And even more unlike animal gametes, haploid spores are fully competent of mitotic proliferation. Yet, despite these differences, gametogenesis shares many fundamental similarities across species.

The following sections outline key insights into the biology of meiosis and gametogenesis that have been obtained from studies of budding yeast sporulation. First, how do cells commit to meiosis and ensure that gene products are present at the proper times? Second, how is regulation of the cell cycle altered to accommodate the unique sequence of events that occurs in meiosis? And finally, how does the organization of the cell change to ensure the reproductive success of the gamete?

1.3.2 Transcriptional regulation in meiosis

Gametogenesis is a cellular differentiation program. In all sexually reproducing organisms, gene regulatory pathways restrict the gametogenesis program to defined sets of conditions. Cells fated to enter gametogenesis are transformed into new cell types, the gametes, with reduced ploidy and specialized cellular architectures tailored to support reproduction. Like other cellular differentiation programs, gametogenesis is driven by a transcriptional program that induces the temporally controlled expression of differentiation genes. In doing so, the transcriptional program of gametogenesis induces the transformation of the progenitor cell into a gamete. Decades of study in yeast have defined the transcriptional mechanisms underlying key steps in gametogenesis.

In all organisms, entry into meiosis must be tightly regulated to ensure that only the correct cell types in the correct locations, destined for reproduction, perform meiosis. Budding yeast is no different, although as a free-living, single-celled organism the meanings of "cell type" and "location" are different.

Every yeast cell has a cell type, called its mating type. Mating type has been extensively studied and reviewed (Herskowitz et al., 1992) and will be outlined only briefly here. Mating type is determined by a single genetic locus called *MAT*. Haploid cells exist as either *MAT***a** or *MAT*α. In *MAT***a** cells, the *MAT* locus contains the genes **a**1 and **a**2. In *MAT*α cells, *MAT* contains the genes α1 and α2. When a *MAT***a** haploid mates with a *MAT*α haploid, a *MAT***a**/α diploid is produced, which is heterozygous at *MAT* and therefore contains all the genes **a**1, **a**2, α1, and α2. Each of the three mating types exhibits unique behaviors and gene expression patterns, and these are ultimately explained by the differences in gene composition at *MAT*. **a**1, α1, and α2 all encode transcription factors that act as master regulators for cell type-specific gene expression. α1 seems to have lost its function during evolution. Important for the regulation of diploid cell behavior, including the ability to enter meiosis, is that in diploid cells, **a**1 and α2 unite to form a heterodimer that acts as a diploid-specific transcriptional repressor. All diploid-specific gene expression patterns are directly or indirectly reliant on transcriptional repression by **a**1/α2.

A key target of the **a**1/α2 repressor is a gene called *RME1* ("*Repressor of MEiosis* 1") (Covitz et al., 1991; Mitchell and Herskowitz, 1986). In haploid cells, where **a**1/α2 is absent, *RME1* is constitutively expressed (Covitz et al., 1991; Mitchell and

Herskowitz, 1986). Rme1 inhibits a second gene called *IME1* ("*Inducer of MEiosis* 1") (Kassir et al., 1988). As the name suggests, it is expression of *IME1* that controls entry into meiosis (Kassir et al., 1988). Rme1, though a repressor by the regulatory logic of its genetic pathway (Figure 1.1), is biochemically a transcriptional activator (van Werven et al., 2012). Rme1 induces the transcription of a noncoding RNA that overlaps the *IME1* promoter and prevents the transcription of *IME1* mRNA (van Werven et al., 2012). A similar noncoding RNA-dependent gene repression mechanism occurs at the *IME4* locus, where a haploid-specific antisense RNA is repressed in diploid cells by the **a**1/α2 repressor to potentiate meiotic entry (Hongay et al., 2006). As haploid cells lacking Rme1 (Mitchell and Herskowitz, 1986) or the *IME1* noncoding RNA (van Werven et al., 2012) are each capable of entering meiosis, this regulatory pathway is the critical determinant of mating type regulation of entry into meiosis. That haploid cells never enter meiosis demonstrates the effectiveness of this noncoding RNA-based gene repression system.

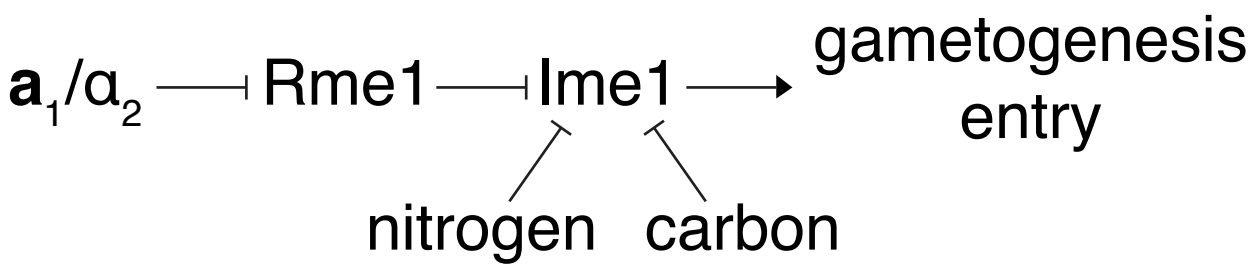

Figure 1.1. Regulation of the entry into gametogenesis. Entry into gametogenesis is governed by the activation of the transcription factor, Ime1. Ime1 is repressed by nutrient cues, including the availability of nitrogen and glucose. The restriction of meiosis to diploid cells acts through the Ime1 repressor Rme1, which is switched off in diploid cells by the **a**1/α2 repressor.

Like in animals, cell type (for yeast, *MAT***a**/α diploid) is not sufficient to promote meiotic entry. Additional environmental cues are required. While in animals developmental signaling pathways from somatic cells promote germ cell differentiation (Fuller and Spradling, 2007), yeast rely on nutritional cues from their environment. *MAT***a**/α cells undergo vegetative (mitotic) growth indefinitely, as long as ample nutrients are available. Entry into gametogenesis only occurs under a specific regime of nutrient deprivation (Figure 1.1), namely in the presence of solely a non-fermentable carbon source (usually acetate) and in the absence of nitrogen (van Werven and Amon, 2011). Glucose, the preferred energy source of yeast, strongly represses meiotic entry (van Werven and Amon, 2011). Like mating

type regulation of meiotic entry, nutritional regulators of meiotic entry act through *IME1* (van Werven and Amon, 2011), though the details are not as well understood and likely involve both transcriptional and post-transcriptional control.

Ime1 promotes entry into meiosis by inducing the transcription of many early meiotic genes (Chu et al., 1998; Neiman, 2011; van Werven and Amon, 2011). One of its key target genes encodes a meiosis-specific kinase called Ime2, which promotes premeiotic DNA replication (Dirick et al., 1998; Smith and Mitchell, 1989; Smith et al., 1990). Ime2 is further described in Section 1.3.3. Ime1 also sets meiotic prophase in motion by inducing the transcription of gene products devoted to the specialized chromosome behaviors that characterize meiotic prophase. Among its targets (Brar et al., 2012; Chu et al., 1998) are *SPO11* (Smith et al., 1990), which encodes the endonuclease responsible for inducing double-strand DNA breaks required for meiotic chromosome pairing (Keeney et al., 1997); subunits of the synaptonemal complex, a structure present on paired homologous chromosomes; and proteins that facilitate the two-step chromosome segregation pattern in meiosis, such as the meiosis-specific cohesin subunit Rec8.

As meiotic prophase leads to profound alterations to the genome, it would seem that entry into meiosis should be an irreversible commitment. Remarkably, this is not the case. Sporulating yeast cultures shifted to rich media abort meiosis and "return to growth." By varying the time of media shift, it was found that cells commit to gametogenesis not at meiotic entry but near the end of meiotic prophase (Dayani et al., 2011; Esposito and Esposito, 1974; Simchen et al., 1972). The stage of commitment to meiosis, termed pachytene, is exactly the same point at which cells with unrepaired DNA breaks arrest (Roeder and Bailis, 2000). The common control point between return to growth and meiotic DNA damage sensing is no coincidence. Both are due to the activity of the second major transcriptional activator in the gametogenesis program: Ndt80 (Hepworth et al., 1998; Prugar et al., 2017; Tung et al., 2000; Wang et al., 2011; Xu et al., 1995).

Like in other cellular differentiation programs, a key feature of meiosis is a transcriptional cascade (Chu et al., 1998; Chu and Herskowitz, 1998; Primig et al., 2000). Ndt80 is the second major transcriptional activator in gametogenesis, and its transcription is induced by the first, Ime1 (Chu and Herskowitz, 1998; Xu et al., 1995). The precise wiring of a transcription factor network can give rise to emergent properties of the system, such as irreversible commitment. This property is evident in meiosis precisely because of the mechanisms by which Ndt80 is regulated.

Ime1 is required for Ndt80 transcription (Chu and Herskowitz, 1998). Even so, the expression of Ndt80 target genes is substantially delayed until later in meiosis (Brar et al., 2012; Cheng et al., 2018; Chu et al., 1998; Chu and Herskowitz, 1998). Among the transcriptional targets of Ndt80 are the polo-like kinase Cdc5 and M-phase cyclin genes (Benjamin et al., 2003; Berchowitz et al., 2013; Chu et al., 1998;

Chu and Herskowitz, 1998; Hepworth et al., 1998; Sourirajan and Lichten, 2008). Their immediate expression would pose a problem to meiosis, because they would promote exit from prophase and entry into the meiotic divisions prior to completion of DNA replication and the characteristic chromosome behaviors of meiotic prophase. Clearly, a delay in Ndt80 *activity* is required. This delay is accomplished by at least two mechanisms. First, Ime1-dependent transcription of *NDT80* is delayed relative to other Ime1 targets (Winter, 2012). This delay is proposed to occur due to the binding of a transcriptional repressor, Sum1 (Winter, 2012). Second, the small amount of Ndt80 protein produced in meiotic prophase is inactivated by posttranslational modification (Hepworth et al., 1998; Roeder and Bailis, 2000; Sopko et al., 2002; Tung et al., 2000; Wang et al., 2011). The target of the DNA damage-sensing pachytene checkpoint is Ndt80 itself, which is phosphorylated by the checkpoint kinase Mek1 to inhibit its nuclear localization (Chen et al., 2018b; Wang et al., 2011). Restricting the activity of Ndt80 by checkpoint signaling thus assures that progression to meiotic chromosome segregation is delayed until genome integrity is restored.

Once the pachytene checkpoint is satisfied, Ndt80 can enter the nucleus and induce the transcription of its target genes. A key feature of Ndt80's regulation is binding its own promoter, creating a positive feedback loop (Winter, 2012). The positive feedback loop in the *NDT80* promoter is directly responsible for the irreversible commitment to meiosis that occurs upon exit from pachytene (Tsuchiya et al., 2014). The transcriptional output resulting from Ndt80 positive feedback is extraordinary. At its peak level of expression, *NDT80* is more highly transcribed than 97% of the yeast genome in a published mRNA-seq dataset (Brar et al., 2012). Induction of *NDT80* transcription in far excess of the required level has been proposed to reinforce the robustness of the commitment to gametogenesis (Winter, 2012). In addition to promoting its own transcription, Ndt80 is thought to activate over 100 (Chu et al., 1998) or perhaps nearly 400 (Cheng et al., 2018) target genes. Among them are cell cycle genes, such as the M-phase cyclins as well as genes required for gamete differentiation (Cheng et al., 2018; Chu et al., 1998; Chu and Herskowitz, 1998). A smaller number of genes are transcribed late in meiosis (Brar et al., 2012; Cheng et al., 2018; Chu et al., 1998; Primig et al., 2000), but the regulators responsible have yet to be identified.

From decades of study in yeast, a compelling model of the gene regulatory logic within gametogenesis has emerged (Figure 1.2). Cell type and environmental cues induce the expression of Ime1, which governs entry into meiosis and meiotic prophase. Once prophase is complete and chromosome architecture is amenable to cell division, and if environmental conditions are unchanged, runaway positive feedback of Ndt80 expression leads to irreversible commitment to the completion of gametogenesis. How does transcription of Ndt80 targets drive meiosis forward? A key target appears to be the polo-like kinase Cdc5, which is sufficient to induce exit from pachytene (Sourirajan and Lichten, 2008). Chromosome segregation in meiosis

I and meiosis II requires M-phase cyclins, which are transcriptional targets of Ndt80 (Benjamin et al., 2003; Berchowitz et al., 2013; Cheng et al., 2018; Chu et al., 1998; Chu and Herskowitz, 1998; Hepworth et al., 1998). By inducing key cell cycle factors through meiosis-specific control mechanisms, Ndt80 acts as the master regulator of the meiotic divisions. How the core cell cycle machinery is adapted to suit the unique needs of meiosis is further described in the following section.

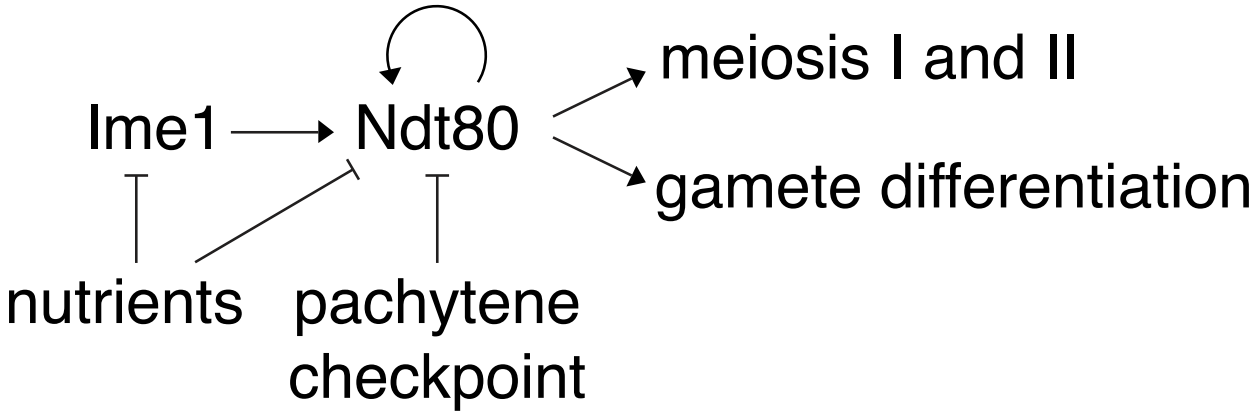

Figure 1.2. Regulation of Ndt80 and commitment to gametogenesis. Ime1 induces the transcription of Ndt80, itself a transcriptional activator. As for Ime1, nutrients inhibit the activity of Ndt80. Ndt80 activity is also restricted by the pachytene checkpoint, which monitors the completion of DNA repair in prophase I. In the absence of nutrients, and upon satisfaction of the pachytene checkpoint, Ndt80 becomes highly transcribed due to a positive feedback loop. High levels of Ndt80 promote entry into the meiotic divisions and induce the gamete differentiation program.

1.3.3 Meiosis-specific cell cycle regulation

The mitotic cell cycle is extensively regulated. Entry into and passage through the cell cycle are controlled by transcriptional as well as posttranslational regulation of cell cycle factors. Ensuring orderly progression through the cell cycle is critical to maintaining the integrity of the genome. Although the order of events in meiosis is somewhat different, meiotic cells use regulators and principles common between mitosis and meiosis, but with variations (Marston and Amon, 2004).

As described in the previous section, entry into the meiotic "cell cycle" (linear rather than cyclical) is controlled by Ime1. Entry into premeiotic S phase is regulated by the kinase Ime2, whose production is controlled by Ime1 (Dirick et al., 1998). Ime2

is highly similar to the cyclin-dependent kinases (CDKs), which are master regulators of cell cycle progression across eukaryotes. During both mitosis and meiosis, CDKs and their cyclin subunits play critical roles in controlling the cell cycle. Unlike typical CDKs, Ime2 kinase activity does not require a cyclin (Benjamin et al., 2003; Berchowitz et al., 2013). Ime2 phosphorylates and induces proteolysis of the CDK inhibitor Sic1, a role performed by the G1 cyclin-CDK complexes in mitosis (Dirick et al., 1998). Removal of Sic1 allows entry into premeiotic S-phase driven by CDK in complex with S-phase cyclins (Dirick et al., 1998). Its role in setting the meiotic cell cycle in motion makes Ime2 a critical target of Ime1.

After the genome is replicated and cells have satisfied the pachytene checkpoint, Ndt80 is induced. Ndt80 activates the transcription of the M-phase cyclin mRNAs *CLB1*, *CLB3*, and *CLB4* that in turn promote the meiotic divisions (Benjamin et al., 2003; Berchowitz et al., 2013; Carlile and Amon, 2008; Chu et al., 1998; Chu and Herskowitz, 1998). The coupling of M-phase cyclin transcription to pachytene exit by Ndt80 is critical, as premature cyclin transcription leads to meiotic errors (Carlile and Amon, 2008; Miller et al., 2012).

Cyclin expression is regulated not only at the transcriptional level but also at the translational level. *CLB1* and *CLB4* mRNAs are immediately translated to promote meiosis I, but *CLB3* mRNA is translationally repressed until the onset of meiosis II (Berchowitz et al., 2013; Carlile and Amon, 2008). Translational repression of *CLB3* mRNA, as well as a subset of other Ndt80 target mRNAs, is conferred by the RNA-binding protein Rim4 (Berchowitz et al., 2013; Berchowitz et al., 2015; Carpenter et al., 2018). At the meiosis I-meiosis II transition, Rim4 is degraded, and its repressed transcripts are accessible to the translation machinery (Berchowitz et al., 2013; Berchowitz et al., 2015; Carpenter et al., 2018). Remarkably, the regulator of Rim4 proteolysis is Ime2 (Berchowitz et al., 2013; Carpenter et al., 2018), providing at least one explanation for the dramatic increase in Ime2 kinase activity that occurs during the meiotic divisions (Benjamin et al., 2003; Berchowitz et al., 2013).

That Ime2 acts not only during premeiotic S phase but also during the meiotic divisions bears a striking resemblance to cell cycle regulation by CDK. CDK is present throughout the cell cycle, but its activity and substrate specificity are dynamically regulated by the cyclin binding partner associated at a given time (Loog and Morgan, 2005). Ime2 is present at all stages of meiosis, but its activity is much higher during premeiotic S-phase and meiosis II than at another other times during meiosis (Benjamin et al., 2003; Berchowitz et al., 2013). How posttranslational regulation of Ime2 directs its stage-specific functions is a fascinating open question.

During mitosis, DNA replication and chromosome segregation (cell division) must occur in a precise, strictly alternating order—one after the other. Extensive regulatory mechanisms ensure that this sequence is not disrupted. One of the most

remarkable aspects of meiosis is its violation of this highly regulated order of events. In meiosis, DNA replication occurs once, and chromosome segregation occurs twice in succession. How does this unique sequence of events occur specifically in meiotic cells?

At the level of cell cycle regulation, meiotic cells perform two M phases with no intervening S phase. In mitosis, the strict alternation between genome duplication and reduction is regulated by cyclin-CDK. In budding yeast, the sole CDK that regulates the cell cycle is Cdc28. High cyclin-Cdc28 activity prevents the assembly of prereplicative complexes at origins of replication (Diffley, 2004). When cells exit mitosis, cyclins are destroyed by proteolysis, and Cdc28 activity is lowered to a level permissive of prereplicative complex loading (Diffley, 2004). Origins of replication are poised but inactive until the next S phase, when they "fire" under control of high cyclin-Cdc28 activity (Diffley, 2004). A plausible model is that meiotic cells prevent rereplication by maintaining an intermediate level of Cdc28 substrate phosphorylation between the meiotic divisions that is permissive for some "resetting" events, such as meiosis I spindle disassembly and centrosome duplication, but not DNA replication (Holt et al., 2007; Marston and Amon, 2004; Marston et al., 2003; Phizicky et al., 2018). Studies suggest dual involvement of Cdc28 and Ime2, which share overlapping substrates (Holt et al., 2007; Phizicky et al., 2018). Key roles may also be played by signaling pathways that antagonize Cdc28 by activating the phosphatase Cdc14 (Holt et al., 2007; Marston and Amon, 2004; Marston et al., 2003).

After meiosis II, cells must fully exit from meiosis and return to G1 so that, upon the return of a nutrient-replete environment, they can re-enter the mitotic cell cycle. In mitosis, cell cycle exit involves inhibiting CDK and reversing the phosphorylation state of its substrates. Mitotic exit is achieved through multiple mechanisms acting in parallel (Sullivan and Morgan, 2007; Weiss, 2012). First, proteolysis of cyclins eliminates ongoing CDK activity. Cyclin proteolysis is controlled by the anaphase-promoting complex (APC), a large protein complex with E3 ubiquitin ligase activity. The APC requires an activator for substrate recognition and catalytic activity, which in mitosis is Cdc20 or Cdh1. In addition to the APC, the phosphatase Cdc14 promotes mitotic exit by reversing the phosphorylation of cyclin-Cdc28 substrates (Jaspersen et al., 1998; Taylor et al., 1997; Visintin et al., 1998). Cdc14 is normally sequestered in the nucleolus in an inactive state, but two signaling pathways called the mitotic exit network (Shou et al., 1999; Visintin et al., 1999) and the Cdc14 early anaphase release network (Stegmeier et al., 2002; Yoshida et al., 2002) promote its release and ability to dephosphorylate its substrates.

The APC and Cdc14 both play roles in coordinating cell cycle exit during meiosis. Like in mitosis, the APC in complex with Cdc20 is required for anaphase and promotes cyclin proteolysis (Marston and Amon, 2004). However, an additional,

meiosis-specific APC activator is present in meiotic cells. This activator, Ama1, is required for gamete formation and may also promote exit from meiosis, though it has earlier functions in meiosis as well (Arguello-Miranda et al., 2017; Diamond et al., 2009; Eisenberg et al., 2018; Okaz et al., 2012). In the absence of Ama1, Ndt80 remains persistently abundant, perhaps suggesting that APC^{Ama1} terminates the Ndt80 transcriptional program by promoting Ndt80 proteolysis (Arguello-Miranda et al., 2017; Eisenberg et al., 2018; Okaz et al., 2012). Like in mitosis, reversal of CDK phosphorylation also occurs at the end of meiosis. Cdc14 is released into the nucleus and cytosol after the meiotic divisions (Attner and Amon, 2012; Marston and Amon, 2004; Marston et al., 2003). The signaling pathway responsible for Cdc14 release in mitosis, the mitotic exit network, is required in meiosis for spindle disassembly as well as spore formation (Attner and Amon, 2012).

The meiotic cell cycle relies on modules shared with mitosis but uses specialized controls. The end result is four faithfully segregated haploid genomes. These genomes are housed in highly specialized cells: the gametes. Production of gametes involves extensive meiosis-specific regulation that extends beyond segregation of the chromosomes.

1.3.4 Cellular remodeling in meiosis

Successful gametogenesis requires not only proper chromosome segregation in meiosis but also differentiation into the gamete cell type. In budding yeast, the differentiated gametes are environmentally resilient spores. Gametes are generated by an unconventional mode of cell division: the daughter cells are assembled *de novo* within the progenitor cell. This unique geometry of cell division requires specialized mechanisms to promote cytokinesis and organelle segregation that appear to be quite different from the mechanisms used in mitosis.

In gametogenesis, the polarized cell division used in mitosis (budding) is replaced with internal partitioning of the cell (Figure 1.3). Cell division by budding uses cell polarization to promote growth of the bud plasma membrane and fortification of the bud compartment with actively transported organelles. When cell division occurs, the bud has nearly grown to the size of the mother cell and contains a full complement of organelles, including the divided nucleus. In gametogenesis, no cell polarity is known to occur. Importantly, mother-daughter cell polarity like in budding is not compatible with the geometry of meiotic cell division. Instead, gametogenesis involves unique cellular remodeling events that transform a single cell into four gametes.

Meiosis II represents the final round of chromosome segregation during meiosis, but it is also the time during which gamete formation begins. Prior to this point, chromosome segregation occurs without cytokinesis. At the meiosis I-meiosis II transition, the two centrosomes (embedded in the nuclear envelope in yeast and

known as spindle pole bodies) duplicate and gain a meiosis-specific composition of subunits on their cytoplasmic face (Bajgier et al., 2001; Knop and Strasser, 2000; Neiman, 2005). These accessory subunits assemble into a structure called the meiotic outer plaque. The meiotic outer plaque cannot nucleate cytoplasmic microtubules due to its lack of γ tubulin. Instead, the meiotic outer plaque is a membrane generation center (Bajgier et al., 2001; Knop and Strasser, 2000; Neiman, 1998; Neiman, 2005).

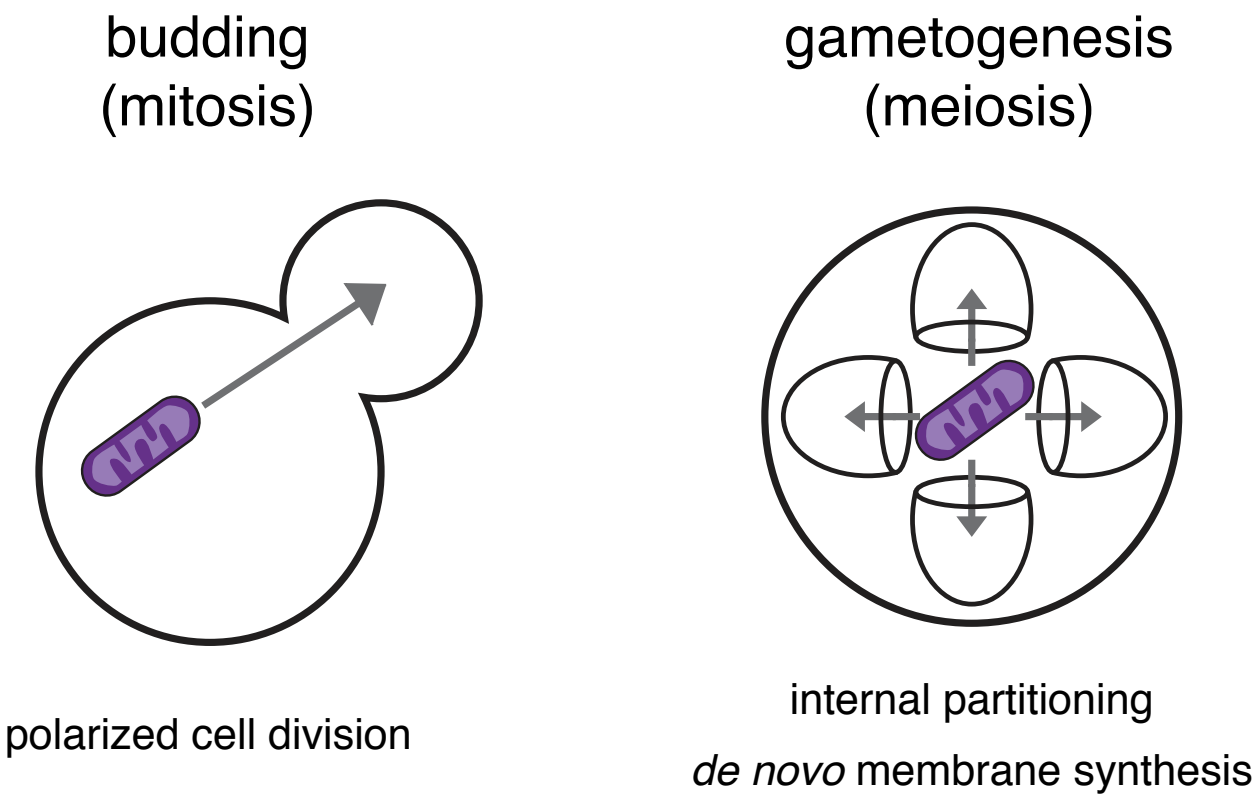

Figure 1.3. Organelle segregation in budding and gametogenesis. In budding (mitotic growth), organelles (e.g. mitochondria) are segregated by transport along the polarized mother-daughter axis into the bud. In gametogenesis (meiotic differentiation), organelles must be simultaneously segregated to four developing gametes, which are enveloped by *de novo* synthesized membranes.

Gamete plasma membranes, called prospore membranes, are nucleated at the meiotic outer plaque and grow by fusion of Golgi-derived vesicles (Neiman, 1998; Neiman, 2005). In essence, daughter cells are formed by redirecting secretion from the plasma membrane to internal prospore membranes. Rerouting of vesicles to the

prospore membrane involves a rewiring of the secretory pathway (Neiman, 1998; Neiman, 2005). A meiosis-specific t-SNARE, called Spo20, localizes to nascent prospore membrane and promotes expansion of the membrane by vesicle fusion (Nakanishi et al., 2004; Neiman, 1998; Neiman, 2005; Neiman, 2011). Anchored at the nucleus-embedded spindle pole body on one end, prospore membranes expand around the nuclear surface and capture organelles and cytoplasm. The lip of the growing prospore membrane is defined by a protein complex called the leading edge complex, which assembles into a ring through which segregated material must pass (Knop and Strasser, 2000; Moreno-Borchart et al., 2001; Suda et al., 2007). After the prospore membrane has grown, the leading edge complex is removed, and the membranes close—a form of cytokinesis (Diamond et al., 2009; Neiman, 2005; Neiman, 2011). Four distinct gamete cells now exist within the progenitor cell.

Formation of viable gametes requires the successful inheritance of organelles. Organelle segregation must occur during the window in meiosis II during which prospore membranes are open. In mitosis, vectoral transport of organelles along actin filaments facilitates the inheritance of many organelles, including the vacuole and mitochondria (Knoblach and Rachubinski, 2015). In gametogenesis, the mechanisms of organelle inheritance are essentially unknown. Studies examining organelle localization have found dramatic differences in meiosis II organelle localization compared to other stages of the yeast life cycle (Gorsich and Shaw, 2004; Miyakawa et al., 1984; Stevens, 1981; Suda et al., 2007). However, the regulation and functional importance of these differences in organelle localization have not been defined.

The work presented in this thesis demonstrates that organelle localization is regulated by the gametogenesis program. Our findings support a model in which segregation of mitochondria requires their detachment from the mother cell plasma membrane—a discarded structure—in favor of their attachment to the nuclear envelope. The nuclear envelope is an inherited structure but critically also the site of prospore membrane synthesis, ensuring mitochondrial segregation during the specialized cell division in gametogenesis.

Chapter 2

Developmentally regulated destruction of the mitochondria-plasma membrane tether in meiosis II

The following chapter contains material derived from a publication on which I am the first author (Sawyer et al., 2019).

2.1 Introduction

Mitochondria are essential organelles that host an array of cellular processes, ranging from ATP production to iron-sulfur cluster assembly. In many cell types, mitochondria are organized into a network of interconnected tubules that is dynamically remodeled by fusion and fission (Friedman and Nunnari, 2014). In addition, the position and motility of mitochondria are regulated to allow proper distribution within the cell and inheritance during cell division (Mishra and Chan, 2014; Westermann, 2014). Although the list of factors that modulate mitochondrial architecture and dynamics continues to expand, relatively little is known about their developmental regulation.

Fusion, fission, anchoring, and transport collectively shape the mitochondrial network. All of these processes are broadly conserved in eukaryotes but have been most extensively characterized in *Saccharomyces cerevisiae*. The budding yeast mitochondrial network exists as a branched structure that is dynamically remodeled by fusion and fission, while maintaining associations with the plasma membrane (Hoffmann and Avers, 1973; Nunnari et al., 1997). Plasma membrane anchoring requires a protein complex called MECA, for mitochondria-ER-cortex anchor (Cerveny et al., 2007; Klecker et al., 2013; Lackner et al., 2013; Ping et al., 2016). MECA belongs to a growing list of protein complexes collectively known as tethers, which establish membrane contact sites between disparate organelles (Elbaz-Alon et al., 2015; Elbaz-Alon et al., 2014; Kornmann et al., 2009; Murley and Nunnari, 2016; Murley et al., 2015). By physically bridging organelles, tethers enable interorganelle communication and establish spatial cellular organization (Eisenberg-Bord et al., 2016; Murley and Nunnari, 2016). Studies in multiple organisms have demonstrated the physiological importance of organelle tethers in controlling metabolism, intracellular signaling, pathogen defense, and organelle inheritance (Eisenberg-Bord et al., 2016; Helle et al., 2013; Prinz, 2014; Schrader et al., 2015). Furthermore, it has been shown that organelle tethers can be dynamically regulated in response to changes in the cellular milieu, including

metabolites and ions (Honscher et al., 2014; Kumagai et al., 2014; Nhek et al., 2010). However, whether and how these structures are subject to developmental regulation to meet the demands of differentiation into new cell types is not clear.

A key cellular differentiation program in budding yeast is gametogenesis, which includes segregation of chromosomes by meiosis and the production of specialized gamete cells called spores. Various organelles, including mitochondria, undergo extensive remodeling during this process (Fuchs and Loidl, 2004; Gorsich and Shaw, 2004; Miyakawa et al., 1984; Neiman, 1998; Stevens, 1981; Suda et al., 2007; Tsai et al., 2014). Mitochondrial distribution changes dramatically during the meiotic divisions, when mitochondria lose their plasma membrane association, instead localizing near the gamete nuclei (Gorsich and Shaw, 2004; Miyakawa et al., 1984; Stevens, 1981). Subsequently, ~50% of the mitochondria from the progenitor cell is inherited by the gametes (Brewer and Fangman, 1980), and the remaining pool is eliminated (Eastwood et al., 2012; Eastwood and Meneghini, 2015). Although little is understood about the mechanisms responsible for mitochondrial reorganization and inheritance during meiosis, many other aspects of this developmental program, including transcriptional and cell cycle control, have been worked out in great detail in this organism (Marston and Amon, 2004; Neiman, 2011; van Werven and Amon, 2011; Winter, 2012). To what extent the previously identified meiotic regulators control mitochondrial dynamics and segregation has been unexplored.

Here, we elucidated how mitochondrial reorganization is coordinated with meiotic development. We observed that mitochondria abruptly detach from the plasma membrane at the onset of anaphase II. To identify the mechanism responsible for regulating mitochondrial detachment, we examined a series of meiotic mutants with defects in meiotic progression. To our surprise, central meiotic regulators, such as the cyclin-dependent kinase CDK1/Cdc28 and the anaphase-promoting complex, were entirely dispensable for mitochondrial detachment. Instead, we found that the transcription factor Ndt80 and the meiosis-specific kinase Ime2 dictate the timing of mitochondrial detachment. Ndt80 controls mitochondrial detachment by inducing the expression of Ime2 and promoting its kinase activity (this study; (Benjamin et al., 2003; Berchowitz et al., 2013). Ime2 phosphorylates both subunits of the MECA complex *in vitro*. Furthermore, Num1 undergoes Ime2-dependent phosphorylation *in vivo*. Finally, we show that Ime2 promotes MECA proteolysis, and this timely destruction of MECA drives mitochondrial detachment. Our results indicate that organelle tethering can be developmentally regulated to facilitate organelle remodeling, a feature of many cellular differentiation programs.

2.2 Results

2.2.1 Mitochondria detach from the plasma membrane in meiosis

To characterize the morphology and dynamic behavior of mitochondria during meiotic differentiation, we monitored cells that simultaneously expressed fluorescent markers of mitochondria (Cit1-GFP) and the nucleus (Htb1-mCherry) using time-lapse microscopy. Prior to the nuclear divisions, the mitochondrial network retained its characteristic morphology, existing as an interconnected tubular structure anchored to the cell cortex. Consistent with previous reports (Gorsich and Shaw, 2004; Miyakawa et al., 1984; Stevens, 1981), we found that mitochondria dissociated from the cell cortex during meiosis II (Figure 2.1A). We term this phenomenon "mitochondrial detachment." Our data indicate that mitochondrial detachment occurs coincident with anaphase II. At the time of mitochondrial detachment, 68% of cells had begun anaphase II (Figure 2.1A). By 10 min after mitochondrial detachment, 90% of cells had initiated anaphase II.

In order to further determine the timing of mitochondrial detachment, we used two additional staging markers. The first marker, GFP-Spo20$^{51-91}$, is an indicator of plasma membrane biogenesis that takes place as part of gamete maturation (Nakanishi et al., 2004; Neiman, 2011). Concomitant with the meiosis I to meiosis II transition, this process, termed prospore membrane formation, begins with fusion of vesicles at the yeast centrosomes, known as spindle pole bodies. As judged by changes in GFP-Spo20$^{51-91}$ localization, mitochondrial detachment occurred after membrane nucleation but prior to the closure of the newly formed plasma membranes (Figure 2.1B).

The second marker, Spc42-GFP, is a component of the spindle pole body. The distance between the duplicated spindle pole bodies is a reliable metric to determine the timing of metaphase to anaphase transition, since the spindle length increases approximately two-fold during this period (Kahana et al., 1995; Palmer et al., 1989; Yeh et al., 1995). We measured when mitochondrial detachment took place with respect to changes in spindle length in cells carrying Spc42-GFP and Cit1-mCardinal. This analysis revealed that mitochondrial detachment occurred at the beginning of anaphase II (Figure 2.1C). Hence, the timing of mitochondrial detachment is precise and occurs with stereotyped timing relative to other well-defined meiotic events.

2.2.2 Many canonical cell cycle regulators are dispensable for mitochondrial detachment

Because mitochondrial detachment occurred simultaneously with anaphase II onset, we reasoned that cell cycle regulators with characterized meiotic functions might jointly control the meiotic divisions and mitochondrial detachment. Since the initial steps of spore formation occur during meiosis II, active coupling of chromosome and organelle segregation could ensure gamete fitness. We monitored mitochondrial detachment and meiotic progression in strains carrying deletion or conditional alleles of genes encoding key cell cycle regulators (Figure 2.2A). We also

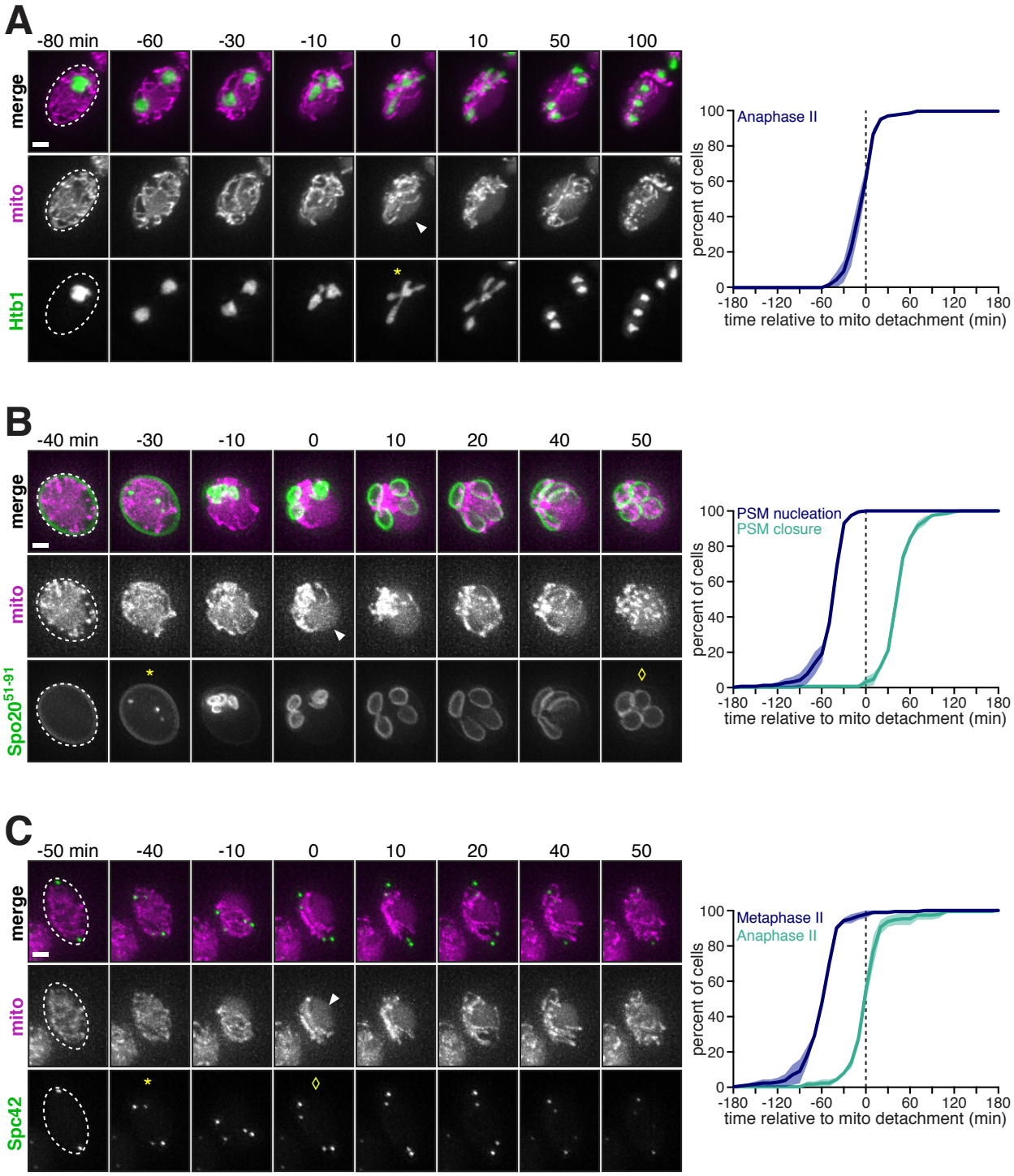

Figure 2.1. Mitochondria detach from the cell cortex during meiosis II. Movie montages and quantifications of cells expressing Cit1-GFP or Cit1-mCardinal to label mitochondria (mito) as well as a meiotic staging marker, imaged every 10 min. Mitochondrial detachment is defined as the abrupt coalescence of mitochondria,

showing restricted rather than uniform localization around the cell cortex, and indicated with an arrowhead. Cell boundaries are indicated with dashed lines. To determine the relative staging compared to other markers (below), mitochondrial detachment is defined to occur at 0 min. Plots show the mean ± range (shaded region) of two independent experiments, with $n \geq 90$ cells counted per experiment per marker. **A.** Mitochondrial detachment relative to the onset of the meiosis II nuclear division (anaphase II), marked by Htb1-mCherry (UB10257). Anaphase II is defined as the first appearance of a four-lobed nuclear morphology (*). **B.** Mitochondrial detachment relative to prospore membrane nucleation and closure, marked by GFP-Spo20$^{51-91}$ prospore membrane marker (UB13131). Prospore membrane nucleation is defined as the first appearance of Spo20$^{51-91}$ puncta (*) and closure as the rounding up of fully elongated prospore membranes (◊). **C.** Mitochondrial detachment relative to metaphase II and anaphase II, marked by Spc42-GFP (UB13129). Metaphase II is defined as the first appearance of two pairs of separated Spc42-GFP dots (*). Anaphase II is defined as the first appearance of concerted movement separating the sister spindle pole bodies in each pair (◊). Scale bars, 2 μm.

---

noted that prior to meiotic entry, all of the mutants examined showed mitochondrial morphology indistinguishable from wild type, indicating that these alleles did not constitutively alter mitochondrial organization (Figure 2.2, B-H). 8 hours after induction of meiosis, the vast majority of wild-type cells contained four distinct nuclei that had not yet assembled into spores. In these cells, mitochondria invariably detached from the cortex and instead localized near the four post-meiotic nuclei (Figure 2.2B).

Among the cell cycle regulators that we analyzed, the polo kinase Cdc5, the anaphase-promoting complex (APC) activator Cdc20, and the cyclin-dependent kinase Cdc28/Cdk1 are all essential for cell viability. To avoid perturbing the mitotic functions of these genes, we depleted *CDC5* and *CDC20* only from meiotic cells by replacing their promoters with the mitosis-specific *CLB2* promoter (Lee and Amon, 2003). To downregulate *CDC28* we utilized a chemical inhibitor sensitive allele, *cdc28-as1* (Bishop et al., 2000). It has been previously reported that each mutant perturbs meiotic chromosome segregation: *cdc5* and *cdc20* mutants are defective in exiting metaphase I (Lee and Amon, 2003), while inactivation of *cdc28-as1* in prophase I with 1-NM-PP1 inhibits meiosis I spindle assembly entirely (Benjamin et al., 2003). In each condition, the expected nuclear division defect was observed. However, mitochondrial detachment was unaffected. Mitochondria not only detached from the plasma membrane but also adopted their perinuclear localization, similar to wild-type cells (Figure 2.2, C-E).

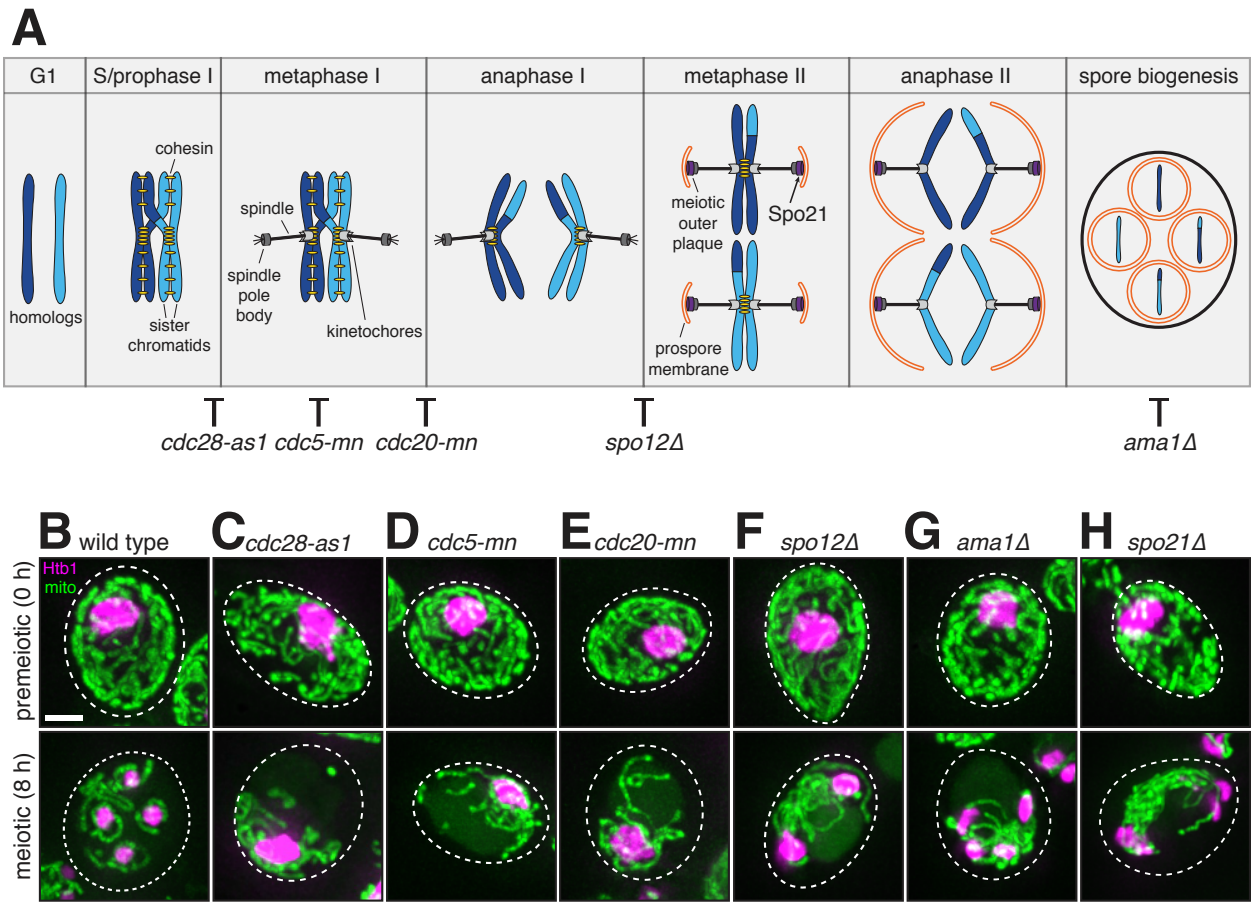

Figure 2.2. Mitochondrial detachment is uncoupled from the meiotic divisions and spore development. A. Schematic of meiotic chromosome segregation and spore development. Meiotic regulators and spore development genes are labeled at key stages for their functions, where disruption of their function perturbs meiotic progression. **B-H.** Maximum intensity projections of fixed wild-type and mutant cells at 0 h in SPO (top) and 8 h in SPO (bottom). Mitochondria (mito), mitoGFP or Cit1-GFP. Nuclei, Htb1-mCherry. Cell boundaries are indicated with dashed lines. **B.** wild type (UB7155) **C.** *cdc28-as1* synchronized by *pGAL-NDT80 GAL4.ER* (UB9494), with 1 μM 1-NM-PP1 and 1 μM ß-estradiol added simultaneously at 5 h **D.** *cdc5-mn*, which is *pCLB2-CDC5* (UB7278) **E.** *cdc20-mn*, which is *pCLB2-CDC20* (UB7343) **F.** *spo12Δ* (UB7345) **G.** *ama1Δ* (UB7533) **H.** *spo21Δ* synchronized by *pGAL-NDT80 GAL4.ER* (UB9239). Scale bar, 2 μm.

In addition to testing essential cell cycle regulators, we also assessed the role of non-essential regulators with defined meiotic functions. The Cdc14 Early Anaphase Release (FEAR) network controls the release of the Cdc28 antagonist phosphatase

Cdc14 (Stegmeier et al., 2002; Yoshida et al., 2002). FEAR network signaling is absent in *spo12Δ* cells, which results in aberrant meiosis I spindle disassembly, culminating in the formation of binucleate post-meiotic cells instead of tetranucleate (Kamieniecki et al., 2005; Klapholz and Esposito, 1980; Marston et al., 2003). In *spo12Δ* cells, mitochondrial detachment was normal (Figure 2.2F). Mitochondrial detachment was also unaffected in *ama1Δ* cells (Figure 2.2G), which lack a meiosis-specific APC activator required for spore biogenesis (Cooper et al., 2000; Diamond et al., 2009).

Finally, we sought to address the possibility that prospore membrane formation is required for mitochondrial detachment, such as through sequestration of mitochondria into spores, since close proximity between mitochondria and prospore membrane has been previously observed (Suda et al., 2007). Synthesis of the prospore membrane requires assembly of a meiosis-specific structure on the cytoplasmic face of the spindle pole body, called the meiotic outer plaque (Knop and Strasser, 2000). In the absence of Spo21 (also known as Mpc70), a meiotic outer plaque component, other subunits fail to localize to the meiotic outer plaque, and therefore prospore membrane formation is completely disrupted (Knop and Strasser, 2000). We found that in *spo21Δ* cells, mitochondrial detachment was entirely unimpeded (Figure 2.2H). From these analyses, we conclude that much of the regulatory scheme that defines meiotic chromosome segregation and cellular differentiation are dispensable for mitochondrial detachment and that other factors must be involved in regulating when and how mitochondria dissociate from the cell cortex.

2.2.3 The meiosis-specific transcription factor Ndt80 is required for mitochondrial detachment

We noted that in wild-type cells, mitochondrial morphology was indistinguishable at meiotic entry and prophase I, with mitochondrial detachment occurring abruptly during the second meiotic division. The master regulator controlling the transition to the meiotic divisions is the transcription factor Ndt80 (Chu and Herskowitz, 1998; Xu et al., 1995). Transcription of *NDT80* mRNA occurs during prophase I, but the ability of Ndt80 protein to localize to the nucleus is restricted by the pachytene checkpoint, which monitors the completion of double-strand break repair requisite for successful chromosome segregation (Chu and Herskowitz, 1998; Hepworth et al., 1998; Tung et al., 2000; Wang et al., 2011). In the absence of *NDT80*, cells exhibit a prolonged arrest during the pachytene stage of prophase I, failing to undergo meiotic divisions and subsequent gamete maturation (Xu et al., 1995).

To determine whether *NDT80* is required for mitochondrial detachment, we examined mitochondrial morphology in a *pGAL-NDT80* strain (Benjamin et al., 2003; Carlile and Amon, 2008). The *pGAL-NDT80* allele allows controlled induction of *NDT80* transcription by a ß-estradiol activatable Gal4 fusion to the estrogen

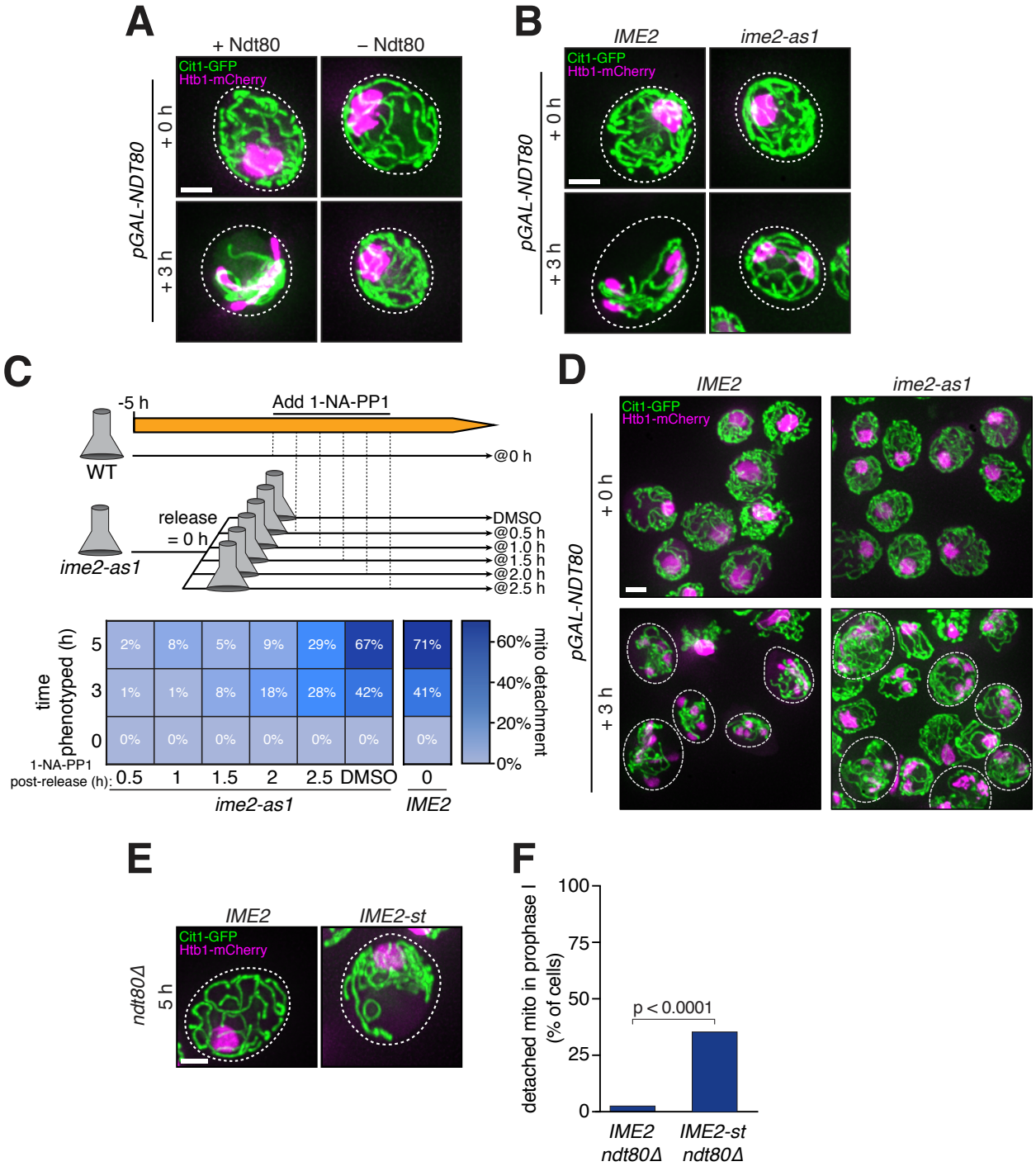

Figure 2.3. Ndt80 and Ime2 regulate mitochondrial detachment. A. Maximum intensity projections of fixed *pGAL-NDT80 GAL4.ER* cells (UB9496) with *NDT80* induced by addition of 1 μM ß-estradiol (+Ndt80) or ethanol vehicle control (–Ndt80). Sporulation cultures were arrested for 5 h, then split and subjected to the

indicated treatment. Cells were imaged 0 h and 3 h after treatment. Mitochondria, Cit1-GFP. Nuclei, Htb1-mCherry. Cell boundaries are indicated with dashed lines. **B.** Maximum intensity projections of fixed *pGAL-NDT80 GAL4.ER* cells containing wild-type *IME2* (UB9158) or *ime2-as1* (UB9844). Sporulation cultures were arrested for 5 h, then 1 μM ß-estradiol and 20 μM 1-NA-PP1 were added simultaneously. Cells were imaged 0 h and 3 h after treatment. Cell boundaries are indicated with dashed lines. **C-D.** Execution point time course, with the timing of Ime2 inhibition varied relative to constant induction of *pGAL-NDT80.* **C.** Top: Schematic of the execution point time course. Wild-type *pGAL-NDT80 GAL4.ER* (UB9158) and *pGAL-NDT80 GAL4.ER ime2-as1* (UB9844) were induced to sporulate and arrested for 5 h, then treated with 1 μM ß-estradiol to induce *NDT80* (time = 0 h). Next, the *ime2-as1* culture was split and treated with 20 μM 1-NA-PP1 at the indicated time points relative to *NDT80* induction. DMSO served as a vehicle control and was added simultaneously with ß-estradiol. The wild-type control was treated with 1-NA-PP1 and ß-estradiol simultaneously. Bottom: Heat map showing the frequency of mitochondrial detachment at 0, 3, and 5 h after *NDT80* induction (i.e., the time of fixation) for each of the execution points. $n = 2200$ total cells counted, with $n \geq 32$ per panel in the heat map. **D.** Maximum intensity projections from wild-type control and the +2.5 h execution point. Cell boundaries are indicated with dashed lines for meiosis II cells only. **E.** Maximum intensity projections of prophase I arrested cells (*ndt80Δ*, 5 h in SPO) containing wild-type *IME2* (UB17328) or *IME2-st* (UB17330). Cell boundaries are indicated with dashed lines. **F.** Quantification of mitochondrial morphology (% of cells with detached mitochondria) for the experiment in panel E. Fisher's exact test $p < 0.0001$ ($n = 100$ per genotype). Scale bars, 2 μm.

---

receptor protein (Gal4.ER) (Benjamin et al., 2003; Carlile and Amon, 2008). In this background, typically >80% of cells perform the meiotic divisions. When we released cells from a 5-h Ndt80 block by addition of ß-estradiol, mitochondrial detachment occurred normally (Figure 2.3A, +Ndt80). However, when the inducer was withheld, mitochondria remained persistently localized to the cell cortex (Figure 2.3A, −Ndt80), indicating that *NDT80* expression is necessary for mitochondrial detachment. *pGAL-NDT80* cells monitored by time-lapse microscopy showed identical behavior (Figure 2.4A). These experiments also confirmed that mitochondrial detachment is developmentally regulated and not an indirect outcome of prolonged nutritional deprivation. We conclude that Ndt80, a key regulator of meiotic events, is required for mitochondrial detachment.

2.2.4 Ime2 kinase is required for mitochondrial detachment

Ndt80 directly regulates the expression of approximately 200 genes (Cheng et al., 2018; Chu and Herskowitz, 1998). Among them, a particularly compelling candidate

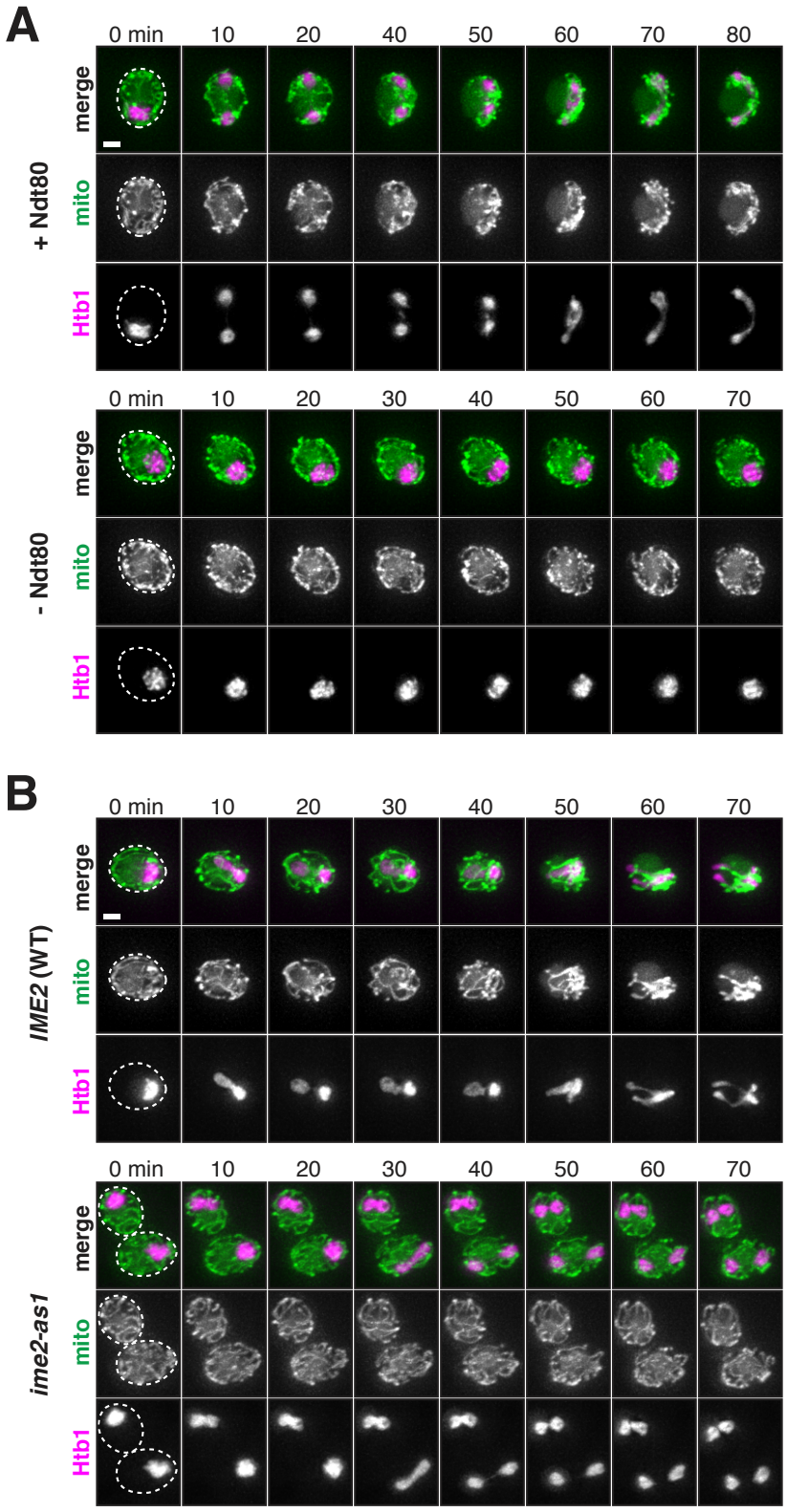
A
0 min
10
20
40
50
60
70
80
merge
mito
Htb1
+ Ndt80
0 min
10
20
30
40
50
60
70
merge
mito
Htb1
- Ndt80
B
0 min
10
20
30
40
50
60
70
merge
mito
Htb1
IME2 (WT)
0 min
10
20
30
40
50
60
70
merge
mito
Htb1
ime2-as1

Figure 2.4. Ndt80 and Ime2 are required for mitochondrial detachment. Movie montages of cells undergoing meiosis. Cells express Cit1-GFP to label mitochondria and Htb1-mCherry to label the nucleus. After the indicated treatments, cells were transferred to a 96-well plate and imaged every 10 min. Dashed lines indicate cell boundaries. Times shown are relative to the first frame. **A.** Movie montages of *pGAL-NDT80 GAL4.ER* (UB9158) cells. After 5 h in SPO medium, the culture was split, and cells were treated with 1 μM ß-estradiol (+Ndt80) or ethanol vehicle control (−Ndt80). **B.** Movie montages of *pGAL-NDT80 GAL4.ER* cells carrying wild-type *IME2* (UB9158) or the *ime2-as1* allele (UB16888). After 5 h in SPO medium, cells were simultaneously treated with 1 μM ß-estradiol and 20 μM 1-NA-PP1. Scale bar, 2 μm.

---

is the meiosis-specific kinase Ime2 (Foiani et al., 1996; Kominami et al., 1993; Nocedal et al., 2017; Smith and Mitchell, 1989; Yoshida et al., 1990). Ime2 belongs to a family of serine/threonine protein kinases displaying sequence similarities to both cyclin-dependent kinases and mitogen-activated protein kinases (Irniger, 2011). Although originally characterized as an early gene required for pre-meiotic S phase (Dirick et al., 1998), Ime2 kinase activity is significantly elevated during meiosis II (Benjamin et al., 2003; Berchowitz et al., 2013). It has been shown that Ndt80 is additionally required for the increase in Ime2 activity during meiosis II, independent of its role in regulating *IME2* expression (Benjamin et al., 2003; Berchowitz et al., 2013).

To determine whether Ime2 is necessary for mitochondrial detachment, we employed a conditional allele, *ime2-as1*, that can be selectively inhibited by the drug 1-NA-PP1 (Benjamin et al., 2003). By controlling the timing of inhibitor treatment, we could bypass the requirement for Ime2 in pre-meiotic S phase. In cells arrested in prophase I by *pGAL-NDT80*, simultaneous addition of ß-estradiol and 1-NA-PP1 resulted in retention of mitochondria at the cortex, even though cells performed meiosis I, as previously reported (Benjamin et al., 2003) (Figure 2.3B). Mitochondrial detachment was normal in *IME2* wild-type cells that were identically treated, ruling out non-specific effects of the drug treatment (Figure 2.3B). We obtained identical results by time-lapse microscopy (Figure 2.4B). These findings show that *IME2* function is necessary for mitochondrial detachment.

2.2.5 Ime2 regulates mitochondrial detachment independent of its role in Ndt80 activation

Our experiments thus far indicate that Ndt80, a transcription factor, and Ime2, a kinase, are involved in mitochondrial detachment. Previous studies found that Ndt80 is required for the elevated activity of Ime2 during the meiotic divisions (Benjamin et al., 2003; Berchowitz et al., 2013), and conversely, Ime2 is required for

the accumulation of Ndt80 and its full activation via phosphorylation (Benjamin et al., 2003; Sopko et al., 2002). Consequently, it was unclear whether the contribution of Ndt80 to the mitochondrial detachment phenotype was primarily by induction of Ime2, or the reverse model where the contribution of Ime2 is through enhancing Ndt80 activity. To distinguish between these possibilities, we induced *pGAL-NDT80* at 5 h but varied the timing of Ime2-as1 inhibition from 0.5 to 2.5 h after *NDT80* induction. We found that mitochondrial detachment was acutely sensitive to Ime2 inactivation. The frequency of mitochondrial detachment showed a graded response over 30-min intervals of drug addition timing, with no drug addition time point recapitulating the high frequency of mitochondrial detachment observed in wild-type cells (Figure 2.3C). As reference, by mRNA-seq (Brar et al., 2012), Ndt80 target genes are induced within ~1 h of *pGAL-NDT80* induction in wild-type cells. Addition of 1-NA-PP1 at 2.5 h after *NDT80* induction resulted in a mild effect on the meiotic divisions, yet mitochondrial detachment was still defective in a substantial fraction of the cells (Figure 2.3, C and D). Though we cannot exclude the possibility that Ime2-as1 inactivation at later execution points might still compromise Ndt80 function, our results are most consistent with the model that the contribution of Ndt80 to mitochondrial detachment is principally through the regulation of Ime2 activity.

Next, we tested whether Ime2 could promote mitochondrial detachment in cells lacking a functional *NDT80* gene (*ndt80Δ*). For this, we used an *IME2* allele that has elevated activity throughout meiosis, *IME2-st* (Sia and Mitchell, 1995). Even though the absence of *NDT80* expression completely blocked meiotic progression, ~40% of the cells carrying the *IME2-st* allele displayed mitochondrial detachment (Figure 2.3, E and F). The remainder had a typical, prophase I mitochondrial morphology. The basis of this heterogeneity is unclear at the moment, though a similar phenotype of incomplete penetrance has been observed in a previous study using the same allele (Berchowitz et al., 2013), potentially suggesting cell-to-cell variation in kinase activity. Nonetheless, these results demonstrate that Ime2 is sufficient to promote mitochondrial detachment and that the requirement of Ime2 for Ndt80 activation and meiotic divisions can be uncoupled from its role in mediating mitochondrial reorganization.

Finally, we sought to determine if Ime2 is active in strains defective in meiotic progression but that are capable of executing mitochondrial detachment. Although the elevated Ime2 kinase activity present during the meiotic divisions is known to require Ndt80 (Benjamin et al., 2003; Berchowitz et al., 2013), the precise requirements for Ime2 activation are unknown. We measured Ime2 kinase activity during meiosis in a subset of the mutants examined in Figure 2.2. We found that, similar to wild-type Ndt80-induced meiotic cells, Ime2 kinase activity is elevated in *cdc5-mn*, *cdc28-as1*, and *cdc20-mn* cells after Ndt80 expression, despite the meiotic arrest phenotypes of these mutants (Figure 2.5, A and B). In contrast, prophase-arrested (−Ndt80) cells do not activate Ime2, as evidenced by persistent low-level

activity (Figure 2.5A). Our results are consistent with the interpretation that Ime2 is activated in a manner dependent on Ndt80 but independent of the cell cycle regulators examined, thereby explaining the uncoupling of mitochondrial detachment and meiotic progression shown in Figure 2.2.

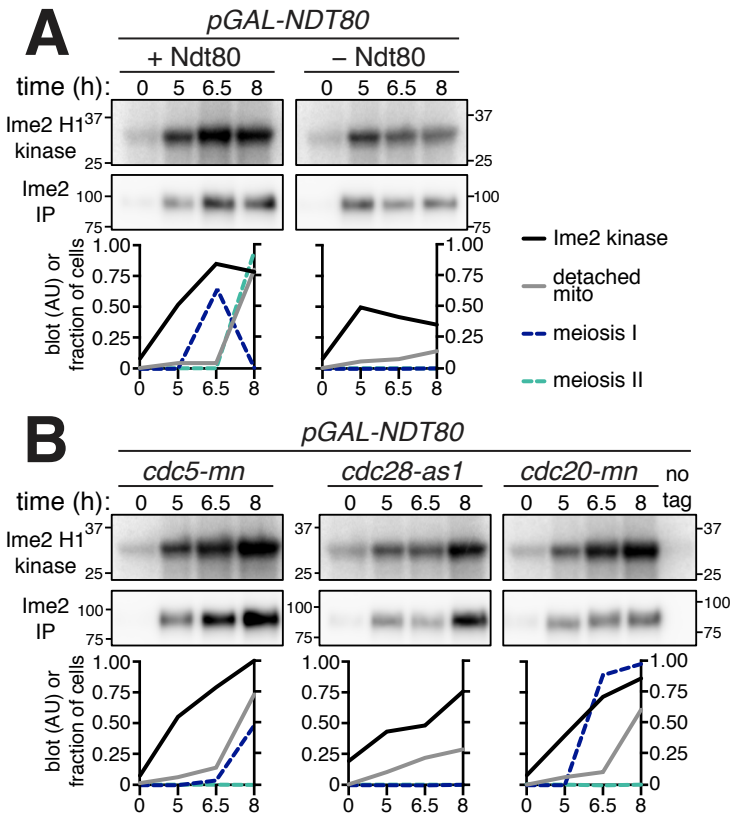

Figure 2.5. Ime2 activation is uncoupled from meiotic progression. A-B. Measurement of Ime2 kinase activity during meiosis in wild type and cell cycle mutants. Ime2-3V5 was immunoprecipitated from lysate collected at the indicated time points. Then, on-bead Ime2-3V5 was incubated with histone H1 and γ-^{32}P ATP. Ime2 kinase activity toward histone H1 was determined by autoradiography, and Ime2-3V5 abundance in the reaction was determined by immunoblotting. Ime2 kinase activity is plotted, with the background from a no-tag control (A15055) subtracted from each value. Values are scaled to the maximum background-subtracted value from the experiment. In addition, mitochondrial detachment frequency was scored using the Cit1-GFP mitochondrial marker and meiotic staging determined by tubulin immunofluorescence (n = 100 cells per time point per condition for each analysis). **A.** *pGAL-NDT80 GAL4.ER* cells (UB10554) were induced to sporulate, then after 5 h treated with 1 μM β-estradiol (+Ndt80) or ethanol vehicle control (–Ndt80). **B.** Sporulating *pGAL-NDT80 GAL4.ER cdc5-mn* (UB18612) and *pGAL-NDT80 GAL4.ER cdc20-mn* (UB18614) cells were treated

with 1 μM ß-estradiol at 5 h. *pGAL-NDT80 GAL4.ER cdc28-as1* (UB18845) cells were simultaneously treated with 1 μM ß-estradiol and 1 μM 1-NM-PP1 at 5 h.

2.2.6 The mitochondria-plasma membrane tether MECA is phosphorylated in an Ime2-dependent manner

How does Ime2 trigger mitochondrial detachment? A simple model would be that Ime2 inhibits the activity of a factor that normally connects mitochondria to the cell cortex. Since Ime2 is a protein kinase, such a factor could be an Ime2 substrate. A clear candidate was the mitochondria-ER-cortex anchor, MECA (Cerveny et al., 2007; Klecker et al., 2013; Lackner et al., 2013). In mitotic cells, MECA tethers mitochondria to the plasma membrane by forming large assemblies at the contact sites between the two membranes (Cerveny et al., 2007; Klecker et al., 2013; Lackner et al., 2013). MECA has two known subunits, Num1 and Mdm36 (Lackner et al., 2013; Ping et al., 2016). While Num1 can directly bind to lipids on both the outer mitochondrial membrane and plasma membrane, Mdm36 helps Num1 assemble into clusters at the membrane contact sites (Lackner et al., 2013; Ping et al., 2016). Interestingly, in the absence of MECA, mitochondria are constitutively detached from the plasma membrane in vegetative cells (Cerveny et al., 2007; Klecker et al., 2013; Lackner et al., 2013), highly reminiscent of the mitochondrial detachment that naturally occurs as part of meiotic differentiation.

In order to test if Ime2 phosphorylates MECA, we first isolated recombinant Mdm36 and performed an *in vitro* kinase assay with constitutively active Ime2 (Ime2-st) purified from yeast. We found that Mdm36 was phosphorylated only in the presence of Ime2, suggesting that it is a direct substrate for the kinase (Figure 2.6, A and B). To analyze Num1, we immunoprecipitated Num1-3V5 from vegetative cells and then performed a similar *in vitro* kinase assay. Similar to Mdm36, we observed Ime2-dependent phosphorylation of Num1 (Figure 2.6C). Together, these results demonstrate that Ime2 can phosphorylate both Num1 and Mdm36 *in vitro*.

We further found that Ime2 regulates MECA phosphorylation *in vivo* (Figure 2.6D). We isolated Num1 from prophase I-arrested cells (*ndt80Δ*) that expressed either wild-type Ime2 or the hyperactive Ime2-st and used label-free mass spectrometry to map phosphorylation sites. This approach led to the identification of four phosphorylated serine residues in Num1, one of which (S1094) was present only when Ime2 activity was high (Figure 2.6D). We used the same strategy to probe *in vivo* Mdm36 phosphorylation sites. However, we were unable to obtain sufficient amounts of the Mdm36-3V5 protein from meiotic cells, for even moderate peptide coverage, and no phosphorylation sites were detected (not shown). We conclude that

Num1, the major subunit of MECA, is phosphorylated in an Ime2-dependent manner during meiosis.

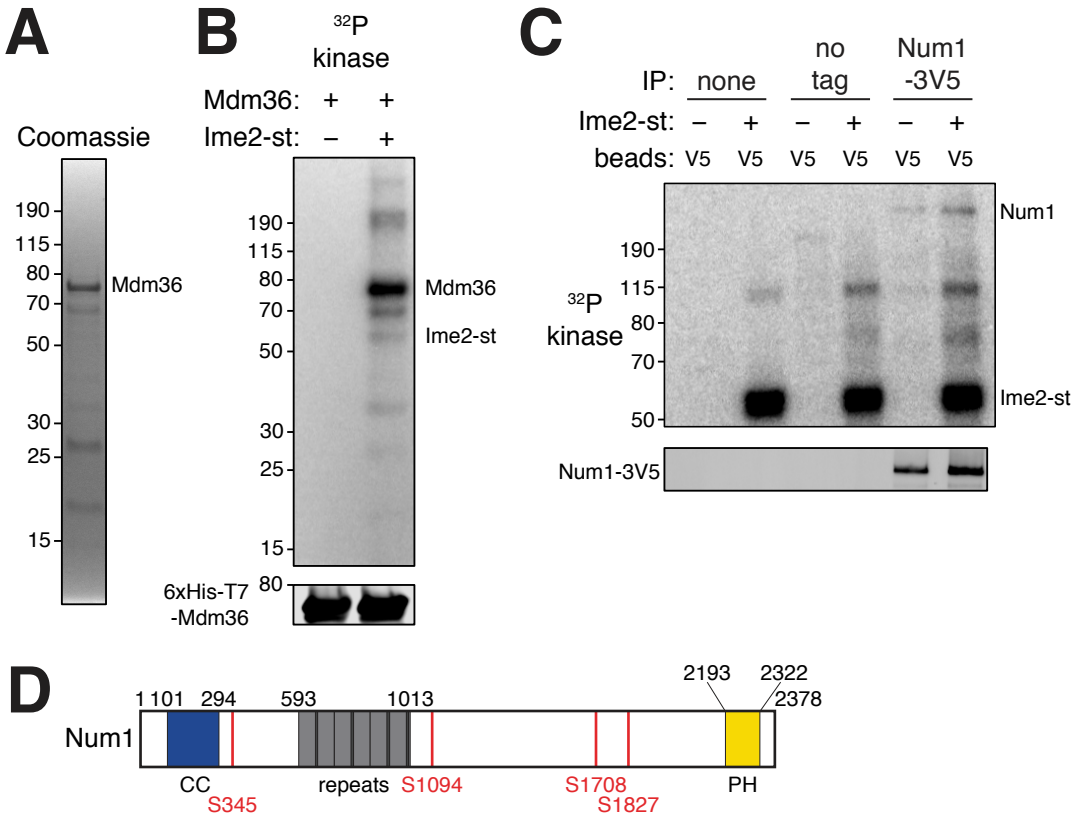

		# of phosphopeptides ± SD (total ± SD)	
peptide	**phosphorylated residue**	**prophase I *ndt80Δ***	**prophase I *ndt80Δ IME2-st***
KY(pS)EKNNMILLSNDSYK	S345	1.7±2.1 (1.7±2.1)	0.7±1.2 (0.7±1.2)
GYHIIDTTTYNELVSNFN(pS)PTLK	S1094	0.0±0.0 (2.3±1.5)	1.3±1.5 (3.0±4.4)
QLVNTT(pS)PCPPITYEDLK	S1708	1.3±1.2 (3.0±1.0)	1.0±1.0 (4.3±2.1)
LVPFEK(pS)NINLK	S1827	3.7±2.1 (3.7±2.1)	2.7±3.1 (2.7±3.1)
	% Num1 coverage	52.4% ± 5.3%	44.2% ± 10.7%

Figure 2.6. Phosphorylation of Num1 and Mdm36 *in vitro* and *in vivo*. A. Coomassie-stained gel of 6xHis-T7-Mdm36 purified from *E. coli*, used in panel B. **B.** *in vitro* kinase assays containing γ-^{32}P ATP, 1 µg recombinant Mdm36, and 3 pmol of Ime2-st purified from yeast or no-kinase control. Reactions were incubated for 15 min at room temperature, then analyzed by SDS-PAGE and autoradiography. Prior to assembling the kinase assay, half of the input was reserved and analyzed by immunoblot. **C.** *in vitro* kinase assay prepared as in panel B, but using on-bead

substrate immunoprecipitated from vegetative cells using agarose beads conjugated with an anti-V5 antibody. Untagged lysate ("no tag") was purified from wild type (UB15) and Num1-3V5 from strain UB12017. Beads never incubated with lysate ("none") were also examined. Prior to assembling the kinase assay, half of the bead volume for each sample was reserved, bound protein eluted, and analyzed by immunoblot. Num1 runs above the highest (190 kDa) ladder band. **D.** Top: Diagram of Num1 domain structure in the SK1 background and *in vivo* phosphorylation sites detected by mass spectrometry (red lines and text). Black numbers refer to amino acid positions that define the domain boundaries. The Num1 amino acid sequence in SK1 differs from the S288C reference genome (Yue et al., 2017). Num1 (SK1) contains six copies of a 64-amino acid repeat, with some repeats separated by a spacer sequence (LEKEVEQ), and an overall length of 2378 amino acids (271 kDa). CC, coiled coil domain; PH, Pleckstrin homology domain. Bottom: Num1 phosphopeptides detected by LC-MS/MS from Num1-3V5 denaturing immunoprecipitation (see Appendix B). Phosphoserine is indicated as (pS). The detected number of phosphopeptides and total peptides (phosphorylated and unmodified combined) as well as the overall sequence coverage of Num1 are shown for three biological replicates (mean ± standard deviation). Num1-3V5 was isolated from *ndt80Δ* negative control cells (UB17332; prophase I *ndt80Δ*) and *ndt80Δ IME2-st* cells (UB16660; prophase I *IME2-st*) after 5 h in SPO medium.

2.2.7 MECA undergoes dynamic changes in meiosis

To investigate a possible role of MECA in regulating mitochondrial dynamics during meiosis, we first examined the localization of Num1 and Mdm36. Similar to previous studies in vegetative cells (Cerveny et al., 2007; Klecker et al., 2013; Kraft and Lackner, 2017; Lackner et al., 2013; Ping et al., 2016; Tang et al., 2012), Num1 and Mdm36 formed prominent clusters at the cell cortex prior to meiosis II (Figure 2.7A); these foci represent contact sites between mitochondria and the plasma membrane. In contrast, meiosis II cells were devoid of Num1 and Mdm36 puncta. We further characterized MECA dynamics in meiosis by monitoring Num1-GFP localization in a strain carrying mitoBFP and Htb1-mCherry. In premeiotic and prophase I cells, we observed many bright Num1-GFP puncta, with mitochondria tethered at the plasma membrane (Figure 2.7B). In contrast, meiosis II cells were largely devoid of the puncta, and mitochondria were detached (Figure 2.7B). The number of Num1 foci and total cellular fluorescence were significantly reduced in meiosis II cells compared to cells from earlier stages (Figure 2.7, C-D). Furthermore, the disappearance of Num1 foci was dependent on Ndt80 expression (Figure 2.7, B-D), but not on Cdc20 (Figure 2.8A), consistent with our previous observations of mitochondrial behavior (Figure 2.2E, Figure 2.3A, and Figure 2.5). These results strongly indicate that the timely detachment of mitochondria from the plasma membrane is driven by developmentally regulated changes in the MECA complex.

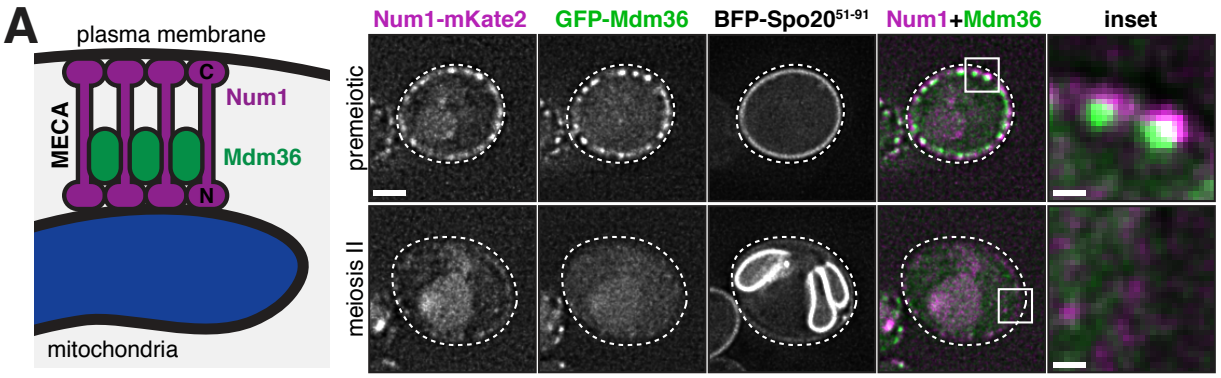
A
plasma membrane
MECA
C
Num1
Mdm36
N
mitochondria
Num1-mKate2
GFP-Mdm36
BFP-Spo20^51-91
Num1+Mdm36
inset
premeiotic
meiosis II

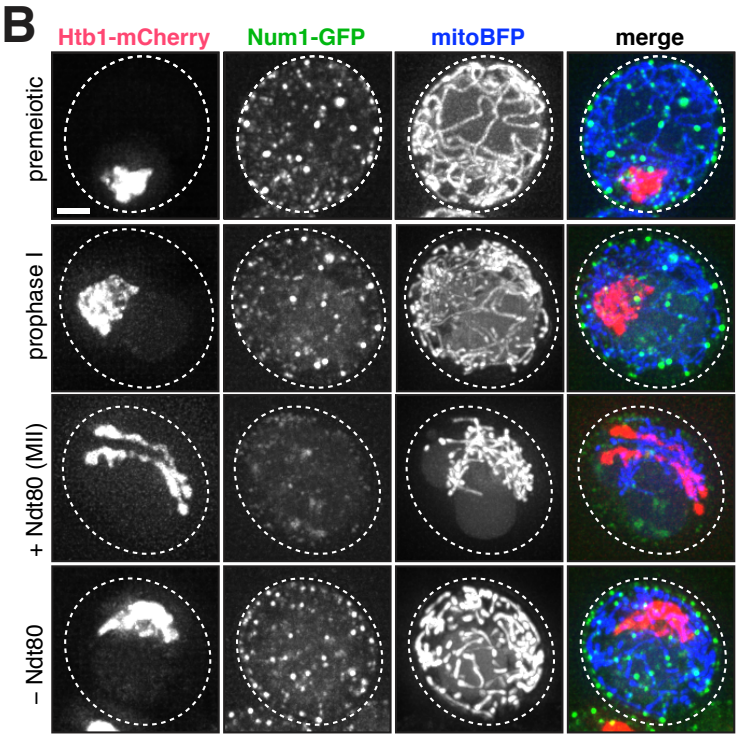
B
Htb1-mCherry
Num1-GFP
mitoBFP
merge
premeiotic
prophase I
+ Ndt80 (MII)
– Ndt80

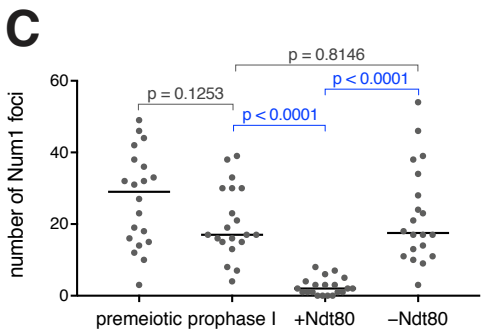
C
number of Num1 foci
p = 0.8146
p < 0.0001
p = 0.1253
p < 0.0001
premeiotic
prophase I
+Ndt80
–Ndt80

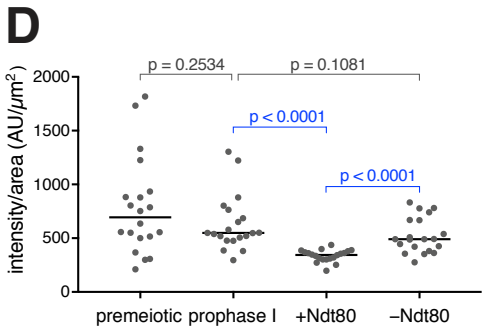
D
intensity/area (AU/μm²)
p = 0.2534
p = 0.1081
p < 0.0001
p < 0.0001
premeiotic
prophase I
+Ndt80
–Ndt80

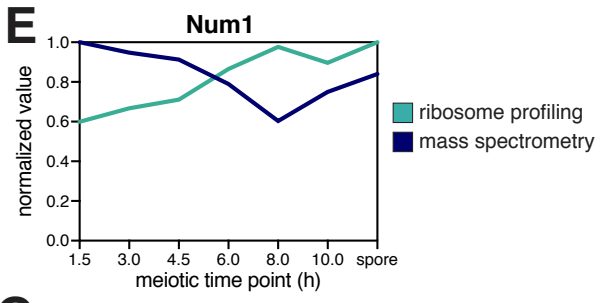
E
Num1
normalized value
ribosome profiling
mass spectrometry
meiotic time point (h)
spore

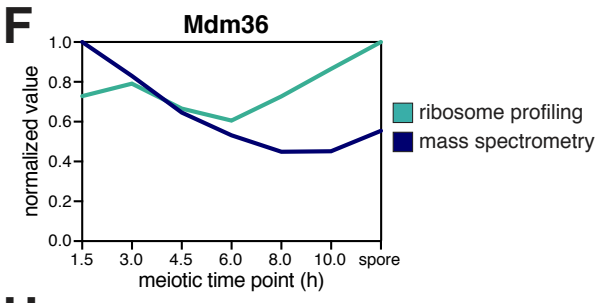
F
Mdm36
normalized value
ribosome profiling
mass spectrometry
meiotic time point (h)
spore

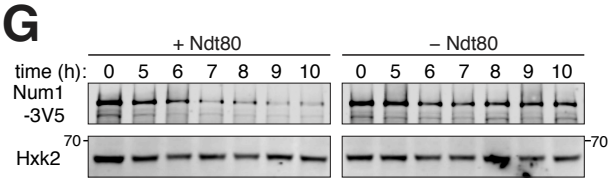
G
+ Ndt80
– Ndt80
time (h):
Num1
-3V5
Hxk2

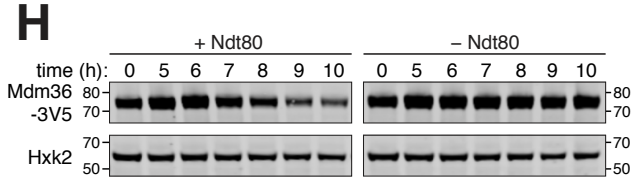
H
+ Ndt80
– Ndt80
time (h):
Mdm36
-3V5
Hxk2

Figure 2.7. MECA is dynamically regulated in meiosis. A. Left: Diagram of the mitochondria-plasma membrane contact site. MECA contains two known subunits, Num1 and Mdm36, and is responsible for tethering mitochondria to the plasma membrane. Right: Localization of MECA subunits, Num1-mKate2 and GFP-Mdm36, in live premeiotic and meiosis II cells (UB16677). Single planes in the z-axis are shown. Meiotic stage was determined by the prospore membrane marker BFP-Spo20$^{51-91}$. **B.** Maximum intensity projections of live *pGAL-NDT80 GAL4.ER* cells (UB15124) showing MECA localization (Num1-GFP), mitochondrial localization (mitoBFP), and nuclei (Htb1-mCherry). Cells were imaged at time of transfer to SPO medium (premeiotic) and 5 h (prophase I). Then, at 5 h, the culture was split and treated with 1 μM ß-estradiol (+Ndt80) or ethanol vehicle control (−Ndt80). Cells from the split cultures were imaged at 8 h. **C-D.** Quantifications of the experiment in panel B. Analysis of the +Ndt80 sample was restricted to meiosis II stage cells. $n = 20$ cells per group. Medians are plotted as horizontal lines. The Mann-Whitney nonparametric test was used to test statistical significance. **C.** Number of Num1-GFP foci per cell (see Appendix B). **D.** Whole-cell Num1-GFP fluorescence quantification from maximum intensity projection (AU, arbitrary units), normalized to cell area. **E-F.** Quantifications of Num1 and Mdm36 steady-state protein levels (mass spectrometry) and synthesis (ribosome profiling) during meiosis from a published dataset (Cheng et al., 2018). **G-H.** Immunoblots of MECA subunits in *pGAL-NDT80 GAL4.ER* strains. Strains were induced to sporulate for 5 h, then flasks were split and treated with 1 μM ß-estradiol (+Ndt80) or ethanol vehicle control (−Ndt80). Hxk2 serves as a loading control. **G.** Blot for Num1-3V5 (UB12402). Num1 runs above the highest (190 kDa) ladder band. **H**. Blot for Mdm36-3V5 (UB13851). Scale bars, 2 μm, except in inset panels, 400 nm.

In a matched ribosome profiling and quantitative mass spectrometry dataset generated from a yeast meiotic time course (Cheng et al., 2018), both Num1 and Mdm36 exhibit dynamic regulation during meiosis. Namely, as assessed by quantitative mass spectrometry, the protein levels of Num1 and Mdm36 decrease as meiosis progresses, reaching their minima at 8 h (Figure 2.7, E and F). We confirmed the decline in protein levels by immunoblotting with strains expressing epitope tagged Num1-3V5 or Mdm36-3V5 from their endogenous loci (Figure 2.7, G and H; Figure 2.9). In each case, protein decline occurred in an Ndt80-dependent manner (Figure 2.7, G and H), suggesting that Num1 and Mdm36 protein levels are actively regulated.

The decline in Num1 and Mdm36 protein levels is not accompanied by a decrease in ribosome footprint density (Figure 2.7, E and F), indicating that the abundance of Num1 and Mdm36 cannot be easily explained by regulation at the level of protein synthesis. Instead, we reasoned that Num1 and Mdm36 are actively degraded. To test whether the reduction in Num1 and Mdm36 protein levels requires the

proteasome, a major conduit for protein degradation, we treated prophase I-arrested cells with the proteasome inhibitor MG-132 and simultaneously released them from the Ndt80-block. Upon MG-132 treatment, Num1 protein levels failed to decline to the extent seen in the control (Figure 2.10A). However, Mdm36 levels continued to decrease (Figure 2.10B). To assess proteasome-dependence by an independent method, we utilized a hypomorphic allele of a 26S proteasome lid subunit, *rpn6-1* (Isono et al., 2005). Consistent with the MG-132 data, in *rpn6-1* cells, the protein levels of Num1, but not Mdm36, were stabilized throughout meiosis (Figure 2.8, B and C), indicating proteasome-dependence for Num1 degradation. To address the possibility that Mdm36 might instead be degraded by autophagy, we utilized the GFP-Mdm36 allele. Since GFP is relatively resistant to vacuolar degradation, autophagic degradation of the tagged protein leads to the accumulation of free GFP in the vacuole (Kanki and Klionsky, 2008). We observed free GFP by immunoblotting in late meiosis (Figure 2.10, C and D), consistent with autophagy-dependent turnover of Mdm36. However, our data do not exclude the possibility of autophagy-independent processing of GFP-Mdm36. Altogether, these analyses reveal that programmed destruction of Num1 and Mdm36 causes the dissolution of MECA assemblies in meiosis II.

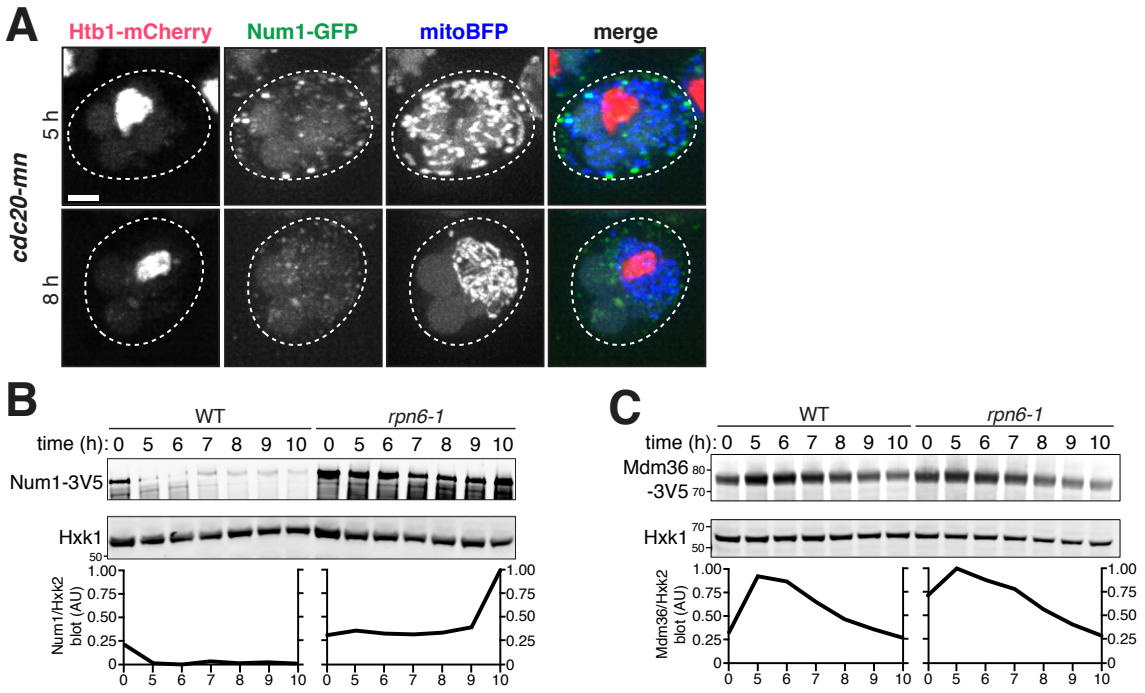

Figure 2.8. Genetic requirements for MECA subunit degradation. A. Maximum intensity projections of live *pGAL-NDT80 GAL4.ER cdc20-mn* (UB16156), which is *pCLB2-CDC20*, imaged after 5 h or 8 h in sporulation media. *NDT80* expression was induced at 5 h by the addition of 1 μM β-estradiol. Mitochondria, mitoBFP. Nuclei, Htb1-mCherry. **B-C.** Immunoblots of MECA subunits in *rpn6-1* mutant background and wild-type control. Strains were induced to sporulate, then 5 h later

1 μM ß-estradiol was added to induce *NDT80*. Band intensity quantifications normalized to the Hxk2 loading control for each time point are shown below the immunoblots. **B.** Num1-3V5 wild type (UB12402) and *rpn6-1* (UB13816). Num1 runs above the highest (190 kDa) ladder band. **C.** Mdm36-3V5 wild type (UB13851) and *rpn6-1* (UB14340). Scale bar, 2 μm.

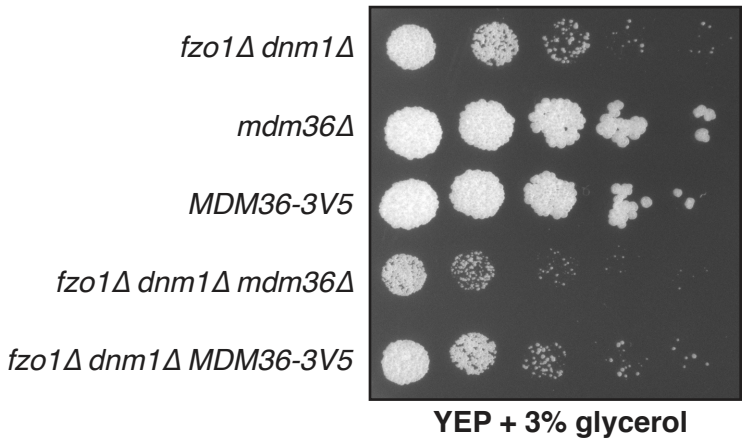

Figure 2.9. *MDM36-3V5* allele is functional. *MDM36-3V5* does not exhibit a synthetic growth defect with the *fzo1Δ dnm1Δ* double mutant, a sensitized background to assess Mdm36 function (Lackner et al., 2013). *MDM36-3V5* (UB13762) and *mdm36Δ* (UB13770) grow normally. *fzo1Δ dnm1Δ* (UB7798) shows diminished growth on YEP + 3% glycerol, and this growth defect is more severe in *fzo1Δ dnm1Δ mdm36Δ* (UB13766), as previously described (Lackner et al., 2013). No synthetic growth defect is observed in *fzo1Δ dnm1Δ MDM36-3V5* (UB13768). Cells were pre-grown overnight on YPG plates, then serially diluted and spotted on the YPG plate shown. The plate was incubated at 30°C for 3 d.

2.2.8 Ime2 induces mitochondrial detachment by promoting MECA degradation

What is the relationship between Ime2 and MECA in mediating mitochondrial detachment? We posited that Ime2 interferes with MECA function during meiosis II by promoting its destruction, thereby triggering mitochondrial detachment. In order to test this hypothesis, we first examined whether Ime2 regulates MECA stability by measuring Num1 and Mdm36 abundance in the *ime2-as1* mutant background. Treatment with 1-NA-PP1 at the time of *pGAL-NDT80* induction attenuated the degradation of Num1 and Mdm36 that was observed in wild-type cells (Figure 2.11, A and B). Monitoring MECA assemblies in single cells yielded similar results (Figure 2.11, C-F). Num1-GFP clusters persisted at later meiotic time points upon

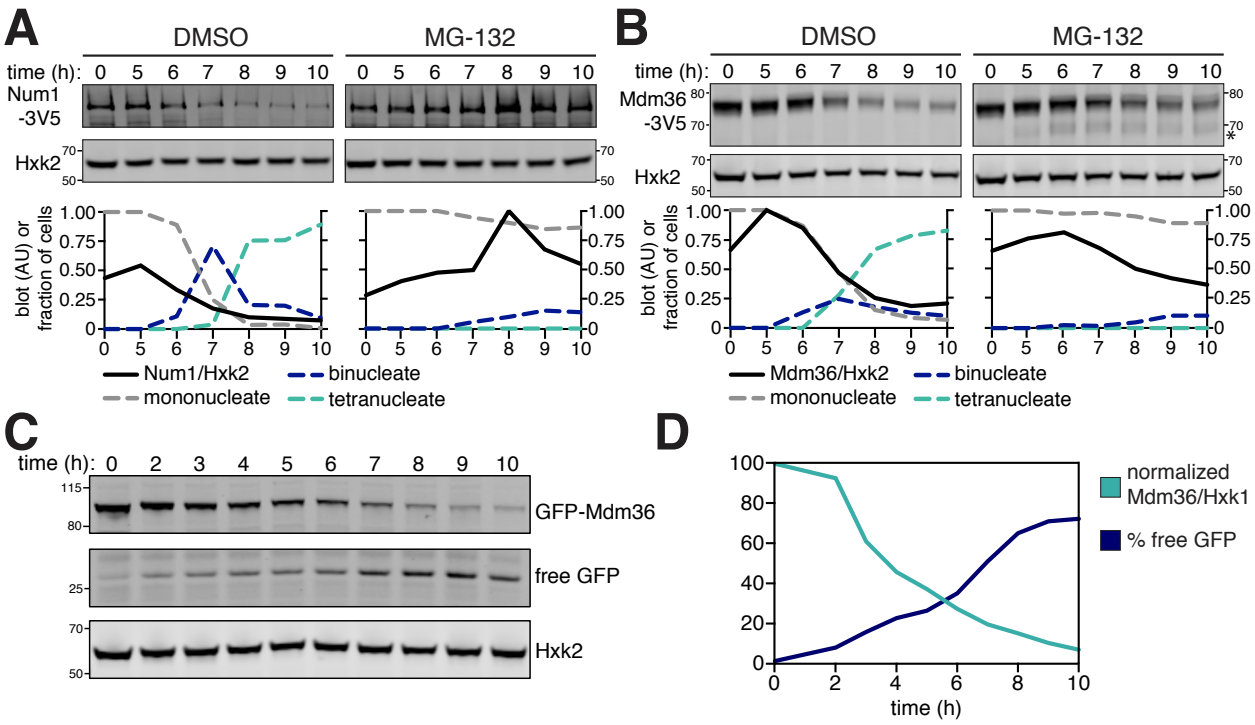

Figure 2.10. MECA is destroyed by the proteasome and autophagy. A-B. Proteasome inhibition during meiosis by treatment with MG-132, compared to a DMSO vehicle control. Flasks were split at 5 h, with one half treated with 100 µM MG-132 and the other half with a DMSO vehicle control. Band intensity quantifications normalized to the Hxk2 loading control and time course staging by DAPI staining for each time point are shown below the immunoblots. **A.** Immunoblot of Num1-3V5 in a *pGAL-NDT80 GAL4.ER* synchronous meiosis (UB13245), where 1 µM ß-estradiol was added to the flasks at 5 h. Num1 runs above the highest (190 kDa) ladder band. **B.** Immunoblot of Mdm36-3V5 (UB16324). The asterisk indicates a band of unknown identity. **C.** Immunoblot autophagy assay of GFP-Mdm36 (UB16326). **D.** Quantification of the blot in panel C. The total level of full-length protein (normalized Mdm36/Hxk2) was calculated as the intensity of the GFP-Mdm36 band divided by the Hxk2 loading control band. Percentages of the maximum value are plotted. The % free GFP value was calculated as the intensity of the free GFP band divided by the summed intensities of the free GFP and GFP-Mdm36 bands.

Ime2 inhibition (Figure 2.11, C-E). Notably, the number of Num1 foci and overall Num1 intensity did not differ significantly between prophase I -arrested (+0 h) and Ime2-inhibited (+3 h) cells. In each case, mitochondria remained attached to the

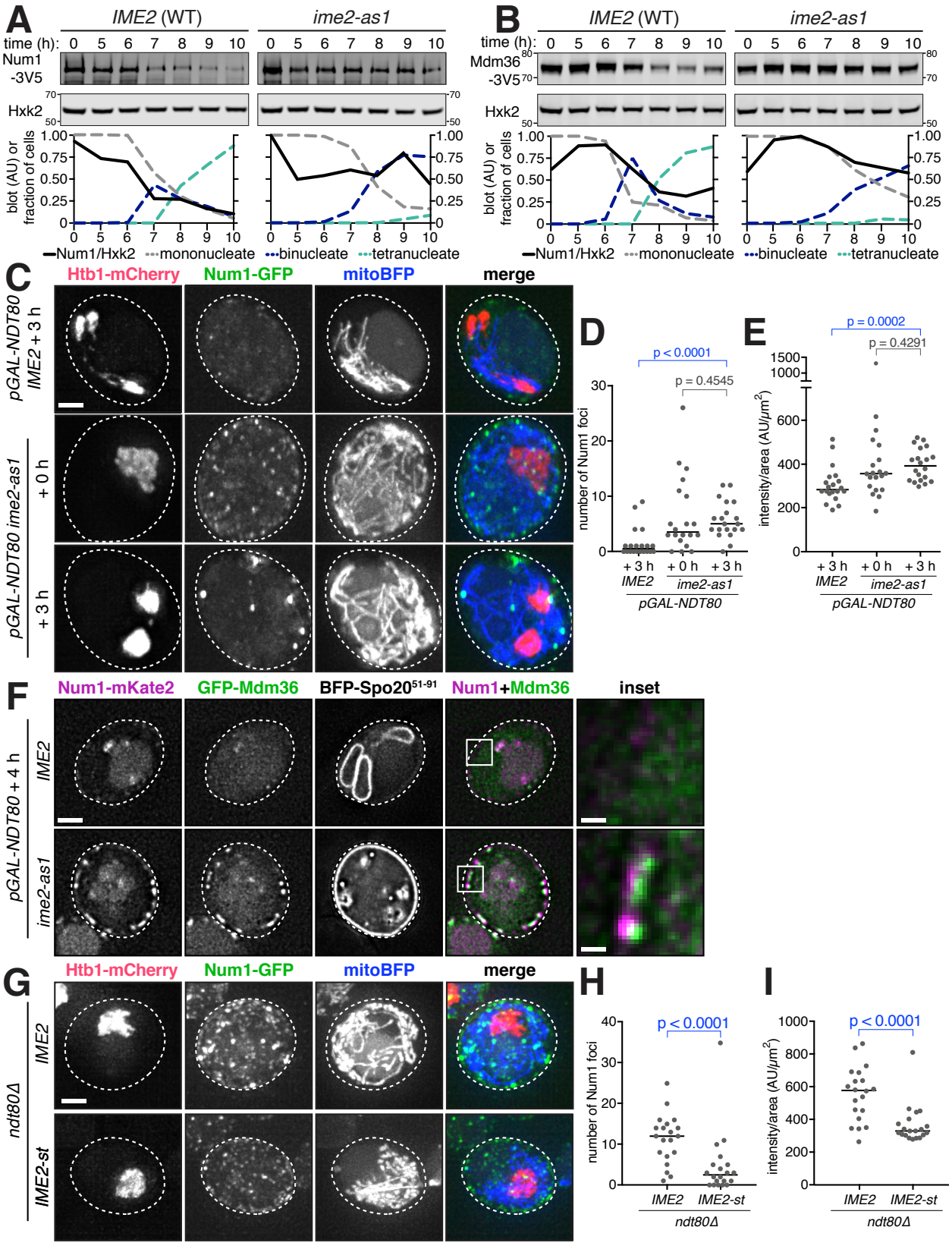
A
IME2 (WT)
ime2-as1
time (h): 0 5 6 7 8 9 10 0 5 6 7 8 9 10
Num1 -3V5
Hxk2
blot (AU) or fraction of cells
Num1/Hxk2
mononucleate
binucleate
tetranucleate
B
IME2 (WT)
ime2-as1
Mdm36 -3V5
Hxk2
C
Htb1-mCherry
Num1-GFP
mitoBFP
merge
pGAL-NDT80 IME2 + 3 h
pGAL-NDT80 ime2-as1
+ 0 h
+ 3 h
D
p < 0.0001
p = 0.4545
number of Num1 foci
+ 3 h IME2
+ 0 h ime2-as1
+ 3 h ime2-as1
pGAL-NDT80
E
p = 0.0002
p = 0.4291
intensity/area (AU/μm²)
F
Num1-mKate2
GFP-Mdm36
BFP-Spo20⁵¹⁻⁹¹
Num1+Mdm36
inset
pGAL-NDT80 + 4 h
IME2
ime2-as1
G
Htb1-mCherry
Num1-GFP
mitoBFP
merge
ndt80Δ
IME2
IME2-st
H
p < 0.0001
number of Num1 foci
IME2
IME2-st
ndt80Δ
I
p < 0.0001
intensity/area (AU/μm²)

Figure 2.11. Ime2 regulates MECA function in meiosis. A-B. Immunoblots of MECA subunits in *pGAL-NDT80 GAL4.ER*. Strains were induced to sporulate, then 5 h later released from prophase I arrest by the addition of 1 μM ß-estradiol to induce *NDT80*. Simultaneously, 20 μM 1-NA-PP1 was added to inhibit *ime2-as1*, with wild-type *IME2* as a control. Band intensity quantifications normalized to the Hxk2 loading control and time course staging by DAPI staining for each time point are shown below the immunoblots. **A.** Num1-3V5 immunoblot in wild type (UB12402) and *ime2-as1* (UB12403). Num1 runs above the highest (190 kDa) ladder band. **B.** Mdm36-3V5 immunoblot in wild type (UB13851) and *ime2-as1* (UB14546). **C.** Maximum intensity projections of live *pGAL-NDT80 GAL4.ER* cells containing wild-type *IME2* (UB15124) or *ime2-as1* (UB16047). Cells were induced to sporulate, then treated with 1 μM ß-estradiol and 20 μM 1-NA-PP1 at 5 h. Images were acquired at the time of ß-estradiol addition (0 h) or 3 h later. Dashed lines indicate cell boundaries. Mitochondria, mitoBFP. Nuclei, Htb1-mCherry. **D-E.** Quantifications for the experiment in panel C. Analysis was restricted to cells that had entered the meiotic divisions. $n = 20$ cells per group. Medians are plotted as horizontal lines. The Mann-Whitney nonparametric test was used to test statistical significance. **D.** Number of Num1-GFP foci per cell (see Appendix B). **E.** Whole-cell Num1-GFP fluorescence quantification from maximum intensity projection, normalized to cell area. **F**. Localization of Num1-mKate2 and GFP-Mdm36 in live *pGAL-NDT80 GAL4.ER* (UB18219) and *pGAL-NDT80 GAL4.ER ime2-as1* (UB18221) cells. After 5 h in SPO medium, the cultures were treated with 1 μM ß-estradiol and 20 μM 1-NA-PP1. Images were acquired 4 h later. Single planes in the z-axis are shown. Entry into the meiotic divisions was staged by the prospore membrane marker BFP-Spo20$^{51-91}$. Note that prospore membranes are misshapen in the *ime2* mutant. **G.** Maximum intensity projections of live wild-type *IME2 ndt80Δ* cells (UB16806) or *IME2-st ndt80Δ* cells (UB16808) arrested in prophase I for 5 h. Cells express the same cellular markers as in panel C. **H-I.** Quantifications of the experiment in panel G. $n = 20$ cells per group. Medians are plotted as horizontal lines. The Mann-Whitney nonparametric test was used to test statistical significance. **H.** Number of Num1-GFP foci per cell (see Appendix B). **I.** Whole-cell Num1-GFP fluorescence quantification from maximum intensity projection, normalized to cell area. Scale bars, 2 μm, except in inset panels, 400 nm.

---

plasma membrane, presumably through the persistent contact sites. Further, Num1 and Mdm36 remained co-localized after Ime2 inhibition (Figure 2.11F). The simplest interpretation of these data is that Ime2-dependent regulation leads to Num1 and Mdm36 degradation, which in turn causes MECA disassembly and mitochondrial detachment in anaphase II.

To further test the involvement of Ime2 in MECA destruction, we examined the impact of expressing the hyperactive Ime2-st kinase on MECA levels in prophase I-

arrested cells. Both the number of Num1 foci and total cellular fluorescence were significantly reduced upon *IME2-st* expression (Figure 2.11, G-I). Our results indicate that elevated Ime2 activity in prophase I is sufficient to trigger premature Num1 degradation.

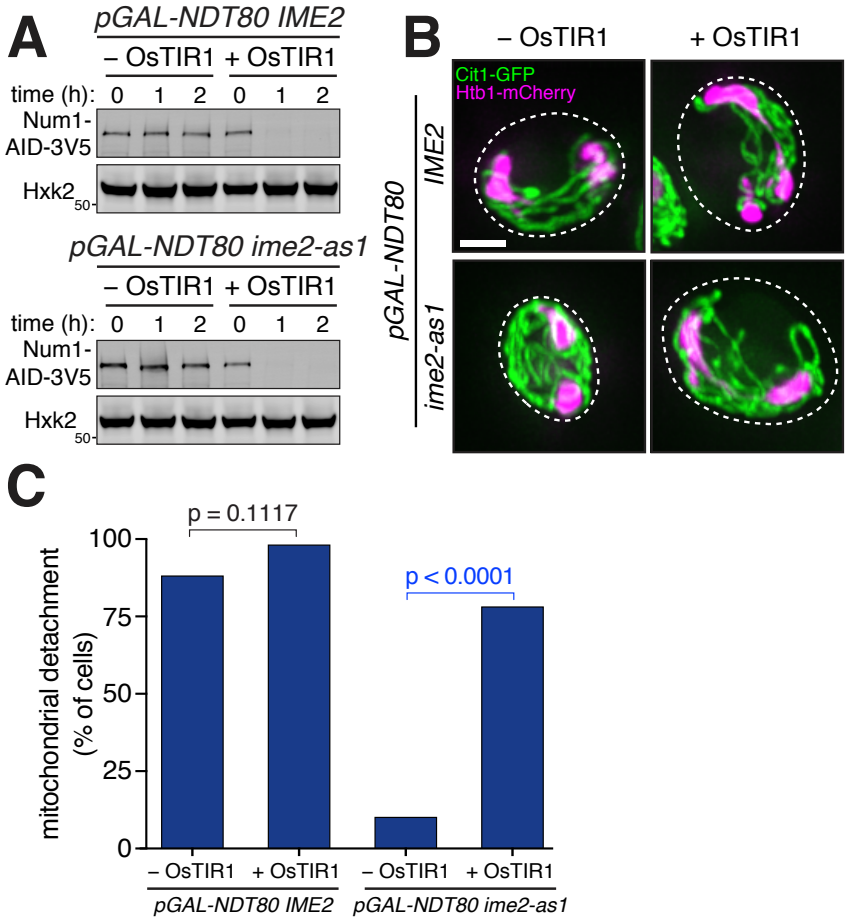

Figure 2.12. Ime2 promotes mitochondrial detachment through MECA destabilization. *pGAL-NDT80 GAL4.ER* cells without OsTIR1 (UB17552) and with *pCUP1-OsTIR1* (UB17548) as well as *pGAL-NDT80 GAL4.ER ime2-as1* cells without OsTIR1 (UB17554) and with *pCUP1-OsTIR1* (UB17550) were induced to sporulate. Then, 1 µM ß-estradiol and 20 µM 1-NA-PP1 were added to the cultures at 5 h. At 6.5 h, 50 µM $CuSO_4$ and 500 µM 3-indoleacetic acid (auxin) were added. **A.** Immunoblot showing Num1-AID-3V5 depletion. Hxk2, loading control. Time indicates hours after addition of auxin and $CuSO_4$ at 6.5 h, a time at which Num1 protein level is already reduced. By band quantification normalized to loading, Num1-AID-3V5 is 2.3x higher in level in *ime2-as1* (no OsTIR1) compared to the wild-type control (no OsTIR1). Num1-AID-3V5 runs above the highest (190 kDa) ladder band. **B.** Maximum intensity projections of cells fixed 2 h after auxin and

$CuSO_4$ addition. Mitochondria, Cit1-GFP. Nuclei, Htb1-mCherry. **C.** Quantification of the frequency of mitochondrial detachment among cells fixed 2 h after auxin and $CuSO_4$ addition. Analysis was restricted to cells that had entered the meiotic divisions. Fisher's exact test p = 0.1117 (*IME2* –OsTIR1 vs. *IME2* +OsTIR1) and p < 0.0001 (*ime2-as1* –OsTIR1 vs. *ime2-as1* +OsTIR1). *n* = 50 cells per genotype. Scale bar, 2 μm.

If Ime2 acts through MECA to promote mitochondrial detachment, then removal of MECA should restore normal mitochondrial dynamics to Ime2-inhibited cells. In order to test this hypothesis, we engineered a version of Num1 that can be degraded in an Ime2-independent manner (Figure 2.12), using the auxin-inducible degron system (Nishimura et al., 2009). We found that forced destruction of Num1 rescued the mitochondrial detachment defect observed in *ime2-as1* cells (Figure 2.12, B and C), highlighting Num1 as a key Ime2 target that is responsible for altering mitochondrial distribution during meiosis.

2.3 Discussion

2.3.1 Regulated destruction of an organelle tether acutely changes intracellular organization

In this study, we have shown that organelle morphogenesis during cellular differentiation can be accomplished by programmed removal of organelle tethers. The mitochondria-ER-cortex anchor (MECA), which normally localizes to and maintains contact sites between mitochondria and the plasma membrane, is inactivated in meiosis II. As a consequence, mitochondria detach from the plasma membrane in a temporally coordinated manner. Mitochondrial detachment is regulated by the meiosis-specific kinase Ime2, which phosphorylates MECA and promotes its destruction (Figure 2.13). Altogether, our study defines a key mechanism that coordinates mitochondrial dynamics with meiotic progression and demonstrates that organelle remodeling can be mediated by posttranslational regulation of organelle tethers.

In vegetative growth, MECA assembly in daughter cells is regulated during the cell cycle (Kraft and Lackner, 2017). Num1 exists in at least two distinct populations, one of which is independent of mitochondria and anchors cytoplasmic dynein at the bud tip (Omer et al., 2018). It is not clear, however, whether vegetative cells regulate the disassembly of MECA in any meaningful way. Once MECA is assembled, it is a very stable anchor: by FRAP, no appreciable recovery was observed for over 20 min (Kraft and Lackner, 2017). Thus, it appears that MECA is a source of stability for an organelle that is otherwise highly dynamic in its

architecture (Friedman and Nunnari, 2014; Mishra and Chan, 2014; Westermann, 2014).

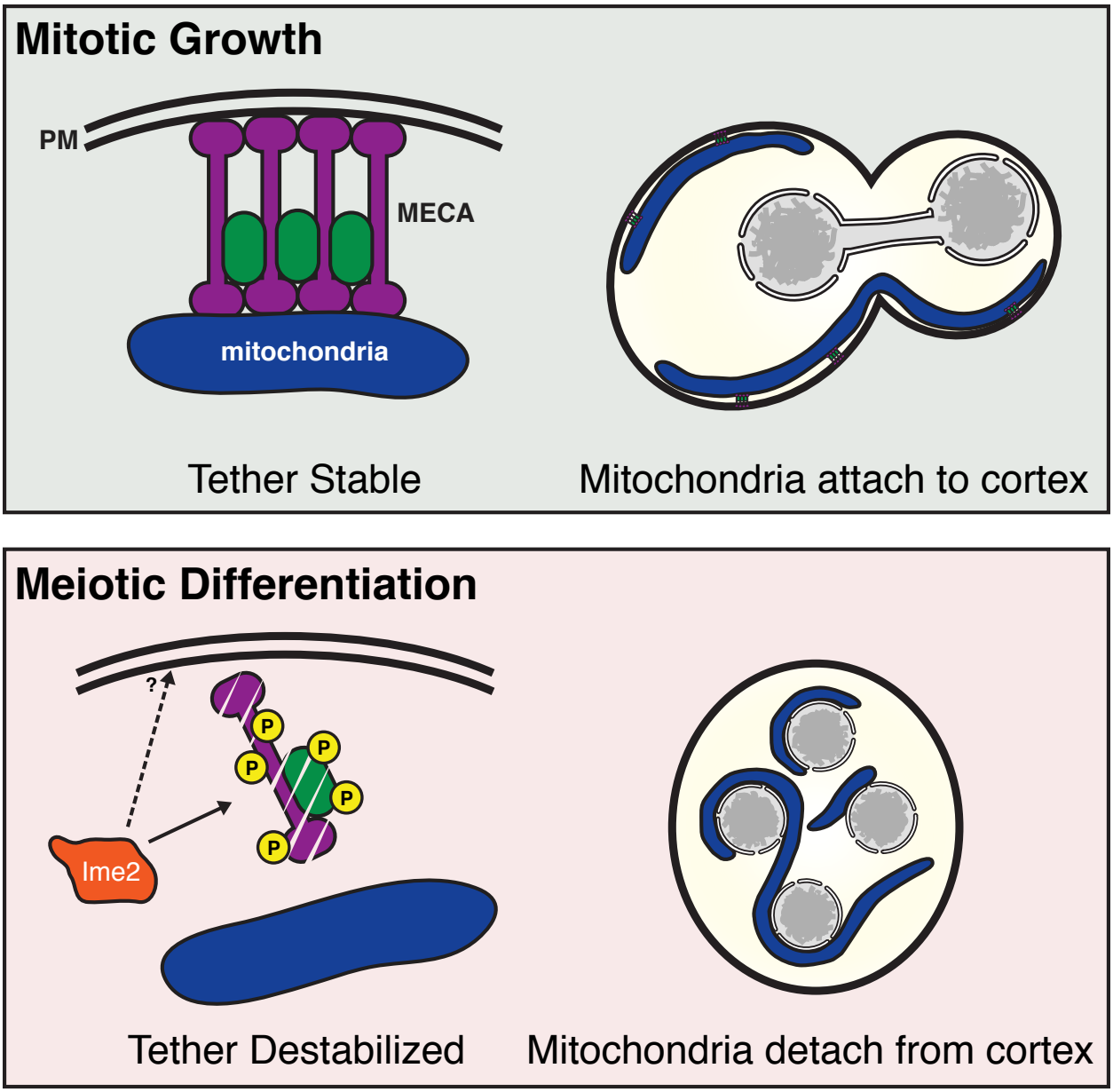

Figure 2.13. Mitochondrial inheritance in mitosis and meiosis. In mitosis, mitochondria remain associated with the cell cortex due to the mitochondria-plasma membrane anchoring activity of MECA. In meiosis, mitochondrial organization is remodeled: mitochondria detach from the plasma membrane and are transmitted to spores. This meiosis-specific mitochondrial remodeling is due to inhibition of MECA by Ime2. As a result of Ime2-dependent phosphorylation, MECA is destroyed and mitochondrial tethering is lost. PM, plasma membrane.

During meiosis, MECA undergoes temporally coordinated disassembly. The timing of MECA destruction is determined by the level of Ime2 activity, which in turn is controlled by the meiotic transcription factor Ndt80. Our study demonstrates that an organelle tether can be developmentally regulated and reveals how this regulation could impact organelle remodeling. A similar principle might apply to other organelles and different developmental contexts.

In meiotic cells, the cortical ER detaches from the plasma membrane in a manner highly reminiscent of mitochondrial detachment (Suda et al., 2007). MECA destruction probably does not explain this behavior. Although ER has been observed in association with MECA by light microscopy and co-immunoprecipitation (Lackner et al., 2013), electron microscopy analysis did not reveal a significant association (Klecker et al., 2013). Additionally, in neither case was it suggested that MECA acts to tether the ER to the plasma membrane. However, it has been recently shown that ER-plasma membrane anchoring proteins, Scs2/22, drive the assembly of a subset of MECA structures (Omer et al., 2018). Therefore it is possible that loss of *SCS2* and/or *SCS22* function during meiosis could also contribute to MECA disassembly, though this perturbation alone is unlikely to explain the full extent of meiotic ER remodeling. ER-plasma membrane contacts are established by additional factors, including Tcb1/2/3 and Ist2, which act redundantly with Scs2/22 (Manford et al., 2012). Based on the finding that removal of any one tether or class of tethers was insufficient for detachment of cortical ER from the plasma membrane, it would appear that meiotic cells have to simultaneously target multiple tethers in order to disrupt ER-plasma membrane contacts. Alternatively, changes intrinsic to the ER or plasma membrane, such as protein or lipid composition, might explain these phenomena. Interestingly, the plasma membrane pool of the lipid phosphatidylinositol 4,5-bisphosphate (PIP_2) is depleted in late meiosis, instead accumulating on prospore membranes (Rudge et al., 2004).

2.3.2 Ime2 is a key regulator of mitochondrial dynamics in meiosis

Our studies reveal a distinct and unanticipated function for Ime2 during meiosis II: regulation of the mitochondria-plasma membrane tether, MECA. Our data support a model in which Ime2 triggers MECA destruction by promoting the phosphorylation of its subunits, thereby causing acute changes in mitochondrial organization (Figure 2.13). Several observations are consistent with this model: First, Ime2 phosphorylates both MECA subunits *in vitro*. Second, inactivation of Ime2 causes stabilization of MECA subunits, persistence of MECA clusters, and retention of contacts between mitochondria and the plasma membrane throughout meiosis. Third, expression of a hyperactive *IME2* allele in prophase I leads to Num1

phosphorylation and results in the premature disassembly of MECA and untimely mitochondrial detachment. Finally, degradation of Num1 by artificial means rescues the mitochondrial detachment defect that occurs in *IME2* inactivated cells. Our data, however, do not rule out the possibility that Ime2 can also influence MECA in an indirect manner (Figure 2.13), for instance through its effect on other, yet to be identified, MECA regulators.

Ime2-dependent destruction of MECA shares similarities with another critical meiotic event: clearance of the translational repressor Rim4. Rim4 assembles into amyloid-like aggregates, which are thought to sequester a group of mRNAs away from ribosomes by binding to their 5' untranslated regions (Berchowitz et al., 2013; Berchowitz et al., 2015; Carpenter et al., 2018). Degradation of Rim4 during meiosis II relieves the translational repression of its targets. Similar to MECA, high Ime2 kinase activity is both necessary and sufficient to disassemble Rim4 aggregates and promote their degradation (Berchowitz et al., 2013; Berchowitz et al., 2015; Carpenter et al., 2018). Rim4 contains a total of 114 serine and threonine residues (S/Ts). Although the initial mass spectrometry suggested the existence of a single Ime2-dependent phosphorylation site, subsequent work identified 39 additional phosphorylation sites. Clearance of Rim4 assemblies is governed by multi-site phosphorylation, with at least 36 S/Ts required for its degradation. Importantly, a threshold amount of phosphorylation, rather than modification of critical residues, is necessary for Rim4 clearance (Carpenter et al., 2018). By comparison, Num1 contains 356 S/Ts. Thus far, mass spectroscopy identified four phosphorylated residues in Num1, one of which appears to be Ime2-dependent. However, this number is likely to be an underestimate, because the peptide coverage for Num1 was less than 60% in our immunoprecipitation-mass spectrometry (IP-MS) analysis. Moreover, unlike the Rim4 IP-MS, our experiments did not include a phospho-peptide enrichment step due to the low expression level of Num1. Adding further to the complexity is the observation that the second MECA subunit, Mdm36, also appears to be phosphorylated by Ime2. Therefore, MECA control by Ime2 is likely to be complex. More thorough analysis will be required to elucidate how phosphorylation affects MECA stability, mitochondrial organization, and inheritance.

2.3.3 Mitochondrial inheritance during gametogenesis

How does mitochondrial detachment lead to meiosis-specific inheritance of the organelle? In budding yeast, mitochondria exhibit four distinct behaviors during meiotic differentiation: (i) abrupt detachment from the mother cell plasma membrane, followed by (ii) extensive contacts with the gamete nuclei, (iii) limited inheritance, and (iv) programmed elimination. Previous electron microscopy data suggested that only about half of the starting mitochondrial population is inherited by the four gametes (Brewer and Fangman, 1980). The remaining mitochondria are eliminated by mega-autophagy that commences at the end of gametogenesis

(Eastwood et al., 2012; Eastwood and Meneghini, 2015). It will be interesting to determine if the two populations of mitochondria, namely the inherited and discarded, are different from one another and whether quality control pathways exist to selectively transmit healthier mitochondria to gametes (Kraft and Lackner, 2018; Neiman, 2011). Perhaps the ability of mitochondria to form direct contact sites with the nuclear envelope, evident in Figure 2.2 and in previous studies (Stevens, 1981; Suda et al., 2007), is part of this selection. Regardless, we propose that the contact sites between mitochondria and nuclear envelope ensure that the mitochondrial genome is inherited during yeast gametogenesis. We further posit that the regulated detachment of mitochondria from the progenitor cell plasma membrane in meiosis II is the first step towards mitochondrial segregation into gametes. Identifying the molecular nature of the mito-nuclear contact sites and their regulation will enhance our understanding of mitochondrial inheritance during meiotic differentiation.

Gametogenesis-specific changes to mitochondrial architecture and inheritance are ubiquitous in metazoan germ cells. For example, primary oocytes of animals contain a unique structure known as the Balbiani body that assembles adjacent to the nucleus (Kloc et al., 2004). The Balbiani body houses a collection of organelles, including mitochondria as well as protein–RNA inclusions, and facilitates their segregation. In *Drosophila* oogenesis, mitochondria are transported between cells, from nurse cells to the oocyte, via a polarized microtubule network that passes through ring canals (Cox and Spradling, 2003). Later, mitochondria are actively tethered to the actin cytoskeleton at the posterior of the oocyte, in proximity to the pole cells that give rise to the germline. Importantly, in the absence of tethering, mtDNA transmission is compromised (Hurd et al., 2016). Although sperm contain mitochondria to meet metabolic demands, they do not transmit genetic information to the zygote. In *Drosophila*, mtDNA is actively destroyed during spermatogenesis (DeLuca and O'Farrell, 2012). In mice, sperm mitochondria are delivered to the zygote, but are depolarized, unable to fuse to maternal mitochondria, and are specifically eliminated by mitophagy (Rojansky et al., 2016). Clearly, mitochondria undergo a plethora of changes during metazoan gametogenesis, which share striking similarities to that observed in budding yeast gametogenesis: namely, nuclear-mitochondrial interactions and programmed mitochondrial elimination. We speculate that the evolutionary conservation of meiotic differentiation between budding yeast and metazoans extends beyond homologous recombination and meiotic chromosome segregation.

Understanding the molecular basis of meiotic specializations to mitochondria is important not only to enhance our understanding of the organelle's physiology but also for its potential impact on human disease and healthspan. It is widely observed that mitochondrial functions decline with age, yet gametogenesis, at least in budding yeast and *C. elegans*, eliminates age-induced cellular damage (Bohnert and Kenyon, 2017; Goudeau and Aguilaniu, 2010; Unal et al., 2011). Therefore, studying

mitochondria in the context of gametogenesis could aid in the development of strategies to counteract mitochondrial dysfunction and disease.

Chapter 3

Nucleus-mitochondria tethering in gametogenesis

3.1 Introduction

Tethers promote the interaction of organelles at specialized domains called membrane contact sites (Eisenberg-Bord et al., 2016; Gatta and Levine, 2017; Lackner, 2019; Prinz, 2014; Scorrano et al., 2019). Through extensive studies in yeast and mammalian cells, a large number of tethers has been identified that together specify a variety of organelle-organelle interactions (Eisenberg-Bord et al., 2016).

Gametogenesis is a cellular differentiation program that involves extensive cellular remodeling. In yeast, gametogenesis appears to involve novel organelle segregation mechanisms, as the morphologies of organelles in gametogenesis are distinct (Fuchs and Loidl, 2004; Gorsich and Shaw, 2004; King et al., 2019; Miyakawa et al., 1984; Roeder and Shaw, 1996; Stevens, 1981; Suda et al., 2007). We previously found that mitochondrial dynamics in meiosis are actively regulated by differentiation factors. Mitochondria detach from the plasma membrane through developmentally regulated proteolysis of an organelle tether (Chapter 2). We (Chapter 2) and others (Gorsich and Shaw, 2004; Miyakawa et al., 1984; Stevens, 1981; Suda et al., 2007) have previously noted that detached mitochondria gain association with the nuclei. However, the basis of this apparently developmentally cued membrane contact site is completely unknown.

Here, we characterized the nucleus-mitochondria contact site in gametogenesis. By light and electron microscopy, we observed that mitochondria form extensive contacts with the nuclear envelope. We determined that nucleus-mitochondria tethering requires the transcription factor Ndt80, indicating that it is developmentally regulated. In contrast to our prior work that found a critical role for Ime2 in regulating the cortical detachment of mitochondria, nucleus-mitochondria tethering was Ime2-independent. We also examined two known ER-mitochondria tethers—ERMES and Ltc1/Lam6—and provide evidence that disfavors a role in this phenomenon, suggesting the involvement of novel factors.

3.2 Results

3.2.1 Mitochondria co-localize with nuclei in meiosis II

To analyze the localization of mitochondria during different stages of meiosis, we labeled mitochondria with Cit1-GFP and stained with DAPI to visualize nuclei. Consistent with the findings presented in Chapter 2, we found that mitochondria localized to the cell cortex in premeiotic cells and during meiotic prophase I (Figure 3.1A). During meiosis II, mitochondria detached from the plasma membrane and gained association with the nuclear periphery (Figure 3.1A), again consistent with findings presented in Chapter 2 and in previous studies (Gorsich and Shaw, 2004; Miyakawa et al., 1984; Suda et al., 2007). Later, a subset of mitochondria were

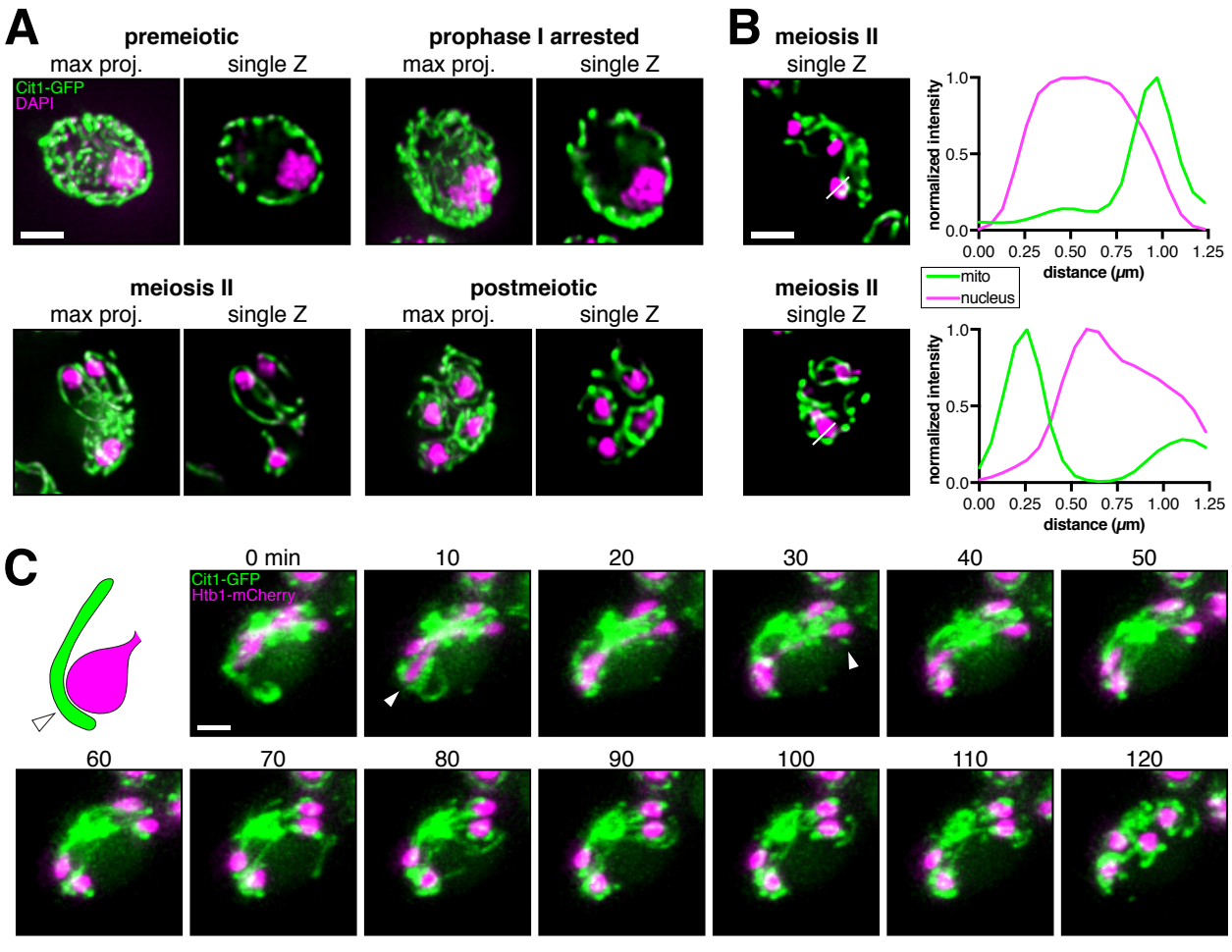

Figure 3.1. Mitochondria co-localize with nuclei in meiosis II. A. Localization of mitochondria relative to the nucleus in different stages of meiosis. *pGAL-NDT80 GAL4.ER* cells (UB10397) were induced to sporulate. Then, after arrest in prophase I for 5 h, cells were released into the meiotic divisions by addition of 1 μM ß-estradiol. Mitochondria, Cit1-GFP. Nuclei, DAPI. Maximum intensity projections (max proj.) or single planes of focus (single Z) of fixed cells are shown. **B.** Linescan analysis of two additional fixed meiosis II cells from the experiment in (A). The lines representing the plotted values are drawn on the micrographs. Fluorescence

intensities are shown scaled to the maximum value for each fluorescent marker for each cell. **C.** Cartoon depicting a mitochondrial tip associating with a nuclear lobe. Movie montage of a live cell (UB10254) undergoing meiosis II. Cit1-GFP, mitochondria. Htb1-mCherry, nuclei. Arrowheads indicate the initiation of a stable nucleus-mitochondria interaction. In the final frame, the nuclei shift positions. Scale bars, 2 μm.

---

tightly associated with gamete nuclei, while some were more distant. The former population will be inherited, while the latter will be discarded (Eastwood and Meneghini, 2015). The proximity between mitochondria and nuclei was striking, as this interaction is not observed during vegetative growth or in earlier stages of meiosis. To verify that mitochondria associate closely with the nuclear envelope, we performed linescan analysis in meiosis II cells. Consistent with the notion that mitochondria tightly associate with the nuclear surface, our analysis indicated a very tight association between Cit1-GFP and DAPI signal in meiosis II cells (Figure 3.1B). Our results indicate that mitochondria associate with the meiosis II nuclei and may form a membrane contact site.

If nucleus-mitochondria associations are a *bona fide* membrane contact site, it might be expected that individual contact sites are stable over time. To test this possibility, we examined the localization of mitochondria (Cit1-GFP) and nuclei (Htb1-mCherry) by time-lapse imaging of live cells. Often, a nascent contact site would be marked by a distinct mitochondrial tubule that remained in contact for long periods of time (Figure 3.1C). In the cell shown, the first nucleus-associated mitochondrial tubule (arrowhead, 10 min) remained associated for nearly 2 h, after which the nuclei change position due to completion of cell division (Figure 3.1C). These results resemble what was found in previous work that examined the mitochondria-plasma membrane contact site. During vegetative growth, the mitochondria-plasma membrane contact site and its tether, Num1, can persist for at least ~30 min (Kraft and Lackner, 2017), and perhaps much longer. In most other regions of the cell, mitochondria are highly dynamic and continually remodeled by fusion, fission, and directed movement. Our analysis indicates that mitochondria initiate stable contacts with the nucleus in meiosis II.

3.2.2 Mitochondria and the nuclear envelope form a membrane contact site

Our results so far suggest that mitochondria likely form a membrane contact site with the nucleus during meiosis II. However, the spatial resolution limit intrinsic to conventional light microscopy precluded us from determining with precision the extent of nucleus-mitochondria contact. To analyze the ultrastructure of mitochondria and nuclei during meiosis II, we subjected highly synchronized cell

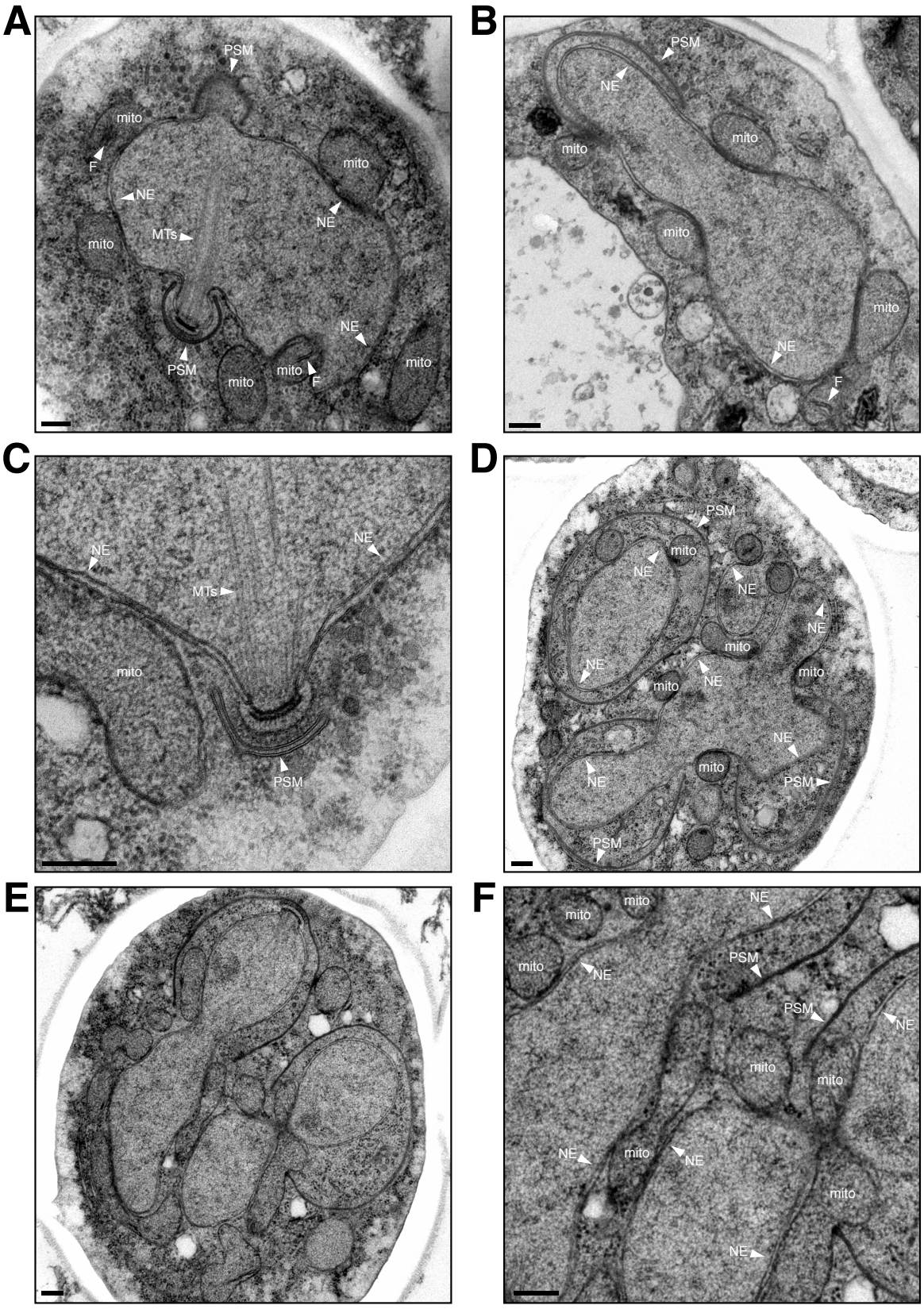
A
PSM
mito
F
NE
mito
NE
MTs
mito
NE
PSM
mito
mito
F
mito
B
PSM
NE
mito
mito
mito
mito
NE
F
C
NE
NE
MTs
mito
PSM
D
PSM
mito
NE
NE
NE
mito
NE
mito
NE
mito
NE
NE
mito
PSM
PSM
E
F
mito
mito
NE
mito
NE
PSM
PSM
NE
mito
mito
NE
mito
NE
mito
NE

Figure 3.2. A nucleus-mitochondria contact site forms during gametogenesis. Transmission electron micrographs of *pGAL-NDT80 GAL4.ER* (UB7055) cells in meiosis II. To obtain synchronous meiosis II cultures, cells were arrested in prophase I for 5 h, then synchronously released into the meiotic divisions by addition of 1 μM ß-estradiol. Progression to meiosis II was monitored by microscopy, and cells were harvested by filtration and high-pressure freezing ~3 h after *pGAL-NDT80* induction (see Appendix B). Note that cristae are not visible in this preparation method. **A-C.** Early meiosis II cells, where prospore membranes are small and have not captured any mitochondria. **A.** Note the two nascent prospore membranes joined by spindle microtubules. The spindle pole body associated with the lower prospore membrane is visible. Some mitochondria contain filamentous structures ("F") of unknown origin. **B.** A cell with a small but growing prospore membrane. Note the distortion of the nucleus by the elongating spindle. A filamentous structure ("F") is visible in the lower mitochondrion. Electron density is present at some nucleus-mitochondria contact sites. **C.** High magnification view of an early meiosis II spindle pole and nucleus-associated mitochondria. Note the spindle pole body where microtubules and nascent prospore membranes are joined. Spherical membrane structures are vesicle precursors of the prospore membrane. **D-F.** Late meiosis II cells, where prospore membranes are large and contain mitochondria. **D.** Late meiosis II cell with elaborate nuclear envelope architecture and associated mitochondria. Note that only a subset of the abundant mitochondria are labeled. Electron dense material is often visible at nucleus-mitochondria contact sites. **E.** Late meiosis II cell and **F.** inset of cell in (E). mito, mitochondria. NE, nuclear envelope. PSM, prospore membrane. MTs, microtubules. F, filaments. Scale bars, 200 nm.

---

populations to high-pressure freezing and freeze substitution. We prepared samples for transmission electron microscopy by thin sectioning of resin-embedded specimens. We found that mitochondria formed abundant contact sites with the nuclear envelope (Figure 3.2; (Stevens, 1981)). Mitochondria were present at the nuclear surface much more frequently than they were present at the plasma membrane or other regions of the cytoplasm. In many cases, elevated electron density was also visible at the contact sites. We also noticed electron-dense filamentous structures present in many mitochondria (Figure 3.2, A, B, and D; Figure 3.4). Although the nature of these filaments is unclear, filamentous structures in yeast mitochondria have recently been noted in electron cryotomograms from vegetative yeast cells (Gan et al., 2019). In any case, the abundance of nucleus-mitochondria contact sites indicates a dramatic shift in localization of the mitochondrial network from the plasma membrane to the nuclear envelope.

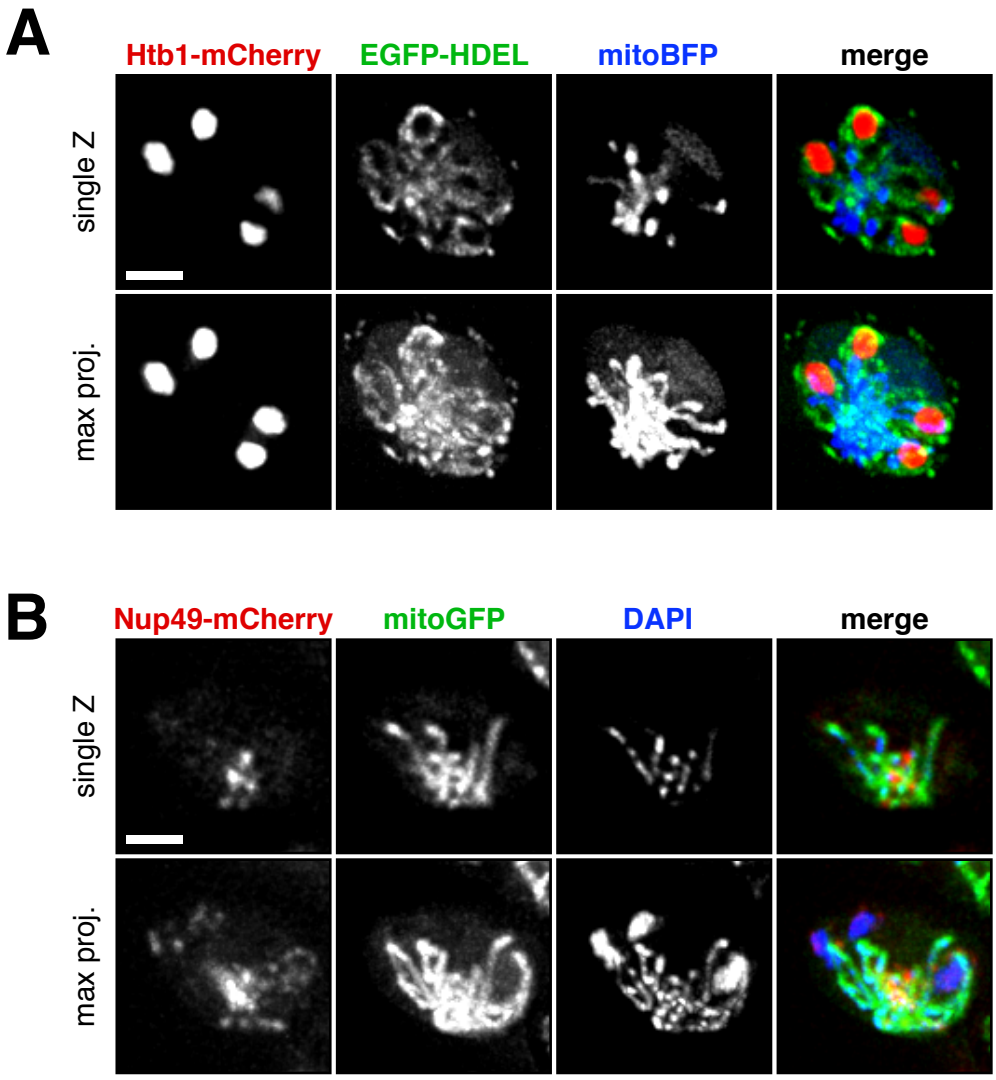

Figure 3.3. Localization of mitochondria in relation to the ER and nuclear pore complexes in meiosis II. Single plane of focus and maximum intensity projections of fixed cells in meiosis II. **A.** A cell (UB7436) expressing markers for nuclei (Htb1-mCherry), ER (EGFP-HDEL), and mitochondria (mitoBFP). **B.** A cell (UB7103) expressing markers for the nuclear pore complex (Nup49-mCherry) and mitochondria (mitoGFP) and stained with DAPI. Note that in the single plane of focus image, only DAPI staining of mtDNA is visible. Scale bars, 2 μm.

During meiosis II, the membrane that will become the plasma membrane of the gamete cells begins to form. This membrane, called the prospore membrane, is nucleated at the spindle pole body. At the meiosis I-meiosis II transition, the

spindle pole body is modified on its cytoplasmic face to facilitate membrane generation by vesicle fusion (Bajgier et al., 2001; Knop and Strasser, 2000; Neiman, 1998; Neiman, 2005). A previous electron microscopy study observed cases where mitochondria were held adjacent to the nuclear envelope as if "sandwiched" between the prospore membrane and the nuclear envelope (Suda et al., 2007). In our analysis, nucleus-mitochondria contact sites were evident even in stages of meiosis II where the prospore membrane had only just begun to form (Figure 3.2, A-C). In cells where the nucleation of the prospore membrane was visible, but where no mitochondria had been inherited by gametes, nucleus-mitochondria contact sites were widely visible (Figure 3.2, A-C). Our results indicate that mitochondria contact the nuclei prior to their segregation to gametes, rather than the reverse model where inherited mitochondria are confined to the perinuclear region.

We next examined cells at later stages of meiosis II. Much like the earlier stages, these cells exhibited abundant nucleus-mitochondria contact sites (Figure 3.2, D-F). In cells where the prospore membrane was extended and enclosed a large lobe of the nucleus, we also observed inheritance of mitochondria. The segregated mitochondria remained tethered to the nuclei, indicating that nucleus-mitochondria tethering persists past the point of initial mitochondrial segregation into gametes. In the late meiosis II cells, the nuclear geometry was heavily distorted. This nuclear expansion may be due at least in part to the need to accommodate two elongated spindles within a single nucleus (Suda et al., 2007), as well as the active segregation of nuclear lobes to gametes.

It is important to note that DNA or chromatin fluorescent markers do not label the regions of the nuclei devoid of chromosomes. At later stages of meiosis II, when chromosomes are clustered at the spindle poles, this volume likely comprises a significant amount of the nucleus. Therefore, the light microscopy analysis in Figure 3.1 may underestimate the true extent of nucleus-mitochondria contact. To address this limitation, we also examined the localization of mitochondria with respect to the ER and to the nuclear pore complex in meiosis II cells (Figure 3.3). Consistent with previous studies (Suda et al., 2007), we found that the cortical ER was reduced in extent in meiosis II, with ER accumulating in a region in between the dividing nuclei. Remarkably, this same region invariably contained the detached mitochondrial network (Figure 3.3A). As the same EGFP-HDEL marker also labels the lumen of the nuclear envelope, we expect that a subset of the signal corresponds to nuclear envelope. To further analyze this possibility, we examined the localization of nuclear pore complexes in relation to mitochondria. As reported in previous studies (Fuchs and Loidl, 2004; King et al., 2019), nuclear pore complexes, as labeled by Nup49-mCherry, localized predominantly away from the meiosis II chromatin masses in a central region of the cell (Figure 3.3B). This region was also crowded with mitochondria, implying contact between mitochondria and the nuclear envelope that is distant from the chromosomes. We conclude that mitochondria are predominately localized to nucleus-mitochondria contact sites in

meiosis II, and that these contact sites likely extend to non-chromatin-containing regions of the nucleus and perhaps also the ER.

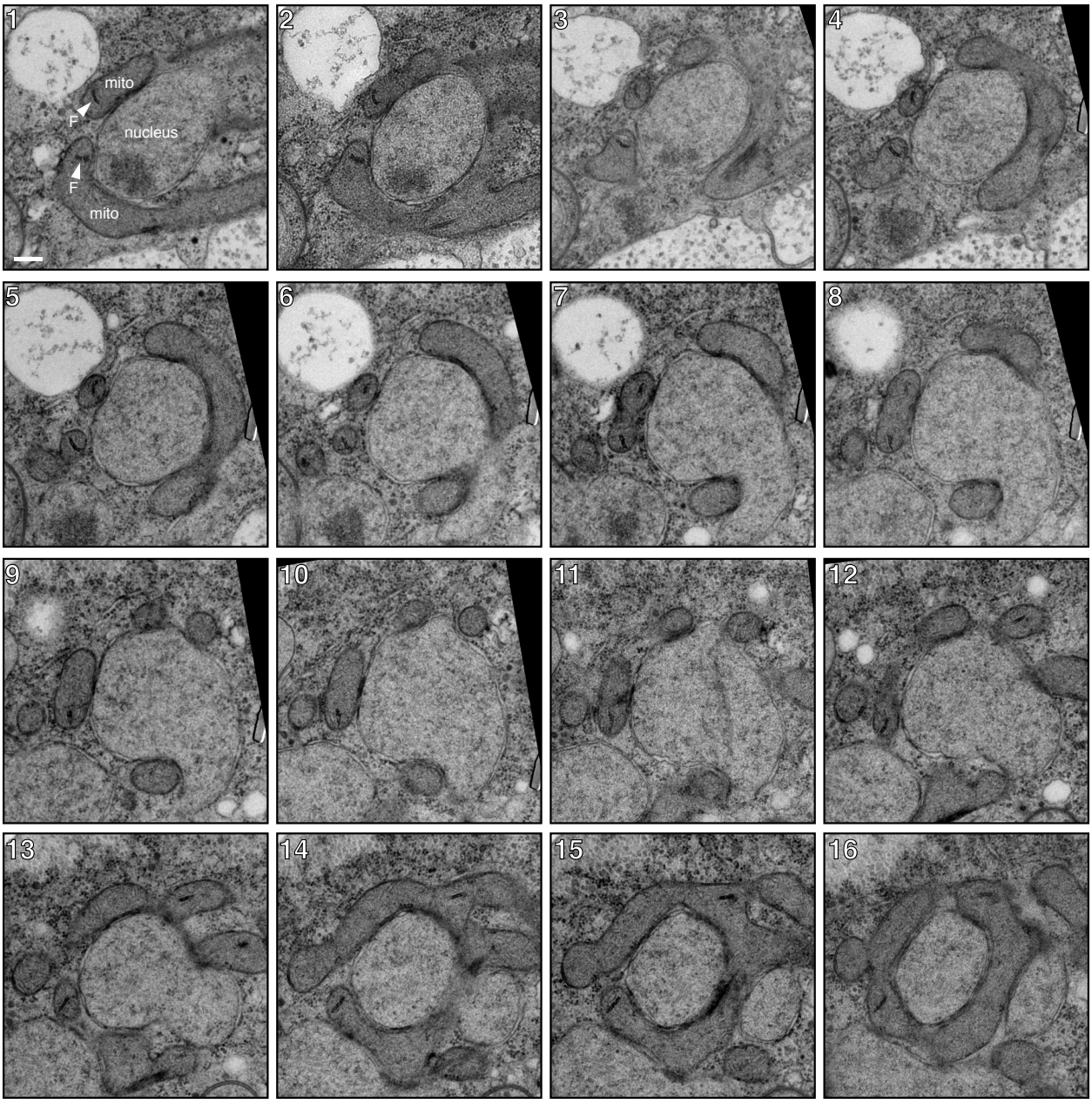

Figure 3.4. The nucleus-mitochondria contact site is extensive over long distances (case 1). Serial section transmission electron micrographs of a UB7055 cell in meiosis II, prepared from the experiment in Figure 3.2. Numbers indicate the section number in the series. Each section was 60 nm thick. Labels in the first section indicate nucleus and mitochondria. Note the abundant filaments in mitochondria and electron density at contact sites. F, filaments. Scale bar, 200 nm.

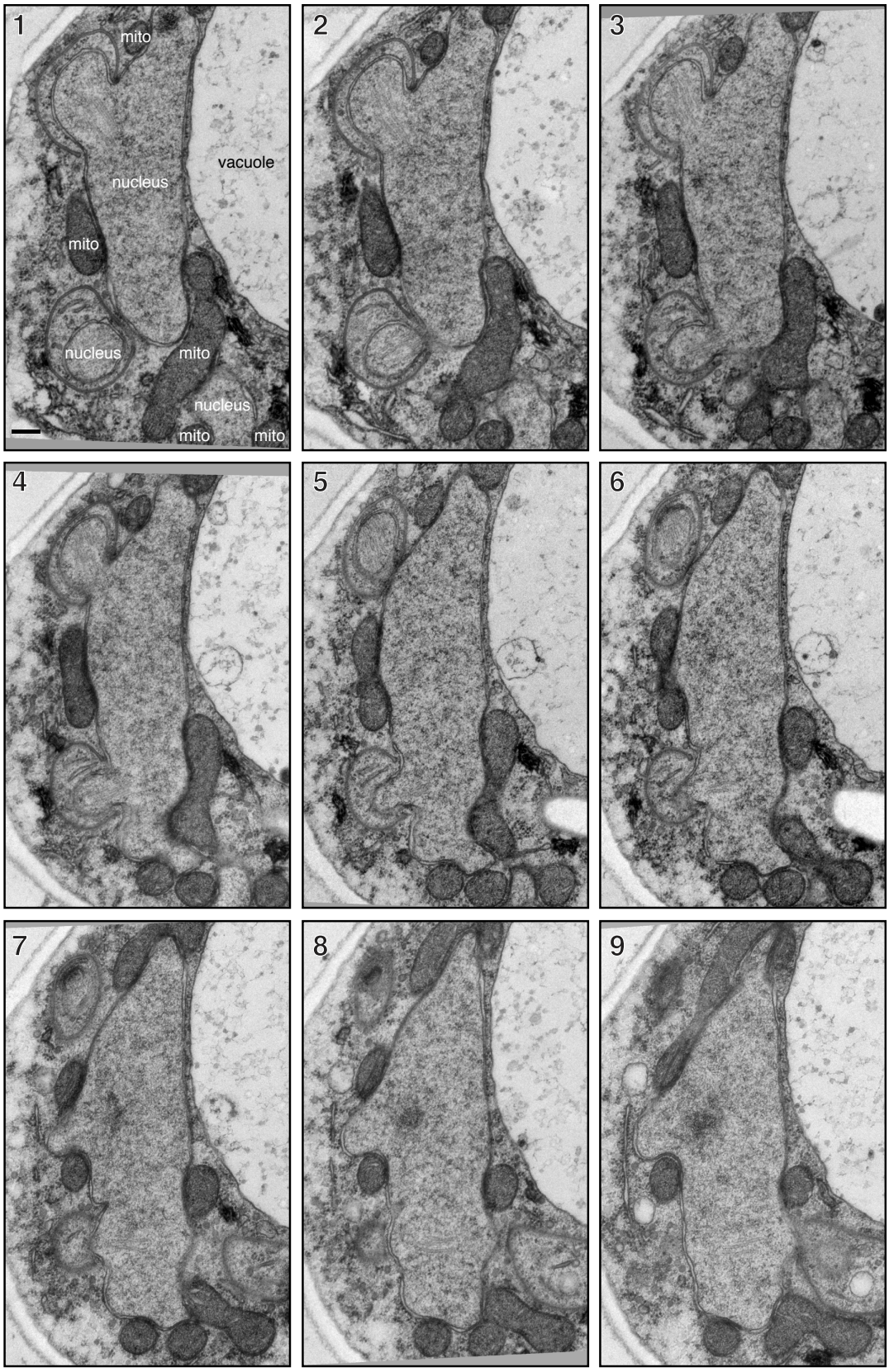

Figure 3.5. The nucleus-mitochondria contact site is extensive over long distances

(case 2). Serial section transmission electron micrographs of a UB7055 cell in meiosis II, prepared from the experiment in Figure 3.2. Numbers indicate the section number in the series. Each section was 60 nm thick. Labels in the first section indicate major organelles. Scale bar, 200 nm.

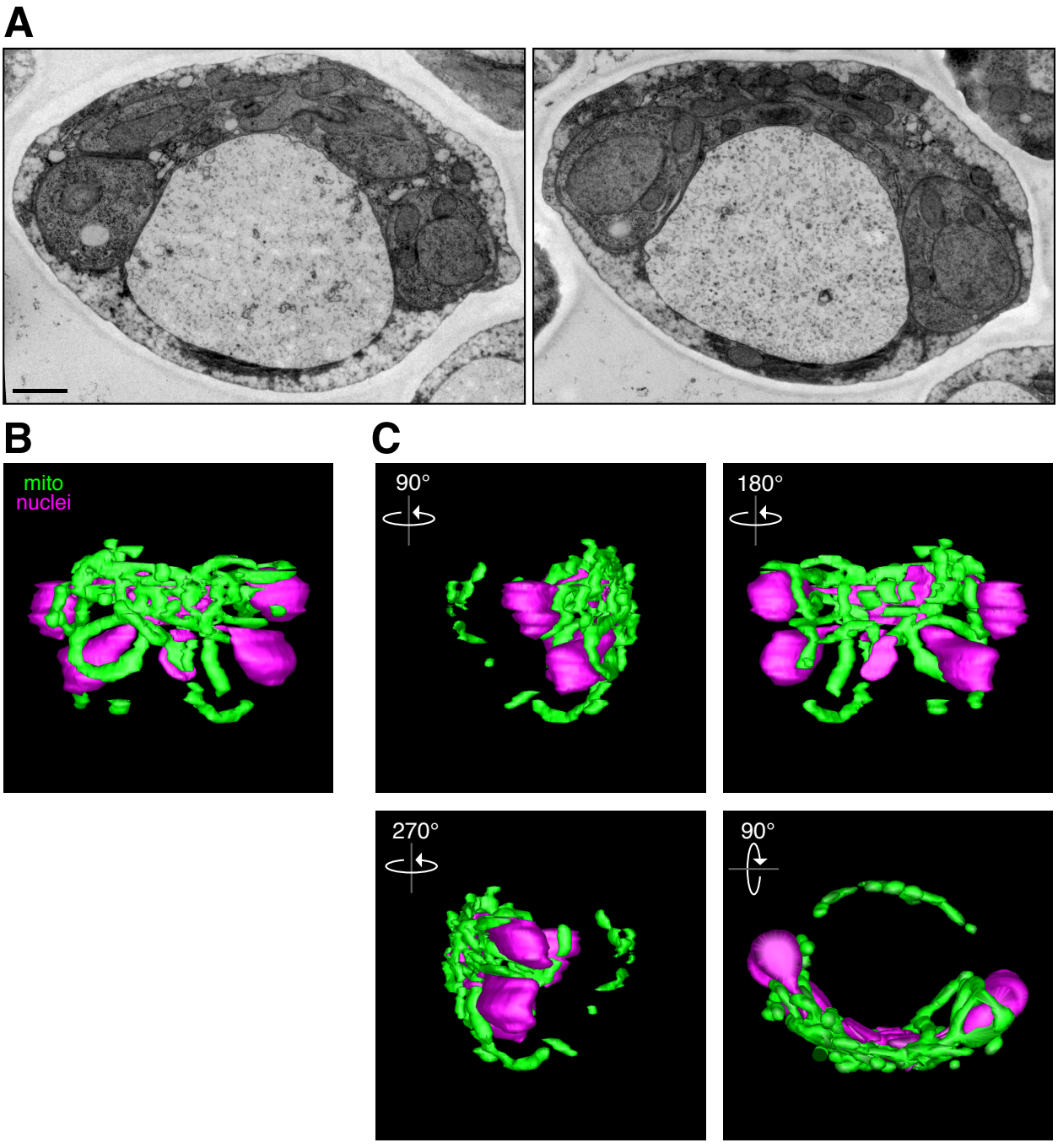

Figure 3.6. Nucleus-mitochondria contact sites extend across the nuclear surface cell-wide. 3D reconstruction of serial section transmission electron micrographs of a

UB7055 cell in meiosis II, prepared from the experiment in Figure 3.2. 57 sections, each 60 nm thick, were used to reconstruct the entire cell volume that contained prospore membranes. Three adjacent sections were missing and interpolated in the final model. **A.** Transmission electron micrographs of two serial sections used in the 3D reconstruction. Scale bar, 600 nm. **B.** The 3D reconstruction. Mitochondria, green. Nuclei, magenta. **C.** Views of the 3D model rotated in space relative to (B).

To further understand the spatial nature and extent of nucleus-mitochondria contact sites at the ultrastructural level, we analyzed the synchronous meiosis II specimens by serial section transmission electron microscopy. This approach allows for 3D electron microscopy. We examined two nuclear regions containing contact sites with mitochondria where prospore membranes were distant (Figures 3.4 and 3.5). In both cases, we observed mitochondria wrapping around the nuclear envelope over considerable distances in three dimensions (Figures 3.4 and 3.5). Electron-dense material was also visible at many of the contact sites. In each case, we observed persistent contact sites over a large number of 60-nm sections: 16 sections, or 960 nm (Figure 3.4), and 9 sections, or 540 nm (Figure 3.5), as well as over considerable distances in the XY plane of each section. In contrast, ER-mitochondria contact sites associated with mitochondrial division in vegetative cells are much more limited in their extent (Friedman et al., 2011). We conclude that nucleus-mitochondria contact sites involve extensive wrapping of mitochondria around the nuclear envelope in space.

To determine the cell-wide extent of nucleus-mitochondria contact, we generated a whole-cell 3D reconstruction that displays segmented mitochondria and nuclear envelope across 57 serial sections (Figure 3.6). The 3D reconstructed cell contained vast nucleus-mitochondria contact. The region of the cell containing the vacuole, as well as the space near the vacuole, was essentially devoid of mitochondria. This region is the large open space in the electron micrographs in Figure 3.6A and also visible in the rotated 3D reconstructions in Figure 3.6C. Nearly the entire mitochondrial network was present on the side of the cell nearest the dividing nuclei. This behavior resembles the coalescence of mitochondria observed by light microscopy (Figures 3.1 and 3.3). Our results demonstrate that nucleus-mitochondria contact sites are abundant, persist over long distances, and capture nearly the entire mitochondrial network.

3.2.3 The nucleus-mitochondria contact site is developmentally regulated

The findings presented in Chapter 2 showed that the mitochondria-plasma membrane contact site is developmentally regulated by the meiotic program. The transcription factor Ndt80 promotes the activation of the kinase Ime2, which in turn induces degradation of the tethering complex MECA. As a nucleus-

mitochondria contact site is not observed in vegetative cells, we propose it might too be under meiosis-specific controls.

In vegetative cells, removal of Num1 leads to constitutive mitochondrial detachment and agglomeration (Lackner et al., 2013). Although no nucleus-mitochondria contacts have been reported in vegetative *num1Δ* cells, we began by addressing the possibility that removal of Num1 in meiosis might yield different behavior. Normally, Num1 degradation in meiosis is regulated by Ndt80 and Ime2 (Chapter 2). In the absence of Ndt80, cells arrest in prophase I with cortically anchored mitochondria. As Ndt80 is also responsible for the expression of many gamete differentiation genes (Cheng et al., 2018; Chu and Herskowitz, 1998; Neiman, 2011), we reasoned that Ndt80 may promote the gain of nucleus-mitochondria tethering in parallel to promoting the loss of mitochondria-cortical tethering through Num1 degradation. To test this possibility, we used the auxin-inducible degron (AID) system (Nishimura et al., 2009) to deplete Num1 from Ndt80-deficient cells. Cells depleted of Num1 contained mitochondria that agglomerated to varying degrees (Figure 3.7A). The locations of these mitochondrial agglomerations were variable, sometimes near nuclei but often in another region of the cell (Figure 3.7A). The strain containing the *NUM1-AID* tag in combination with the *pCUP1-osTIR1* transgene (but not the −osTIR1 control) exhibited mitochondrial detachment without induction. Even so, in the absence of Ndt80 no nucleus-mitochondria tethering was evident. We conclude that a Ndt80-dependent process is required for productive nucleus-mitochondria contacts after detachment of mitochondria from the cortex.

MECA stability, and by extension the mitochondria-plasma membrane contact site, is governed only indirectly by Ndt80. Ndt80 promotes MECA destruction by activating the kinase Ime2. Experimental inactivation of Ime2 during the meiotic divisions blocks mitochondrial detachment, even if Ndt80 is active (Chapter 2). Accordingly, we sought to determine whether Ime2 might *promote* nucleus-mitochondria tethering in a similar manner as it *prevents* mitochondria-plasma membrane tethering. To test the potential involvement of Ime2, we induced *pGAL-NDT80* in control cells and in cells containing the ATP analog-sensitive allele of *IME2*, *ime2-as1* (Benjamin et al., 2003; Berchowitz et al., 2013). Under these conditions, Ndt80 is partially active and cells enter the meiotic divisions but are defective in meiosis II (Benjamin et al., 2003; Berchowitz et al., 2013). Cells in the meiotic divisions contained nucleus-mitochondria contact sites, whether or not Ime2 was active (Figure 3.7B). In binucleate *ime2-as1* cells, mitochondria still contacted the nuclei (Figure 3.7B). We conclude that Ime2 is dispensable for nucleus-mitochondria contact sites.

From our previous analysis, we identified a key role for Ime2 in promoting destruction of the mitochondria-plasma membrane contact site and its tether, MECA (Chapter 2). The finding that Ime2 was not required for nucleus-

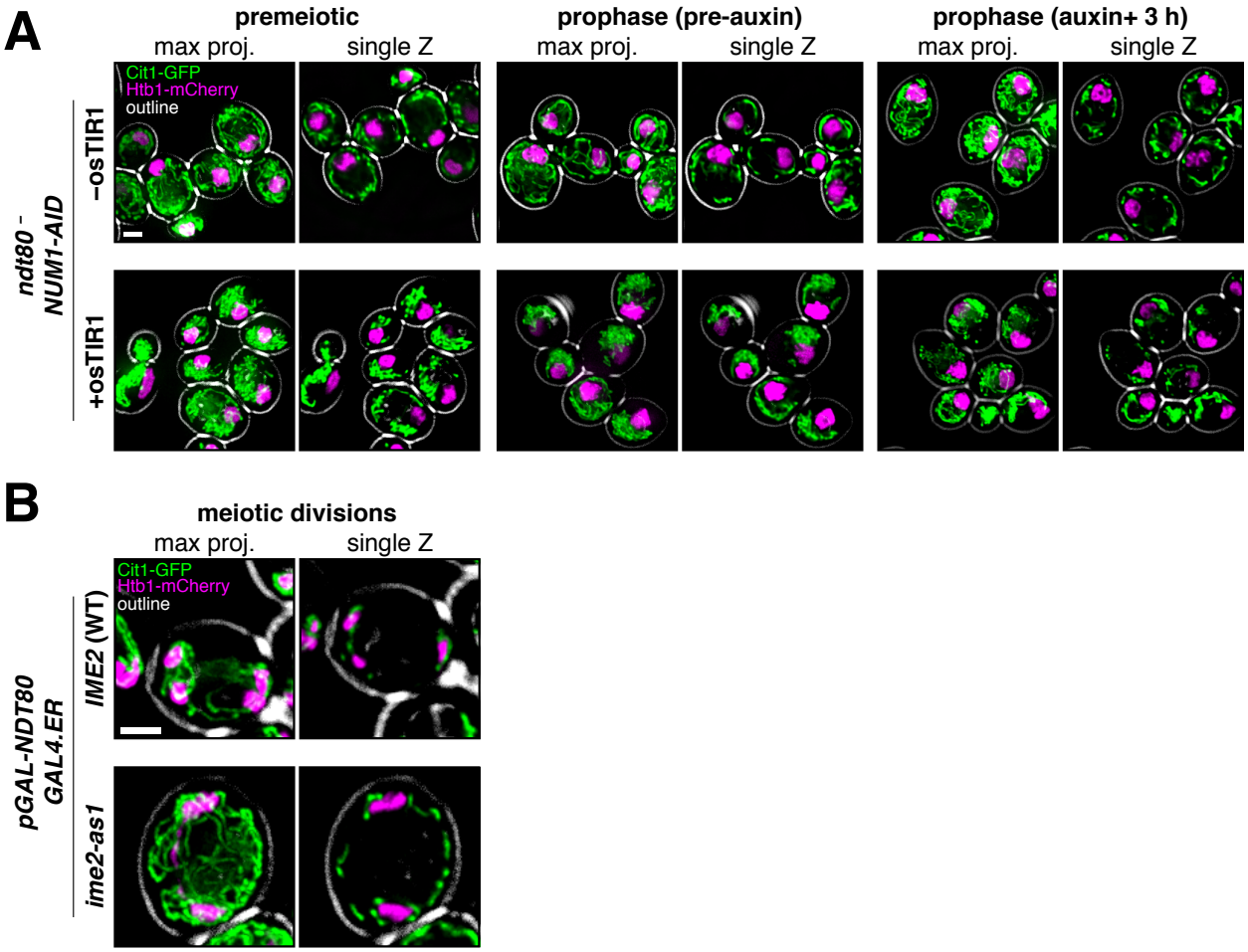

Figure 3.7. The nucleus-mitochondria contact site is developmentally regulated by Ndt80 but not by Ime2. A. Localization of mitochondria in uninduced *pGAL-NDT80 GAL4.ER NUM1-AID* cells (effectively *ndt80*$^-$) containing *pCUP1-osTIR1* (UB17548) or control (UB17552). In both cases, cells were induced to sporulate for 4 h 50 min, then treated with 50 µM $CuSO_4$ to induce *osTIR1* expression. Then at 5 h, cells were treated with 500 µM 3-indoleacetic acid (auxin). The conditional depletion was not fully effective, because cells contained detached mitochondria even prior to treatment, which was dependent on the presence of the *pCUP1-osTIR1* transgene. Fixed cells were examined for the localization of mitochondria (Cit1-GFP) and nuclei (Htb1-mCherry). Maximum intensity projections (max proj.) and single planes of focus (single Z) are shown. Cell outlines are derived from a transmission light image. **B.** Localization of mitochondria in fixed *pGAL-NDT80 GAL4.ER* (UB9158) and *pGAL-NDT80 GAL4.ER ime2-as1* (UB9844) cells during the meiotic divisions. Cells were induced to sporulate, then treated with 1 µM ß-estradiol and 20 µM 1-NA-PP1 at 5 h. Scale bars, 2 µm.

mitochondria contact sites was contrary to our expectations and implied that cortical tethering by MECA and the nucleus-mitochondria contact site should not be mutually exclusive. Accordingly, we monitored the presence of the nucleus-mitochondria contact site in cells triple-labeled for mitochondria, the nucleus, and Num1-GFP. In Ime2-inhibited cells, we found that cortical Num1-GFP puncta could tether the mitochondrial network to the cortex, while simultaneously some mitochondria formed contact sites with the nuclei (Figure 3.8). In control cells, the Num1-GFP puncta were diminished and only nucleus-mitochondria contact sites were evident (Figure 3.8). Our data indicate that nucleus-mitochondria tethering can be induced in Ime2-deficient cells, where it can co-exist with MECA-mediated cortical tethering of mitochondria.

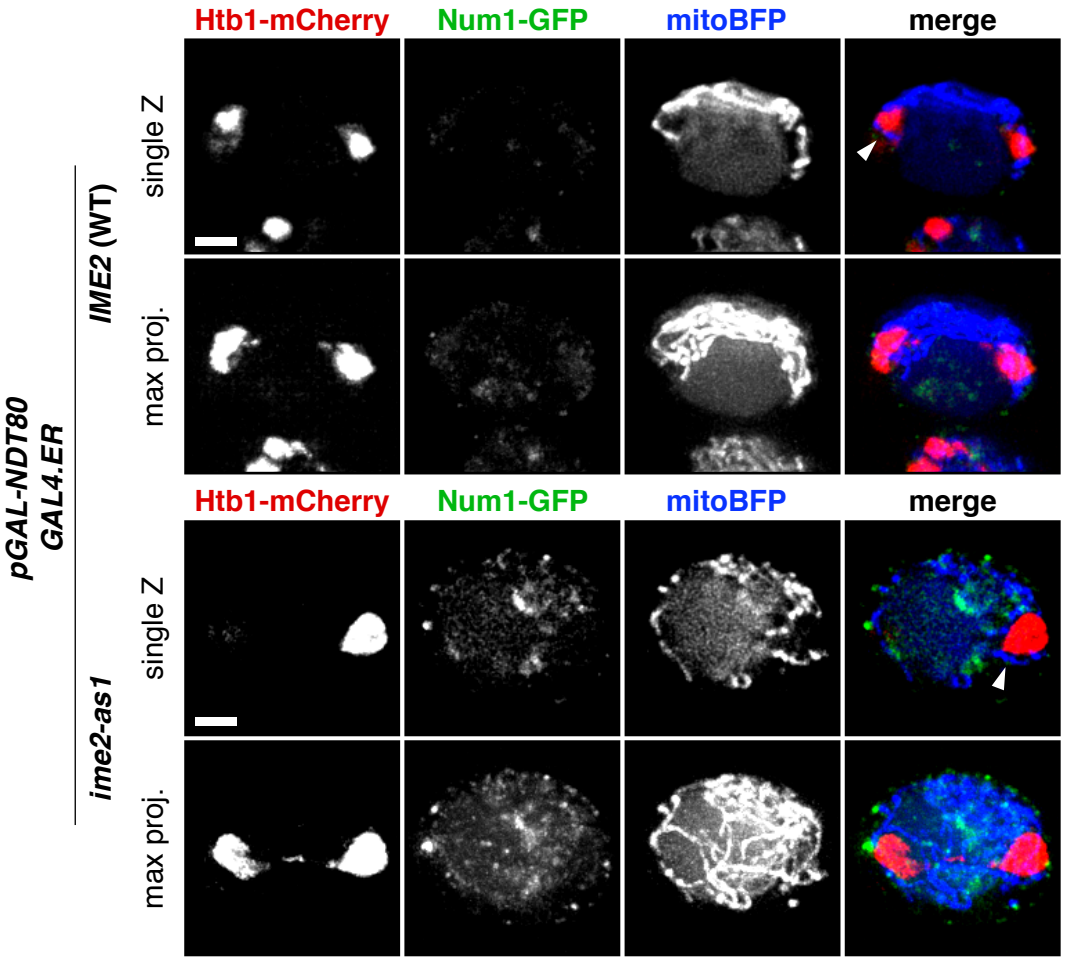

Figure 3.8. Num1 and the nucleus-mitochondria contact site can coexist.

Localization of Num1-GFP and nucleus-mitochondria contact sites in live *pGAL-NDT80 GAL4.ER* control (UB15124) or *pGAL-NDT80 GAL4.ER ime2-as1* (UB16047) cells. Cells were induced to sporulate, then treated with 1 μM ß-estradiol and 20 μM 1-NA-PP1 at 5 h. Cells were imaged 3 h later. At this time point, many control cells were in meiosis II and lacked Num1-GFP puncta, while many *ime2-as1* cells were binucleate and contained Num1-GFP puncta. Arrowheads, nucleus-mitochondria contact sites. Scale bars, 2 μm.

Taken together, our results demonstrate that, while Ndt80 and Ime2 are required for MECA destruction (Chapter 2), Ndt80—but not Ime2—is required for nucleus-mitochondria tethering. One interpretation of these results is that MECA destruction is primarily governed by posttranslational control, while nucleus-mitochondria tethering might be governed by transcription of a Ndt80 target gene that promotes the new tethering interaction.

3.2.4 Analysis of meiotic gene expression data suggests tether candidates

To address the possibility that a direct or indirect target of Ndt80 might initiate nucleus-mitochondria tethering, we analyzed a genome-wide ribosome profiling dataset (Brar et al., 2012) to assemble a list of candidate genes. This dataset contains measurements of protein synthesis (ribosome footprint density) for every gene across a dense meiotic timecourse. To identify candidate tethering factors from this dataset, we reasoned that a candidate gene should be synthesized during the meiotic divisions after Ndt80 is activated. Accordingly, we calculated the fold-induction of each gene by dividing the maximum ribosome footprint density during the meiotic divisions by its mean ribosome footprint density in premeiotic and prophase I-arrested (Ndt80-deficient) cells. In total, 140 genes met an arbitrary induction threshold of 30-fold or more. Of those, 92 genes had irrelevant annotated functions (and so were excluded); 20 genes had annotated functions related to lipids, membranes, or organelles, or had known meiotic defects; and 28 genes had unknown function (Table 3.1). We also included 10 cherry-picked candidates that did not meet the expression criteria but have known involvement in mitochondrial tethering or spore viability (Table 3.1).

In determining a screening approach, we considered the possibility that nucleus-mitochondria tethering could be genetically redundant. Genetic redundancy—that is, absence of a tethering defect in mutants lacking a single tether—has been observed for many other membrane contact sites (Eisenberg-Bord et al., 2016; Scorrano et al., 2019). To circumvent this limitation, we decided to examine the localization of the candidates in wild-type cells rather than assess the functional consequences of each single-gene deletion mutant. We attempted to construct a superfolder-GFP-tagged allele of each gene at its endogenous locus, but due to

Table 3.1. Candidate tethering factors for nucleus-mitochondria contact site.

ORF Name	Gene Name	Fold Induction
YGL230C	YGL230C	1518.0
YFL012W	YFL012W	955.1
YOR214C	SPR2	832.5
YJR107W	LIH1	553.8
YDR042C	YDR042C	489.4
YOR313C	SPS4	484.4
YPR078C	YPR078C	453.1
YCR045C	RRT12	391.0
YBR076W	ECM8	385.8
YNL019C	YNL019C	361.6
YJL160C	PIR5	344.6
YKR015C	YKR015C	280.8
YNL034W	YNL034W	268.0
YBR063C	YBR063C	213.4
YCL021W-A	YCL021W-A	212.0
YDR317W	HIM1	180.6
YJL016W	TPH3	174.9
YLR012C	YLR012C	166.9
YFL040W	YFL040W	164.2
YER085C	YER085C	148.9
YHR185C	PFS1	148.4
YFR012W	DCV1	146.0
YGR273C	YGR273C	140.1
YOL024W	YOL024W	139.5
YEL023C	YEL023C	132.5
YDR326C	YSP2	117.1
YML119W	YML119W	103.9
YNL204C	SPS18	103.0
YPR027C	YPR027C	95.0
YDL218W	YDL218W	88.3
YJL043W	YJL043W	86.4
YHL028W	WSC4	86.3
YKL050C	YKL050C	82.1
YBR250W	SPO23	74.4
YNL033W	YNL033W	74.2
YOR298W	MUM3	73.4
YLR049C	MLO50	69.8
YNL128W	TEP1	64.9
YIL037C	PRM2	52.8
YLR031W	YLR031W	52.8
YOR365C	YOR365C	49.7
YLR372W	ELO3	47.0
YPL192C	PRM3	43.3
YDL186W	YDL186W	42.3
YGR066C	YGR066C	34.2
YDR281C	PHM6	33.8
YEL025C	YEL025C	32.0
YLR072W	LTC1	17.9
YPR140W	TAZ1	14.2
YAR042W	SWH1	2.6
YHL044W	YHL044W	1.7
YDL222C	FMP45	1.7
YLR253W	MCP2	1.0
YDL077C	VPS39	0.7
YPR091C	NVJ2	0.6
YLL006W	MMM1	0.4
YOR228C	MCP1	0.3

technical difficulties our strain construction was not reliable (not shown). Instead, we pursued two highly promising candidates already known to mediate tethering between mitochondria and the ER.

3.2.5 Localization of the ERMES complex and Ltc1/Lam6 in meiosis

In vegetative growth, the ER-Mitochondria Encounter Structure (ERMES) is responsible for ER-mitochondria tethering (Kornmann et al., 2009). As the nuclear envelope is an extension of the ER, we reasoned that ERMES might play a role in forming the meiosis-specific nucleus-mitochondria contact site. We monitored the localization of the integral ER membrane subunit of ERMES, Mmm1-GFP (Kornmann et al., 2009), relative to mitochondria (Cit1-mCardinal) and the nucleus (DAPI). Mmm1 is essential for ER-mitochondria tethering and for maintaining normal mitochondrial morphology in vegetative cells (Kornmann et al., 2009). If ERMES is the nucleus-mitochondria tether, it should localize to contact sites between the nucleus and mitochondria. In premeiotic cells and in meiosis I, we observed a punctate distribution of Mmm1-GFP that colocalized with mitochondria (Figure 3.9, A and B). This localization is consistent with previous studies in vegetative cells (Kornmann et al., 2009; Murley et al., 2013). However, Mmm1-GFP puncta were much more abundant than in previous studies, perhaps due to the considerable expansion of mitochondrial biomass that occurs in respiring cells. In meiosis II, we observed that Mmm1-GFP foci localized to detached mitochondria but were generally absent from the nucleus-mitochondria contact sites (Figure 3.9C). Instead, its localization was reminiscent of the colocalization between ER, mitochondria, and nuclear pores described above (Figure 3.3) In postmeiotic cells, ERMES localized near the nuclei, presumably because mitochondria and ER were already inherited (Figure 3.9D). Due to its apparent absence from the nucleus-mitochondria contact site, we concluded that ERMES was likely not responsible for tethering. However, we cannot exclude the possibility that a minor pool of ERMES localizes to the contact site and promotes tethering. We also cannot exclude the possibility that the meiosis II ERMES puncta are present at nucleus-mitochondria contact sites, but at regions of the nucleus that do not contain DAPI-stained chromatin.

Although ERMES plays a key role in ER-mitochondria tethering, a sterol transporter was found to physically associate with ERMES sites and also promote ER-mitochondria tethering (Elbaz-Alon et al., 2015; Gatta et al., 2015; Murley et al., 2015; Tong et al., 2018). This transporter, Ltc1/Lam6, localizes to the ER-mitochondria contact site independent of ERMES (Elbaz-Alon et al., 2015; Murley et al., 2015) as well as to other membrane contact sites. Given its pre-existing ability to localize to ER-mitochondria contact sites, as well as its flexibility to

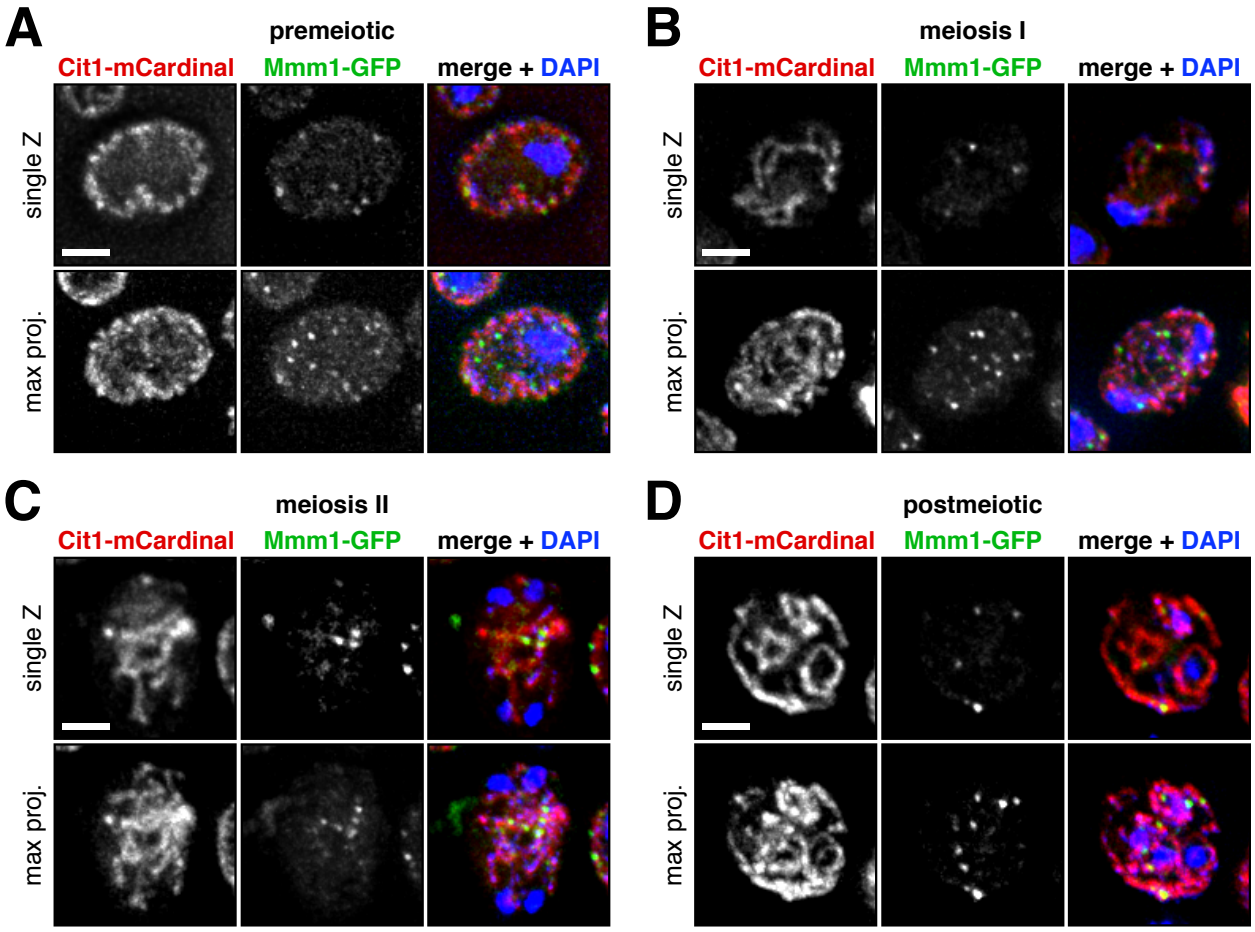

Figure 3.9. Localization of the ERMES complex during gametogenesis. Localization of ERMES subunit Mmm1-GFP in fixed cells (UB19945). Localization of the ERMES complex was determined relative to mitochondria (Cit1-mCardinal) and nuclei (DAPI) at different stages of meiosis: **A.** premeiotic **B.** meiosis I **C.** meiosis II **D.** postmeiotic. Scale bars, 2 µm.

localize to multiple membrane contact sites, we reasoned Ltc1/Lam6 might localize to the nucleus-mitochondria contact site. We monitored the localization of Ltc1-GFP relative to mitochondria and nuclei. In premeiotic cells and in meiosis I, Ltc1-GFP appeared as faint puncta that colocalized with mitochondria (Figure 3.10, A and B). Patchy signal also appeared associated with the vacuole, which may indicate turnover of the protein. However, some fluorescent background signal is also present in the vacuole in meiotic cells (not shown). In meiosis II, faint signal was also visible around mitochondria, sometimes occurring near nuclei, but also elsewhere (Figure 3.10C). In postmeiotic cells, Ltc1-GFP remained localized to

mitochondria, which at this stage are largely perinuclear (Figure 3.10D). Our data are consistent with Ltc1/Lam6 playing a role in nucleus-mitochondria tethering. However, as the protein was lowly abundant, it was difficult to conclusively determine the degree to which it localized to the contact site when mitochondria first encounter the nuclei. Accordingly, we next sought to determine whether Ltc1/Lam6 presence at the contact site might be functionally relevant.

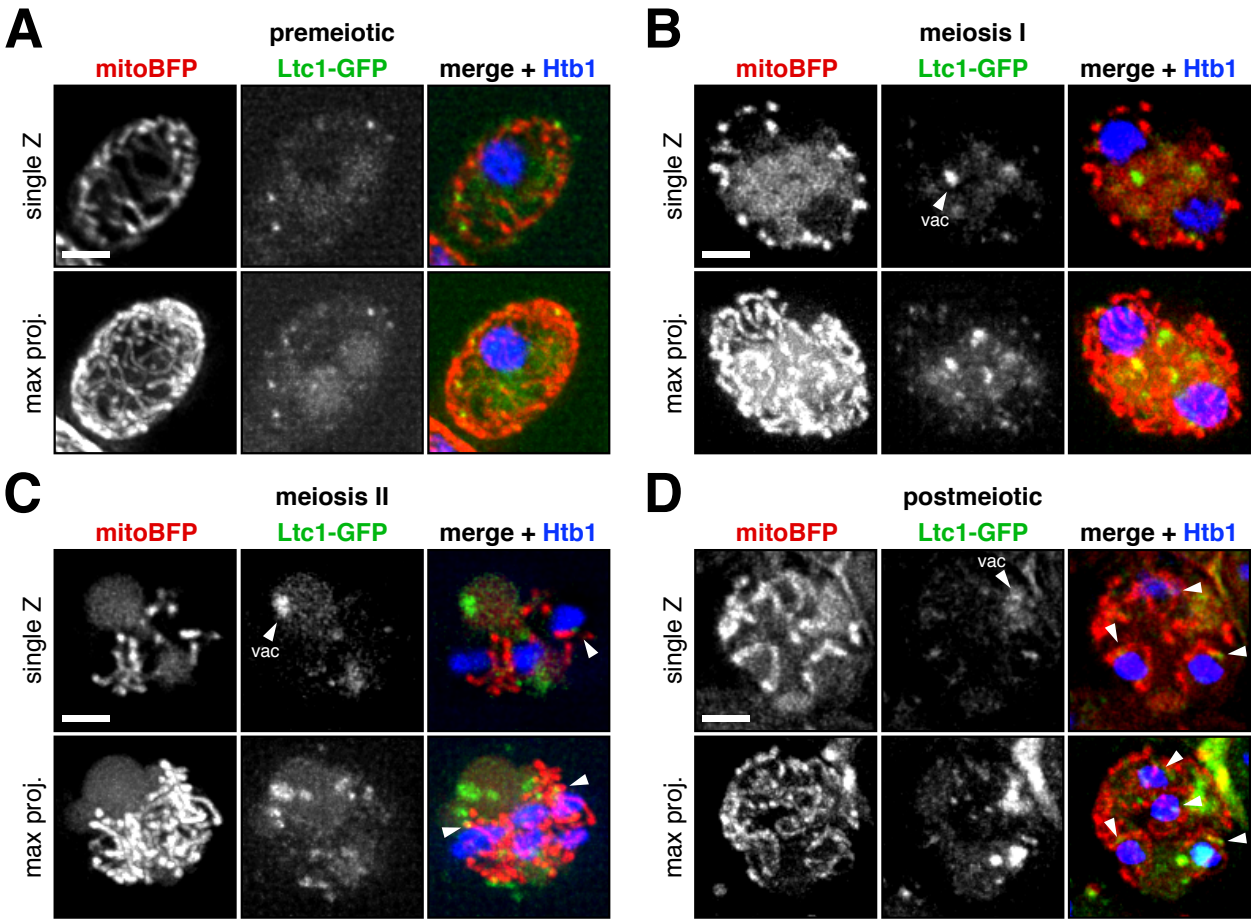

Figure 3.10. Localization of Ltc1 during gametogenesis. Localization of Ltc1-GFP in live cells (UB20120). We found that formaldehyde fixation does not faithfully preserve Ltc1-GFP localization (not shown). Localization was determined relative to mitochondria (mitoBFP) and nuclei (Htb1-mCherry) at different stages of meiosis: **A.** premeiotic **B.** meiosis I **C.** meiosis II **D.** postmeiotic. Arrowheads, Ltc1-GFP foci at nucleus-mitochondria contact sites. vac, vacuolar signal. Scale bars, 2 μm.

3.2.6 Ltc1/Lam6 is neither necessary nor sufficient for nucleus-mitochondria tethering

To further test the potential involvement of Ltc1/Lam6 in nucleus-mitochondria tethering, we analyzed the consequence of *LTC1/LAM6* deletion. Unlike ERMES, which is essential for respiration (and, by extension, gametogenesis), deletion of *LTC1/LAM6* does not affect the ability of cells to utilize a non-fermentable carbon source (Gatta et al., 2015; Murley et al., 2015). Using time-lapse microscopy, we tested *ltc1Δ* cells for defects in nucleus-mitochondria tethering. We observed no defects in tethering (Figure 3.11). Further, we observed that *ltc1Δ* cells effectively segregated mitochondria to gametes, demonstrating the dispensability of Ltc1 to the meiotic mitochondrial segregation program. We conclude that Ltc1/Lam6 is not essential for nucleus-mitochondria tethering or mitochondrial inheritance.

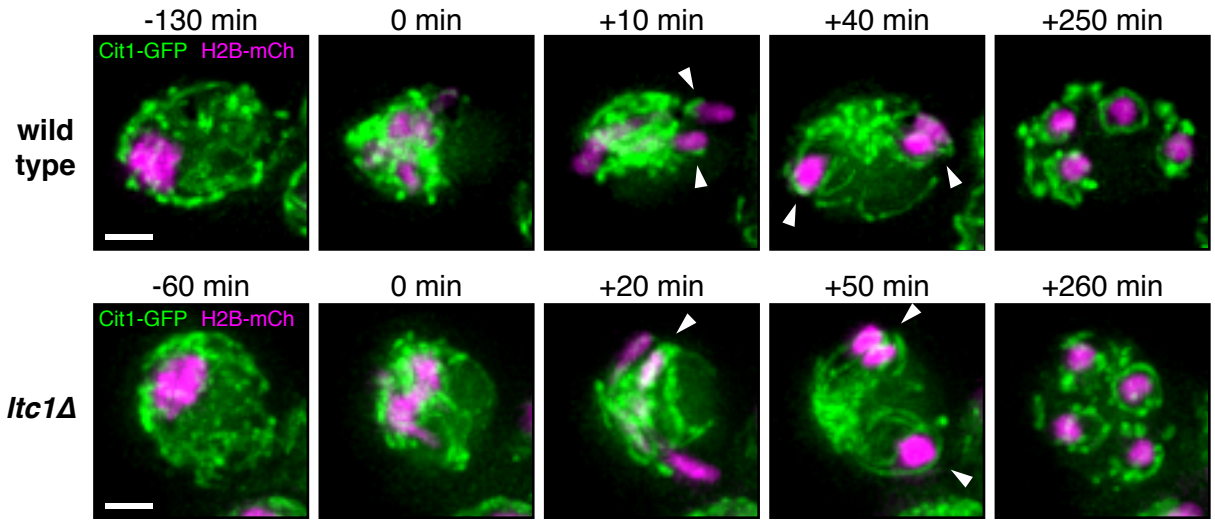

Figure 3.11. Ltc1 is not required for nucleus-mitochondria tethering. Maximum intensity projections of live wild-type (UB10254) and *ltc1Δ* (UB20463) cells in meiosis examined by time lapse microscopy. Nuclei, Htb1-mCherry. Mitochondria, Cit1-GFP. Time is shown relative to anaphase II onset. Arrowheads, nucleus-mitochondria contact sites. Scale bars, 2 μm.

Although we did not observe a clear requirement for Ltc1/Lam6 in nucleus-mitochondria tethering, the same is true for ER-mitochondria tethering in vegetative cells. Ltc1/Lam6 is not required for tethering, but it is synthetically lethal with deletions of ERMES complex subunits (Elbaz-Alon et al., 2015; Murley et al., 2015). Notably, overexpression of GFP-Ltc1/Lam6 leads to a marked expansion of ER-mitochondria contact sites (Elbaz-Alon et al., 2015). To test if

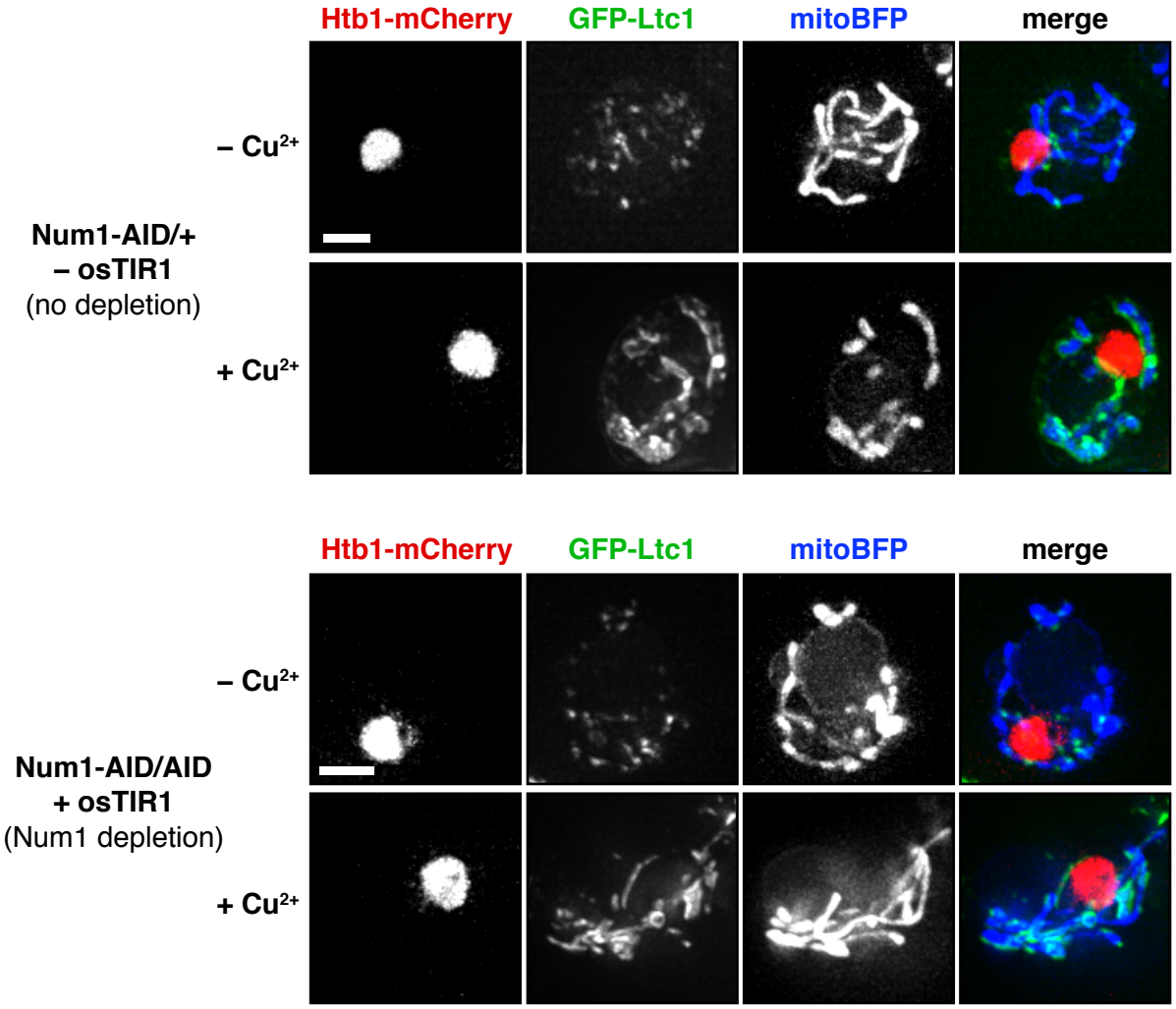

Figure 3.12. GFP-Ltc1 overexpression is not sufficient to induce nucleus-mitochondria tethering. Maximum intensity projections of live cells containing ectopic *pCUP1-GFP-LTC1* construct. Cells heterozygous for *NUM1-AID* and lacking *osTIR1* (UB20737) or homozygous for *NUM1-AID* and containing *pCUP1-osTIR1* (UB20735) were grown in YPD + clonNAT to post-diauxie, pre-saturated growth. Then, cultures were split and treated with 50 μM $CuSO_4$ for 2 h or grown untreated for 2 h. For imaging, cells were pelleted, washed once with synthetic complete medium, and imaged in synthetic complete medium. Nuclei, Htb1-mCherry. Mitochondria, mitoBFP. Fluorescence intensities are not equally scaled, because copper-induced *GFP-LTC1* is far more abundant than in the uninduced controls. Scale bars, 2 μm.

Ltc1/Lam6 is sufficient to induce nucleus-mitochondria tethering but might normally act in parallel to redundant factors, we examined the consequences of *GFP-LTC1/LAM6* overexpression in vegetative cells (Figure 3.12). To do so, we integrated an ectopic copy of *GFP-LTC1/LAM6* driven by the copper-inducible *CUP1* promoter. In agreement with the published data (Elbaz-Alon et al., 2015), overexpressed GFP-Ltc1/Lam6 localized to multiple intracellular locations. In the absence of induction, low levels of GFP-Ltc1/Lam6 were produced due to copper in the medium and predominantly localized in a punctate pattern (Figure 3.12, no depletion). The GFP-Ltc1/Lam6 puncta probably represent ER-mitochondria contact sites (Elbaz-Alon et al., 2015), which when overexpressed coat the mitochondria (Figure 3.12, no depletion). Importantly, we did not observe formation of a nucleus-mitochondria contact site upon *GFP-LTC1/LAM6* induction. To address the possibility that nucleus-mitochondria tethering by Ltc1/Lam6 might require removal of Num1, we used the Num1-AID allele to abolish cortical mitochondrial anchoring in the *GFP-LTC1/LAM6* overexpressing strain. Simultaneous Num1 depletion and *GFP-LTC1/LAM6* overexpression still did not result in nucleus-mitochondria tethering (Figure 3.12, Num1 depletion). Instead, in Num1-AID osTIR1-expressing cells, mitochondria agglomerated seemingly at random and to a similar extent whether or not *GFP-LTC1/LAM6* was induced (Figure 3.12, Num1 depletion). GFP-Ltc1/Lam6 localized to the agglomerated mitochondria like in the control. Our results indicate that Ltc1/Lam6 is neither necessary nor sufficient for nucleus-mitochondria tethering.

3.3 Discussion

3.3.1 Mitochondrial segregation by formation of a nucleus-mitochondria contact site

In this work we demonstrated that a developmentally regulated nucleus-mitochondria contact site is formed during yeast gametogenesis. This finding was consistent with previous reports of nucleus-mitochondria proximity by light and electron microscopy analysis (Gorsich and Shaw, 2004; Miyakawa et al., 1984; Stevens, 1981; Suda et al., 2007). By imaging meiosis II and postmeiotic cells in time lapse, we noted that nucleus-mitochondria contact sites form and can persist for ~2 h (Figure 3.1). Temporal contact site persistence is also a feature of the mitochondria-plasma membrane contact site in vegetative cells. This stability is due to the prolonged association between mitochondria and the cortical tether, MECA (Kraft and Lackner, 2017). The persistent association of mitochondria and nuclei in meiotic differentiation suggests the contact site might be important in organelle inheritance (Figure 3.13).

To further study the nucleus-mitochondria contact site, we examined meiotic cells by transmission electron microscopy (Figures 3.2, 3.4, 3.5, and 3.6). Essentially the whole mitochondrial network contacted the nuclei. This contact persisted over long

distances and often involved wrapping of mitochondria around the nuclear surface. The behavior we observed at the nucleus-mitochondria contact site is quite different from the ER-mitochondria and mitochondria-plasma membrane contact sites, where spatially restricted tether points exist (Kornmann et al., 2009; Kraft and Lackner, 2017; Lackner et al., 2013; Murley et al., 2013). In contrast, the nucleus-vacuole junction and its tether proteins, Vac8 and Nvj1, spread across the entire region of nucleus-vacuole contact (Pan et al., 2000). This variety indicates that tether-mediated membrane contact sites can range from minute structures to extended surfaces of organelle interaction.

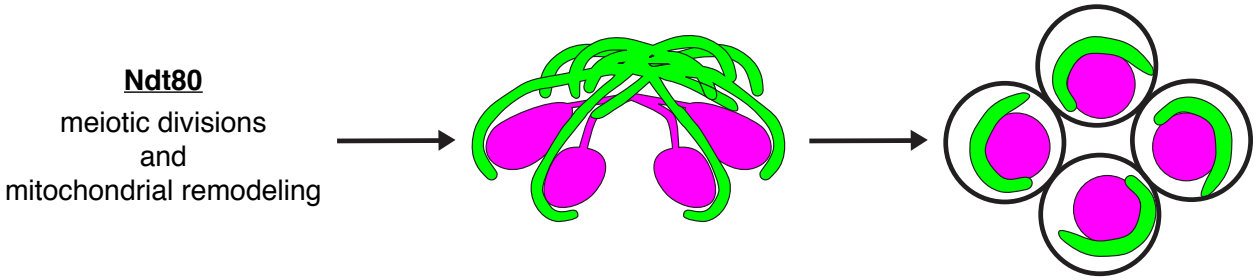

Figure 3.13. Model of nucleus-mitochondria contact and mitochondrial inheritance. Ndt80 promotes both the meiotic divisions and mitochondrial dynamics. During the meiotic divisions, mitochondria tether to the nucleus and are ultimately segregated to gametes.

In Chapter 2, we demonstrated that the transcription factor Ndt80 promotes the activation of a protein kinase, Ime2, which in turn leads to MECA destruction and detachment of mitochondria from the plasma membrane. When we performed similar manipulations, the results were slightly different for the nucleus-mitochondria contact site. While Ndt80 proved to be essential, Ime2 was not (Figure 3.7). This result suggests that Ndt80-dependent transcription plays a critical role not only in promoting the meiotic divisions but also in establishing the nucleus-mitochondria contact site (Figure 3.13). We also observed that Ime2-inhibited cells contained dually tethered mitochondria: to the plasma membrane by Num1 as well as to the nucleus (Figure 3.8). It would be interesting to test whether this competition must be resolved in favor of the nucleus-mitochondria contact site to permit the inheritance of mitochondria. As Ime2 inhibition prevents gamete formation, this possibility could be addressed by overexpressing MECA in wild-type cells expressing Ndt80.

3.3.2 Identity of the nucleus-mitochondria tether

What is responsible for nucleus-mitochondria tethering? An attractive model is that a single protein or protein complex is under the transcriptional control of Ndt80 and promotes nucleus-mitochondria tethering. We addressed the possibility that Ltc1/Lam6 might be the responsible factor. Although the protein is low in abundance, a population of Ltc1/Lam6 localizes near the nucleus-mitochondria contact site (Figure 3.10). However, deletion of Ltc1/Lam6 did not influence nucleus-mitochondria tethering or mitochondrial inheritance (Figure 3.11). Overproduction of GFP-Ltc1/Lam6, even in combination with Num1 depletion, also failed to induce nucleus-mitochondria tethering (Figure 3.12). Although we cannot exclude the possibility that more extensive manipulation is required, such as simultaneous cortical ER and mitochondrial detachment in combination with *GFP-LTC1/LAM6* overexpression, it appears unlikely that Ltc1/Lam6 is the responsible tether. We also disfavor the potential involvement of ERMES due to its apparent exclusion from nascent nucleus-mitochondria contact sites (Figure 3.9). However, analysis of the consequences of ERMES depletion in meiosis would still be informative. We also cannot exclude the possibility that the ERMES foci represent a spatially restricted population of nucleus-mitochondria contact sites, as nuclear envelope containing nuclear pore complexes but not chromatin is present at that location (Figure 3.3). In addition, we did not examine the potential involvement of the endoplasmic reticulum membrane protein complex, which has also been demonstrated to tether the ER and mitochondria (Lahiri et al., 2014). Perhaps other constitutively present tethers could also be responsible through regulated changes in localization.

Unbiased methods could aid in the discovery of the molecular basis of tethering. The extended duration of nucleus-mitochondria contact (~2 h) prior to spore formation makes this system amenable to proximity labeling proteomics, such as the recently developed TurboID system (Branon et al., 2018). In addition, genetic screens for tether-defective mutants could be successful in identifying the proteins responsible.

It is also possible that a much more sophisticated scenario is set in motion by Ndt80. It is increasingly appreciated that deletion of one tether can lead to compensatory remodeling of other contact sites, even in an unchanging, nutrient-replete environment (Eisenberg-Bord et al., 2016; Scorrano et al., 2019). Might it be the case that Ndt80 promotes widespread contact site remodeling through a combination of direct and indirect effects? It is possible that the nucleus-vacuole junction is destroyed by Ndt80, because the nuclei but not vacuoles are segregated to gametes (Roeder and Shaw, 1996; Suda et al., 2007). Consistently, the Nvj1 subunit of the bipartite tether disappears during meiosis II (Tsai et al., 2014). (The other subunit, Vac8, was not examined). It would be of great interest to systematically survey the known membrane contact sites and their tethers through meiosis to determine which are reduced and which are expanded. It is conceivable

that a constitutively present tether could specify nucleus-mitochondria contact in the context of the unique organelle 'interactome' present in meiosis II.

3.3.3 Mitochondrial remodeling in gametogenesis

Nucleus-mitochondria tethering occurs as part of a larger cellular remodeling program during yeast gametogenesis. Mitochondria (Chapter 2) and the cortical ER (Suda et al., 2007) detach from the plasma membrane; gamete plasma membranes are generated *de novo* by a rewiring of the secretory pathway (Neiman, 1998; Neiman, 2005); and the nucleus is highly distorted (Figures 3.2, 3.5, and 3.6), with only a limited nuclear compartment segregated to gametes (Fuchs and Loidl, 2004; King et al., 2019). Identifying the organelle-shaping activities underlying each process would provide insights into how cellular remodeling is coordinated in gametogenesis.

Organelle remodeling during gametogenesis also occurs in other organisms. Nucleus-mitochondria tethering by Milton occurs during *Drosophila* spermatogenesis (Aldridge et al., 2007), and long Oskar induces mitochondrial tethering to the posterior pole of the *Drosophila* oocyte (Hurd et al., 2016). During early stages of *Drosophila* oogenesis, concerted mitochondrial movements from nurse cells into the oocyte occur along microtubule tracks (Cox and Spradling, 2003). In the oocyte, mitochondria join a host of other organelles—including derivatives of the ER and Golgi—as well as mRNAs to form a highly conserved structure in animals called the Balbiani body (Kloc et al., 2004). An electron dense material, termed nuage, associates with mitochondria and Balbiani body components at the perinuclear region (Kloc et al., 2004). Intriguingly, we also observed electron dense material between nuclei and mitochondria in many cases (Figures 3.2, 3.4 and 3.5). Further, the location where mitochondria, nuclear pores, and the ER colocalize in meiosis II (Figure 3.3) was recently shown to contain localized mRNAs (Jin et al., 2015). As the molecular compositions and functions of Balbiani bodies and nuage are open questions, it will be interesting to see whether any similarities with yeast will emerge. Such commonality would indicate the conservation of an ancient gametogenesis organelle remodeling program.

Chapter 4

Conclusions

4.1 Regulation of mitochondrial tethering in meiotic differentiation

In this work we analyzed the developmentally regulated behaviors of mitochondria in yeast gametogenesis. The morphology and spatial positioning of mitochondria are highly regulated in vegetative cells. Thus, the marked departure from the standard mitochondrial network architecture that occurs in gametogenesis provides an exciting opportunity to study unexplored facets of mitochondrial biology in the highly tractable yeast model system. Our analysis, in combination with previous studies (Eastwood et al., 2012; Eastwood and Meneghini, 2015; Gorsich and Shaw, 2004; Miyakawa et al., 1984; Stevens, 1981; Suda et al., 2007), suggests four principal steps in the mitochondrial remodeling program in gametogenesis: (1) detachment of mitochondria from the plasma membrane, (2) establishment of nucleus-mitochondria tethering, (3) limited inheritance of mitochondria by gametes, and (4) active elimination of gamete-excluded mitochondria (Figure 4.1).

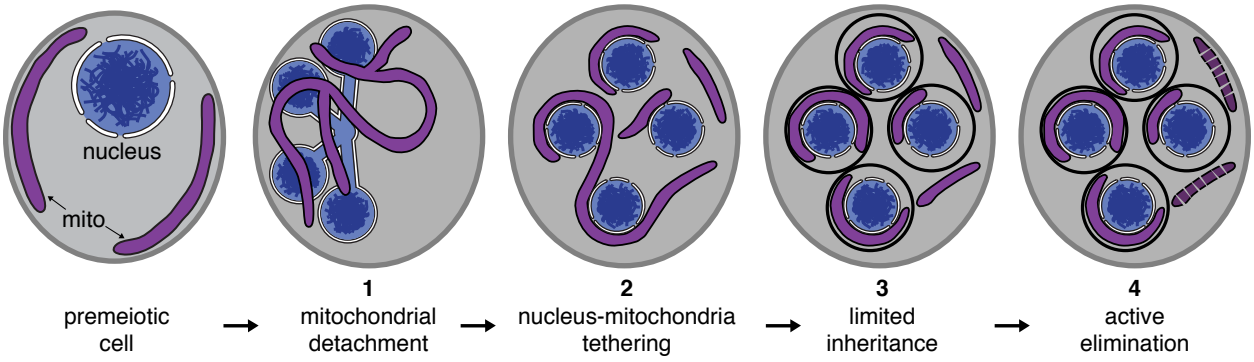

Figure 4.1. The hallmarks of mitochondrial dynamics in gametogenesis. Mitochondria exhibit four distinct behaviors during gametogenesis. (1) Mitochondria detach from the plasma membrane in anaphase II. (2) Mitochondria are tethered to nuclei. (3) A limited amount of mitochondria is inherited by gametes. (4) The gamete-excluded mitochondria are actively eliminated.

4.1.1 Mitochondrial detachment from the plasma membrane

Mitochondrial detachment from the plasma membrane occurs during anaphase II and is regulated by the gametogenesis program. Mitochondrial detachment requires the transcription factor Ndt80 and the protein kinase Ime2 (Figures 2.3 and 2.4). By genetic analysis, we determined that the requirement for Ndt80 is due to its role in Ime2 activation, because expression of a constitutively active allele of Ime2 can restore mitochondrial detachment to *ndt80Δ* cells (Figure 2.3, E and F). Ime2 induces mitochondrial detachment by promoting the destruction of MECA, the protein complex responsible for mitochondria-plasma membrane tethering (Figures 2.7 and 2.11). Recombinant Ime2 phosphorylates the MECA subunits Num1 and Mdm36 *in vitro* (Figure 2.6), suggesting that Ime2 may directly phosphorylate MECA to inactivate tethering in cells. Ime2 leads to MECA proteolysis, which in the case of Num1 requires the proteasome (Figures 2.8 and 2.10). By coupling tether destruction to tightly regulated differentiation factors (Ndt80 and Ime2), meiotic cells ensure timely mitochondrial remodeling during gametogenesis.

4.1.2 Establishment of nucleus-mitochondria tethering

The next step in mitochondrial remodeling is establishment of nucleus-mitochondria tethering. Nucleus-mitochondria tethering requires Ndt80 but not Ime2 (Figure 3.7). Mitochondria form extended contact sites with the elaborate nuclear structure present in meiosis II cells (Figures 3.2, 3.4, 3.5, and 3.6). Mitochondria wrap around the nuclear envelope over long distances and in three dimensions. The extensive surface area of the nucleus-mitochondria contact site is striking, because ER-mitochondria and mitochondria-plasma membrane contact sites exist over much shorter distances (Kornmann et al., 2009; Kraft and Lackner, 2017; Lackner et al., 2013; Murley et al., 2013). We examined the localization of two known ER-mitochondria tethers—ERMES and Ltc1/Lam6—to address the possibility they might mediate nucleus-mitochondria tethering in gametogenesis. ERMES localized to mitochondria in the central region of the detached mass of mitochondria, but we did not detect any ERMES puncta at nascent nucleus-mitochondria contact sites (Figure 3.9). However, it is possible that ERMES tethers mitochondria to the region of the nucleus containing nuclear pore complexes but not chromatin (Figure 3.3). Ltc1/Lam6 did localize to the contact site (Figure 3.10), but deletion of *LTC1/LAM6* did not prevent nucleus-mitochondria tethering (Figure 3.11). In addition, overexpression of *GFP-LTC1/LAM6* was not sufficient to induce ectopic nucleus-mitochondria contacts (Figure 3.12). It is possible that Ltc1/Lam6 localizes to the contact site downstream of other factors responsible for initially establishing the contact site. Further work will be required to define the molecular composition of the nucleus-mitochondria contact site and the factors responsible for its creation.

4.1.3 Relation and regulation of plasma membrane and nuclear tethers

How are mitochondrial detachment from the plasma membrane and the gain of the new nucleus-mitochondria contact site coordinated? The detached mitochondria in wild-type meiosis II cells do not resemble the mitochondrial agglomerations in *num1Δ* vegetative cells (Cerveny et al., 2007; Klecker et al., 2013; Lackner et al., 2013) or in prophase I-arrested cells depleted of Num1 (Figure 3.7A). Instead, the mitochondrial network seems to immediately attach to the nuclear envelope. This conclusion is suggested by several observations. First, the detached mitochondria localize to the perinuclear region by electron microscopy (Figures 3.2, 3.4, 3.5, and 3.6), including in early meiosis II prior to prospore membrane growth (Figure 3.2, A-C). Second, detached mitochondria have a highly stereotyped localization by light microscopy. Mitochondria accumulate in a small region of the cell that is always localized near the midzone of the dividing anaphase II nuclei—a location that also contains nuclear envelope marked by nuclear pores (Figure 3.3). The immediate mitochondria-nuclear association is probably a consequence of how the two mitochondrial contact sites are regulated. Destruction of the mitochondria-plasma membrane contact site requires Ndt80 but is further delayed by the requirement for Ime2 activation at the meiosis I-meiosis II transition. However, partial nucleus-mitochondria tethering is visible in Ime2-inhibited cells (Figures 3.7B and 3.8). This finding indicates that the nucleus-mitochondria contact site is poised after Ndt80 is activated, prior to the bulk detachment of the mitochondrial network that is induced by Ime2 in meiosis II.

Why do meiotic cells regulate mitochondrial tethering using Ndt80 and Ime2? Ndt80 is the master regulator of the meiotic divisions and gamete differentiation (Chu et al., 1998; Chu and Herskowitz, 1998; Winter, 2012; Xu et al., 1995). Tying mitochondrial remodeling to Ndt80 activation ensures the mitochondrial segregation program occurs in synchrony with the rest of the gamete biogenesis program. As an appropriately timed transcriptional activator, Ndt80 is the ideal regulator for promoting nucleus-mitochondria tethering (perhaps by transcriptional induction of one or more tethers). Through an unknown mechanism, Ndt80 promotes Ime2 activation, which is both necessary and sufficient for MECA proteolysis and mitochondrial detachment (Chapter 2). Therefore, a single master regulator (Ndt80) controls both aspects of mitochondrial tether remodeling. The fact that nucleus-mitochondria tethering appears limited in Ime2-inhibited cells (Figures 3.7B and 3.8)—a condition in which MECA is stable—suggests that the nucleus-mitochondria tether may be weaker than MECA. Alternatively, the differences in nuclear morphology between meiosis I and in meiosis II could contribute. Once the molecular identity of the nucleus-mitochondria tether is established, more direct experiments (such as tether overexpression) can be performed to test the relative strengths of the opposing tether forces.

The replacement of cortical mitochondrial tethering by nucleus-mitochondria tethering likely facilitates mitochondrial inheritance. The mother cell plasma

membrane is not transmitted to gametes, which instead are bound by *de novo* synthesized plasma membranes (Neiman, 1998; Neiman, 2005). The mother cell plasma membrane becomes a part of the ascus. The gamete plasma membranes are not synthesized at random, but are specifically nucleated at the spindle pole body embedded in the nuclear envelope (Bajgier et al., 2001; Knop and Strasser, 2000; Neiman, 1998; Neiman, 2005). This organization likely guarantees the inheritance of perinuclear material, such as tethered mitochondria. Thus, it appears that meiotic cells ensure mitochondrial inheritance by replacing mitochondrial tethering to a discarded structure (the mother cell plasma membrane) with mitochondrial tethering to an inherited structure (the nuclear envelope).

Our findings also have broader implications on the regulation of meiosis. Widely used conditions that arrest meiotic progression generally failed to arrest mitochondrial remodeling. Mitochondrial detachment was unimpeded by meiotic inactivation of many key regulators of meiotic progression, such as the polo-like kinase Cdc5 (Figure 2.2). Although we did not specifically analyze it, it is evident in many of these images that nucleus-mitochondria tethering also occurs (Figure 2.2). What appears to be precocious mitochondrial detachment (for example, occurring in mononucleate cells that have not performed any meiotic divisions) is actually timed by Ndt80 and Ime2, just as in wild type. Consistent with this notion, we found that Ime2 kinase activity—which normally is high in premeiotic S phase and meiosis II—was still activated in cells arrested by inactivation of Cdc28, Cdc5, or Cdc20 (Figure 2.5). Importantly, Ime2 activity remained low in Ndt80-deficient cells (Figure 2.5). This result is fascinating, because it implies that cells either monitor progression through the two meiotic divisions in a manner independent of successful chromosome segregation, or they do not monitor meiotic progression at all post-Ndt80. It would be interesting to monitor Ime2 activity (or use mitochondrial detachment as a proxy) in an expanded collection of meiotic perturbations. For example, does the meiosis I spindle assembly checkpoint arrest Ime2 activation? This question could also be systematically addressed by genetic screening for Ime2 activators, such as by monitoring ectopic mitochondrial detachment in *ndt80Δ* cells, which contain ample Ime2 protein but low Ime2 activity (Benjamin et al., 2003; Berchowitz et al., 2013). It also remains completely unknown how substrate specificity is achieved for Ime2. Ime2 kinase activity is high in both premeiotic S phase and meiosis II, but its meiosis II substrates are not targeted in premeiotic S phase. Although Ime2 does not require any accessory factors *in vitro*, perhaps in cells temporally regulated Ime2 specificity factors or posttranslational modifications provide additional regulation. All of these points raise interesting questions about how meiotic progression and the coupling of meiotic division to gamete differentiation are regulated.

4.1.4 Limited inheritance of mitochondria

During gamete differentiation, mitochondrial segregation occurs in the time period during which prospore membranes are open. Measurements from transmission electron microscopy indicate that approximately half of the mitochondrial volume is segregated to spores (Brewer and Fangman, 1980). After plasma membrane detachment and nuclear association, limited inheritance is the third feature of mitochondrial dynamics in gametogenesis. As the four gametes together comprise only ~30% of the volume of the progenitor cell, mitochondria are actually over-inherited relative to what would be predicted if all cytoplasmic elements were segregated proportionally (Brewer and Fangman, 1980). What limits their inheritance to ~50%? Perhaps the gamete cytoplasm is crowded, and as an over-represented organelle the better question might by "why are so many mitochondria inherited?" It is also possible that the geometries of mitochondria and gametes constrain inheritance. Mitochondria adhere to the nuclei by wrapping (Chapter 3), and due to its penetrance, it is reasonable to assume that this mechanism governs inheritance. Mitochondria are confined to the limited two-dimensional nuclear surface, perhaps constraining the amount that can be segregated to gametes. Mitochondria are also constrained by physical forces, such that mitochondria cannot be loaded into spores beyond the capacity of packing forces to deform the rod-like organelle.

4.1.5 Active elimination of gamete-excluded mitochondria

Regardless of the origins of their limited inheritance, what follows is the fourth event in meiotic mitochondrial dynamics: active elimination. Mitochondria left in the gamete-excluded cytoplasm (ascus) are cleared by mega-autophagy (Eastwood et al., 2012). Mega-autophagy leads to the destruction of gamete-excluded material by exposing them to proteases released from lysed vacuoles/lysosomes (Eastwood et al., 2012). Remarkably, like in other programmed cell death programs, mitochondria may be the executioners responsible for mega-autophagy. Digestion of gamete-excluded chromatin and RNA viruses in postmeiotic cells requires the mitochondrially localized nuclease, endonuclease G, called Nuc1 in budding yeast (Eastwood et al., 2012; Gao et al., 2019). Prior to mega-autophagy, mitochondria outside the gametes—but not mitochondria inside the gametes—lose membrane potential, perhaps indicative of permeabilization (Eastwood et al., 2012; Eastwood and Meneghini, 2015). More work will be required to determine the precise origins (mitochondrial or otherwise) of mega-autophagy-inducing signals and effectors. It will also be of interest to investigate whether gamete-excluded mitochondria are predestined for that fate, such as due to pre-existing dysfunction or a physiological specialization induced by the gametogenesis program.

4.2 Roles for organelle tethering in cell biology and development

The subcellular localization and interactions of mitochondria with other organelles are determined in large part by tethers, which promote the formation of membrane contact sites.

4.2.1 The functions of tethers

As the numbers of molecularly defined tethers and contact sites grow, so too do their ascribed functions. A key function of tethers is likely in lipid homeostasis, which has been extensively described (Eisenberg-Bord et al., 2016; Gatta and Levine, 2017; Helle et al., 2013; Kopec et al., 2010; Reinisch and De Camilli, 2016; Saheki and De Camilli, 2017; Schrader et al., 2015). A fundamental problem that tethers likely solve is the isolation of some organelles, such as mitochondria, from vesicular trafficking pathways. However, this notion is not the whole story, as lipid transport at membrane contact sites also occurs between organelles that could in principle transfer lipids by vesicular transport, such as the plasma membrane and the ER (Manford et al., 2012; Saheki et al., 2016; Saheki and De Camilli, 2017). Clearly, membrane contact sites layer regulatory functions on top of the essential requirement that membrane-bound organelles have access to lipids.

Tethers also play roles in organelle inheritance. In vegetative growth, mitochondria are tethered in the mother cell by Num1 and in the daughter by Mmr1 (Cerveny et al., 2007; Chen et al., 2018a; Klecker et al., 2013; Kraft and Lackner, 2017; Lackner et al., 2013; Swayne et al., 2011). It has been proposed that the competing tethering activities of Num1 and Mmr1 balance mitochondrial distribution between the mother and daughter cell. In support of this model, *num1Δ* and *mmr1Δ* exhibit strong genetic suppression—deletion of both genes alleviates the growth defect of either single mutant (Hoppins et al., 2011; Lackner et al., 2013). That Num1 and Mmr1 contact mitochondria through similar biochemical means (cardiolipin binding and self-interaction) further reinforces this notion (Chen et al., 2018a; Ping et al., 2016). Our work suggests that nucleus-mitochondria tethering likely facilitates the inheritance of mitochondria during gametogenesis (Chapter 3).

Finally, tethers facilitate interorganelle communication. The ER-mitochondria contact site cues mitochondrial DNA replication and mitochondrial division (Friedman et al., 2011; Lewis et al., 2016; Meeusen and Nunnari, 2003; Murley et al., 2013). ER-endosome contact sites couple endosome fission to cargo sorting and maturation (Hoyer et al., 2018; Rowland et al., 2014). The number of known cellular processes where interorganelle communication plays a key role will certainly grow with more kinetic studies.

4.2.2 Regulation of tethers

From many functional studies, it is clear that tethers play key roles in cell biology. Because the organization of cells is highly diverse and in part determined by

tethers, regulation of tethers likely plays an important role in determining the morphological diversity of cells. At present, examples are sparse. The vacuole-mitochondria (vCLAMP) and ER-mitochondria (ERMES) contact sites are regulated by carbon source (Honscher et al., 2014). In glycerol-containing medium, where respiration is required for growth, ERMES sites increase in number, and vCLAMP sites are diminished (Honscher et al., 2014). Reduction in vCLAMP tethering is due to inhibitory phosphorylation of the vCLAMP subunit Vps39 (Honscher et al., 2014). We also found that inhibitory phosphorylation can lead to destruction of a contact site: Ime2 phosphorylates MECA to destroy the mitochondria-plasma membrane contact site (Chapter 2). Tether phosphorylation may be a general means to regulate contact site activity.

Tethers may also be regulated by protein-protein interactions. Starvation and other environmental stresses lead to altered lipid composition of the vacuolar membrane, which causes the induction of spatially segregated sterol-rich domains (Toulmay and Prinz, 2013). This behavior requires the tether and sterol transporter Ltc1 (Murley et al., 2013). Importantly, deletion of the Ltc1 binding partners on mitochondria (Tom70 and Tom71) leads to ectopic vacuolar domain formation under nutrient-rich conditions, suggesting regulation of Ltc1 activity by its interaction partners (Murley et al., 2013).

Nutrient state can regulate the extent and types of tethering. It will be important to determine how nutritional cues lead to contact site remodeling. A plausible explanation is that nutrient-responsive kinases, such as protein kinase A and TOR, could promote tether phosphorylation to regulate their activities. Nutrient-responsive changes to tether protein synthesis or degradation are also possible, as are changes to targeting factors or organelle membrane composition. Examining tethers under different nutritional conditions promises to greatly expand our understanding of contact sites.

Cellular differentiation is also a context where tethers are likely to be regulated. In this work, we demonstrated that the regulation of two contact sites occurs in yeast gametogenesis. The mitochondria-plasma membrane site is destroyed by the action of the protein kinase Ime2 (Chapter 2), and the nucleus-mitochondria contact site is established by an Ndt80-dependent process (Chapter 3). Gametogenesis likely involves extensive regulation of tethers, beyond those examined here. Age-induced damage, including protein aggregates and nucleolar material, associate with a gamete-excluded nuclear compartment (King et al., 2019). As the material appears immobilized, tethering factors are likely involved (King et al., 2019). The excluded material is ultimately destroyed by vacuolar lysis (King et al., 2019). The mother cell vacuole lyses in developmentally regulated mega-autophagy, and daughter cells regenerate vacuoles *de novo* (Eastwood et al., 2012; Roeder and Shaw, 1996). Therefore, it is plausible that tethers that interact with the vacuole could be down-regulated or undergo changes in subcellular localization. Indeed, Nvj1, which

mediates tethering between the nucleus and the vacuole (Pan et al., 2000), disappears from the vacuole in meiosis II (Tsai et al., 2014). It will be interesting to examine whether vCLAMP components are similarly redistributed.

Beyond exclusion of the vacuole, the cell is fundamentally remodeled in gametogenesis. Examination of organelles during gametogenesis has revealed remarkable specialization in their morphologies and segregation modalities as compared to vegetative growth (Gorsich and Shaw, 2004; Miyakawa et al., 1984; Roeder and Shaw, 1996; Stevens, 1981; Suda et al., 2007). The extent to which these behaviors are controlled by tethers remains largely unknown. Of particular interest is the endoplasmic reticulum, which like the mitochondrial network is normally anchored to the plasma membrane. Along with mitochondria, the ER loses its cortical attachment during meiosis II (Suda et al., 2007). In vegetative growth, ER-plasma membrane tethering is controlled by six functionally redundant tethers (Manford et al., 2012). Do meiotic cells simultaneously target all six, or do they exploit another mechanism, such as changing the lipid composition of the ER or plasma membrane? Alternatively, it is conceivable that weakening ER-cortical anchoring by inactivation of one or a few tethers could lead to ER detachment in combination with competing forces from another tether. One possible source of the competing force is mitochondria. The ER and mitochondria are already tethered by ERMES (Kornmann et al., 2009)—an interaction that may be maintained in detached ER and mitochondria in meiosis II (Figures 3.3 and 3.9). Perhaps detached mitochondria could pull on weakly tethered ER through their cortical detachment, nuclear associations, and movement into gametes.

Gametogenesis in yeast provides an excellent natural context to study cellular remodeling and tether regulation. Remodeling of cellular organization is profound, but very little is understood about how it occurs. As the localization of organelles in many cases opposes their localization in vegetative cells, it is highly likely that regulation of tethers is involved. A great deal can be learned by leveraging the strengths of the yeast model system to address this problem.

4.2.3 A cellular systems view of organelle tethers

The behaviors of membrane contact sites and tethers can change in response to genetic or environmental perturbations as well as developmental cues. A recurring theme in the membrane contact site field is that inhibition of one tether can be compensated for by other tethers (Eisenberg-Bord et al., 2016; Scorrano et al., 2019). Three mechanisms have been described that can lead to tether compensation: (1) acquisition of suppressor mutations, (2) redundant tethers at shared contact sites, and (3) compensatory remodeling of other contact sites.

First, compensation for a tether deficit can occur through acquiring new mutations that alleviate the mutant phenotype. ERMES mutants grow slowly on fermentable

carbon sources and not at all on nonfermentable carbon sources (Kornmann et al., 2009). However, unlinked suppressors frequently arise that completely alleviate the mutant growth phenotype (Lang et al., 2015). Remarkably, the suppressor mutations were located in a single gene, *VPS13* (Lang et al., 2015). Thus, in this case, tether compensation occurs through selection for mutants that obtain a wild-type growth rate through acquiring suppressor mutations.

Second, compensation can occur due to multiple tethers specifying the same organelle-organelle interaction. For example, ERMES (Kornmann et al., 2009), Ltc1/Lam6 (Elbaz-Alon et al., 2015; Murley et al., 2015), and the ER membrane complex (Lahiri et al., 2014) all specify ER-mitochondria contact sites. Deletion of any one tether is compatible with viability. However, deletion of ERMES and Ltc1/Lam6 in combination is lethal (Elbaz-Alon et al., 2015; Murley et al., 2015), as is deletion of ERMES and the ER membrane complex (Lahiri et al., 2014). Similarly, six tethers act in a redundant fashion to tether the ER to the plasma membrane, and removal of all six is required for constitutive ER detachment (Manford et al., 2012).

The third mechanism involves remodeling of one contact site to compensate for a deficit at another contact site. This behavior has been observed for the vCLAMP and ERMES. When vCLAMP is absent, ERMES becomes more abundant; when ERMES is absent, vCLAMP becomes more abundant (Elbaz-Alon et al., 2014). Deletion of both ERMES and vCLAMP is lethal (Elbaz-Alon et al., 2014), emphasizing the importance of the ability of the two pathways to balance one another.

It is important to appreciate that *active* compensation occurs in cases like the balance between vCLAMP and ERMES. It is not simply that one tether is sufficient to support a function shared with the other tether. What actually occurs is more sophisticated: in the absence of one tether, the second tether and its associated contact site are remodeled to expand the activity of the contact site. Identifying the molecular mechanisms underlying this type of compensatory contact site remodeling is arguably one of the most important unanswered questions in the field.

The observation that perturbation of one contact site can lead to remodeling of other contact sites also has broader implications on contact site regulation. If a small perturbation can "upset the balance," there may be widespread consequences on cellular organization. An intricate series of compensatory interactions could lead to unpredictable emergent behaviors. For example, deletion of ERMES induces expansion of the expansion of vCLAMP. What happens in the context of meiosis, when the vacuole (and presumably its contact sites) are discarded? A domino effect leading to down- and up-regulation of myriad tethers, even tethers unrelated to the ER, vacuole, or mitochondria, might occur in response.

It is conceivable that such a "domino effect" could occur in wild-type gametogenesis. At least three contact sites are destroyed: the mitochondria-plasma membrane contact site (Chapter 2), the ER-plasma membrane contact site (Suda et al., 2007), and the nucleus-vacuole contact site (Tsai et al., 2014); and at least one contact site is created: the nucleus-mitochondria contact site (Chapter 3). This list is almost certainly incomplete, as contact sites are largely uncharacterized in gametogenesis. It is possible that regulation of only a few contact sites in gametogenesis could lead to widespread changes in cellular organization by triggering pre-existing compensatory mechanisms that change the locations or strengths of tethers.

Altered gene expression or posttranslational regulation of tethers by environment-responsive signaling or differentiation programs adds another layer of complexity. If some tethers are transcriptionally induced by differentiation factors, while others are not, the patterns of compensation between tethers could be completely different when compared to nutrient-replete, vegetative growth conditions. For example, Ysp2 is induced over 100-fold during the meiotic divisions (Table 3.1). Ysp2 is a sterol-binding protein structurally similar to Ltc1/Lam6 but that localizes to ER-plasma membrane contact sites (Gatta et al., 2015). Upon 100-fold overexpression, in combination with widespread contact site remodeling, Ysp2 may localize to different, less-preferred contact sites. Likewise, Ltc1/Lam6 expression is induced 17.9-fold during the meiotic divisions (Table 3.1). Ltc1/Lam6 is already known to modify the extent of membrane contact sites depending on its expression level in vegetative cells (Elbaz-Alon et al., 2014). By studying the roles for differentiation-specific controls on tether activity, it will be possible to determine the importance of tether regulation to contact site remodeling.

How might compensatory contact site remodeling occur? One possibility is through competing interactions. The balance in one condition might be upset by another condition, leading to different outcomes. For example, tethers that share a common and limiting protein binding partner or organelle binding modality could compete with one another. When one tether is lost, the other gains expanded interaction capacity. Although untested, this mechanism could plausibly provide cross-talk between the nucleus-vacuole junction and Ltc1/Lam6 contact sites, as both rely on Vac8 to contact the vacuole (Elbaz-Alon et al., 2015; Murley et al., 2015; Pan et al., 2000).

Another possible mechanism of contact site compensation is through signaling pathways. Organelles can signal stress through a variety of mechanisms. For example, lipid or protein folding stress in the ER leads to a transcriptional response termed the unfolded protein response (Walter and Ron, 2011). Plasma membrane stress leads to a rapid response regulated by TORC2 and its effector kinase Ypk1, which alleviates stress through both transcriptional and non-transcriptional means (Roelants et al., 2017). It is conceivable that signaling pathways could monitor

contact site or organelle integrity, leading to remodeling of distant contact sites when one is compromised.

The organelle tethering field has benefited greatly from detailed catalogs of contact sites and tethers made possible by studies in the highly tractable yeast and mammalian cell systems (Eisenberg-Bord et al., 2016). The next great challenge is to determine how the tethers are regulated and to what extent organisms use tethers to effect cellular remodeling. Although the astounding morphological diversity of cells has been long appreciated, the mechanisms responsible for generating this diversity are rarely understood. This understanding can only come from expanding cell biological studies into multicellular organisms and *in vitro* cell culture differentiation models. Advances in technology make such approaches increasingly feasible (Drubin and Hyman, 2017; Liu et al., 2018).

It will be informative to examine organelle contact sites in differentiation models where dramatic cellular remodeling occurs. Promising cases include myogenesis, where the specialized sarcoplasmic reticulum contacts mitochondria to exchange Ca^{2+} (Dorn and Maack, 2013); neural differentiation, where extreme cell shape constrains the geometry of organelles; specialist secretory cells like B cells, which greatly expand the ER (Kirk et al., 2010); and oogenesis, where organelles assemble into germ cell-specific structures such as Balbiani bodies (Kloc et al., 2004). Cases in which organelle behaviors run counter to the wild-type functions of tethers are also likely to prove fruitful, as was the case for Num1 (Chapter 2). Embracing the immense diversity of cell types will enhance our understanding of tethers, their regulation, and their importance to organismal health.

References

AhYoung, A.P., J. Jiang, J. Zhang, X. Khoi Dang, J.A. Loo, Z.H. Zhou, and P.F. Egea. 2015. Conserved SMP domains of the ERMES complex bind phospholipids and mediate tether assembly. *Proc Natl Acad Sci U S A*. 112:E3179-3188.

Aldridge, A.C., L.P. Benson, M.M. Siegenthaler, B.T. Whigham, R.S. Stowers, and K.G. Hales. 2007. Roles for Drp1, a dynamin-related protein, and milton, a kinesin-associated protein, in mitochondrial segregation, unfurling and elongation during Drosophila spermatogenesis. *Fly (Austin)*. 1:38-46.

Altmann, K., M. Frank, D. Neumann, S. Jakobs, and B. Westermann. 2008. The class V myosin motor protein, Myo2, plays a major role in mitochondrial motility in Saccharomyces cerevisiae. *J Cell Biol*. 181:119-130.

Anand, R., G. Memisoglu, and J. Haber. 2017. Cas9-mediated gene editing in Saccharomyces cerevisiae. *Protocol Exchange*.

Arguello-Miranda, O., I. Zagoriy, V. Mengoli, J. Rojas, K. Jonak, T. Oz, P. Graf, and W. Zachariae. 2017. Casein Kinase 1 Coordinates Cohesin Cleavage, Gametogenesis, and Exit from M Phase in Meiosis II. *Dev Cell*. 40:37-52.

Ashburner, M., C.A. Ball, J.A. Blake, D. Botstein, H. Butler, J.M. Cherry, A.P. Davis, K. Dolinski, S.S. Dwight, J.T. Eppig, M.A. Harris, D.P. Hill, L. Issel-Tarver, A. Kasarskis, S. Lewis, J.C. Matese, J.E. Richardson, M. Ringwald, G.M. Rubin, and G. Sherlock. 2000. Gene ontology: tool for the unification of biology. The Gene Ontology Consortium. *Nat Genet*. 25:25-29.

Attner, M.A., and A. Amon. 2012. Control of the mitotic exit network during meiosis. *Mol Biol Cell*. 23:3122-3132.

Bachofen, V., R.J. Schweyen, K. Wolf, and F. Kaudewitz. 1972. Quantitative selection of respiratory deficient mutants in yeasts by triphenyltetrazolium chloride. *Z Naturforsch B*. 27:252-256.

Bajgier, B.K., M. Malzone, M. Nickas, and A.M. Neiman. 2001. SPO21 is required for meiosis-specific modification of the spindle pole body in yeast. *Mol Biol Cell*. 12:1611-1621.

Bean, B.D.M., S.K. Dziurdzik, K.L. Kolehmainen, C.M.S. Fowler, W.K. Kwong, L.I. Grad, M. Davey, C. Schluter, and E. Conibear. 2018. Competitive organelle-specific adaptors recruit Vps13 to membrane contact sites. *J Cell Biol*. 217:3593-3607.

Benjamin, K.R., C. Zhang, K.M. Shokat, and I. Herskowitz. 2003. Control of landmark events in meiosis by the CDK Cdc28 and the meiosis-specific kinase Ime2. *Genes Dev*. 17:1524-1539.

Berchowitz, L.E., A.S. Gajadhar, F.J. van Werven, A.A. De Rosa, M.L. Samoylova, G.A. Brar, Y. Xu, C. Xiao, B. Futcher, J.S. Weissman, F.M. White, and A. Amon. 2013. A developmentally regulated translational control pathway establishes the meiotic chromosome segregation pattern. *Genes Dev*. 27:2147-2163.

Berchowitz, L.E., G. Kabachinski, M.R. Walker, T.M. Carlile, W.V. Gilbert, T.U. Schwartz, and A. Amon. 2015. Regulated Formation of an Amyloid-like Translational Repressor Governs Gametogenesis. *Cell*. 163:406-418.

Bishop, A.C., J.A. Ubersax, D.T. Petsch, D.P. Matheos, N.S. Gray, J. Blethrow, E. Shimizu, J.Z. Tsien, P.G. Schultz, M.D. Rose, J.L. Wood, D.O. Morgan, and K.M. Shokat. 2000. A chemical switch for inhibitor-sensitive alleles of any protein kinase. *Nature*. 407:395-401.

Bleazard, W., J.M. McCaffery, E.J. King, S. Bale, A. Mozdy, Q. Tieu, J. Nunnari, and J.M. Shaw. 1999. The dynamin-related GTPase Dnm1 regulates mitochondrial fission in yeast. *Nat Cell Biol*. 1:298-304.

Bohnert, K.A., and C. Kenyon. 2017. A lysosomal switch triggers proteostasis renewal in the immortal C. elegans germ lineage. *Nature*. 551:629-633.

Boldogh, I.R., S.L. Ramcharan, H.C. Yang, and L.A. Pon. 2004. A type V myosin (Myo2p) and a Rab-like G-protein (Ypt11p) are required for retention of newly inherited mitochondria in yeast cells during cell division. *Mol Biol Cell*. 15:3994-4002.

Boldogh, I.R., H.C. Yang, W.D. Nowakowski, S.L. Karmon, L.G. Hays, J.R. Yates, 3rd, and L.A. Pon. 2001. Arp2/3 complex and actin dynamics are required for actin-based mitochondrial motility in yeast. *Proc Natl Acad Sci U S A*. 98:3162-3167.

Branon, T.C., J.A. Bosch, A.D. Sanchez, N.D. Udeshi, T. Svinkina, S.A. Carr, J.L. Feldman, N. Perrimon, and A.Y. Ting. 2018. Efficient proximity labeling in living cells and organisms with TurboID. *Nat Biotechnol*. 36:880-887.

Brar, G.A., M. Yassour, N. Friedman, A. Regev, N.T. Ingolia, and J.S. Weissman. 2012. High-resolution view of the yeast meiotic program revealed by ribosome profiling. *Science*. 335:552-557.

Brewer, B.J., and W.L. Fangman. 1980. Preferential inclusion of extrachromosomal genetic elements in yeast meiotic spores. *Proc Natl Acad Sci U S A*. 77:5380-5384.

Carbon, S., A. Ireland, C.J. Mungall, S. Shu, B. Marshall, S. Lewis, G.O.H. Ami, and G. Web Presence Working. 2009. AmiGO: online access to ontology and annotation data. *Bioinformatics*. 25:288-289.

Carlile, T.M., and A. Amon. 2008. Meiosis I is established through division-specific translational control of a cyclin. *Cell*. 133:280-291.

Carpenter, K., R.B. Bell, J. Yunus, A. Amon, and L.E. Berchowitz. 2018. Phosphorylation-Mediated Clearance of Amyloid-like Assemblies in Meiosis. *Dev Cell*. 45:392-405 e396.

Cerveny, K.L., S.L. Studer, R.E. Jensen, and H. Sesaki. 2007. Yeast mitochondrial division and distribution require the cortical num1 protein. *Dev Cell*. 12:363-375.

Chen, H., S.A. Detmer, A.J. Ewald, E.E. Griffin, S.E. Fraser, and D.C. Chan. 2003. Mitofusins Mfn1 and Mfn2 coordinately regulate mitochondrial fusion and are essential for embryonic development. *J Cell Biol*. 160:189-200.

Chen, W., H.A. Ping, and L.L. Lackner. 2018a. Direct membrane binding and self-interaction contribute to Mmr1 function in mitochondrial inheritance. *Mol Biol Cell*. 29:2346-2357.

Chen, X., R. Gaglione, T. Leong, L. Bednor, T. de Los Santos, E. Luk, M. Airola, and N.M. Hollingsworth. 2018b. Mek1 coordinates meiotic progression with DNA break repair by directly phosphorylating and inhibiting the yeast pachytene exit regulator Ndt80. *PLoS Genet*. 14:e1007832.

Cheng, Z., G.M. Otto, E.N. Powers, A. Keskin, P. Mertins, S.A. Carr, M. Jovanovic, and G.A. Brar. 2018. Pervasive, Coordinated Protein-Level Changes Driven by Transcript Isoform Switching during Meiosis. *Cell*. 172:910-923 e916.

Chernyakov, I., F. Santiago-Tirado, and A. Bretscher. 2013. Active segregation of yeast mitochondria by Myo2 is essential and mediated by Mmr1 and Ypt11. *Curr Biol*. 23:1818-1824.

Christianson, T.W., R.S. Sikorski, M. Dante, J.H. Shero, and P. Hieter. 1992. Multifunctional yeast high-copy-number shuttle vectors. *Gene*. 110:119-122.

Chu, J., R.D. Haynes, S.Y. Corbel, P. Li, E. Gonzalez-Gonzalez, J.S. Burg, N.J. Ataie, A.J. Lam, P.J. Cranfill, M.A. Baird, M.W. Davidson, H.L. Ng, K.C. Garcia, C.H. Contag, K. Shen, H.M. Blau, and M.Z. Lin. 2014. Non-invasive intravital imaging of cellular differentiation with a bright red-excitable fluorescent protein. *Nat Methods*. 11:572-578.

Chu, S., J. DeRisi, M. Eisen, J. Mulholland, D. Botstein, P.O. Brown, and I. Herskowitz. 1998. The transcriptional program of sporulation in budding yeast. *Science*. 282:699-705.

Chu, S., and I. Herskowitz. 1998. Gametogenesis in yeast is regulated by a transcriptional cascade dependent on Ndt80. *Mol Cell*. 1:685-696.

Cipolat, S., O. Martins de Brito, B. Dal Zilio, and L. Scorrano. 2004. OPA1 requires mitofusin 1 to promote mitochondrial fusion. *Proc Natl Acad Sci U S A*. 101:15927-15932.

Cociorva, D., L.T. D, and J.R. Yates. 2007. Validation of tandem mass spectrometry database search results using DTASelect. *Curr Protoc Bioinformatics*. Chapter 13:Unit 13 14.

Consortium, T.G.O. 2019. The Gene Ontology Resource: 20 years and still GOing strong. *Nucleic Acids Res*. 47:D330-D338.

Cooper, K.F., M.J. Mallory, D.B. Egeland, M. Jarnik, and R. Strich. 2000. Ama1p is a meiosis-specific regulator of the anaphase promoting complex/cyclosome in yeast. *Proc Natl Acad Sci U S A*. 97:14548-14553.

Covitz, P.A., I. Herskowitz, and A.P. Mitchell. 1991. The yeast RME1 gene encodes a putative zinc finger protein that is directly repressed by a1-alpha 2. *Genes Dev*. 5:1982-1989.

Cox, R.T., and A.C. Spradling. 2003. A Balbiani body and the fusome mediate mitochondrial inheritance during Drosophila oogenesis. *Development*. 130:1579-1590.

Dayani, Y., G. Simchen, and M. Lichten. 2011. Meiotic recombination intermediates are resolved with minimal crossover formation during return-to-growth, an analogue of the mitotic cell cycle. *PLoS Genet*. 7:e1002083.

DeLuca, S.Z., and P.H. O'Farrell. 2012. Barriers to male transmission of mitochondrial DNA in sperm development. *Dev Cell*. 22:660-668.

Diamond, A.E., J.S. Park, I. Inoue, H. Tachikawa, and A.M. Neiman. 2009. The anaphase promoting complex targeting subunit Ama1 links meiotic exit to cytokinesis during sporulation in Saccharomyces cerevisiae. *Mol Biol Cell*. 20:134-145.

Diffley, J.F. 2004. Regulation of early events in chromosome replication. *Curr Biol*. 14:R778-786.

Dirick, L., L. Goetsch, G. Ammerer, and B. Byers. 1998. Regulation of meiotic S phase by Ime2 and a Clb5,6-associated kinase in Saccharomyces cerevisiae. *Science*. 281:1854-1857.

Dorn, G.W., 2nd, and C. Maack. 2013. SR and mitochondria: calcium cross-talk between kissing cousins. *J Mol Cell Cardiol*. 55:42-49.

Drubin, D.G., and A.A. Hyman. 2017. Stem cells: the new "model organism". *Mol Biol Cell*. 28:1409-1411.

Dujon, B. 1981. Mitochondrial Genetics and Functions. *In* The Molecular Biology of the Yeast Saccharomyces: Life Cycle and Inheritance. Vol. 11A. J.N.J. Strathern, E. W.; Broach, J. R., editor. Cold Spring Harbor Laboratory Press, New York. 505-635.

Eastwood, M.D., S.W. Cheung, K.Y. Lee, J. Moffat, and M.D. Meneghini. 2012. Developmentally programmed nuclear destruction during yeast gametogenesis. *Dev Cell*. 23:35-44.

Eastwood, M.D., and M.D. Meneghini. 2015. Developmental Coordination of Gamete Differentiation with Programmed Cell Death in Sporulating Yeast. *Eukaryot Cell*. 14:858-867.

Eisenberg, A.R., A. Higdon, A. Keskin, S. Hodapp, M. Jovanovic, and G.A. Brar. 2018. Precise Post-translational Tuning Occurs for Most Protein Complex Components during Meiosis. *Cell Rep*. 25:3603-3617 e3602.

Eisenberg-Bord, M., N. Shai, M. Schuldiner, and M. Bohnert. 2016. A Tether Is a Tether Is a Tether: Tethering at Membrane Contact Sites. *Dev Cell*. 39:395-409.

Elbaz-Alon, Y., M. Eisenberg-Bord, V. Shinder, S.B. Stiller, E. Shimoni, N. Wiedemann, T. Geiger, and M. Schuldiner. 2015. Lam6 Regulates the Extent of Contacts between Organelles. *Cell Rep*. 12:7-14.

Elbaz-Alon, Y., E. Rosenfeld-Gur, V. Shinder, A.H. Futerman, T. Geiger, and M. Schuldiner. 2014. A dynamic interface between vacuoles and mitochondria in yeast. *Dev Cell*. 30:95-102.

Engel, S.R., F.S. Dietrich, D.G. Fisk, G. Binkley, R. Balakrishnan, M.C. Costanzo, S.S. Dwight, B.C. Hitz, K. Karra, R.S. Nash, S. Weng, E.D. Wong, P. Lloyd, M.S. Skrzypek, S.R. Miyasato, M. Simison, and J.M. Cherry. 2014. The

reference genome sequence of Saccharomyces cerevisiae: then and now. *G3 (Bethesda)*. 4:389-398.
Esposito, R.E., and M.S. Esposito. 1974. Genetic recombination and commitment to meiosis in Saccharomyces. *Proc Natl Acad Sci U S A*. 71:3172-3176.
Ferla, M.P., J.C. Thrash, S.J. Giovannoni, and W.M. Patrick. 2013. New rRNA gene-based phylogenies of the Alphaproteobacteria provide perspective on major groups, mitochondrial ancestry and phylogenetic instability. *PLoS One*. 8:e83383.
Foiani, M., E. Nadjar-Boger, R. Capone, S. Sagee, T. Hashimshoni, and Y. Kassir. 1996. A meiosis-specific protein kinase, Ime2, is required for the correct timing of DNA replication and for spore formation in yeast meiosis. *Mol Gen Genet*. 253:278-288.
Fox, T.D. 2012. Mitochondrial protein synthesis, import, and assembly. *Genetics*. 192:1203-1234.
Friedman, J.R., M. Kannan, A. Toulmay, C.H. Jan, J.S. Weissman, W.A. Prinz, and J. Nunnari. 2018. Lipid Homeostasis Is Maintained by Dual Targeting of the Mitochondrial PE Biosynthesis Enzyme to the ER. *Dev Cell*. 44:261-270 e266.
Friedman, J.R., L.L. Lackner, M. West, J.R. DiBenedetto, J. Nunnari, and G.K. Voeltz. 2011. ER tubules mark sites of mitochondrial division. *Science*. 334:358-362.
Friedman, J.R., A. Mourier, J. Yamada, J.M. McCaffery, and J. Nunnari. 2015. MICOS coordinates with respiratory complexes and lipids to establish mitochondrial inner membrane architecture. *Elife*. 4.
Friedman, J.R., and J. Nunnari. 2014. Mitochondrial form and function. *Nature*. 505:335-343.
Fuchs, J., and J. Loidl. 2004. Behaviour of nucleolus organizing regions (NORs) and nucleoli during mitotic and meiotic divisions in budding yeast. *Chromosome Res*. 12:427-438.
Fuller, M.T. 1993. Spermatogenesis. *In* The Development of Drosophila melanogaster. Vol. 1. M. Bate and A.M. Arias, editors. Cold Spring Harbor Laboratory Press, New York.
Fuller, M.T., and A.C. Spradling. 2007. Male and female Drosophila germline stem cells: two versions of immortality. *Science*. 316:402-404.
Gan, L., C.T. Ng, C. Chen, and S. Cai. 2019. A collection of yeast cellular electron cryotomography data. *bioRxiv*.
Gao, J., S. Chau, F. Chowdhury, T. Zhou, S. Hossain, A. Mcquibban, and M.D. Meneghini. 2019. Meiotic viral attenuation through an ancestral apoptotic pathway. *bioRxiv*.
Gatta, A.T., and T.P. Levine. 2017. Piecing Together the Patchwork of Contact Sites. *Trends Cell Biol*. 27:214-229.
Gatta, A.T., L.H. Wong, Y.Y. Sere, D.M. Calderon-Norena, S. Cockcroft, A.K. Menon, and T.P. Levine. 2015. A new family of StART domain proteins at membrane contact sites has a role in ER-PM sterol transport. *Elife*. 4.

Gorsich, S.W., and J.M. Shaw. 2004. Importance of mitochondrial dynamics during meiosis and sporulation. *Mol Biol Cell*. 15:4369-4381.
Goudeau, J., and H. Aguilaniu. 2010. Carbonylated proteins are eliminated during reproduction in C. elegans. *Aging Cell*. 9:991-1003.
Graef, M., J.R. Friedman, C. Graham, M. Babu, and J. Nunnari. 2013. ER exit sites are physical and functional core autophagosome biogenesis components. *Mol Biol Cell*. 24:2918-2931.
Hales, K.G., and M.T. Fuller. 1997. Developmentally regulated mitochondrial fusion mediated by a conserved, novel, predicted GTPase. *Cell*. 90:121-129.
Heil-Chapdelaine, R.A., J.R. Oberle, and J.A. Cooper. 2000. The cortical protein Num1p is essential for dynein-dependent interactions of microtubules with the cortex. *J Cell Biol*. 151:1337-1344.
Helle, S.C., G. Kanfer, K. Kolar, A. Lang, A.H. Michel, and B. Kornmann. 2013. Organization and function of membrane contact sites. *Biochim Biophys Acta*. 1833:2526-2541.
Helle, S.C.J., Q. Feng, M.J. Aebersold, L. Hirt, R.R. Gruter, A. Vahid, A. Sirianni, S. Mostowy, J.G. Snedeker, A. Saric, T. Idema, T. Zambelli, and B. Kornmann. 2017. Mechanical force induces mitochondrial fission. *Elife*. 6.
Henderson, K.A., A.L. Hughes, and D.E. Gottschling. 2014. Mother-daughter asymmetry of pH underlies aging and rejuvenation in yeast. *Elife*. 3:e03504.
Hepworth, S.R., H. Friesen, and J. Segall. 1998. NDT80 and the meiotic recombination checkpoint regulate expression of middle sporulation-specific genes in Saccharomyces cerevisiae. *Mol Cell Biol*. 18:5750-5761.
Hermann, G.J., J.W. Thatcher, J.P. Mills, K.G. Hales, M.T. Fuller, J. Nunnari, and J.M. Shaw. 1998. Mitochondrial fusion in yeast requires the transmembrane GTPase Fzo1p. *J Cell Biol*. 143:359-373.
Herskowitz, I., J. Rine, and J. Strathern. 1992. 11 Mating-type Determination and Mating-type Interconversion in Saccharomyces cerevisiae.
Higuchi, R., J.D. Vevea, T.C. Swayne, R. Chojnowski, V. Hill, I.R. Boldogh, and L.A. Pon. 2013. Actin dynamics affect mitochondrial quality control and aging in budding yeast. *Curr Biol*. 23:2417-2422.
Higuchi-Sanabria, R., T.C. Swayne, I.R. Boldogh, and L.A. Pon. 2016. Live-Cell Imaging of Mitochondria and the Actin Cytoskeleton in Budding Yeast. *Methods Mol Biol*. 1365:25-62.
Hoffmann, H.P., and C.J. Avers. 1973. Mitochondrion of yeast: ultrastructural evidence for one giant, branched organelle per cell. *Science*. 181:749-751.
Holt, L.J., J.E. Hutti, L.C. Cantley, and D.O. Morgan. 2007. Evolution of Ime2 phosphorylation sites on Cdk1 substrates provides a mechanism to limit the effects of the phosphatase Cdc14 in meiosis. *Mol Cell*. 25:689-702.
Hongay, C.F., P.L. Grisafi, T. Galitski, and G.R. Fink. 2006. Antisense transcription controls cell fate in Saccharomyces cerevisiae. *Cell*. 127:735-745.
Honscher, C., M. Mari, K. Auffarth, M. Bohnert, J. Griffith, W. Geerts, M. van der Laan, M. Cabrera, F. Reggiori, and C. Ungermann. 2014. Cellular

metabolism regulates contact sites between vacuoles and mitochondria. *Dev Cell*. 30:86-94.
Hoppins, S., S.R. Collins, A. Cassidy-Stone, E. Hummel, R.M. Devay, L.L. Lackner, B. Westermann, M. Schuldiner, J.S. Weissman, and J. Nunnari. 2011. A mitochondrial-focused genetic interaction map reveals a scaffold-like complex required for inner membrane organization in mitochondria. *J Cell Biol*. 195:323-340.
Hoyer, M.J., P.J. Chitwood, C.C. Ebmeier, J.F. Striepen, R.Z. Qi, W.M. Old, and G.K. Voeltz. 2018. A Novel Class of ER Membrane Proteins Regulates ER-Associated Endosome Fission. *Cell*. 175:254-265 e214.
Hughes, A.L., and D.E. Gottschling. 2012. An early age increase in vacuolar pH limits mitochondrial function and lifespan in yeast. *Nature*. 492:261-265.
Hughes, A.L., C.E. Hughes, K.A. Henderson, N. Yazvenko, and D.E. Gottschling. 2016. Selective sorting and destruction of mitochondrial membrane proteins in aged yeast. *Elife*. 5.
Hurd, T.R., B. Herrmann, J. Sauerwald, J. Sanny, M. Grosch, and R. Lehmann. 2016. Long Oskar Controls Mitochondrial Inheritance in Drosophila melanogaster. *Dev Cell*. 39:560-571.
Irniger, S. 2011. The Ime2 protein kinase family in fungi: more duties than just meiosis. *Mol Microbiol*. 80:1-13.
Isono, E., N. Saito, N. Kamata, Y. Saeki, and E.A. Toh. 2005. Functional analysis of Rpn6p, a lid component of the 26 S proteasome, using temperature-sensitive rpn6 mutants of the yeast Saccharomyces cerevisiae. *J Biol Chem*. 280:6537-6547.
Itoh, T., E.A. Toh, and Y. Matsui. 2004. Mmr1p is a mitochondrial factor for Myo2p-dependent inheritance of mitochondria in the budding yeast. *EMBO J*. 23:2520-2530.
Jajoo, R., Y. Jung, D. Huh, M.P. Viana, S.M. Rafelski, M. Springer, and J. Paulsson. 2016. Accurate concentration control of mitochondria and nucleoids. *Science*. 351:169-172.
Jambhekar, A., and A. Amon. 2008. Control of meiosis by respiration. *Curr Biol*. 18:969-975.
Jan, C.H., C.C. Williams, and J.S. Weissman. 2014. Principles of ER cotranslational translocation revealed by proximity-specific ribosome profiling. *Science*. 346:1257521.
Janke, C., M.M. Magiera, N. Rathfelder, C. Taxis, S. Reber, H. Maekawa, A. Moreno-Borchart, G. Doenges, E. Schwob, E. Schiebel, and M. Knop. 2004. A versatile toolbox for PCR-based tagging of yeast genes: new fluorescent proteins, more markers and promoter substitution cassettes. *Yeast*. 21:947-962.
Jaspersen, S.L., J.F. Charles, R.L. Tinker-Kulberg, and D.O. Morgan. 1998. A late mitotic regulatory network controlling cyclin destruction in Saccharomyces cerevisiae. *Mol Biol Cell*. 9:2803-2817.

Jin, L., K. Zhang, Y. Xu, R. Sternglanz, and A.M. Neiman. 2015. Sequestration of mRNAs Modulates the Timing of Translation during Meiosis in Budding Yeast. *Mol Cell Biol*. 35:3448-3458.
Kahana, J.A., B.J. Schnapp, and P.A. Silver. 1995. Kinetics of spindle pole body separation in budding yeast. *Proc Natl Acad Sci U S A*. 92:9707-9711.
Kalia, R., R.Y. Wang, A. Yusuf, P.V. Thomas, D.A. Agard, J.M. Shaw, and A. Frost. 2018. Structural basis of mitochondrial receptor binding and constriction by DRP1. *Nature*. 558:401-405.
Kamieniecki, R.J., L. Liu, and D.S. Dawson. 2005. FEAR but not MEN genes are required for exit from meiosis I. *Cell Cycle*. 4:1093-1098.
Kanfer, G., T. Courtheoux, M. Peterka, S. Meier, M. Soste, A. Melnik, K. Reis, P. Aspenstrom, M. Peter, P. Picotti, and B. Kornmann. 2015. Mitotic redistribution of the mitochondrial network by Miro and Cenp-F. *Nat Commun*. 6:8015.
Kanki, T., D. Kang, and D.J. Klionsky. 2009a. Monitoring mitophagy in yeast: the Om45-GFP processing assay. *Autophagy*. 5:1186-1189.
Kanki, T., and D.J. Klionsky. 2008. Mitophagy in yeast occurs through a selective mechanism. *J Biol Chem*. 283:32386-32393.
Kanki, T., K. Wang, M. Baba, C.R. Bartholomew, M.A. Lynch-Day, Z. Du, J. Geng, K. Mao, Z. Yang, W.L. Yen, and D.J. Klionsky. 2009b. A genomic screen for yeast mutants defective in selective mitochondria autophagy. *Mol Biol Cell*. 20:4730-4738.
Kanki, T., K. Wang, Y. Cao, M. Baba, and D.J. Klionsky. 2009c. Atg32 is a mitochondrial protein that confers selectivity during mitophagy. *Dev Cell*. 17:98-109.
Kassir, Y., D. Granot, and G. Simchen. 1988. IME1, a positive regulator gene of meiosis in S. cerevisiae. *Cell*. 52:853-862.
Katajisto, P., J. Dohla, C.L. Chaffer, N. Pentinmikko, N. Marjanovic, S. Iqbal, R. Zoncu, W. Chen, R.A. Weinberg, and D.M. Sabatini. 2015. Stem cells. Asymmetric apportioning of aged mitochondria between daughter cells is required for stemness. *Science*. 348:340-343.
Keeney, S., C.N. Giroux, and N. Kleckner. 1997. Meiosis-specific DNA double-strand breaks are catalyzed by Spo11, a member of a widely conserved protein family. *Cell*. 88:375-384.
King, G.A., J.S. Goodman, K. Chetlapalli, J.G. Schick, D.M. Jorgens, K.L. McDonald, and E. Ünal. 2019. Meiotic cellular rejuvenation is coupled to nuclear remodeling in budding yeast. *bioRxiv*.
Kirk, S.J., J.M. Cliff, J.A. Thomas, and T.H. Ward. 2010. Biogenesis of secretory organelles during B cell differentiation. *J Leukoc Biol*. 87:245-255.
Klapholz, S., and R.E. Esposito. 1980. Isolation of SPO12-1 and SPO13-1 from a natural variant of yeast that undergoes a single meiotic division. *Genetics*. 96:567-588.

Klecker, T., D. Scholz, J. Fortsch, and B. Westermann. 2013. The yeast cell cortical protein Num1 integrates mitochondrial dynamics into cellular architecture. *J Cell Sci*. 126:2924-2930.
Kloc, M., S. Bilinski, and L.D. Etkin. 2004. The Balbiani body and germ cell determinants: 150 years later. *Curr Top Dev Biol*. 59:1-36.
Knoblach, B., and R.A. Rachubinski. 2015. Sharing the cell's bounty - organelle inheritance in yeast. *J Cell Sci*. 128:621-630.
Knop, M., and K. Strasser. 2000. Role of the spindle pole body of yeast in mediating assembly of the prospore membrane during meiosis. *EMBO J*. 19:3657-3667.
Kominami, K., Y. Sakata, M. Sakai, and I. Yamashita. 1993. Protein kinase activity associated with the IME2 gene product, a meiotic inducer in the yeast Saccharomyces cerevisiae. *Biosci Biotechnol Biochem*. 57:1731-1735.
Kopec, K.O., V. Alva, and A.N. Lupas. 2010. Homology of SMP domains to the TULIP superfamily of lipid-binding proteins provides a structural basis for lipid exchange between ER and mitochondria. *Bioinformatics*. 26:1927-1931.
Kormanec, J., I. Schaaff-Gerstenschlager, F.K. Zimmermann, D. Perecko, and H. Kuntzel. 1991. Nuclear migration in Saccharomyces cerevisiae is controlled by the highly repetitive 313 kDa NUM1 protein. *Mol Gen Genet*. 230:277-287.
Kornmann, B., E. Currie, S.R. Collins, M. Schuldiner, J. Nunnari, J.S. Weissman, and P. Walter. 2009. An ER-mitochondria tethering complex revealed by a synthetic biology screen. *Science*. 325:477-481.
Korobova, F., V. Ramabhadran, and H.N. Higgs. 2013. An actin-dependent step in mitochondrial fission mediated by the ER-associated formin INF2. *Science*. 339:464-467.
Kraft, L.M., and L.L. Lackner. 2017. Mitochondria-driven assembly of a cortical anchor for mitochondria and dynein. *J Cell Biol*. 216:3061-3071.
Kraft, L.M., and L.L. Lackner. 2018. Mitochondrial anchors: Positioning mitochondria and more. *Biochem Biophys Res Commun*. 500:2-8.
Kremer, J.R., D.N. Mastronarde, and J.R. McIntosh. 1996. Computer visualization of three-dimensional image data using IMOD. *J Struct Biol*. 116:71-76.
Kumagai, K., M. Kawano-Kawada, and K. Hanada. 2014. Phosphoregulation of the ceramide transport protein CERT at serine 315 in the interaction with VAMP-associated protein (VAP) for inter-organelle trafficking of ceramide in mammalian cells. *J Biol Chem*. 289:10748-10760.
Kumar, N., M. Leonzino, W. Hancock-Cerutti, F.A. Horenkamp, P. Li, J.A. Lees, H. Wheeler, K.M. Reinisch, and P. De Camilli. 2018. VPS13A and VPS13C are lipid transport proteins differentially localized at ER contact sites. *J Cell Biol*. 217:3625-3639.
Lackner, L.L. 2019. The Expanding and Unexpected Functions of Mitochondria Contact Sites. *Trends Cell Biol*.
Lackner, L.L., H. Ping, M. Graef, A. Murley, and J. Nunnari. 2013. Endoplasmic reticulum-associated mitochondria-cortex tether functions in the distribution and inheritance of mitochondria. *Proc Natl Acad Sci U S A*. 110:E458-467.

Lahiri, S., J.T. Chao, S. Tavassoli, A.K. Wong, V. Choudhary, B.P. Young, C.J. Loewen, and W.A. Prinz. 2014. A conserved endoplasmic reticulum membrane protein complex (EMC) facilitates phospholipid transfer from the ER to mitochondria. *PLoS Biol*. 12:e1001969.

Lammers, L.G., and S.M. Markus. 2015. The dynein cortical anchor Num1 activates dynein motility by relieving Pac1/LIS1-mediated inhibition. *J Cell Biol*. 211:309-322.

Lane, N. 2006. Power, Sex, Suicide: Mitochondria and the Meaning of Life. Oxford University Press.

Lang, A.B., A.T. John Peter, P. Walter, and B. Kornmann. 2015. ER-mitochondrial junctions can be bypassed by dominant mutations in the endosomal protein Vps13. *J Cell Biol*. 210:883-890.

Lazarou, M., D.A. Sliter, L.A. Kane, S.A. Sarraf, C. Wang, J.L. Burman, D.P. Sideris, A.I. Fogel, and R.J. Youle. 2015. The ubiquitin kinase PINK1 recruits autophagy receptors to induce mitophagy. *Nature*. 524:309-314.

Lee, B.H., and A. Amon. 2003. Role of Polo-like kinase CDC5 in programming meiosis I chromosome segregation. *Science*. 300:482-486.

Lee, J.E., L.M. Westrate, H. Wu, C. Page, and G.K. Voeltz. 2016. Multiple dynamin family members collaborate to drive mitochondrial division. *Nature*. 540:139-143.

Lewis, S.C., L.F. Uchiyama, and J. Nunnari. 2016. ER-mitochondria contacts couple mtDNA synthesis with mitochondrial division in human cells. *Science*. 353:aaf5549.

Liu, T.L., S. Upadhyayula, D.E. Milkie, V. Singh, K. Wang, I.A. Swinburne, K.R. Mosaliganti, Z.M. Collins, T.W. Hiscock, J. Shea, A.Q. Kohrman, T.N. Medwig, D. Dambournet, R. Forster, B. Cunniff, Y. Ruan, H. Yashiro, S. Scholpp, E.M. Meyerowitz, D. Hockemeyer, D.G. Drubin, B.L. Martin, D.Q. Matus, M. Koyama, S.G. Megason, T. Kirchhausen, and E. Betzig. 2018. Observing the cell in its native state: Imaging subcellular dynamics in multicellular organisms. *Science*. 360.

Longtine, M.S., A. McKenzie, 3rd, D.J. Demarini, N.G. Shah, A. Wach, A. Brachat, P. Philippsen, and J.R. Pringle. 1998. Additional modules for versatile and economical PCR-based gene deletion and modification in Saccharomyces cerevisiae. *Yeast*. 14:953-961.

Loog, M., and D.O. Morgan. 2005. Cyclin specificity in the phosphorylation of cyclin-dependent kinase substrates. *Nature*. 434:104-108.

Ma, H., and P.H. O'Farrell. 2016. Selfish drive can trump function when animal mitochondrial genomes compete. *Nat Genet*. 48:798-802.

Manford, A.G., C.J. Stefan, H.L. Yuan, J.A. Macgurn, and S.D. Emr. 2012. ER-to-plasma membrane tethering proteins regulate cell signaling and ER morphology. *Dev Cell*. 23:1129-1140.

Marston, A.L., and A. Amon. 2004. Meiosis: cell-cycle controls shuffle and deal. *Nat Rev Mol Cell Biol*. 5:983-997.

Marston, A.L., B.H. Lee, and A. Amon. 2003. The Cdc14 phosphatase and the FEAR network control meiotic spindle disassembly and chromosome segregation. *Dev Cell*. 4:711-726.
McDonald, K., and T. Muller-Reichert. 2002. Cryomethods for thin section electron microscopy. *Methods Enzymol*. 351:96-123.
McDonald, K.L. 2014. Out with the old and in with the new: rapid specimen preparation procedures for electron microscopy of sectioned biological material. *Protoplasma*. 251:429-448.
McDonald, K.L., and R.I. Webb. 2011. Freeze substitution in 3 hours or less. *J Microsc*. 243:227-233.
McDonald, W.H., D.L. Tabb, R.G. Sadygov, M.J. MacCoss, J. Venable, J. Graumann, J.R. Johnson, D. Cociorva, and J.R. Yates, 3rd. 2004. MS1, MS2, and SQT-three unified, compact, and easily parsed file formats for the storage of shotgun proteomic spectra and identifications. *Rapid Commun Mass Spectrom*. 18:2162-2168.
Meeusen, S., J.M. McCaffery, and J. Nunnari. 2004. Mitochondrial fusion intermediates revealed in vitro. *Science*. 305:1747-1752.
Meeusen, S., and J. Nunnari. 2003. Evidence for a two membrane-spanning autonomous mitochondrial DNA replisome. *J Cell Biol*. 163:503-510.
Miller, M.P., E. Unal, G.A. Brar, and A. Amon. 2012. Meiosis I chromosome segregation is established through regulation of microtubule-kinetochore interactions. *Elife*. 1:e00117.
Mishra, P., and D.C. Chan. 2014. Mitochondrial dynamics and inheritance during cell division, development and disease. *Nat Rev Mol Cell Biol*. 15:634-646.
Mitchell, A.P., and I. Herskowitz. 1986. Activation of meiosis and sporulation by repression of the RME1 product in yeast. *Nature*. 319:738-742.
Miyakawa, I., H. Aoi, N. Sando, and T. Kuroiwa. 1984. Fluorescence microscopic studies of mitochondrial nucleoids during meiosis and sporulation in the yeast, Saccharomyces cerevisiae. *J Cell Sci*. 66:21-38.
Moreno-Borchart, A.C., K. Strasser, M.G. Finkbeiner, A. Shevchenko, A. Shevchenko, and M. Knop. 2001. Prospore membrane formation linked to the leading edge protein (LEP) coat assembly. *EMBO J*. 20:6946-6957.
Mortimer, R.K., and J.R. Johnston. 1959. Life span of individual yeast cells. *Nature*. 183:1751-1752.
Murley, A., L.L. Lackner, C. Osman, M. West, G.K. Voeltz, P. Walter, and J. Nunnari. 2013. ER-associated mitochondrial division links the distribution of mitochondria and mitochondrial DNA in yeast. *Elife*. 2:e00422.
Murley, A., and J. Nunnari. 2016. The Emerging Network of Mitochondria-Organelle Contacts. *Mol Cell*. 61:648-653.
Murley, A., R.D. Sarsam, A. Toulmay, J. Yamada, W.A. Prinz, and J. Nunnari. 2015. Ltc1 is an ER-localized sterol transporter and a component of ER-mitochondria and ER-vacuole contacts. *J Cell Biol*. 209:539-548.

Nakanishi, H., P. de los Santos, and A.M. Neiman. 2004. Positive and negative regulation of a SNARE protein by control of intracellular localization. *Mol Biol Cell*. 15:1802-1815.
Neiman, A.M. 1998. Prospore membrane formation defines a developmentally regulated branch of the secretory pathway in yeast. *J Cell Biol*. 140:29-37.
Neiman, A.M. 2005. Ascospore formation in the yeast Saccharomyces cerevisiae. *Microbiol Mol Biol Rev*. 69:565-584.
Neiman, A.M. 2011. Sporulation in the budding yeast Saccharomyces cerevisiae. *Genetics*. 189:737-765.
Nhek, S., M. Ngo, X. Yang, M.M. Ng, S.J. Field, J.M. Asara, N.D. Ridgway, and A. Toker. 2010. Regulation of oxysterol-binding protein Golgi localization through protein kinase D-mediated phosphorylation. *Mol Biol Cell*. 21:2327-2337.
Nishimura, K., T. Fukagawa, H. Takisawa, T. Kakimoto, and M. Kanemaki. 2009. An auxin-based degron system for the rapid depletion of proteins in nonplant cells. *Nat Methods*. 6:917-922.
Nocedal, I., E. Mancera, and A.D. Johnson. 2017. Gene regulatory network plasticity predates a switch in function of a conserved transcription regulator. *Elife*. 6.
Nunnari, J., W.F. Marshall, A. Straight, A. Murray, J.W. Sedat, and P. Walter. 1997. Mitochondrial transmission during mating in Saccharomyces cerevisiae is determined by mitochondrial fusion and fission and the intramitochondrial segregation of mitochondrial DNA. *Mol Biol Cell*. 8:1233-1242.
Ogur, M., R. St. John, and S. Nagai. 1957. Tetrazolium overlay technique for population studies of respiration deficiency in yeast. *Science*. 125:928-929.
Okaz, E., O. Arguello-Miranda, A. Bogdanova, P.K. Vinod, J.J. Lipp, Z. Markova, I. Zagoriy, B. Novak, and W. Zachariae. 2012. Meiotic prophase requires proteolysis of M phase regulators mediated by the meiosis-specific APC/CAma1. *Cell*. 151:603-618.
Omer, S., S.R. Greenberg, and W.L. Lee. 2018. Cortical dynein pulling mechanism is regulated by differentially targeted attachment molecule Num1. *Elife*. 7.
Osman, C., T.R. Noriega, V. Okreglak, J.C. Fung, and P. Walter. 2015. Integrity of the yeast mitochondrial genome, but not its distribution and inheritance, relies on mitochondrial fission and fusion. *Proc Natl Acad Sci U S A*. 112:E947-956.
Padmore, R., L. Cao, and N. Kleckner. 1991. Temporal comparison of recombination and synaptonemal complex formation during meiosis in S. cerevisiae. *Cell*. 66:1239-1256.
Palmer, R.E., M. Koval, and D. Koshland. 1989. The dynamics of chromosome movement in the budding yeast Saccharomyces cerevisiae. *J Cell Biol*. 109:3355-3366.
Pan, X., P. Roberts, Y. Chen, E. Kvam, N. Shulga, K. Huang, S. Lemmon, and D.S. Goldfarb. 2000. Nucleus-vacuole junctions in Saccharomyces cerevisiae are

formed through the direct interaction of Vac8p with Nvj1p. *Mol Biol Cell*. 11:2445-2457.
Park, S.K., J.D. Venable, T. Xu, and J.R. Yates, 3rd. 2008. A quantitative analysis software tool for mass spectrometry-based proteomics. *Nat Methods*. 5:319-322.
Peng, J., J.E. Elias, C.C. Thoreen, L.J. Licklider, and S.P. Gygi. 2003. Evaluation of multidimensional chromatography coupled with tandem mass spectrometry (LC/LC-MS/MS) for large-scale protein analysis: the yeast proteome. *J Proteome Res*. 2:43-50.
Phizicky, D.V., L.E. Berchowitz, and S.P. Bell. 2018. Multiple kinases inhibit origin licensing and helicase activation to ensure reductive cell division during meiosis. *Elife*. 7.
Ping, H.A., L.M. Kraft, W. Chen, A.E. Nilles, and L.L. Lackner. 2016. Num1 anchors mitochondria to the plasma membrane via two domains with different lipid binding specificities. *J Cell Biol*. 213:513-524.
Primig, M., R.M. Williams, E.A. Winzeler, G.G. Tevzadze, A.R. Conway, S.Y. Hwang, R.W. Davis, and R.E. Esposito. 2000. The core meiotic transcriptome in budding yeasts. *Nat Genet*. 26:415-423.
Prinz, W.A. 2014. Bridging the gap: membrane contact sites in signaling, metabolism, and organelle dynamics. *J Cell Biol*. 205:759-769.
Prugar, E., C. Burnett, X. Chen, and N.M. Hollingsworth. 2017. Coordination of Double Strand Break Repair and Meiotic Progression in Yeast by a Mek1-Ndt80 Negative Feedback Loop. *Genetics*. 206:497-512.
Reggiori, F., and D.J. Klionsky. 2013. Autophagic processes in yeast: mechanism, machinery and regulation. *Genetics*. 194:341-361.
Reinisch, K.M., and P. De Camilli. 2016. SMP-domain proteins at membrane contact sites: Structure and function. *Biochim Biophys Acta*. 1861:924-927.
Reynolds, E.S. 1963. The use of lead citrate at high pH as an electron-opaque stain in electron microscopy. *J Cell Biol*. 17:208-212.
Rockmill, B., E.J. Lambie, and G.S. Roeder. 1991. Spore Enrichment. *In* Guide to Yeast Genetics and Molecular Biology. Vol. 194. C. Guthrie and G.R. Fink, editors. Academic Press. 146-149.
Roeder, A.D., and J.M. Shaw. 1996. Vacuole partitioning during meiotic division in yeast. *Genetics*. 144:445-458.
Roeder, G.S., and J.M. Bailis. 2000. The pachytene checkpoint. *Trends Genet*. 16:395-403.
Roelants, F.M., K.L. Leskoske, M.N. Martinez Marshall, M.N. Locke, and J. Thorner. 2017. The TORC2-Dependent Signaling Network in the Yeast Saccharomyces cerevisiae. *Biomolecules*. 7.
Rojansky, R., M.Y. Cha, and D.C. Chan. 2016. Elimination of paternal mitochondria in mouse embryos occurs through autophagic degradation dependent on PARKIN and MUL1. *Elife*. 5.

Rossanese, O.W., C.A. Reinke, B.J. Bevis, A.T. Hammond, I.B. Sears, J. O'Connor, and B.S. Glick. 2001. A role for actin, Cdc1p, and Myo2p in the inheritance of late Golgi elements in Saccharomyces cerevisiae. *J Cell Biol*. 153:47-62.

Rowland, A.A., P.J. Chitwood, M.J. Phillips, and G.K. Voeltz. 2014. ER contact sites define the position and timing of endosome fission. *Cell*. 159:1027-1041.

Rudge, S.A., V.A. Sciorra, M. Iwamoto, C. Zhou, T. Strahl, A.J. Morris, J. Thorner, and J. Engebrecht. 2004. Roles of phosphoinositides and of Spo14p (phospholipase D)-generated phosphatidic acid during yeast sporulation. *Mol Biol Cell*. 15:207-218.

Saheki, Y., X. Bian, C.M. Schauder, Y. Sawaki, M.A. Surma, C. Klose, F. Pincet, K.M. Reinisch, and P. De Camilli. 2016. Control of plasma membrane lipid homeostasis by the extended synaptotagmins. *Nat Cell Biol*. 18:504-515.

Saheki, Y., and P. De Camilli. 2017. Endoplasmic Reticulum-Plasma Membrane Contact Sites. *Annu Rev Biochem*. 86:659-684.

Sawyer, E.M., E.C. Brunner, Y. Hwang, L.E. Ivey, O. Brown, M. Bannon, D. Akrobetu, K.E. Sheaffer, O. Morgan, C.O. Field, N. Suresh, M.G. Gordon, E.T. Gunnell, L.A. Regruto, C.G. Wood, M.T. Fuller, and K.G. Hales. 2017. Testis-specific ATP synthase peripheral stalk subunits required for tissue-specific mitochondrial morphogenesis in Drosophila. *BMC Cell Biol*. 18:16.

Sawyer, E.M., P.R. Joshi, V. Jorgensen, J. Yunus, L.E. Berchowitz, and E. Unal. 2019. Developmental regulation of an organelle tether coordinates mitochondrial remodeling in meiosis. *J Cell Biol*. 218:559-579.

Schauder, C.M., X. Wu, Y. Saheki, P. Narayanaswamy, F. Torta, M.R. Wenk, P. De Camilli, and K.M. Reinisch. 2014. Structure of a lipid-bound extended synaptotagmin indicates a role in lipid transfer. *Nature*. 510:552-555.

Schindelin, J., I. Arganda-Carreras, E. Frise, V. Kaynig, M. Longair, T. Pietzsch, S. Preibisch, C. Rueden, S. Saalfeld, B. Schmid, J.Y. Tinevez, D.J. White, V. Hartenstein, K. Eliceiri, P. Tomancak, and A. Cardona. 2012. Fiji: an open-source platform for biological-image analysis. *Nat Methods*. 9:676-682.

Schrader, M., L.F. Godinho, J.L. Costello, and M. Islinger. 2015. The different facets of organelle interplay-an overview of organelle interactions. *Front Cell Dev Biol*. 3:56.

Schwarz, T.L. 2013. Mitochondrial trafficking in neurons. *Cold Spring Harb Perspect Biol*. 5.

Scorrano, L., M.A. De Matteis, S. Emr, F. Giordano, G. Hajnoczky, B. Kornmann, L.L. Lackner, T.P. Levine, L. Pellegrini, K. Reinisch, R. Rizzuto, T. Simmen, H. Stenmark, C. Ungermann, and M. Schuldiner. 2019. Coming together to define membrane contact sites. *Nat Commun*. 10:1287.

Sheff, M.A., and K.S. Thorn. 2004. Optimized cassettes for fluorescent protein tagging in Saccharomyces cerevisiae. *Yeast*. 21:661-670.

Shou, W., J.H. Seol, A. Shevchenko, C. Baskerville, D. Moazed, Z.W. Chen, J. Jang, A. Shevchenko, H. Charbonneau, and R.J. Deshaies. 1999. Exit from mitosis is triggered by Tem1-dependent release of the protein phosphatase Cdc14 from nucleolar RENT complex. *Cell*. 97:233-244.

Sia, R.A., and A.P. Mitchell. 1995. Stimulation of later functions of the yeast meiotic protein kinase Ime2p by the IDS2 gene product. *Mol Cell Biol*. 15:5279-5287.
Sieber, M.H., M.B. Thomsen, and A.C. Spradling. 2016. Electron Transport Chain Remodeling by GSK3 during Oogenesis Connects Nutrient State to Reproduction. *Cell*. 164:420-432.
Simchen, G., R. Pinon, and Y. Salts. 1972. Sporulation in Saccharomyces cerevisiae: premeiotic DNA synthesis, readiness and commitment. *Exp Cell Res*. 75:207-218.
Smirnova, E., D.L. Shurland, S.N. Ryazantsev, and A.M. van der Bliek. 1998. A human dynamin-related protein controls the distribution of mitochondria. *J Cell Biol*. 143:351-358.
Smith, H.E., and A.P. Mitchell. 1989. A transcriptional cascade governs entry into meiosis in Saccharomyces cerevisiae. *Mol Cell Biol*. 9:2142-2152.
Smith, H.E., S.S. Su, L. Neigeborn, S.E. Driscoll, and A.P. Mitchell. 1990. Role of IME1 expression in regulation of meiosis in Saccharomyces cerevisiae. *Mol Cell Biol*. 10:6103-6113.
Sopko, R., S. Raithatha, and D. Stuart. 2002. Phosphorylation and maximal activity of Saccharomyces cerevisiae meiosis-specific transcription factor Ndt80 is dependent on Ime2. *Mol Cell Biol*. 22:7024-7040.
Sourirajan, A., and M. Lichten. 2008. Polo-like kinase Cdc5 drives exit from pachytene during budding yeast meiosis. *Genes Dev*. 22:2627-2632.
Stegmeier, F., R. Visintin, and A. Amon. 2002. Separase, polo kinase, the kinetochore protein Slk19, and Spo12 function in a network that controls Cdc14 localization during early anaphase. *Cell*. 108:207-220.
Stevens, B. 1981. Mitochondrial Structure. *In* The Molecular Biology of the Yeast Saccharomyces: Life Cycle and Inheritance. Vol. 11A. J.N.J. Strathern, E. W.; Broach, J. R., editor. Cold Spring Harbor Laboratory Press, New York. 471-504.
Stowers, R.S., L.J. Megeath, J. Gorska-Andrzejak, I.A. Meinertzhagen, and T.L. Schwarz. 2002. Axonal transport of mitochondria to synapses depends on milton, a novel Drosophila protein. *Neuron*. 36:1063-1077.
Suda, Y., H. Nakanishi, E.M. Mathieson, and A.M. Neiman. 2007. Alternative modes of organellar segregation during sporulation in Saccharomyces cerevisiae. *Eukaryot Cell*. 6:2009-2017.
Sullivan, M., and D.O. Morgan. 2007. Finishing mitosis, one step at a time. *Nat Rev Mol Cell Biol*. 8:894-903.
Swayne, T.C., C. Zhou, I.R. Boldogh, J.K. Charalel, J.R. McFaline-Figueroa, S. Thoms, C. Yang, G. Leung, J. McInnes, R. Erdmann, and L.A. Pon. 2011. Role for cER and Mmr1p in anchorage of mitochondria at sites of polarized surface growth in budding yeast. *Curr Biol*. 21:1994-1999.
Tabb, D.L., W.H. McDonald, and J.R. Yates, 3rd. 2002. DTASelect and Contrast: tools for assembling and comparing protein identifications from shotgun proteomics. *J Proteome Res*. 1:21-26.

Tang, X., B.S. Germain, and W.L. Lee. 2012. A novel patch assembly domain in Num1 mediates dynein anchoring at the cortex during spindle positioning. *J Cell Biol*. 196:743-756.

Taylor, G.S., Y. Liu, C. Baskerville, and H. Charbonneau. 1997. The activity of Cdc14p, an oligomeric dual specificity protein phosphatase from Saccharomyces cerevisiae, is required for cell cycle progression. *J Biol Chem*. 272:24054-24063.

Teixeira, F.K., C.G. Sanchez, T.R. Hurd, J.R. Seifert, B. Czech, J.B. Preall, G.J. Hannon, and R. Lehmann. 2015. ATP synthase promotes germ cell differentiation independent of oxidative phosphorylation. *Nat Cell Biol*. 17:689-696.

Tieu, Q., and J. Nunnari. 2000. Mdv1p is a WD repeat protein that interacts with the dynamin-related GTPase, Dnm1p, to trigger mitochondrial division. *J Cell Biol*. 151:353-366.

Tong, J., M.K. Manik, and Y.J. Im. 2018. Structural basis of sterol recognition and nonvesicular transport by lipid transfer proteins anchored at membrane contact sites. *Proc Natl Acad Sci U S A*. 115:E856-E865.

Toulmay, A., and W.A. Prinz. 2013. Direct imaging reveals stable, micrometer-scale lipid domains that segregate proteins in live cells. *J Cell Biol*. 202:35-44.

Tsai, I.T., J.L. Lin, Y.H. Chiang, Y.C. Chuang, S.S. Liang, C.N. Chuang, T.N. Huang, and T.F. Wang. 2014. Interorganelle interactions and inheritance patterns of nuclei and vacuoles in budding yeast meiosis. *Autophagy*. 10:285-295.

Tsuchiya, D., Y. Yang, and S. Lacefield. 2014. Positive feedback of NDT80 expression ensures irreversible meiotic commitment in budding yeast. *PLoS Genet*. 10:e1004398.

Tung, K.S., E.J. Hong, and G.S. Roeder. 2000. The pachytene checkpoint prevents accumulation and phosphorylation of the meiosis-specific transcription factor Ndt80. *Proc Natl Acad Sci U S A*. 97:12187-12192.

Unal, E., B. Kinde, and A. Amon. 2011. Gametogenesis eliminates age-induced cellular damage and resets life span in yeast. *Science*. 332:1554-1557.

Vale, R.D. 1987. Intracellular transport using microtubule-based motors. *Annu Rev Cell Biol*. 3:347-378.

van Werven, F.J., and A. Amon. 2011. Regulation of entry into gametogenesis. *Philos Trans R Soc Lond B Biol Sci*. 366:3521-3531.

van Werven, F.J., G. Neuert, N. Hendrick, A. Lardenois, S. Buratowski, A. van Oudenaarden, M. Primig, and A. Amon. 2012. Transcription of two long noncoding RNAs mediates mating-type control of gametogenesis in budding yeast. *Cell*. 150:1170-1181.

Veatch, J.R., M.A. McMurray, Z.W. Nelson, and D.E. Gottschling. 2009. Mitochondrial dysfunction leads to nuclear genome instability via an iron-sulfur cluster defect. *Cell*. 137:1247-1258.

Visintin, R., K. Craig, E.S. Hwang, S. Prinz, M. Tyers, and A. Amon. 1998. The phosphatase Cdc14 triggers mitotic exit by reversal of Cdk-dependent phosphorylation. *Mol Cell*. 2:709-718.
Visintin, R., E.S. Hwang, and A. Amon. 1999. Cfi1 prevents premature exit from mitosis by anchoring Cdc14 phosphatase in the nucleolus. *Nature*. 398:818-823.
Wagstaff, J.E., S. Klapholz, and R.E. Esposito. 1982. Meiosis in haploid yeast. *Proc Natl Acad Sci U S A*. 79:2986-2990.
Walter, P., and D. Ron. 2011. The unfolded protein response: from stress pathway to homeostatic regulation. *Science*. 334:1081-1086.
Wang, Y., C.Y. Chang, J.F. Wu, and K.S. Tung. 2011. Nuclear localization of the meiosis-specific transcription factor Ndt80 is regulated by the pachytene checkpoint. *Mol Biol Cell*. 22:1878-1886.
Wang, Z., and M. Wu. 2015. An integrated phylogenomic approach toward pinpointing the origin of mitochondria. *Sci Rep*. 5:7949.
Washburn, M.P., D. Wolters, and J.R. Yates, 3rd. 2001. Large-scale analysis of the yeast proteome by multidimensional protein identification technology. *Nat Biotechnol*. 19:242-247.
Waters, M.G., and S.R. Pfeffer. 1999. Membrane tethering in intracellular transport. *Curr Opin Cell Biol*. 11:453-459.
Weidberg, H., F. Moretto, G. Spedale, A. Amon, and F.J. van Werven. 2016. Nutrient Control of Yeast Gametogenesis Is Mediated by TORC1, PKA and Energy Availability. *PLoS Genet*. 12:e1006075.
Weiss, E.L. 2012. Mitotic exit and separation of mother and daughter cells. *Genetics*. 192:1165-1202.
Westermann, B. 2014. Mitochondrial inheritance in yeast. *Biochim Biophys Acta*. 1837:1039-1046.
Williams, C.C., C.H. Jan, and J.S. Weissman. 2014. Targeting and plasticity of mitochondrial proteins revealed by proximity-specific ribosome profiling. *Science*. 346:748-751.
Winter, E. 2012. The Sum1/Ndt80 transcriptional switch and commitment to meiosis in Saccharomyces cerevisiae. *Microbiol Mol Biol Rev*. 76:1-15.
Xu, L., M. Ajimura, R. Padmore, C. Klein, and N. Kleckner. 1995. NDT80, a meiosis-specific gene required for exit from pachytene in Saccharomyces cerevisiae. *Mol Cell Biol*. 15:6572-6581.
Xu, T., S.K. Park, J.D. Venable, J.A. Wohlschlegel, J.K. Diedrich, D. Cociorva, B. Lu, L. Liao, J. Hewel, X. Han, C.C.L. Wong, B. Fonslow, C. Delahunty, Y. Gao, H. Shah, and J.R. Yates, 3rd. 2015. ProLuCID: An improved SEQUEST-like algorithm with enhanced sensitivity and specificity. *J Proteomics*. 129:16-24.
Yaffe, M.P., N. Stuurman, and R.D. Vale. 2003. Mitochondrial positioning in fission yeast is driven by association with dynamic microtubules and mitotic spindle poles. *Proc Natl Acad Sci U S A*. 100:11424-11428.

Yeh, E., R.V. Skibbens, J.W. Cheng, E.D. Salmon, and K. Bloom. 1995. Spindle dynamics and cell cycle regulation of dynein in the budding yeast, Saccharomyces cerevisiae. *J Cell Biol*. 130:687-700.

Yoshida, M., H. Kawaguchi, Y. Sakata, K. Kominami, M. Hirano, H. Shima, R. Akada, and I. Yamashita. 1990. Initiation of meiosis and sporulation in Saccharomyces cerevisiae requires a novel protein kinase homologue. *Mol Gen Genet*. 221:176-186.

Yoshida, S., K. Asakawa, and A. Toh-e. 2002. Mitotic exit network controls the localization of Cdc14 to the spindle pole body in Saccharomyces cerevisiae. *Curr Biol*. 12:944-950.

Youk, H., and W.A. Lim. 2014. Secreting and sensing the same molecule allows cells to achieve versatile social behaviors. *Science*. 343:1242782.

Yu, J.W., J.M. Mendrola, A. Audhya, S. Singh, D. Keleti, D.B. DeWald, D. Murray, S.D. Emr, and M.A. Lemmon. 2004. Genome-wide analysis of membrane targeting by S. cerevisiae pleckstrin homology domains. *Mol Cell*. 13:677-688.

Yue, J.X., J. Li, L. Aigrain, J. Hallin, K. Persson, K. Oliver, A. Bergstrom, P. Coupland, J. Warringer, M.C. Lagomarsino, G. Fischer, R. Durbin, and G. Liti. 2017. Contrasting evolutionary genome dynamics between domesticated and wild yeasts. *Nat Genet*. 49:913-924.

Zick, M., R. Rabl, and A.S. Reichert. 2009. Cristae formation-linking ultrastructure and function of mitochondria. *Biochim Biophys Acta*. 1793:5-19.

Appendix A

Other Results

A.1 mtDNA segregation in meiosis

A.1.1 Introduction

A distinguishing feature of mitochondria is that they contain their own genome. The mitochondrial DNA (mtDNA) is a remnant of the bacterial ancestor that gave rise to mitochondria (Ferla et al., 2013; Lane, 2006; Wang and Wu, 2015). In most organisms, mtDNA is essential for viability. However, in budding yeast, mtDNA is dispensable in the presence of a fermentable carbon source such as dextrose (glucose). Mutants that lack functional mtDNA are called "petite," due to the small colonies formed by these strains (Dujon, 1981). Strains with functional mtDNA are called "grande." The petite phenotype can be unambiguously determined by the inability to grow on a nonfermentable carbon source such as glycerol.

Petite mutants can arise spontaneously during vegetative growth, and when they do exhibit a non-Mendelian inheritance pattern (Dujon, 1981). The petite phenotype in yeast has been extensively reviewed (Dujon, 1981) and will be only outlined here. In cases where the mitochondrial genome is absent (ρ^0), outcrossing to a wild-type (ρ^+) strain always yields the meiotic segregation pattern 0:4 petite:grande. In cases where the genome is present but nonfunctional (ρ^-), the segregation pattern is most often the same 0:4 petite:grande. However, in exceptional cases the segregation pattern is reversed. 4:0 petite:grande often occur, as well as other tetrad types. Such 'dominant' petites can be viewed as non-Mendelian antimorphs and are called "suppressive petites" or "hypersuppressive petites," depending on the magnitude of the effect. The molecular basis of petite suppressiveness is loss of the mtDNA protein-coding genes in favor of origins of replication. Essentially, the mitochondrial genome becomes a parasite that out-replicates the competitor ρ^+ genomes.

Here, we examined the inheritance pattern of the spontaneous petite phenotype when it arises in meiosis rather than in vegetative growth. The segregation pattern of spontaneous petite mutants suggests sporadic mitochondrial catastrophe during meiosis, rather than spore-autonomous acquisition of the petite phenotype. This was surprising, because respiration is required throughout meiosis (Jambhekar and Amon, 2008; Weidberg et al., 2016). We also performed a genetic screen to identify mutants with elevated spore petite frequencies, but we were ultimately not successful. However, in the process of designing the screen we developed tools that will be useful for future work.

A.1.2 Inheritance pattern of the petite phenotype in meiosis

This work began with the observation that, although uncommon, petite spore clones occasionally arise during tetrad dissection. Oftentimes, a tetrad would contain 4 petite spore clones (Figure A.1A). Previous studies demonstrated that the ability to respire is required for transcription of *IME1*, which encodes the transcription factor that promotes entry into meiosis (Jambhekar and Amon, 2008; Weidberg et al., 2016). Remarkably, in conditions where wild-type strains can be induced to sporulate in rich medium (by chemical inhibition of the TOR and PKA nutrient sensing pathways), respiratory-deficient mutants are still unable to sporulate (Weidberg et al., 2016). This finding indicates that there is a distinct requirement for respiration during the meiotic divisions and gamete formation. In light of those results, our observation of petite gametes was paradoxical: how are petite meiotic products formed, when the developmental program that gives rise to them is dependent on respiration?

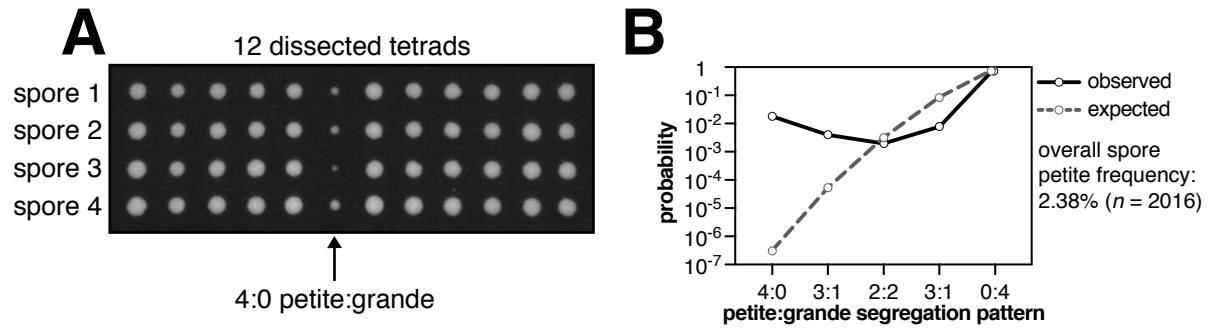

Figure A.1. Petite mutants arise spontaneously but spore non-autonomously during meiosis. A. An example of a spontaneous 4:0 petite:grande tetrad (UB8338 x UB18405). The dissected tetrad indicated by an arrow contains 4 petite spore clones, while all other tetrads contained 4 grande spore clones. The petite phenotype was tested by replica plating to a YPG plate (not shown). **B.** Frequency of each petite tetrad type in dissected tetrads (n = 504 tetrads). In total, 48 petite spore clones and 1968 grande spore clones were identified (overall petite frequency = 2.38%). The binomial distribution was used to calculate the expected frequencies of each tetrad type based on the overall petite frequency. The observed distribution of tetrad types as well as the expected values from the binomial model are plotted. The y-axis is represented on a $\log_{10}$ scale. Tetrads were of mixed genotypes, but no mutants that affect mitochondrial function were considered.

We first considered the possibility that spores might acquire the petite phenotype independently of one another after meiosis. Because we assessed respiratory function by replica plating after colonies had already grown, it was possible that cells acquired the petite phenotype during germination or subsequent vegetative growth. To address this possibility, we examined the distribution of different tetrad types containing petite and grande spore clones. In total, we examined 504 tetrads (2016 spores) and measured an overall spore petite frequency of 2.38% (48/2016). Next, we considered whether petite spores arose independently and at random, or whether spores derived from the same tetrad had correlated fates. The first possibility would indicate that the petite phenotype was acquired during germination or vegetative growth, while the second possibility suggests a meiotic catastrophe.

Considering that each spore can be either petite or grande, five tetrad types are possible: 4:0 petite:grande, 3:1 petite:grande, 2:2 petite:grande, 1:3 petite:grande, and 0:4 petite:grande. Because only two outcomes for each spore are possible (petite or grande), the expected frequencies of each tetrad type are predicted by the binomial distribution. (The same distribution governs a series of coin flips: what is the probability of flipping 4 heads in a row? 3 heads and 1 tails?) If spores become petite autonomously and at random (i.e., if like a coin flip, the result of one trial does not influence the probability of the next), the five possible tetrad types should follow the binomial model. Instead, the data strongly contradicted the expected tetrad frequencies given by the binomial distribution (Figure A.1B). The 4:0 petite:grande tetrad type, which is predicted to be the most uncommon, was 10^5 times more common than predicted by the binomial model. Our data indicate that the petite spore phenotype is not spore-autonomous. Instead, the fates of spores within the same tetrad were highly correlated and consistent with mitochondrial catastrophe during the gametogenesis program.

A.1.3 A screen for meiotic petite mutants

Because spores within a tetrad generally co-acquired the petite phenotype, we reasoned that the low-level petite frequency of spores could be due to sporadic catastrophes during meiosis. For example, the fidelity of mtDNA segregation to spores could be ~98%, and ~2% of the time spores do not inherit mtDNA. Further, we reasoned that the low but non-zero frequency of petite spores in wild type might indicate that mutants with heightened spore petite frequencies could be obtained by mutagenesis. To genetically dissect the spore petite phenotype, we aimed to perform a genetic screen.

Genetic screening in meiosis is complicated by the fact that *MAT***a** or *MAT*α haploids do not enter meiosis, even under nutrient deprivation. To circumvent this limitation, we generated a *MAT***a** haploid strain that contains an ectopic *MAT*α cassette integrated at the *URA3* locus (Figure A.2A). Conveniently, because this

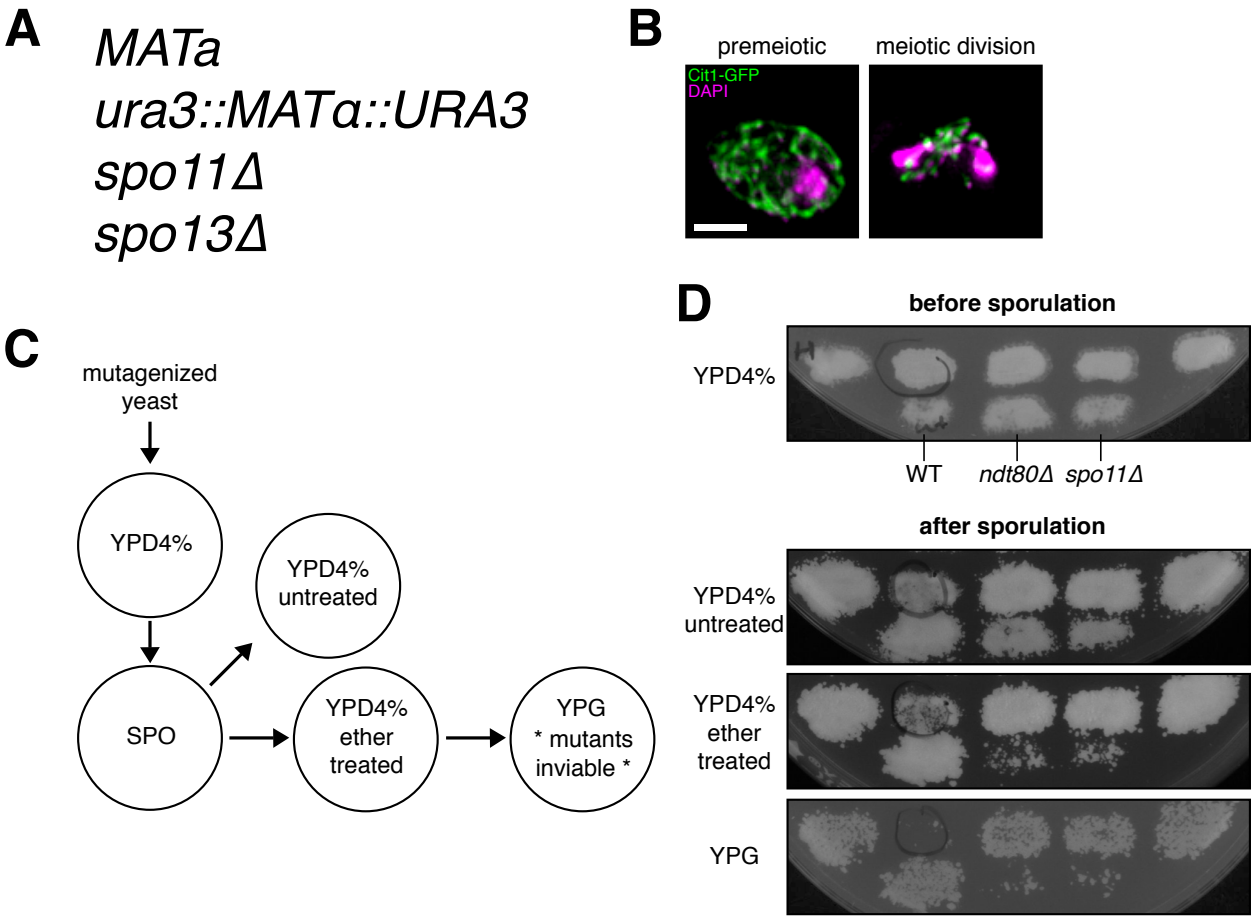

Figure A.2. A genetic screen to identify meiotic petite mutants. A. The genotype of the wild-type haploid sporulator strain. **B.** Maximum intensity projections of fixed haploid sporulator strain expressing Cit1-GFP to label mitochondria and stained with DAPI (UB9897). **C.** Diagram of screen replica plating approach. YPD4%, YPD solid medium with 4% dextrose. YPG, identical medium except 3% glycerol replaces dextrose. SPO, sporulation plate. **D.** Example plate phenotypes of controls and a meiotic petite mutant (circled in pen). WT, wild type, can sporulate and give rise to viable, ether-resistant spores. *ndt80Δ* cannot sporulate and so all cells should be ether sensitive. *spo11Δ* forms inviable spores, and unsporulated cells should be ether sensitive.

allele was generated by a plasmid-based "ends-in" transformation, the *MAT***a** *ura3*::*MAT*α::*URA3* strain can be reverted to *MAT***a** *ura3* by selection for spontaneous plasmid "pop-outs" on 5-fluoroorotic acid. Cells treated with 5-fluoroorotic acid produce 5-fluorouracil, a toxic compound, in a reaction that

depends on Ura3. Therefore, loss of *URA3* (and in this case, *MAT*α as well as *URA3*) can be selected for using 5-fluoroorotic acid medium.

Although "pseudodiploid" strains can enter meiosis, spore viability is poor due to the incompatibility of a haploid genome with two meiotic divisions. To overcome this limitation, we performed the screen in a *spo11Δ spo13Δ* background (Figure A.2A), where no DNA breaks occur in prophase I, and only a single equational round of chromosome segregation occurs (Klapholz and Esposito, 1980; Wagstaff et al., 1982). We termed this genetic background the "haploid sporulator." Essentially, meiosis is converted into mitosis, but the gamete differentiation program that accompanies meiosis remains intact (Wagstaff et al., 1982). To confirm that is the case, we monitored the localization of mitochondria during the single meiotic division in the haploid sporulator background. We observed normal mitochondrial dynamics (Figure A.2B), indicating that the strain can successfully undergo cellular remodeling in gametogenesis.

To perform the meiotic petite screen, we subjected the haploid sporulator strain to high-dose ethyl methanesulfonate mutagenesis. After treatment with 3% ethyl methanesulfonate for 80 min, 50% or 75% of cells died (2 replicates) based on counting colony-forming units on YPD4% plates. We plated the mutagenized cells on YPD4% to obtain single colonies and expanded them into patches on solid YPD4% medium. In total, we examined 12,910 mutants. To assess the meiotic petite phenotype, we transferred the patched mutants through a series of plate conditions by a replica plating strategy (Figure A.2C). Mutant patches were first replica plated to sporulation (SPO) medium, then replica plated to two YPD4% plates. One was allowed to grow as a control, and the other was treated with ether vapor to kill unsporulated cells (Rockmill et al., 1991). After patches grew on the ether-treated plate, we replica plated to YPG to assess the petite phenotype. Mutants that grew on all plates except the YPG plate were scored as meiotic petite mutants (Figure A.2D). We identified a total of 64 mutants that met these criteria and proceeded to secondary screening.

In the secondary screening, we repeated the replica plating assay. We found that in general the phenotypes were not reproducible. In particular, many mutants appeared to have a strong cell adhesion phenotype that caused poor cell transfer during replica plating. In these cases, it is likely that the mutants were selected based on this technical artifact. In the remaining cases, through follow-up experiments with liquid sporulation and plating, we determined that the initial phenotype could be explained through low sporulation efficiency or constitutively elevated petite frequency. In summary, none of the mutants possessed the meiotic petite phenotype.

Although our screen was not successful in identifying mutants with the phenotype of interest, in the process we validated the haploid sporulator as a general tool for

genetic screening in meiosis. During development of the screening method, we also tested a method for genetic selection of petites that could be useful for future work. This method uses a chemical compound, triphenyl tetrazolium chloride (TTC; Figure A.3A) spread on the top of YPD agar. Although TTC is generally used as a colorimetric indicator for respiratory activity (Ogur et al., 1957), the dye is also toxic to respiring cells—but not to respiratory deficient cells—at high concentrations (Bachofen et al., 1972). We found that top-spread 25 μg/mL TTC effectively killed grande cells but not the respiratory-deficient *pet100Δ* mutant (Figure A.3B). The few wild-type control cells that grew on the TTC plates (Figure A.3B) proved to be spontaneous petite mutants when tested for their ability to grow on the nonfermentable carbon source YPG (3% glycerol) without TTC. Consistent with the high stringency of the drug, no growth was observed on YPG plates top-spread with TTC, regardless of strain genotype. This result indicates that respiration and the 25 μg/mL dose of TTC are mutually exclusive. We conclude that top-spread TTC on agar plates is an effective means for selecting petite mutants.

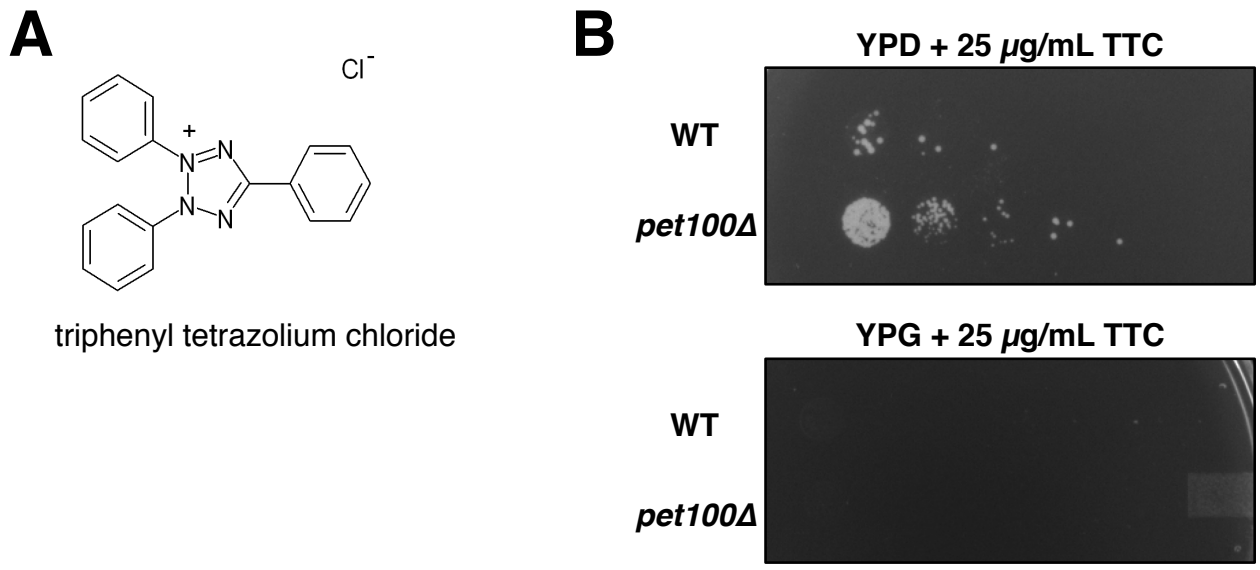

Figure A.3. A method for selecting petite mutants by triphenyl tetrazolium chloride (TTC) top-spreading. A. The structure of triphenyl tetrazolium chloride. **B.** Serial dilution plating assay of wild type (UB15) and the respiratory-deficient *pet100Δ* mutant (UB2781) on YPD (2% dextrose) or YPG (3% glycerol) treated with TTC and grown for 3 d at 30°C. Both plates were top-spread with TTC for a final concentration of 25 μg/mL (assuming plate volumes of 30 mL and free diffusion of TTC through the plate). The wild-type (UB15) TTC-resistant colonies were unable to grow when transferred to a YPG plate lacking TTC (not shown), indicating that they are spontaneous petite mutants and not escapers of the selection.

A.1.4 Discussion

In this work we analyzed the inheritance pattern of the respiratory-deficient petite phenotype in gametogenesis. Because petite mutants cannot enter meiosis, we concluded that the petite condition must be acquired during or after gametogenesis. By tetrad analysis, we found that spores derived from the same tetrad had highly correlated fates. The 4:0 petite:grande tetrad class was 10^5 times more common than predicted to occur if the petite phenotype were acquired spore-autonomously. This observation indicates that the petite phenotype arises during gametogenesis.

How do petites arise during gametogenesis? Our observation was surprising, because respiratory function is required not only for meiotic entry but also during meiosis (Jambhekar and Amon, 2008; Weidberg et al., 2016). However, our statistical analysis only indicated that gametes were *fated* to the petite phenotype during gametogenesis, not that the diploid progenitors were wholly respiratory deficient. There are several models that can explain our data. First, a catastrophe could occur during the late stages of gametogenesis where mitochondria are segregated to spores. Cases of petite spores could arise from rare situations where the mitochondrial network failed to adequately detach from the plasma membrane (Chapter 2) or attach to the nuclear envelope (Chapter 3). Because mitochondria are essential for viability, and it is only absence or dysfunction of the mtDNA that gives rise to the petite phenotype, some mitochondrial inheritance would have to occur in these cells. Second, our observation could be due to a mixed population of mtDNA (petite and grande) in the progenitor cell giving rise to solely or mostly petite gametes. As selfish "suppressive" petite mtDNAs have been long known to occur spontaneously in vegetative growth (Dujon, 1981), it is possible they could arise during gametogenesis. This notion could be tested by outcrossing petite spore clones to a ρ^+ strain and measuring suppressiveness. If the spontaneous petites are suppressive, it would be interesting to determine whether the suppressive petite mtDNAs exploit a gametogenesis-specific mitochondrial inheritance bottleneck. An inheritance bottleneck for mtDNA has been observed in *Drosophila* oogenesis (Hurd et al., 2016), which can be exploited by selfish mitochondrial genomes (Ma and O'Farrell, 2016). In yeast, by electron microscopy analysis, only about half of the mitochondrial volume is transmitted to yeast gametes (Brewer and Fangman, 1980). However, restrictions on mtDNA inheritance have not been defined. Alternatively, the suppressive petite mtDNAs could overtake the population of mtDNAs during germination and vegetative growth of the colony. These two possibilities could be distinguished through mtDNA sequencing, mtDNA nucleoid imaging technologies (Osman et al., 2015), or DNA FISH, which should be able to directly examine healthy and dysfunctional mtDNAs throughout the gametogenesis program and in subsequent germination. A third possibility is that the microenvironment of particular tetrads leads to mtDNA damage and loss of respiratory capacity. Testing the predictions of these three models could illuminate

what inheritance and quality control pathways might exist in gametogenesis, and perhaps how rogue mtDNAs could exploit them.

Although our genetic screen to identify mutants that commonly—instead of rarely—form petite gametes did not succeed, we developed a useful tool in the process. The haploid sporulator strain (Figure A.2A; (Wagstaff et al., 1982)) allows standard yeast genetic analysis to be easily applied to meiosis. As most mutations are recessive, beginning with a haploid strain is critical to the success of yeast genetic screens. The haploid sporulator strain will be generally useful for screens aiming to study the cellular remodeling aspects of the gamete differentiation program. Although the meiotic chromosome segregation pattern is suppressed in this strain, phenotypically normal gametes are still produced. An additional advantage we have introduced is that selection on 5-FOA yields *MAT***a** haploids isogenic to the original mutant, making it possible to perform crosses for complementation analysis and genetic mapping. In any situation where recessive mutations with meiotic phenotypes are desired, the haploid sporulator strain could prove a valuable tool.

A.2 Expression patterns of mitochondrial proteins in meiosis

A.2.1 Introduction

Gametogenesis is a cellular differentiation program that involves dynamic regulation of gene expression (Brar et al., 2012; Cheng et al., 2018; Chu et al., 1998; Primig et al., 2000). Although by their nature meiosis-specific genes exhibit temporally regulated expression, genes common to mitosis and meiosis often also exhibit dynamic regulation (Brar et al., 2012; Cheng et al., 2018; Chu et al., 1998; Primig et al., 2000).

The mitochondrial proteome is a mosaic of proteins encoded in the nuclear genome and in the mitochondrial genome. The yeast mitochondrial genome encodes rRNAs and tRNAs but only eight proteins (Engel et al., 2014; Fox, 2012). The large majority of mitochondrial proteins are synthesized on cytosolic ribosomes and imported into the organelle (Fox, 2012).

Here, we examined the expression patterns of mitochondrial genes encoded in the nuclear and mitochondrial genomes by analyzing published genome-wide datasets. A subset of mitochondrial inner membrane proteins were highly induced in saturated culture. Proteins associated with mtDNA exhibited dynamically regulated expression, with three critical mtDNA replication factors being co-expressed during the meiotic divisions. The mitochondrial RNA polymerase was repressed during most of meiosis, and mitochondrially encoded mRNAs were reduced in their expression during that time. These expression patterns are consistent with—but fall short of demonstrating—mtDNA amplification occurring during a period of mitochondrial transcriptional quiescence.

A.2.2 Results

To analyze expression patterns during meiosis for genes encoding mitochondrial proteins, we began by analyzing the expression of mitochondrial membrane proteins using a published dataset (Brar et al., 2012). In this study, two meiotic timecourses were densely sampled and analyzed by mRNA-seq and ribosome profiling. Ribosome profiling provides a quantitative measurement of ribosome occupancy on mRNAs, which by inference provides the rate of protein synthesis. The expression patterns of mitochondrial membrane proteins varied considerably, but four clusters were apparent (Figure A.4A). When the genes in each cluster were analyzed for enriched gene ontology terms by AmiGO 2 (Ashburner et al., 2000; Carbon et al., 2009; Consortium, 2019), we found that three of the four clusters showed no significantly enriched terms (besides generic mitochondrial membrane terms, which were the basis of their original selection). The remaining cluster (cluster 3) contains genes with much higher expression levels in saturated culture than in any stages of meiosis, and a subset are additionally down-regulated during meiosis II and some of the meiosis I time points (Figure A.4A). Cluster 3 was enriched for four mitochondrial inner membrane protein complexes: the respiratory complexes III and V, the MICOS complex, and the Tim23 protein import complex (Figure A.4A). Except for the Tim23 complex, for which half of its subunits were present in this cluster, all or nearly all subunits were present for the enriched protein complexes. We conclude that mitochondrial membrane proteins are not uniformly expressed during meiosis but instead often exhibit dynamic regulation. Further, a subset of inner membrane protein complexes are highly expressed in saturated culture.

To further examine the regulation of the mitochondrial proteome, we next examined the regulation of nuclear genome-encoded factors that control mitochondrial gene expression. The mitochondrial ribosome contains mtDNA-derived rRNAs, but its protein subunits are encoded in the nuclear genome. The expression patterns of the protein components of the large and small mitochondrial ribosomal subunits were quite similar (Figure A.4B). The proteins were nearly universally highly expressed in saturated culture, much like Cluster 3 above. This commonality could indicate a coordination between the expression of the nuclear and mitochondrially encoded inner membrane proteins. In addition, many mitochondrial ribosome subunits were up-regulated during meiosis II. However, as noted previously (Brar et al., 2012), perhaps the most striking feature of these data was that mitochondrial ribosomes are much more heavily expressed during meiosis than the cytosolic ribosomes and translation machinery, which are heavily down-regulated.

Next we examined the expression of nuclear genome-encoded factors with functions directly regulated to mtDNA maintenance. Three proteins, the mtDNA DNA polymerase Mip1, the HMG family mtDNA packing protein Abf2, and the replicative ssDNA binding protein Rim1, were all up-regulated during the meiotic

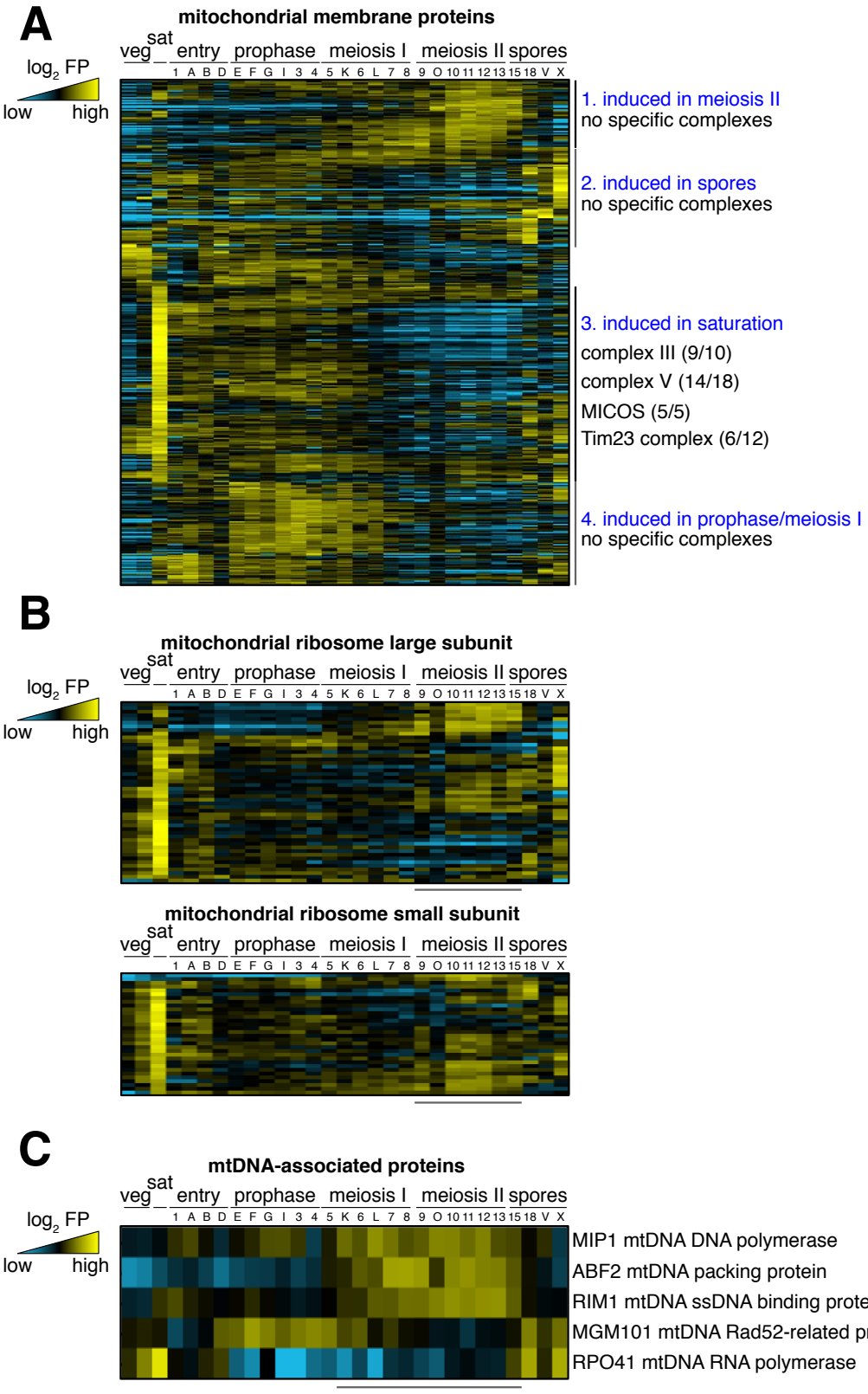
A
mitochondrial membrane proteins
log2 FP
low
high
veg
sat
entry
prophase
meiosis I
meiosis II
spores
1 A B D E F G I 3 4 5 K 6 L 7 8 9 O 10 11 12 13 15 18 V X
1. induced in meiosis II
no specific complexes
2. induced in spores
no specific complexes
3. induced in saturation
complex III (9/10)
complex V (14/18)
MICOS (5/5)
Tim23 complex (6/12)
4. induced in prophase/meiosis I
no specific complexes
B
mitochondrial ribosome large subunit
mitochondrial ribosome small subunit
C
mtDNA-associated proteins
MIP1 mtDNA DNA polymerase
ABF2 mtDNA packing protein
RIM1 mtDNA ssDNA binding protein
MGM101 mtDNA Rad52-related protein
RPO41 mtDNA RNA polymerase

Figure A.4. Ribosome profiling expression patterns of mitochondrial proteins. Clustered heat maps of cytosolic ribosome footprint density during vegetative growth, saturation, and meiosis. Stages of meiosis are indicated above, and alphanumeric meiotic time points are indicated from the original study (Brar et al., 2012). Expression level is normalized by gene, and genes are clustered. **A.** Cytosolic ribosome footprint density for mitochondrial membrane proteins. The gene list was obtained from Gene Ontology. Four clusters are apparent: (1) induced during the meiotic divisions, (2) induced in spores, (3) highly expressed in saturation, and (4) induced in prophase and meiosis I. Cluster 3 is labeled with selected GO cellular components determined by AmiGO 2 (Ashburner et al., 2000; Carbon et al., 2009; Consortium, 2019). Fractions indicate the number of genes for the GO term in the cluster out of the total number of genes assigned to that GO term. Clusters 1, 2, and 4 do not contain any significantly enriched cellular components besides generic mitochondrial membrane terms. **B.** Cytosolic ribosome footprint density for genes encoding components of the mitochondrial ribosome. Bars indicate meiotic time window where many subunits are upregulated. **C.** Cytosolic ribosome footprint density for proteins associated with mtDNA. Gene names and their functions are indicated next to the heatmap. Bar indicates time window where *MIP1*, *ABF2*, and *RIM1* are induced and *MGM101* is repressed.

---

divisions (Figure A.4C). The Rad52-like mitochondrial protein Mgm101 was well-expressed at most stages of meiosis but strikingly down-regulated during the meiotic divisions, giving an expression pattern anti-correlated to the previously mentioned factors (Figure A.4C). Finally, the mitochondrial RNA polymerase, Rpo41, was strongly repressed throughout meiosis, not returning until spore packaging (Figure A.4C). Interestingly, when Rpo41 returned, Mip1, Abf2, and Rim1 were suddenly down-regulated again. The data indicate that proteins acting directly on mtDNA exhibit dynamic and apparently coordinated expression patterns.

Because the dataset suggested temporal regulation of mtDNA factors, we next examined whether mitochondrially encoded mRNAs were differentially expressed during meiosis. We examined the abundances of six of the eight mitochondrially encoded mRNAs in a total RNA-seq meiotic dataset (Cheng et al., 2018), which should efficiently capture mitochondrial transcripts. We found that all six transcripts were markedly down-regulated during meiosis and later returned in later stages and in spores (Figure A.5). The expression patterns for the mitochondrial transcripts very clearly mirrored the decline and return of Rpo41 synthesis (Figure A.5). This apparent coordination suggests that expression of the mtDNA-encoded transcripts might be regulated by the abundance of the RNA polymerase.

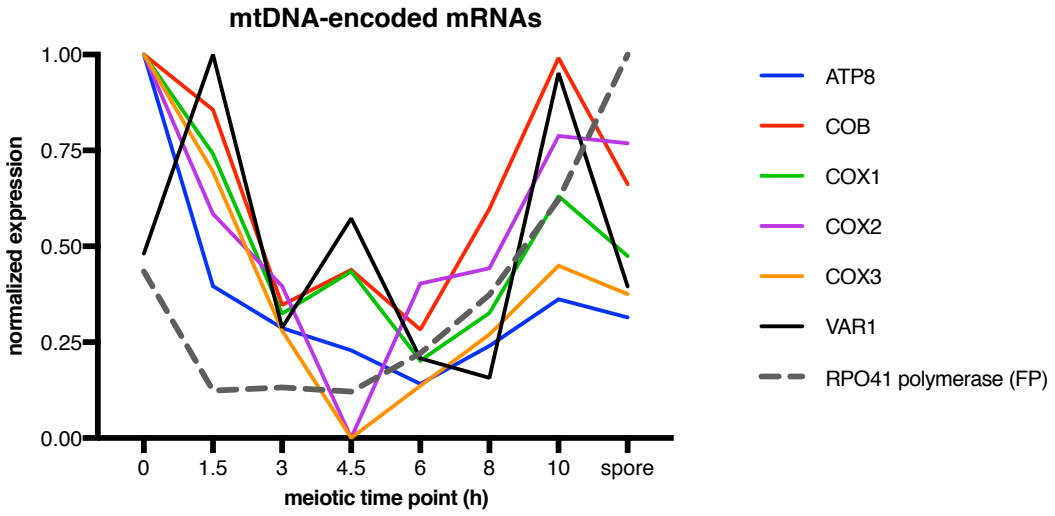

Figure A.5. Abundances of mitochondrially encoded protein-coding mRNAs in meiosis. Analysis of a published total RNA-seq dataset (Cheng et al., 2018). The RPKM values were normalized to the maximum values for each gene in the meiotic time course. *OLI1* and *ATP6* mRNAs had very low (sometimes 0) RPKM values and were excluded from this analysis. The ribosome footprint density (protein synthesis rate) for the nuclear genome-encoded mitochondrial RNA polymerase (Rpo41) is plotted with a dashed line.

A.2.3 Discussion

In this work we examined the expression of mitochondrial genes through the dynamic developmental program of meiosis. This analysis was possible due to high quality genome-wide sequencing datasets for yeast meiosis (Brar et al., 2012; Cheng et al., 2018). As cells rely on respiration during meiosis due to nutritional controls, it seems reasonable that cells would uniformly express mitochondrial proteins throughout meiosis. Instead, the patterns of gene expression were dynamic (Figures A.4 and A.5). We noted particularly striking expression patterns for the subunits of respiratory complex III and complex V as well as the mitochondrial inner membrane structuring MICOS complex. In each case, the subunits were much more highly translated in saturated culture than in any stages of meiosis. MICOS has been implicated in modulating cristae structure and the arrangement of respiratory complexes (Friedman et al., 2015), perhaps indicating developmental regulation of the structure of cristae. Such regulation has been observed in male gametogenesis in *Drosophila*, where a gametogenesis-specific ATP synthase subunit is expressed to modulate mitochondrial ultrastructure (Sawyer et al., 2017). In female *Drosophila*, complex V subunits—but not other respiratory complex subunits—are required for

gametogenesis due to their regulation of cristae remodeling (Teixeira et al., 2015). The metabolic activity of oocyte mitochondria is also dynamically regulated. Transient reduction in respiratory complexes I and V lead to reduced metabolic activity and altered cristae structure that is reversed prior to embryogenesis (Sieber et al., 2016). Perhaps remodeling of cristae and the respiratory complexes are conserved features of gametogenesis.

We also noticed that mtDNA replication and transcription machineries were dynamically regulated during gametogenesis (Figure A.4). The DNA polymerase, the protein responsible for packaging mtDNA, and the ssDNA binding protein were coordinately up-regulated during the meiotic divisions. This up-regulation could potentially promote mtDNA replication. Future work to address this possibility, such as 5-ethynyl-2′-deoxyuridine pulse labeling, would conclusively address whether replication of the mitochondrial genome is dynamically regulated during gametogenesis. A burst of mtDNA synthesis during meiosis could explain the surprising tendency of dysfunctional mtDNAs to arise during gametogenesis (Section A.1). Perhaps most surprising was that the mitochondrial RNA polymerase was strongly repressed during meiosis (Figures A.4 and A.5). This down-regulation coincided with a marked decline in the levels of transcripts encoded by the mitochondrial genome (Figures A.5). These patterns suggest that the replication and expression of the mitochondrial genome are developmentally regulated. Both would be fascinating directions for future study with implications for homeostasis of the mitochondrial genome in diverse biological contexts.

A.3 Mitophagy in meiosis

A.3.1 Introduction

Macroautophagy (here, "autophagy") is a conserved process that sequesters and destroys subcellular components, and the underlying pathway has been intensely studied in yeast (Reggiori and Klionsky, 2013). In brief, materials destined for degradation are first isolated in a nascent double-membrane compartment called the phagophore. The phagophore matures into a closed double-membrane compartment called the autophagosome, which fuses with the vacuole and releases the inner membrane-bound compartment containing cargo as an "autophagic body." The autophagic body is destroyed by degradative enzymes in the vacuole. Autophagy is commonly referred to as "selective" or "nonselective." In selective autophagy, the contents of the phagophore are actively determined. In nonselective autophagy, they are not.

Mitochondria can be degraded by selective autophagy, termed mitophagy. In yeast, mitophagy relies on a mitochondria-localized protein, Atg32, which directs the autophagy machinery to the organelle (Kanki and Klionsky, 2008; Kanki et al., 2009b; Kanki et al., 2009c). Yeast autophagy studies generally induce autophagy by

nitrogen starvation or treatment with rapamycin. However, how autophagy is regulated in a natural, developmental context such as gametogenesis is poorly understood. Strikingly, many autophagy genes, such as *ATG8* and the mitophagy receptor *ATG32* are temporally regulated during gametogenesis (Brar et al., 2012).

Here, we examined mitophagy during different stages of gametogenesis. We found that mitophagy is essentially uniform throughout gametogenesis and degrades substrates with diverse mitochondrial localizations. Mitophagy is dependent on the known receptor, Atg32.

A.3.2 Results

To examine mitophagy during meiosis we used an established immunoblotting assay (Kanki et al., 2009a). In this assay, the protein of interest is tagged with GFP. In the absence of autophagy, the protein runs at its full molecular weight by SDS-PAGE. When degraded by autophagy, the protein-GFP fusion is processed in a manner that leaves only the GFP intact. The ratio of free GFP to total signal is a semi-quantitative indicator of the level of autophagy. To begin, we examined an abundant mitochondrial outer membrane protein, Om45, that is the most commonly used target for this assay. We found that Om45-GFP ran only at its full length during the premeiotic time point (0 h). During all subsequent stages of meiosis, processed free GFP was visible at an essentially identical level (Figure A.6A). The processing depended on Atg32 (Figure A.6A), indicating that mitophagy in meiosis occurs through the known Atg32 pathway. We conclude that mitophagy occurs throughout gametogenesis and is regulated by the known receptor Atg32.

Next we examined the nucleoid-associated protein Abf2 by the same immunoblot autophagy assay. Our results were identical to what was observed with Om45. Abf2-GFP was not degraded at the premeiotic time point, but free GFP was visible at all other time points examined and at a stable level (Figure A.6B). Interestingly, high free GFP signal was observed at 24 h, indicating ongoing autophagy or delayed clearance of the processed GFP (Figure A.6B). We conclude that meiotic autophagy extends not only to mitochondrial membrane proteins but also to proteins associated with the mitochondrial genome.

Having established that Atg32 is required for mitophagy in meiosis, we next sought to determine the consequence of mitophagy inhibition. To do so, we examined the localization of the mitochondrial protein Om45-GFP in cells expressing a marker of the prospore membrane, Rrt5-mKate2. In wild-type cells, a subset of mitochondria were segregated to gametes, and the remaining (uninherited) pool of mitochondria eventually disappeared (Figure A.7). However, in *atg32Δ* cells, a substantial amount of mitochondrial mass persisted even long after spore formation (Figure A.7). Our data indicate that Atg32 is required for the efficient clearance of mitochondria during gametogenesis. Because the vacuole normally lyses late in

meiosis to clear uninherited material, our findings suggest that vacuolar lysis might be impaired in *atg32Δ* cells or that Atg32 plays a role in promoting degradation of mitochondria even after vacuolar lysis.

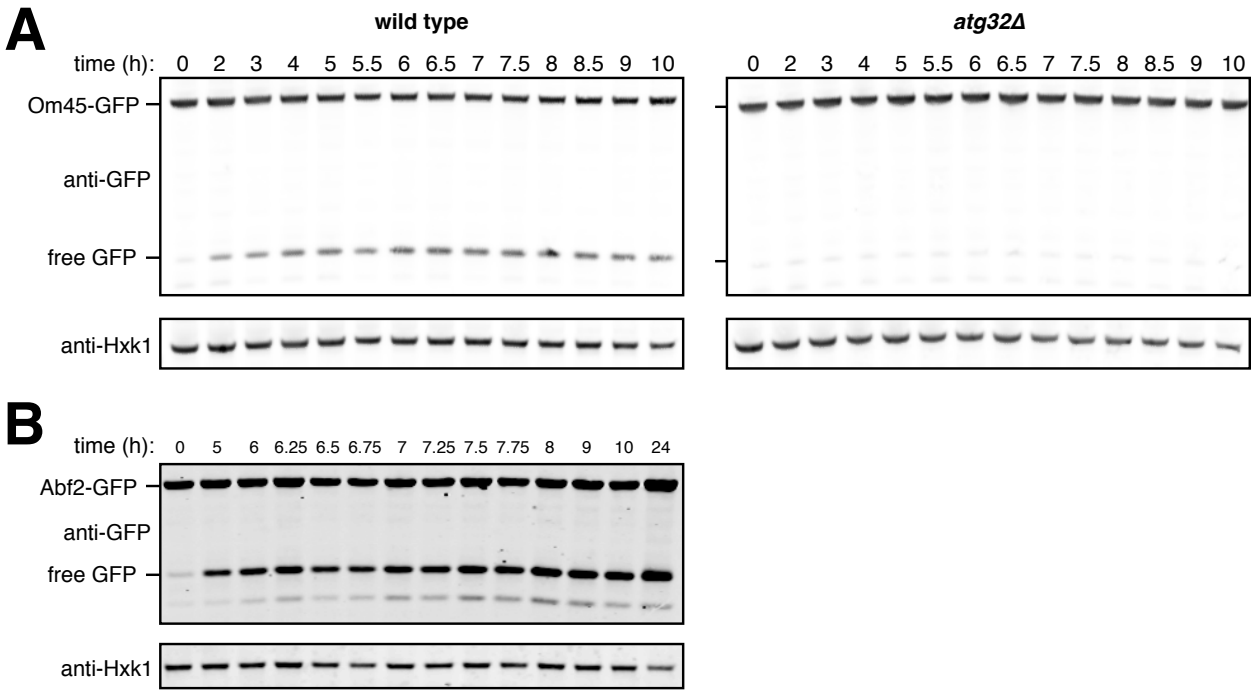

Figure A.6. Mitochondrial proteins are degraded by autophagy in meiosis. Immunoblot autophagy assays of GFP-tagged mitochondrial proteins through meiotic time courses. **A.** Om45-GFP autophagy in wild type (UB3286) and *atg32Δ* (UB3284). **B.** Abf2-GFP (UB8503) autophagy. Cells were induced to sporulate for 5 h, then *pGAL-NDT80 GAL4.ER* induced by addition of 1 μM ß-estradiol.

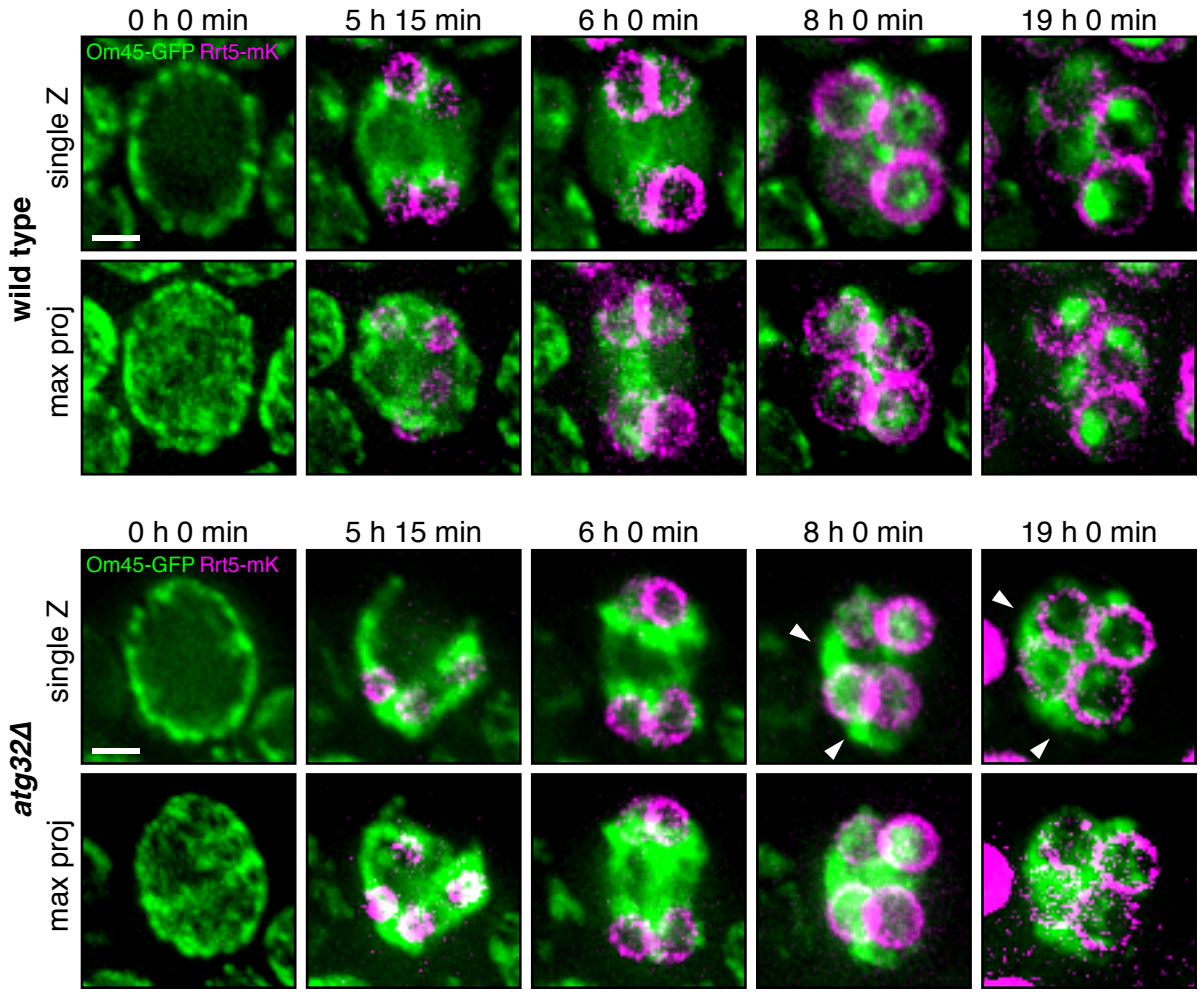

Figure A.7. Atg32 promotes removal of uninherited mitochondria. Time-lapse microscopy showing the localization of mitochondria in live wild-type (UB3521) and *atg32Δ* (UB3494) cells. Mitochondria, Om45-GFP. Prospore membrane, Rrt5-mKate2. The Rrt5-mKate2 channel is shown with high contrast due to low signal in most time points. Time is relative to the first frame, which was the initial frame acquired in the experiment. Arrowheads, spore-excluded mitochondria.

A.3.3 Discussion

Autophagy is a major degradative pathway in the cell. In meiosis, autophagy genes are dynamically regulated (Brar et al., 2012). The significance of autophagy gene temporal regulation in meiosis is not understood, nor are the potential stage-specific functions of autophagy that this regulation might promote. Interestingly, an exotic form of autophagy termed "mega-autophagy" occurs during the latest stages of yeast gametogenesis (Eastwood et al., 2012; Eastwood and Meneghini, 2015). In postmeiotic cells, the vacuole is permeabilized and lyses, leading to the destruction

of spore-excluded material not by their delivery to the vacuole but by the delivery of vacuolar proteases to the material (Eastwood et al., 2012; Eastwood and Meneghini, 2015). In cells containing age-associated damage, vacuolar lysis is used to degrade the damaged material after it is specifically sequestered away from gametes (King et al., 2019). It is therefore surprising that deletion of Atg32 leads to persistence of mitochondria outside the gametes. It is unexpected that Atg32 would have any role in mitochondrial degradation during mega-autophagy, because mitochondria should be directly exposed to the contents of the vacuolar lumen. Our current data are consistent with at least three possibilities: (1) vacuolar lysis requires Atg32, (2) Atg32 is required for efficient mitochondrial degradation even after vacuolar lysis, or (3) Atg32-deficient cells accumulate a quantity of mitochondria that overwhelms the mega-autophagy degradation pathway. Distinguishing between these possibilities, such as by monitoring vacuolar morphology in *atg32Δ* cells, will be of great interest. Finally, what other specializations to autophagy might occur in gametogenesis remains an interesting and open question.

In yeast, mitophagy is not known to specifically degrade damaged mitochondria. In contrast, in animal cells, the PINK1/PARKIN mitochondrial quality control pathway can induce mitophagy of damaged mitochondria (Lazarou et al., 2015). Although no PINK1/PARKIN homologs have been described in yeast, and unlike animals, yeast do not respond to mitochondrial membrane depolarization by inducing mitophagy (Kanki et al., 2009b), an analogous quality control mechanism could conceivably exist. Indeed, old yeast cells induce mitochondrial degradation through a mechanism that relies on core autophagy machinery but not Atg32 (Hughes et al., 2016). Interestingly, this age-induced degradation pathway can be recapitulated by treatment of cells with the V-ATPase inhibitor concanamycin A (Hughes et al., 2016). Further study of mitochondrial control pathways, and their potential involvement in gametogenesis, could provide insights into mechanisms that ensure the integrity of organelles during developmental processes.

Appendix B

Methods

B.1 Yeast strains, plasmids, and culture methods

B.1.1 Strains and plasmids

All yeast strains used in this study are derivatives of SK1 (Padmore et al., 1991), except for B114, and are described in Table B.1. The Ndt80 block-release system and associated strains were described previously (Benjamin et al., 2003; Carlile and Amon, 2008) and contain *pGAL-NDT80* and *GAL4.ER* transgenes. The PP1 analog sensitive kinase alleles *cdc28-as1* (F88G) (Bishop et al., 2000) and *ime2-as1* (M146G) (Benjamin et al., 2003) were previously described. The *IME2-st* allele was described previously (Sia and Mitchell, 1995) and lacks the C-terminal 241 amino acids. Meiotic-null alleles generated by promoter replacement using *pCLB2* were described previously for *CDC5* and *CDC20* (Lee and Amon, 2003). The *rpn6-1* (*435Y) allele was described previously (Isono et al., 2005), and the His3MX6-marked SK1 version of the strain was described previously (Carpenter et al., 2018). The untagged control strain, A15055, for the Ime2-3V5 IP experiment was described previously (Berchowitz et al., 2013). The auxin-inducible degron system was described previously (Nishimura et al., 2009). In this study, we used TIR1 from *Oryza sativa* under regulation of a copper-inducible promoter, *pCUP1*. The *pCUP1-OsTIR1* construct was cloned into the *HIS3* single integration vector pNH603 (Youk and Lim, 2014), but modified to remove homology to the *DED1* locus (a gift from Leon Chan). The Num1-AID allele carried a C-terminal IAA7 degron followed by a 3V5 tag. The IAA7-3V5 tagging plasmid was a gift from Leon Chan.

Yeast transformation was performed using the lithium acetate method. C-terminal tagging was performed using a PCR-mediated technique previously described (Janke et al., 2004; Longtine et al., 1998). As some C-terminally tagged alleles of *MDM36* are not functional, we verified functionality of *MDM36-3V5* using an established assay (Fig. S3; (Lackner et al., 2013)). We constructed a *LEU2*-selectable GFP(S65T) tagging plasmid by replacing the selectable marker in pFA6a-GFP(S65T)-His3MX6 with *Candida glabrata LEU2* (*cgLEU2*), amplified from pLC605 (a gift from Leon Chan). The 3V5 tagging plasmid was a gift from Vincent Guacci.

To visualize mitochondria, we employed several different strategies. First, we C-terminally tagged *CIT1* with a fluorescent protein, as described (Higuchi-Sanabria et al., 2016), using GFP(S65T) or mCardinal (Chu et al., 2014). The mCardinal

yeast tagging plasmid was a gift from Ryo Higuchi-Sanabria. We also expressed the Su9 mitochondrial targeting sequence (MTS) from *Neurospora crassa* fused to yEGFP under regulation of a *pGPD1* promoter, expressed from a pNH603 single integration plasmid (Youk and Lim, 2014), but modified to remove homology to the *DED1* locus (a gift from Leon Chan). Additionally, we expressed a mitoBFP construct from a pRS424 plasmid modified to carry a KanMX or NatMX marker instead of *TRP1* (termed pRS(2μ)-KanMX or -NatMX). The mitoBFP construct was described as pYES-TagBFP (Murley et al., 2013), and pRS424 was described previously (Christianson et al., 1992). We also used a 2μ plasmid containing a *URA3* marker and mito-TagBFP (mitoBFP; pUB812) that was previously described (Friedman et al., 2015).

To visualize the prospore membrane, we fused amino acids 51-91 from Spo20 (Nakanishi et al., 2004) to the C terminus of link-yEGFP (Sheff and Thorn, 2004) or mTagBFP2, under regulation of the *ATG8* promoter (amplified from pRS306-2xyEGFP-ATG8 (Graef et al., 2013)), subcloned into the *LEU2* integrating plasmid pLC605 (a gift from Leon Chan) or a pRS(2μ), drug-selectable plasmid (described above). We also used the prospore membrane marker Rrt5-mKate2, whose localization was discovered fortuitously (Elçin Ünal, personal communication).

To visualize the endoplasmic reticulum, we integrated a plasmid encoding an ER-retained GFP. The EGFP-HDEL plasmid (pUB606) contains the Kar2 signal sequence fused to EGFP with a C-terminal HDEL tetrapeptide and was described previously (Rossanese et al., 2001).

To generate the *GFP-MDM36* strain, we used a Cas9-mediated genome editing strategy similar to a described method (Anand et al., 2017). Annealed oligonucleotides encoding the gRNA (5'-GAACACTTACTACTATAGCA-3') were inserted into a centromeric plasmid carrying a *URA3* marker and *pPGK1-Cas9* (a gift from Gavin Schlissel), generating pUB1395. Then, pUB1395 and a repair template were co-transformed into yeast, the plasmid was lost by streaking cells without selection, and the presence of the yEGFP tag was confirmed by PCR and sequencing.

To overexpress *GFP-LTC1/LAM6*, we inserted the *LTC1/LAM6* ORF amplified from SK1 genomic DNA downstream of the pCUP1 promoter and GFP. We cloned the insert into the *LEU2* integrating plasmid pLC605 (a gift from Leon Chan).

To purify Mdm36 from *E. coli*, we used an IPTG-inducible expression plasmid described previously as pET22b mod T7prom::H6-T7-Mdm36 (Ping et al., 2016) and provided by Laura Lackner. (See below for protein purification method).

Table B.1. Strains used in this study.

Strain	Genotype
UB15 (SK1 wild type*)	SK1 *MAT***a***/MATα ho::LYS2/ho::LYS2 lys2/lys2 ura3/ura3/ leu2::hisG/leu2::hisG his3::hisG/his3::hisG trp1::hisG/trp1::hisG*
UB2781	SK1 *MAT***a***/MATα pet100::KanMX6/pet100::KanMX6*
UB3284	SK1 *MAT***a***/MATα atg32::KanMX/atg32::KanMX OM45-GFP::KanMX/OM45-GFP::KanMX*
UB3286	SK1 *MAT***a***/MATα OM45-GFP::KanMX/OM45-GFP::KanMX*
UB3494	SK1 *MAT***a***/MATα atg32::KanMX/atg32::KanMX OM45-GFP::KanMX/OM45-GFP::KanMX RRT5-mKate2::KanMX/RRT5-mKate2::KanMX*
UB3521	SK1 *MAT***a***/MATα OM45-GFP::KanMX/OM45-GFP::KanMX RRT5-mKate2::KanMX/RRT5-mKate2::KanMX*
UB7055	SK1 *MAT***a***/MATα pGAL-NDT80::TRP1/pGAL-NDT80::TRP1 ura3::pGPD1-GAL4(848).ER::URA3/ura3::pGPD1-GAL4(848).ER::URA3 his3::pGPD1-Su9 MTS-yEGFP::HIS3/his3::hisG HTB1-mCherry::His3MX6/+*
UB7103	SK1 *MAT***a***/MATα his3::pGPD1-Su9 MTS-yEGFP::HIS3/his3::hisG NUP49-mCherry::KanMX/+*
UB7155	SK1 *MAT***a***/MATα HTB1-mCherry::His3MX6/HTB1-mCherry::His3MX6 his3::pGPD1-Su9 MTS-yEGFP::HIS3/his3::pGPD1-Su9 MTS-yEGFP::HIS3*
UB7278	SK1 *MAT***a***/MATα HTB1-mCherry::His3MX6/HTB1-mCherry::His3MX6 his3::pGPD1-Su9 MTS-yEGFP::HIS3/his3::pGPD1-Su9 MTS-yEGFP::HIS3 pCLB2-3HA-CDC5::KanMX6/pCLB2-3HA-CDC5::KanMX6*
UB7343	SK1 *MAT***a***/MATα HTB1-mCherry::His3MX6/HTB1-mCherry::His3MX6 his3::pGPD1-Su9 MTS-yEGFP::HIS3/his3::pGPD1-Su9 MTS-yEGFP::HIS3 pCLB2-CDC20::KanMX6/pCLB2-CDC20::KanMX6*
UB7345	SK1 *MAT***a***/MATα HTB1-mCherry::His3MX6/HTB1-mCherry::His3MX6 his3::pGPD1-Su9 MTS-yEGFP::HIS3/his3::pGPD1-Su9 MTS-yEGFP::HIS3 spo12::LEU2/spo12::LEU2*
UB7436	SK1 *MAT***a***/MATα trp1::EGFP-HDEL::TRP1/trp1::EGFP-HDEL::TRP1 HTB1-mCherry::His3MX6/HTB1-mCherry::His3MX6 2μ(URA3)-pADH1-mitoBFP*(pUB812)
UB7533	SK1 *MAT***a***/MATα HTB1-mCherry::His3MX6/HTB1-mCherry::His3MX6 his3::pGPD1-Su9 MTS-yEGFP::HIS3/his3::pGPD1-Su9 MTS-yEGFP::HIS3*

	ama1::HIS3/ama1::HIS3
UB7798	SK1 *MAT***a** *fzo1::KanMX6 dnm1::NatMX4*
UB8338	SK1 *MAT***a** *CIT1-mCardinal::His3MX6*
UB8503	SK1 *MAT***a***/MATα pGAL-NDT80::TRP1/pGAL-NDT80::TRP1 ura3::pGPD1-GAL4(848).ER::URA3/ura3::pGPD1-GAL4(848).ER::URA3 ABF2-GFP::KanMX/ABF2-GFP::KanMX HTB1-mCherry::His3MX6/HTB1-mCherry::His3MX6*
UB9158	SK1 *MAT***a***/MATα pGAL-NDT80::TRP1/pGAL-NDT80::TRP1 ura3::pGPD1-GAL4(848).ER::URA3/ura3::pGPD1-GAL4(848).ER::URA3 CIT1-GFP::His3MX6/CIT1-GFP::His3MX6 HTB1-mCherry::His3MX6/HTB1-mCherry::His3MX6*
UB9239	SK1 *MAT***a***/MATα pGAL-NDT80::TRP1/pGAL-NDT80::TRP1 ura3::pGPD1-GAL4(848).ER::URA3/ura3::pGPD1-GAL4(848).ER::URA3 CIT1-GFP::His3MX6/CIT1-GFP::His3MX6 HTB1-mCherry::His3MX6/HTB1-mCherry::His3MX6 spo21::hphNT1/spo21::hphNT1*
UB9494	SK1 *MAT***a***/MATα pGAL-NDT80::TRP1/pGAL-NDT80::TRP1 ura3::pGPD1-GAL4(848).ER::URA3/ura3::pGPD1-GAL4(848).ER::URA3 CIT1-GFP::His3MX6/+ HTB1-mCherry::His3MX6/+ ZIP1^GFP(700)/+ cdc28-as1/cdc28-as1*
UB9496	SK1 *MAT***a***/MATα pGAL-NDT80::TRP1/pGAL-NDT80::TRP1 ura3::pGPD1-GAL4(848).ER::URA3/ura3::pGPD1-GAL4(848).ER::URA3 CIT1-GFP::His3MX6/+ HTB1-mCherry::His3MX6/+ ZIP1^GFP(700)/+*
UB9844	SK1 *MAT***a***/MATα pGAL-NDT80::TRP1/pGAL-NDT80::TRP1 ura3::pGPD1-GAL4(848).ER::URA3/ura3::pGPD1-GAL4(848).ER::URA3 CIT1-GFP::His3MX6/+ HTB1-mCherry::His3MX6/+ ime2-as1/ime2-as1*
UB9897	SK1 *MAT***a** *spo11::TRP1 spo13::KanMX CIT1-GFP::His3MX6 ura3::MATα::URA3*
UB10254	SK1 *MAT***a***/MATα CIT1-GFP::His3MX6/CIT1-GFP::His3MX6 HTB1-mCherry::His3MX6/HTB1-mCherry::His3MX6*
UB10397	SK1 *MAT***a***/MATα pGAL-NDT80::TRP1/pGAL-NDT80::TRP1 ura3::pGPD1-GAL4(848).ER::URA3/ura3::pGPD1-GAL4(848).ER::URA3 CIT1-GFP::His3MX6/CIT1-GFP::His3MX6*
UB10554	SK1 *MAT***a***/MATα pGAL-NDT80::TRP1/pGAL-NDT80::TRP1 ura3::pGPD1-GAL4(848).ER::URA3/ura3::pGPD1-GAL4(848).ER::URA3 IME2-3V5::His3MX6/IME2-3V5::His3MX6 CIT1-GFP::His3MX6/CIT1-GFP::His3MX6*
UB12017	SK1 *MAT***a***/MATα NUM1-3V5::KanMX6/NUM1-3V5::KanMX6*
UB12402	SK1 *MAT***a***/MATα pGAL-NDT80::TRP1/pGAL-NDT80::TRP1 ura3::pGPD1-GAL4(848).ER::URA3/ura3::pGPD1-GAL4(848).ER::URA3 NUM1-3V5::KanMX6/NUM1-3V5::KanMX6*
UB12403	SK1 *MAT***a***/MATα pGAL-NDT80::TRP1/pGAL-NDT80::TRP1*

	ura3::pGPD1-GAL4(848).ER::URA3/ura3::pGPD1-GAL4(848).ER::URA3 NUM1-3V5::KanMX6/NUM1-3V5::KanMX6 ime2-as1/ime2-as1
UB13129	SK1 *MAT***a***/MATα CIT1-mCardinal::His3MX6/CIT1-mCardinal::His3MX6 SPC42-GFP::KanMX/SPC42-GFP::KanMX*
UB13131	SK1 *MAT***a***/MATα CIT1-mCardinal::His3MX6/CIT1-mCardinal::His3MX6 leu2::pATG8-link-yEGFP-SPO20$^{51-91}$::LEU2/ leu2::pATG8-link-yEGFP-SPO20$^{51-91}$::LEU2*
UB13245	SK1 *MAT***a***/MATα pGAL-NDT80::TRP1/pGAL-NDT80::TRP1 ura3::pGPD1-GAL4(848).ER::URA3/ura3::pGPD1-GAL4(848).ER::URA3 NUM1-3V5::KanMX6/NUM1-3V5::KanMX6 pdr5::hphMX6/pdr5::hphMX6*
UB13762	SK1 *MAT***a** *MDM36-3V5::KanMX6*
UB13766	SK1 *MAT***a** *fzo1::KanMX6 dnm1::NatMX4 mdm36::hphNT1*
UB13768	SK1 *MAT***a** *fzo1::KanMX6 dnm1::NatMX4 MDM36-3V5::KanMX6*
UB13770	SK1 *MAT***a** *mdm36::hphNT1*
UB13816	SK1 *MAT***a***/MATα pGAL-NDT80::TRP1/pGAL-NDT80::TRP1 ura3::pGPD1-GAL4(848).ER::URA3/ura3::pGPD1-GAL4(848).ER::URA3 NUM1-3V5::KanMX6/NUM1-3V5::KanMX6 rpn6-1::His3MX6/rpn6-1::His3MX6*
UB13851	SK1 *MAT***a***/MATα pGAL-NDT80::TRP1/pGAL-NDT80::TRP1 ura3::pGPD1-GAL4(848).ER::URA3/ura3::pGPD1-GAL4(848).ER::URA3 MDM36-3V5::KanMX6/MDM36-3V5::KanMX6*
UB14340	SK1 *MAT***a***/MATα pGAL-NDT80::TRP1/pGAL-NDT80::TRP1 ura3::pGPD1-GAL4(848).ER::URA3/ura3::pGPD1-GAL4(848).ER::URA3 MDM36-3V5::KanMX6/MDM36-3V5::KanMX6 rpn6-1::His3MX6/rpn6-1::His3MX6*
UB14546	SK1 *MAT***a***/MATα pGAL-NDT80::TRP1/pGAL-NDT80::TRP1 ura3::pGPD1-GAL4(848).ER::URA3/ura3::pGPD1-GAL4(848).ER::URA3 MDM36-3V5::KanMX6/MDM36-3V5::KanMX6 ime2-as1/ime2-as1*
UB15124	SK1 *MAT***a***/MATα pGAL-NDT80::TRP1/pGAL-NDT80::TRP1 ura3::pGPD1-GAL4(848).ER::URA3/ura3::pGPD1-GAL4(848).ER::URA3 HTB1-mCherry::His3MX6/HTB1-mCherry::His3MX6 NUM1-GFP::cgLEU2/NUM1-GFP::cgLEU2 pRS(2μ)-KanMX-pGPD1-mitoBFP*
UB16047	SK1 *MAT***a***/MATα pGAL-NDT80::TRP1/pGAL-NDT80::TRP1 ura3::pGPD1-GAL4(848).ER::URA3/ura3::pGPD1-GAL4(848).ER::URA3 HTB1-mCherry::His3MX6/HTB1-mCherry::His3MX6 NUM1-GFP::cgLEU2/NUM1-GFP::cgLEU2 ime2-as1/ime2-as1 pRS(2μ)-KanMX-pGPD1-mitoBFP*
UB16156	SK1 *MAT***a***/MATα pGAL-NDT80::TRP1/pGAL-NDT80::TRP1 ura3::pGPD1-GAL4(848).ER::URA3/ura3::pGPD1-*

	GAL4(848).ER::URA3 HTB1-mCherry::His3MX6/HTB1-mCherry::His3MX6 NUM1-GFP::cgLEU2/NUM1-GFP::cgLEU2 pCLB2-CDC20::KanMX6/pCLB2-CDC20::KanMX6 pRS(2μ)-NanMX-pGPD1-mitoBFP
UB16162	SK1 *MAT***a***/MATα HTB1-mCherry::His3MX6/HTB1-mCherry::His3MX6 NUM1-GFP::cgLEU2/NUM1-GFP::cgLEU2 pRS(2μ)-KanMX-pGPD1-mitoBFP*
UB16324	SK1 *MAT***a***/MATα MDM36-3V5::KanMX6/ MDM36-3V5::KanMX6 pdr5::hphMX6/pdr5::hphMX6*
UB16326	SK1 *MAT***a***/MATα yEGFP-MDM36/yEGFP-MDM36*
UB16660	SK1 *MAT***a***/MATα pGAL-NDT80::TRP1/ndt80::LEU2 ura3::pGPD1-GAL4(848).ER::URA3/ura3::pGPD1-GAL4(848).ER::URA3 NUM1-3V5::KanMX6/+ IME2-st/+*
UB16677	SK1 *MAT***a***/MATα NUM1-mKate2::His3MX6/NUM1-mKate2::His3MX6 yEGFP-MDM36/yEGFP-MDM36 pRS(2μ)-NatMX-pATG8-mTagBFP2-SPO20*$^{51\text{-}91}$
UB16683	SK1 *MAT***a***/MATα HTB1-mCherry::His3MX6/HTB1-mCherry::His3MX6 yEGFP-MDM36/yEGFP-MDM36 pRS(2μ)-NatMX-pGPD1-mitoBFP*
UB16806	SK1 *MAT***a***/MATα pGAL-NDT80::TRP1/pGAL-NDT80::TRP1 ura3::pGPD1-GAL4(848).ER::URA3/ura3::pGPD1-GAL4(848).ER::URA3 CLB3-3HA::KanMX/+ RIM4-3V5::HIS3/+ NUM1-GFP::cgLEU2/NUM1-GFP::cgLEU2 HTB1-mCherry::His3MX6/+ pRS(2μ)-NatMX-pGPD1-mitoBFP*
UB16808	SK1 *MAT***a***/MATα pGAL-NDT80::TRP1/pGAL-NDT80::TRP1 ura3::pGPD1-GAL4(848).ER::URA3/ura3::pGPD1-GAL4(848).ER::URA3 CLB3-3HA::KanMX/+ RIM4-3V5::HIS3/+ NUM1-GFP::cgLEU2/NUM1-GFP::cgLEU2 HTB1-mCherry::His3MX6/+ IME2-st/+ pRS(2μ)-NatMX-pGPD1-mitoBFP*
UB16888	SK1 *MAT***a***/MATα pGAL-NDT80::TRP1/pGAL-NDT80::TRP1 ura3::pGPD1-GAL4(848).ER::URA3/ura3::pGPD1-GAL4(848).ER::URA3 ime2-as1/ime2-as1 CIT1-GFP::His3MX6/CIT1-GFP::His3MX6 HTB1-mCherry::His3MX6/HTB1-mCherry::His3MX6*
UB17328	SK1 *MAT***a***/MATα ndt80::LEU2/ndt80::LEU2 HTB1-mCherry::His3MX6/+ CIT1-GFP::His3MX6/+*
UB17330	SK1 *MAT***a***/MATα ndt80::LEU2/ndt80::LEU2 HTB1-mCherry::His3MX6/+ CIT1-GFP::His3MX6/+ IME2-st/+*
UB17332	SK1 *MAT***a***/MATα pGAL-NDT80::TRP1/ndt80::LEU2 ura3::pGPD1-GAL4(848).ER::URA3/ura3::pGPD1-GAL4(848).ER::URA3 NUM1-3V5::KanMX6/+*
UB17548	SK1 *MAT***a***/MATα pGAL-NDT80::TRP1/pGAL-NDT80::TRP1 ura3::pGPD1-GAL4(848).ER::URA3/ura3::pGPD1-GAL4(848).ER::URA3 his3::pCUP1-osTIR1::HIS3/his3::pCUP1-*

	osTIR1::HIS3 NUM1-IAA7-3V5::KanMX/NUM1-IAA7-3V5::KanMX CIT1-GFP::His3MX6/CIT1-GFP::His3MX6 HTB1-mCherry::His3MX6/HTB1-mCherry::His3MX6
UB17550	SK1 *MAT***a***/MATα pGAL-NDT80::TRP1/pGAL-NDT80::TRP1 ura3::pGPD1-GAL4(848).ER::URA3/ura3::pGPD1-GAL4(848).ER::URA3 his3::pCUP1-osTIR1::HIS3/his3::pCUP1-osTIR1::HIS3 ime2-as1/ime2-as1 NUM1-IAA7-3V5::KanMX/NUM1-IAA7-3V5::KanMX CIT1-GFP::His3MX6/CIT1-GFP::His3MX6 HTB1-mCherry::His3MX6/HTB1-mCherry::His3MX6*
UB17552	SK1 *MAT***a***/MATα pGAL-NDT80::TRP1/pGAL-NDT80::TRP1 ura3::pGPD1-GAL4(848).ER::URA3/ura3::pGPD1-GAL4(848).ER::URA3 NUM1-IAA7-3V5::KanMX/NUM1-IAA7-3V5::KanMX CIT1-GFP::His3MX6/CIT1-GFP::His3MX6 HTB1-mCherry::His3MX6/HTB1-mCherry::His3MX6*
UB17554	SK1 *MAT***a***/MATα pGAL-NDT80::TRP1/pGAL-NDT80::TRP1 ura3::pGPD1-GAL4(848).ER::URA3/ura3::pGPD1-GAL4(848).ER::URA3 ime2-as1/ime2-as1 NUM1-IAA7-3V5::KanMX/NUM1-IAA7-3V5::KanMX CIT1-GFP::His3MX6/CIT1-GFP::His3MX6 HTB1-mCherry::His3MX6/HTB1-mCherry::His3MX6*
UB18219	SK1 *MAT***a***/MATα pGAL-NDT80::TRP1/pGAL-NDT80::TRP1 ura3::pGPD1-GAL4(848).ER::URA3/ura3::pGPD1-GAL4(848).ER::URA3 NUM1-mKate2::His3MX6/NUM1-mKate2::His3MX6 yEGFP-MDM36/yEGFP-MDM36 pRS(2μ)-NatMX-pATG8-mTagBFP2-SPO20$^{51-91}$*
UB18221	SK1 *MAT***a***/MATα pGAL-NDT80::TRP1/pGAL-NDT80::TRP1 ura3::pGPD1-GAL4(848).ER::URA3/ura3::pGPD1-GAL4(848).ER::URA3 ime2-as1/ime2-as1 NUM1-mKate2::His3MX6/NUM1-mKate2::His3MX6 yEGFP-MDM36/yEGFP-MDM36 pRS(2μ)-NatMX-pATG8-mTagBFP2-SPO20$^{51-91}$*
UB18405	SK1 *MATα URA(CEN)-pCUP1-GFP-PH-8*
UB18612	SK1 *MAT***a***/MATα pGAL-NDT80::TRP1/pGAL-NDT80::TRP1 ura3::pGPD1-GAL4(848).ER::URA3/ura3::pGPD1-GAL4(848).ER::URA3 IME2-3V5::His3MX6/IME2-3V5::His3MX6 CIT1-GFP::His3MX6/CIT1-GFP::His3MX6 pCLB2-3HA-CDC5::KanMX6/pCLB2-3HA-CDC5::KanMX6*
UB18614	SK1 *MAT***a***/MATα pGAL-NDT80::TRP1/pGAL-NDT80::TRP1 ura3::pGPD1-GAL4(848).ER::URA3/ura3::pGPD1-GAL4(848).ER::URA3 IME2-3V5::His3MX6/IME2-3V5::His3MX6 CIT1-GFP::His3MX6/CIT1-GFP::His3MX6 pCLB2-CDC20::KanMX6/pCLB2-CDC20::KanMX6*
UB18845	SK1 *MAT***a***/MATα pGAL-NDT80::TRP1/pGAL-NDT80::TRP1 ura3::pGPD1-GAL4(848).ER::URA3/ura3::pGPD1-*

	GAL4(848).ER::URA3 IME2-3V5::His3MX6/IME2-3V5::His3MX6 CIT1-GFP::His3MX6/CIT1-GFP::His3MX6 cdc28-as1/cdc28-as1
UB19945	SK1 *MAT***a***/MATα CIT1-mCardinal::His3MX6/+ MMM1-GFP::cgLEU2/+*
UB20120	SK1 *MAT***a***/MATα HTB1-mCherry::His3MX6/+ LTC1-GFP::TRP1/+ pRS(2μ)-NatMX-pGPD1-mitoBFP*
UB20463	SK1 *MAT***a***/MATα HTB1-mCherry::His3MX6/HTB1-mCherry::His3MX6 CIT1-GFP::His3MX6/CIT1-GFP::His3MX6 ltc1::hphNT1/ltc1::hphNT1*
UB20735	SK1 *MAT***a***/MATα pGAL-NDT80::TRP1/pGAL-NDT80::TRP1 ura3::pGPD1-GAL4(848).ER::URA3/ura3::pGPD1-GAL4(848).ER::URA3 NUM1-IAA7-3V5::KanMX/NUM1-IAA7-3V5::KanMX leu2::pCUP1-GFP-LTC1::LEU2/leu2::hisG HTB1-mCherry::His3MX6/+ pRS(2μ)-NatMX-pGPD1-mitoBFP*
UB20737	SK1 *MAT***a***/MATα pGAL-NDT80::TRP1/pGAL-NDT80::TRP1 ura3::pGPD1-GAL4(848).ER::URA3/ura3::pGPD1-GAL4(848).ER::URA3 NUM1-IAA7-3V5::KanMX/+ leu2::pCUP1-GFP-LTC1::LEU2/leu2::hisG HTB1-mCherry::His3MX6/+ pRS(2μ)-NatMX-pGPD1-mitoBFP*
A15055	SK1 *MAT***a***/MATα pGAL-NDT80::TRP1/pGAL-NDT80::TRP1 ura3::pGPD1-GAL4(848).ER::URA3/ura3::pGPD1-GAL4(848).ER::URA3 CLB3-3HA::KanMX/CLB3-3HA::KanMX*
B114	W303 *MAT***a** *ade2-1 trp1-1 leu2-3,112 his3-11,15 ura3-1 can1-100 bar1Δ lys2::hisG pep4Δ leu2::pGAL-IME2-st-3xFLAG::LEU2*

* Strain UB15 is the background to all other strains, except B114, which is a derivative of W303. For brevity, the wild-type background genotype does not appear in the other strain genotypes.

Table B.2. Plasmids used in this study.

Plasmid Name	Description	Genbank accession number
pUB1	pFA6a-KanMX6	
pUB4	pFA6a-GFP(S65T)-KanMX6	
pUB5	pFA6a-GFP(S65T)-TRP1	
pUB86	pFA6a-mKate2-KanMX6	
pUB153	pFA6a-NatMX4	
pUB217	pFA6a-hphNT1	
pUB294	3V5-KanMX6 tagging plasmid	
pUB606	YIplac204-pTPI1-KAR2$^{1-45}$-EGFP-HDEL	
pUB679	pNH603-pGPD1-Su9 MTS-yEGFP	MK178572

pUB763	pFA6a-IAA7-3V5-KanMX6	
pUB812	pVT100u-mito-TagBFP (2μ-URA3)	
pUB867	pFA6a-GFP(S65T)-His3MX6	
pUB868	pFA6a-mCardinal-His3MX6	
pUB949	pLC605-pATG8-link-yEGFP-SPO20$^{51-91}$	MK178573
pUB972	pRS(2μ)-KanMX-pGPD1-mitoBFP	MK178574
pUB976	pNH603-pCUP1-OsTIR1	
pUB1004	pFA6a-GFP(S65T)-cgLEU2	MK178575
pUB1375	pRS(2μ)-NatMX-pGPD1-mitoBFP	MK178576
pUB1392	pRS(2μ)-NatMX-pATG8-mTagBFP2-SPO20$^{51-91}$	MK178577
pUB1395	URA/CEN-Cas9-MDM36(gRNA3)	MK178578
pUB1429	pET22b mod T7prom::H6-T7-Mdm36	
pUB1638	pLC605-pCUP1-GFP-LTC1	

The sequences of plasmids generated by the work in Chapter 2 are available from Genbank under the indicated accession numbers.

B.1.2 Sporulation

Unless indicated otherwise, cells were induced to sporulate by a traditional starvation synchronization method. At all steps, flasks were shaken at 275 rpm. First, cells were grown in YPD (1% yeast extract, 2% peptone, 2% glucose, 22.4 mg/L uracil, and 80 mg/L tryptophan) for ~24 h at room temperature to reach saturation ($OD_{600} \geq 10$). The YPD culture was used to inoculate BYTA medium (1% yeast extract, 2% bacto tryptone, 1% potassium acetate, 50 mM potassium phthalate) to $OD_{600} = 0.25$ and grown for ~16 h at 30°C to reach $OD_{600} \geq 5$. Then, the cells were pelleted, washed with sterile water, and resuspended to a density of $OD_{600} = 1.85$ in SPO media (0.5% potassium acetate, 0.02% raffinose, pH 7). Cultures were shaken at 30°C for the duration of the experiment. In cases where selection for plasmids was necessary, G418 (Geneticin) or nourseothricin (clonNAT) were added to YPD and BYTA cultures at concentrations of 200 μg/mL and 100 μg/mL, respectively. For selection of the *URA3* mitoBFP plasmid (pUB812), cells were grown in SD-Ura medium instead of YPD.

In experiments utilizing synchronization by the Ndt80 block-release system, cells carrying the *pGAL-NDT80* and *GAL4.ER* transgenes were induced to sporulate as described above. After 5 h in SPO medium, ß-estradiol was added to a final concentration of 1 μM from a 5 mM stock (in ethanol) to induce *NDT80* expression.

During the course of this work, it was discovered that cells sporulate more efficiently in a modified sporulation medium (2% potassium acetate, 0.02% raffinose, 39.6 mg/L adenine, 39.9 mg/L uracil, 20.1 mg/L histidine, 11.8 mg/L leucine, 20 mg/L tryptophan, in Arrowhead 100% Mountain Spring Water).

B.1.3 Tetrad analysis

Cells were sporulated on solid SPO medium (1% potassium acetate, 20 mg/L adenine, 20 mg/L arginine, 20 mg/L methionine, 30 mg/L lysine, 30 mg/L tyrosine, 50 mg/L phenylalanine, 200 mg/L threonine) for at least 24 h. Then a small scraping of asci was digested in 20 μL of 1 mg/mL zymolyase-100T for 8 min at room temperature. To halt digestion, 1 mL of sterile water was added and the cells were transferred to ice. 15 μL of digested cell suspension was dripped on a YPD plate and tetrads were dissected using a micromanipulator mounted on a Zeiss Axio Scope.A1. Growth was assessed after incubation at 30°C for 2 d. To score the petite phenotype, spore colonies were replica plated to a YPG plate and incubated at 30°C for 1 d.

B.1.4 Serial dilution plating assay

Overnight cultures (in YPD, unless otherwise indicated) were diluted to OD_{600} = 0.1, sonicated, and serially diluted. Each serial dilution was 5-fold, with OD_{600} = 0.1 being the most concentrated (six total cell suspensions). 3 μL of each cell suspension was spotted on the indicated plates.

B.1.5 Drug treatments

Shokat inhibitors. The Shokat inhibitors 1-NA-PP1 and 1-NM-PP1 were provided by Kevan Shokat (UCSF). Both inhibitors were prepared as 10 mM stock solutions in DMSO and used at concentrations specific to the kinase (1 μM 1-NM-PP1 to inhibit *cdc28-as1* and 20 μM 1-NA-PP1 to inhibit *ime2-as1*).

MG-132. MG-132 (Sigma; sold as Z-Leu-Leu-Leu-al [cat. no. C2211]) was dissolved in DMSO to generate a 100 mM stock solution. The stock solution was stored frozen at -20°C and discarded after 30 d. MG-132 was used at a final concentration of 100 μM.

Auxin. Auxin (Sigma; sold as 3-indoleacetic acid [cat. no. I2886]) was dissolved in DMSO on the day of use to generate a 1 M stock solution. Auxin was used at a final concentration of 500 μM.

TTC. Triphenyl tetrazolium chloride (TTC; MP Biomedicals) was prepared as a 50 mg/mL stock in water. TTC stock solution was top-spread with beads onto pre-poured agar plates containing ~30 mL of solid medium to give the desired concentration. It was assumed that the TTC was able to freely diffuse through the

medium. In initial experiments, TTC was added to cooled molten agar but did not show any activity even at high concentrations, suggesting heat intolerance of the compound.

B.2 Light microscopy

B.2.1 Microscopy

All images were acquired using a DeltaVision Elite widefield fluorescence microscope (GE Healthcare, Sunnyvale, CA) and a PCO Edge sCMOS camera, operated by their associated softWoRx software. Time-lapse imaging experiments were performed in an environmental chamber heated to 30°C, with images acquired using a 60X/NA1.42 oil-immersion plan apochromat objective. Cells were maintained on concanavalin A-coated, glass-bottom 96-well plates (Corning). Every 10 min or every 15 min, a stack of 8 Z positions (1 μm step size) was acquired, with mCherry (32% intensity, 25 ms exposure) and FITC (10% intensity, 25 ms exposure) filter sets. All other imaging experiments were acquired at ambient temperature (~22°C) using a 100X/NA1.40 oil-immersion plan apochromat objective.

All live cells were imaged in SPO medium (0.5% potassium acetate, 0.02% raffinose) or synthetic complete medium (2% dextrose, yeast nitrogen base with amino acids), as indicated.

Where indicated, cells were fixed at room temperature for 15 min by adding formaldehyde (final concentration of 3.7%) directly to the culture medium. To halt fixation, cells were washed once with 100 mM potassium phosphate, pH 6.4, and stored in 100 mM potassium phosphate pH 7.5 with 1.2 M sorbitol at 4°C. All fixed samples were imaged in 100 mM potassium phosphate pH 7.5 with 1.2 M sorbitol.

All images were deconvolved in softWoRx software (GE Healthcare) using a 3D iterative constrained deconvolution algorithm (enhanced ratio) with 15 iterations. Linear adjustments to brightness and contrast were made in FIJI (Schindelin et al., 2012).

B.2.2 Image analysis

Num1-GFP spot number and Num1-GFP fluorescence intensity were measured in FIJI. First, the mean background intensity was measured in a 155 x 155 pixel square containing no cells. This value was then subtracted from each pixel in the image. Next, cells were manually traced, and the Find Maxima function was run to identify spots (noise tolerance = 1500) within the traced region. In addition, the total fluorescence intensity (IntDen) and area were measured for each cell.

Linescan analysis was performed in FIJI using the Plot Profile function.

B.2.3 Statistical analysis

All tests of statistical significance were nonparametric (Mann-Whitney Test or Fisher's Exact Test) and performed in Prism (GraphPad Software). The results from all statistical tests are reported as two-tailed p-values.

B.2.4 Time course staging by DAPI staining and tubulin immunofluorescence

Cells collected from meiotic culture at the desired time points were fixed in 3.7% formaldehyde overnight at 4°C. Then, cells were pelleted, washed once with 100 mM potassium phosphate, pH 6.4, and stored in 100 mM potassium phosphate, pH 7.5, with 1.2 M sorbitol at 4°C.

For DAPI staining, cells were mounted on poly-L-lysine coated multi-well slides. Then, slides were submerged in -20°C methanol for 3 min followed by -20°C acetone for 10 s. After drying, the slide was filled with VECTASHIELD Antifade Mounting Medium with DAPI (Vector Labs, Burlingame, CA) and sealed with a cover slip. For tubulin immunofluorescence, fixed cells were resuspended in 200 µL of 100 mM potassium phosphate, pH 7.5, with 1.2 M sorbitol, to which 20 µL of glusulase (Perkin-Elmer) and 6 µL of 10 mg/mL zymolyase 100T (MP Biomedicals, Santa Ana, CA) was added to obtain spheroplasts. Digestions were incubated at 30°C with rotation for 2-3 h. Completion of the digestion was monitored by sensitivity of a small aliquot of cells to lysis in the presence of 0.5% SDS. Spheroplasts were gently pelleted (900 x g) and gently resuspended in 500 µL of 100 mM potassium phosphate, pH 7.5, with 1.2 M sorbitol as a wash step. Spheroplasts were then pelleted again and resuspended in 10-50 µL of 100 mM potassium phosphate, pH 7.5, with 1.2 M sorbitol. Spheroplasts were mounted on poly-L-lysine coated multi-well slides. Then, slides were submerged in -20°C methanol for 3 min followed by -20°C acetone for 10 s. Next, spheroplasts were incubated with a 1:200 dilution of a rat anti-tubulin antibody (RRID:AB_325005, MCA78G, Bio-Rad) suspended in PBS-BSA (5 mM potassium phosphate, 15 mM NaCl, 1% bovine serum albumin, 0.1% sodium azide). After 1-3 h in a wet chamber, primary antibody was removed, the wells were washed twice with PBS-BSA, and then incubated with a 1:200 dilution of a pre-absorbed anti-rat FITC-conjugated secondary antibody (RRID:AB_2340652, 712-095-153, Jackson ImmunoResearch Labs). After incubation at room temperature for 1 h, antibody was removed, and the wells were washed twice with PBS-BSA. Then, the slide was filled with VECTASHIELD Antifade Mounting Medium with DAPI (Vector Labs, Burlingame, CA) and sealed with a cover slip.

B.2.5 DAPI staining of fixed cells expressing fluorescent proteins

To preserve organelle localization by chemical fixation while also permitting DNA staining, cells were fixed by adding 37% formaldehyde directly to the culture

medium to a final concentration of 3.7% formaldehyde. Cell suspensions were mixed by inversion and incubated at room temperature for 15 min. Then, cells were pelleted at 1900 x g for 2 min, washed once with 100 mM potassium phosphate pH 6.4, pelleted again at 1900 x g for 2 min, and resuspended in 100 mM potassium phosphate, pH 7.5, with 1.2 M sorbitol at 4°C for storage.

To DAPI stain, 8 µL of cell suspension for each sample was spotted onto a poly-L-lysine-treated multi-well slide (Teflon-coated; Tekdon). After cells adhered (1-5 min), the suspensions were removed. To permeabilize cells for DAPI staining, the slide was submerged in 70% ethanol for ~15 s. Ethanol was removed with an aspirator, then slides were mounted in DAPI mount (Vector Labs) and sealed with a 24-60 mm #1 coverslip and nail polish.

B.3 Electron microscopy

B.3.1 Electron microscopy sample preparation

Samples for thin section transmission electron microscopy were prepared by a high-pressure freezing and fast freeze substitution method (McDonald and Muller-Reichert, 2002; McDonald, 2014; McDonald and Webb, 2011). In brief, cells were harvested from meiotic culture by vacuum filtration onto nitrocellulose filters. Then cells were scrape-loaded into 50-µm or 100-µm-deep high pressure freezing specimen carriers (McDonald and Muller-Reichert, 2002). Samples were frozen in a Bal-Tec HPM-010 high-pressure freezer (Bal-Tec AG) and stored in liquid nitrogen.

Frozen samples were transferred to cryovials containing 1.5 mL of 1% osmium tetroxide, 0.1% uranyl acetate, and 5% water in acetone at -195°C for fixation and fast freeze substitution using a published method (McDonald, 2014; McDonald and Webb, 2011). Addition of 5% water during freeze substitution improves membrane contrast. For fast freeze substitution, the cryovials were transferred to a -195°C metal block and horizontally shaken at 125 rpm for 3 h in a thermally insulated box. After 3 h, the samples had warmed to 20°C.

Next, samples were infiltrated with Epon-Araldite resin using a graded resin series (McDonald, 2014). Cells were rinsed 4-5 times in acetone and removed from the planchettes. Then cells were infiltrated with Epon-Araldite resin in increasing increments of 25% over 3 h. To change resin, cells were pelleted at 6,000 x g for 1 min. Then samples were treated with pure resin, changed every 30 min, 3 times. Afterwards, samples were mounted in pure resin and confined between two PTFE-coated slides. The samples were cured for 2 h at 100°C.

Resin-embedded samples were mounted in blocks and cut into 60-nm-thick serial sections using a Reichert-Jung Ultracut E microtome. Ribbons containing the serial sections were transferred to 1 x 2 mm slot grids covered with 0.6% Formvar.

Sections were post-stained with 1% uranyl acetate for 10 min, then with lead citrate for 10 min (Reynolds, 1963).

B.3.2 Electron microscopy

Cells were imaged on a FEI Tecnai 12 transmission electron microscope (120 kV). Images were adjusted for brightness and contrast and serial sections assembled into image stacks in FIJI (Schindelin et al., 2012). For short section series representing a single contact site, the stack registration tools in FIJI were sometimes successful in aligning the individual section images. However, for longer series, manual registration was necessary (see below).

B.3.3 3D reconstructions of electron microscopy data

During image acquisition, some sections were imaged twice to capture the entire cell area. These sections corresponded to the center of the cell, where the diameter is large. Before proceeding, image pairs were stitched together in Adobe Photoshop CS6 using the Photomerge function. Then, images were assembled into a TIF stack with FIJI.

Further processing was performed using IMOD (Kremer et al., 1996). First, the image stack was converted from TIF to MRC format. Next, the image stack was aligned into register manually using the Midas function within the eTomo package in IMOD. Warp adjustments were made where judged necessary due to grid deformation. Using the aligned images, mitochondria and nuclear envelope were manually segmented in IMOD and rendered as 3D models. As three adjacent sections were missing within the 57-section (3420 nm) series, the segmented features were interpolated across the missing sections.

B.4 Protein methods

B.4.1 Immunoblotting

To harvest protein, 3.7 OD_{600} equivalents of cells were pelleted and resuspended in 1 mL of 5% trichloroacetic acid (TCA) and incubated at 4°C for ≥10 min. Then, cells were washed with 1 mL of TE50 pH 7.5 (50 mM Tris, 1 mM EDTA), and finally with 1 mL of acetone, then allowed to dry completely. To extract protein, ~100 µL of glass beads and 100 µL of lysis buffer (TE50 pH 7.5, 2.75 mM DTT, 1X cOmplete EDTA-free protease inhibitor cocktail [Roche]) were added to the pellet and shaken using a Mini-Beadbeater-96 (BioSpec). Next, 50 µL of 3X SDS sample buffer (187.5 mM Tris pH 6.8, 6% β-mercaptoethanol, 30% glycerol, 9% SDS, 0.05% bromophenol blue) was added, and the mixture heated for 5 min. We found that recovery of Num1 was enhanced by heating at 50°C rather than boiling.

Proteins were separated by SDS-PAGE using Bolt 4-12% Bis-Tris Plus Gels (Thermo Fisher) and transferred onto membranes. For Num1, we transferred to a 0.45 μm Immobilon-FL PVDF membrane (LI-COR Biosciences, Lincoln, NE) in a Mini-PROTEAN Tetra tank (BioRad) filled with 25 mM Tris, 192 mM glycine, and 9% methanol, run at 180 mA (max 80 V) for 3 h. For all other blots, we transferred to a 0.45 μm nitrocellulose membrane (BioRad) using a semi-dry transfer system (Trans-Blot Turbo) and its supplied transfer buffer (BioRad). Membranes were blocked for 30 min with Odyssey Blocking Buffer (PBS) (LI-COR Biosciences) at room temperature, then incubated overnight at 4°C with primary antibody mixtures diluted in Odyssey Blocking Buffer (PBS) with 0.1% Tween-20. For detection of V5 epitope, we used a mouse anti-V5 antibody (RRID:AB_2556564, R960-25, Thermo Fisher) at a 1:2000 dilution. For detection of GFP, we used a mouse anti-GFP antibody (RRID:AB_2313808, 632381, Clontech) at a 1:2000 dilution. For detection of T7 epitope, we used a mouse anti-T7 antibody (RRID: AB_11211744, 69522, EMD Millipore) at a 1:2000 dilution. As a loading control, we used a rabbit anti-hexokinase (Hxk1) antibody (RRID:AB_2629457, H2035, US Biological, Salem, MA) at 1:10,000 dilution or a rabbit anti-hexokinase (Hxk2) antibody (RRID:AB_219918, 100-4159, Rockland, Limerick, PA) at 1:15,000 dilution. For secondary detection, we used an anti-mouse secondary antibody conjugated to IRDye 800CW at a 1:15,000 dilution (RRID:AB_621847, 926–32212, LI-COR Biosciences) and an anti-rabbit antibody conjugated to IRDye 680RD at a 1:15,000 dilution (RRID:AB_10956166, 926–68071, LI-COR Biosciences) in Odyssey Blocking Buffer (PBS) with 0.01% Tween-20. Blots were imaged using an Odyssey CLx scanner (LI-COR Biosciences), and band intensities were quantified using the Image Studio software associated with the scanner.

B.4.2 Protein purification

Purification of His-tagged Mdm36 was performed as described (Ping et al., 2016) with minor modifications. In brief, 500-mL cultures of Rosetta 2(DE3) *E. coli* (Novagen) bearing expression plasmids and growing in log phase were induced with 250 μM IPTG for 16 h at 18°C. Then, cells were harvested by centrifugation, the pellet resuspended in resuspension buffer (RB, 20 mM Tris pH 8, 500 mM NaCl, 1.89 mM 2-mercaptoethanol), and lysed by 3 freeze-thaw cycles and sonication. Clarified lysates were mixed with 1/7 volume of Ni-NTA agarose (Qiagen) and rotated end-over-end for 1 h at 4°C. Beads were washed in a conical tube with RB, then loaded into a chromatography column and washed with 500 mL of RB + 30 mM imidazole. Protein was eluted with RB + 300 mM imidazole, then dialyzed against 20 mM Tris pH 8, 500 mM NaCl. Last, glycerol was added to 10%, proteins were aliquotted, and flash-frozen in liquid nitrogen. Protein concentration was estimated by A280.

Ime2-st kinase was purified from yeast (B114), described previously as yDP159 (Phizicky et al., 2018), with minor modifications. Strain B114 contains a pGAL-

IME2-st-3xFLAG expression plasmid with a *LEU2* selectable marker. First, a 100-mL culture of SC -Leu with strain B114 was grown overnight with shaking at 30°C. The following day, this culture was used to inoculate 4 L of YEP + 2% glycerol (8 x 500-mL cultures in 2-L baffled flasks) and grown overnight with shaking at 30°C. The following day when the culture reached OD_{600} 1.2, expression of pGAL-IME2-st-3xFLAG was induced by the addition of galactose to a final concentration of 2%. (The protein contains amino acids 1-404 of Ime2 fused to a 3x FLAG epitope at the C terminus). After an additional 6 h of growth, cells were harvested by centrifugation at 4°C.

The yeast pellet was then resuspended in 35 mL of lysis buffer (50 mM HEPES pH 7.6, 10% glycerol, 5 mM Mg-Acetate, 1 mM EDTA, 1 mM EGTA, 1 M sorbitol, 0.02% NP-40, 2 mM ATP, 0.5 M KCl, 1X Halt protease and phosphatase inhibitors) and cells were drop-frozen in liquid nitrogen. Frozen cells were lysed under liquid nitrogen in a Waring blender. The resulting powder was thawed and clarified for 1 h at 20,000 rpm at 4°C in a JA-20 rotor. The supernatant was adjusted to 0.3 M KCl and clarified again at 25,000 x g for 15 min at 4°C.

To isolate the tagged protein, lysate was incubated with 1 mL of equilibrated FLAG resin (Sigma) for 2 hours with rotation at 4°C. Then, the lysate/resin was transferred to a gravity flow column (at 4°C) and washed with 20 mL H buffer containing 0.3 M KCl, 0.01% NP-40. Beads were washed again with 10 mL H buffer containing 0.3 M KGlut, 0.01% NP-40. Proteins were eluted with 5 mL H buffer containing 0.15 mg/ml 3xFLAG Peptide and 0.3 M KGlut (5 x 1-mL elutions incubated for 30 min each). The eluate was subsequently concentrated by ultrafiltration (10 kDa MWCO, Vivaspin) and then run through a Superdex 75 column (GE Healthcare) equilibrated with H buffer containing 0.3 M KGlut, 1 mM ATP, 0.01% NP-40 using a ActaPur FPLC (GE Healthcare). Peak Ime2-st fractions were pooled, aliquotted, and stored at -80°C.

B.4.3 Ime2 IP *in vitro* kinase assay

Measurement of Ime2 kinase activity *in vitro* was performed similar to a described method (Berchowitz et al., 2013). At each time point, cell pellets from 2 mL of SPO culture were harvested by centrifugation and snap-frozen in liquid nitrogen. Pellets were thawed on ice, and 220 µL of NP-40 lysis buffer (50 mM Tris pH 7.5, 150 mM NaCl, 1% NP-40) with protease and phosphatase inhibitors (60 mM ß-glycerophosphate, 0.1 mM sodium orthovanadate, 15 mM *p*-Nitrophenylphosphate, 0.095 U/mL aprotinin (Sigma), 0.1 mg/mL leupeptin (Sigma), 1 mM PMSF (Sigma), 1 mM DTT, 1X fungal-specific protease inhibitor cocktail (Sigma)) was added. Cells were lysed in a Fast-Prep (MP Bio) using zirconia beads (BioSpec). Lysates were clarified by centrifugation twice at 16,000 x g for 10 min. Ime2-3V5 immunoprecipitation was performed using 15 µL of anti-V5 agarose beads (Sigma)

for 2 h at 4°C. IP samples were washed twice with NP-40 lysis buffer, then twice with 25 mM MOPS (pH 7.2).

For kinase reactions, agarose beads with bound Ime2-3V5 were incubated with 6 µL of buffer HBII (25 mM MOPS pH 7.2, 15 mM $MgCl_2$, 5 mM EGTA, 1 mM DTT, 0.02 mg/mL leupeptin, 0.04 U/mL aprotinin, 0.1 mM sodium orthovanadate, 15 mM *p*-Nitrophenylphosphate) for 15 min at room temperature, followed by the addition of 10 µL kinase reaction mixture (25 mM MOPS pH 7.2, 2 mg/mL Histone H1 (Sigma), 0.2 mM ATP) containing 50 nCi γ-^{32}P ATP. Kinase reactions were incubated for 15 min at room temperature and stopped by the addition of 10 µL of 3X SDS loading buffer and boiling (5 min). Kinase reactions were separated on a 4-15% SDS Criterion TGX PAGE gel (Bio-Rad) and transferred to a nitrocellulose membrane. The membrane was cut, with the half containing histone H1 subjected to autoradiography (imaged with a Typhoon scanner, GE Healthcare) and the half containing Ime2-3V5 analyzed by immunoblotting. Ime2 kinase activity was determined by measuring the intensities of the histone H1 autoradiography band for each time point, with the background signal from a no-tag control subtracted. We found measurements of specific activity unreliable due to stage-specific differences in intrinsic Ime2 stability.

B.4.4 MECA subunit *in vitro* kinase assays

Ime2-st kinase and recombinant Mdm36 substrate was purified as described above. Immunoprecipitated substrates were purified as follows. 50 OD_{600} equivalents of cells growing in YPD were pelleted, resuspended in 10 mM Tris pH 7.5, pelleted again, and flash-frozen in liquid nitrogen. Frozen pellets were thawed on ice and resuspended in 300 µL of NP-40 lysis buffer (50 mM Tris pH 7.5, 150 mM NaCl, 1% NP-40, 5% glycerol) containing 1 mM DTT, 1 mM EDTA, 3X cOmplete Ultra Protease Inhibitors without EDTA (Roche), and 1X PhosSTOP phosphatase inhibitors (Roche). Cells were broken on a Mini-Beadbeater-96, and extracts were clarified by centrifugation at 15,000 x g for 15 min. Total protein concentration was determined by Bradford Assay (BioRad). For each IP, 1 mg of total protein was incubated with 15 µL of V5 agarose beads (Sigma) in a total IP volume of 200 µL. Two parallel IPs were run for each sample. After incubation with extract for 2 h at 4°C, beads were washed with NP-40 lysis buffer supplemented with protease and phosphatase inhibitors. Then, the beads from duplicate IPs were pooled and washed 3 more times with NP-40 lysis buffer supplemented with inhibitors and twice with 25 mM MOPS. Then, beads were split for the kinase assay (+Ime2-st and –Ime2-st). Prior to setting up the kinase assay, half of the bead volumes of each tube were reserved for immunoblotting. Proteins were eluted from the beads by incubation in 1X SDS sample buffer (62.5 mM Tris pH 6.8, 2% ß-mercaptoethanol, 10% glycerol, 3% SDS, 0.017% bromophenol blue) for 5 min at 50°C.

For the kinase assay, recombinant or on-bead substrate was incubated with 6 µL of HBII (15 mM MOPS, 15 mM $MgCl_2$, 5 mM EGTA, 1 mM EDTA, 3X cOmplete Ultra without EDTA, 1X PhosSTOP) for 15 min at room temperature. Then, solution 1 was prepared (1.1 µL of 100 mM ATP, 275 µL of water, 3 µL 6000 Ci/mmol 10 mCi/mL γ-^{32}P ATP). The kinase reaction was assembled by adding 5 µL of solution 1 and 2 µL of 1.5 µM Ime2-st to the substrate in HBII, resulting in a final volume of 16 µL in 25 mM MOPS. After 15 min at room temperature, reactions were stopped with 3X SDS sample buffer, heated, and run on a SDS-PAGE gel. The gels were fixed in 10% methanol, 10% acetic acid, dried, and exposed to a phosphor screen. Screens were imaged using a Typhoon scanner (GE Healthcare).

B.4.5 Denaturing immunoprecipitation and mass spectrometry

To generate denatured protein extracts, cells were first pelleted in multiples of 9.25 OD_{600} equivalents (i.e., 5 mL of SPO culture), then resuspended in 2/5 culture volume of 5% TCA at 4°C and distributed into tubes such that each contained 9.25 OD_{600} equivalents. After incubation overnight at 4°C, cells were pelleted, washed once with acetone, and dried completely. To break pellets, 100 µL of zirconia beads and 150 µL of TE50 pH 7.5, 2.75 mM DTT, 1X PhosSTOP (Roche) and 3X cOmplete Ultra EDTA Free (Roche), were added to each tube. Pellets were disrupted on a Mini-Beadbeater-96. Then, SDS was added to 1%, extracts were denatured by heating at 50°C for 5 min, and NP-40 lysis buffer (50 mM Tris pH 7.5, 150 mM NaCl, 1% NP-40, 5% glycerol) was added, supplemented with 1X PhosSTOP and 3X cOmplete Ultra EDTA Free, to a final volume of 1.5 mL (i.e., diluting SDS to 0.1%). Cleared lysates pooled from 5 tubes were added to V5 agarose beads (Sigma), incubated for 2 h at 4°C with rotation, and then washed twice with each: (1) 50 mM Tris pH 7.5, 1 M NaCl, 1 mM EDTA, 1% NP40; (2) 50 mM Tris pH 7.5, 150 mM NaCl, 10 mM $MgCl_2$, 0.05% NP-40, 5% glycerol; and (3) 50 mM Tris pH 7.5, 150 mM NaCl, 10 mM $MgCl_2$, 5% glycerol. After washes, 1X SDS sample buffer was added to the beads, and proteins were eluted by heating at 50°C for 5 min. Eluted proteins were separated by SDS-PAGE, then stained using a Colloidal Blue Staining Kit (Invitrogen).

Gel bands containing the desired protein were excised, washed for 20 min in 500 µL of 100 mM NH_4HCO_3, then incubated at 50°C for 15 min in 150 µL of 100 mM NH_4HCO_3 and 2.8 mM DTT. 10 µL of 100 mM iodoacetamide was then added to the cooled gel band mixtures and incubated for 15 min in the dark at room temperature. Then the gel slice was washed in 500 µL of equal parts 100 mM NH_4HCO_3 and acetonitrile with shaking for 20 min. Gel slices were shrunk by soaking in 50 µL of acetonitrile for 15 min. Then the supernatant was removed, and residual solvent was removed in a speed vac. Gel fragments were rehydrated with 10 µL of 25 mM NH_4HCO_3 containing sequencing grade modified trypsin (Promega), incubated at room temperature for 15 min, then supplemented with additional trypsin to completely cover the gel slices. Digestion was allowed to continue overnight at 37°C.

Then, the supernatant; two washes with 60% acetonitrile, 0.1% formic acid; and one wash with acetonitrile were all combined and dried completely in a speed vac.

Mass spectrometry was performed by the Vincent J. Coates Proteomics/Mass Spectrometry Laboratory at UC Berkeley. mudPIT methods were used in order to achieve good sequence coverage of target proteins in a complex mixture. A nano LC column was packed in a 100 µm inner diameter glass capillary with an emitter tip. The column consisted of 10 cm of Polaris c18 5 µm packing material (Varian), followed by 4 cm of Partisphere 5 SCX (Whatman). The column was loaded by use of a pressure bomb and washed extensively with buffer A (see below). The column was then directly coupled to an electrospray ionization source mounted on a Thermo-Fisher LTQ XL linear ion trap mass spectrometer. An Agilent 1200 HPLC equipped with a split line so as to deliver a flow rate of 300 nL/min was used for chromatography. Peptides were eluted using an 8-step mudPIT procedure (Washburn et al., 2001). Buffer A was 5% acetonitrile, 0.02% heptaflurobutyric acid (HBFA). Buffer B was 80% acetonitrile, 0.02% HBFA. Buffer C was 250 mM ammonium acetate, 5% acetonitrile, 0.02% HBFA. Buffer D was same as buffer C, but with 500 mM ammonium acetate.

Protein identification was performed with Integrated Proteomics Pipeline (IP2, Integrated Proteomics Applications, Inc., San Diego, CA) using ProLuCID/Sequest, DTASelect2, and Census (Cociorva et al., 2007; Park et al., 2008; Tabb et al., 2002; Xu et al., 2015). Tandem mass spectra were extracted into ms1 and ms2 files from raw files using RawExtractor (McDonald et al., 2004). Data were searched against the SK1 sequence of the target protein (Yue et al., 2017) plus the yeast database supplemented with sequences of common contaminants and concatenated to a decoy database in which the sequence for each entry in the original database was reversed (Peng et al., 2003). LTQ data was searched with 3000.0 milli-amu precursor tolerance, and the fragment ions were restricted to a 600.0 ppm tolerance. All searches were parallelized and searched on the VJC proteomics cluster. Search space included all fully tryptic peptide candidates with no missed cleavage restrictions. Carbamidomethylation (+57.02146) of cysteine was considered a static modification. We required 1 peptide per protein and both tryptic termini for each protein identification. The ProLuCID search results were assembled and filtered using the DTASelect program (Cociorva et al., 2007; Tabb et al., 2002) with a peptide false discovery rate (FDR) of 0.001 for single peptides and a peptide FDR of 0.005 for additional peptides for the same protein. Under such filtering conditions, the estimated false discovery rate for peptides was never more than 0.5%. Spectra for individual posttranslational modifications of interest were manually inspected.